

**NEW TECHNIQUES IN COHERENT OPTICAL SPECTROSCOPY:
OPTICAL DEPHASING AND RADIATIONLESS
PROCESSES IN MOLECULES**

**Thesis by
Thomas Edward Orlowski**

**In Partial Fulfillment of the Requirements
for the Degree of
Doctor of Philosophy**

**California Institute of Technology
Pasadena, California**

1979

(Submitted August 14, 1978)

To my parents, Eugene and Sophie, whose countless sacrifices have made my entire education possible.

ACKNOWLEDGMENTS

First, I would like to acknowledge the help and encouragement of my research advisor, Professor Ahmed Zewail. In the two years that we have worked together, his endless supply of scientific ideas, his ability to work tirelessly and his desire to strike out boldly into new areas have taught me a lot about what it means to be a creative and productive scientist.

Several other faculty members have helped me considerably during my stay. First, I wish to thank my former advisor, Professor G. Wilse Robinson, for giving me the opportunity to work independently, discovering the joys and pains of doing research. I look back upon those years fondly for they gave me some time to make mistakes and to learn from them. I ended up with a better understanding of the patience and perserverence required to do science. Second, I wish to thank Professor Vincent McKoy for his support and advice during the time I was trying to decide upon a new course of research. His guidance and continuing interest in my welfare since that time have left a deep impression upon me. Third, I wish to thank Professor Fred Anson for being my "substitute advisor" during the second and third years of my stay. He patiently handled all of the administrative work necessary to keep the money coming and his support and confidence are greatly appreciated. Fourth, I would like to thank Professor Jack Beauchamp for giving me the opportunity to learn ICR spectroscopy without making demands on my time or future plans. Finally I would like to thank the rest of the chemistry faculty for their interest in my work and support throughout my five years here at Caltech.

Next, I wish to thank the members of the Zewail group for their friendship, help, criticism and scientific curiosity. Working in the sub-basement of Noyes has truly been a more satisfying and productive experience for me because of the enthusiasm and skills that we have shared. I especially want to thank: Duane Smith for his overall experimental expertise and help in the design of equipment as well as for sharing his ideas in photography and music; Rajiv Shah for many spirited discussions in optics and electrodynamics; Dan Dawson for his help in setting up the laboratory and in doing "the first experiment"; Bill Lambert for countless hours in the lab helping me finish "one last experiment," and Barry Swartz, Doug Godar, Dave Millar, Joe Perry, Albert Nichols, Roy Mead, and Sam Batchelder for their help and interest in my work. A very special thanks goes to Kevin Jones who has helped me immeasurably in almost every aspect of my work. I have benefitted greatly from his theoretical understanding of and his physical insight into the concepts involved in the problems we have worked on. His genuine interest in all aspects of science has stimulated my enthusiasm as well. I would also like to thank Jackie Berg, the last official member of the Robinson group at Caltech, for her friendship and help throughout my stay and Professor Benjamin Freiser for collaborating with me and teaching me some ICR photochemistry as well as for his friendship and continuing interest in my work.

I sincerely want to express my gratitude and warmest thanks to Joyce Lundstedt for being such a patient and hard-working secretary these past two years and for working so hard (many days late into the night) organizing and masterfully typing most of this thesis. Her dedication and

interest in all of the details has certainly made the job easier and less painful. I also want to thank Beth Cooper for her help in typing part of this thesis and Ruth Stratton for the expert job she did in typing all of the propositions. These three people have definitely made what appeared to be an impossible task at the beginning a reality. Last but certainly not least, I wish to thank Adria McMillan for her help and friendship throughout my stay. In the early stages her knowledge and skills concerning every aspect of grant finances and protocol were invaluable.

My work could not have been completed without the expert help of the Chemistry shops. At every stage of experimentation, I have relied on the advice of William Schuelke, Erich Siegel, and Irving Moskovitz in the design of several components crucial to the apparatus. I have received more than my share of favors from these people and wish to acknowledge all of the shop personnel who not only built the equipment but kept it in excellent repair as well. In addition, I wish to thank Fran Bennett and Brax Evans for constantly putting up with my persistent requests and for handling my purchase orders in an efficient manner.

Next, I want to acknowledge the National Science Foundation and the Chemistry Department of the California Institute of Technology for their support throughout my graduate education.

Finally, I want to express my love for two very special friends that I have made here and my thanks for the profound influence they have had upon my life and my happiness. Bruce Parkinson has given me a better perspective of what friendship means. He generously shared much that he had with me, including his home and his knowledge of photography.

Last and certainly most of all, I want to express my love for Diane and the joy that she has brought into my life. Our strength together is without bound. Her confidence and spirit have kindled within me a new beginning.

I am grateful to everyone in the Caltech community for making my graduate education the most enlightening period in my life.

ABSTRACT

The objectives of this thesis are to develop new high-resolution (± 3 MHz) coherent nonlinear optical spectroscopic techniques and to utilize them to examine the nature of line broadening processes in optical transitions of isolated large and small molecules. By measuring the coherent and incoherent transients observed either in the forward direction along the laser beam (absorption) or at right-angles to the exciting beam (emission), these techniques allow one to determine optical T_1 (the longitudinal relaxation time) and optical T_2 (the transverse relaxation time). From T_1 and T_2 one can obtain under certain circumstances, both the radiative and nonradiative (T_1) contributions as well as the pure dephasing (T_2') contribution to the total homogeneous linewidth ($1/\pi T_2$) of the optical transition.

Two molecules are examined in detail. Iodine was chosen to demonstrate the new techniques because its conventional spectroscopy is well-known and to examine dephasing and decay processes important for small molecules. It was studied in the gas phase and in a molecular beam. Condensed phase experiments were performed on single crystals of pentacene isolated in a p-terphenyl host to obtain information about the nature of radiationless transitions and dephasing processes important in this large molecule.

The optical transition that was studied in iodine is $X^1\Sigma_g^+ \rightarrow B^3\Pi_{0+u}$. Using LADS (Laser Acoustic Diffraction Spectroscopy) for obtaining nanosecond time resolution with a narrowband single-mode dye laser and the IRD (Incoherent Resonance Decay) method whereby

population dynamics and the coherence in the system can be obtained by monitoring the spontaneous emission, the following Stern-Volmer relationship was obtained for iodine:

$$\frac{1}{T_1} (\mu\text{sec}^{-1}) = (0.783 \pm 0.032) + (0.0143 \pm 0.0005) P(\text{mtorr}) \quad .$$

This relationship provides a zero-pressure radiative lifetime of $1.28 \pm 0.05 \mu\text{sec}$ and a nonradiative collisional quenching cross section of $\sigma^2 = 70 \pm 2 \text{ \AA}^2$. These results agree with those obtained in previous studies with broadband excitation indicating that excitation bandwidth is unimportant for T_1 processes in small molecules. Using the electro-optic method of laser frequency switching, an optical nutation was observed in iodine whose Rabi oscillation frequency ($\mu \cdot \epsilon / \hbar$) provided the dipole moment for the transition ($\mu = 0.05$ Debye) after determining the laser field amplitude (ϵ). The Rabi frequency was also obtained from a coherent oscillation observed on top of the IRD signal in iodine at low pressure. This oscillation decayed by T_2 and the overall IRD signal provided T_1 such that both the coherence and decay of the system were obtained simply by monitoring the spontaneous emission. The homogeneous linewidth of the transition was measured using the 3-pulse photon echo method. At 10 mtorr pressure it was found to be 579 kHz. This is almost three orders of magnitude less than the inhomogeneous (Doppler) linewidth of ca. 400 MHz. Molecular beam experiments provided the radiative lifetime ($1.24 \pm 0.02 \mu\text{sec}$) of iodine in a collisionless environment from which the radiative contribution (22%, 128 kHz) to the total homogeneous linewidth was obtained. Assuming that radiative

losses from the lower level of the system can be neglected it was also determined that 38 kHz (7%) of the homogeneous linewidth is due to non-radiative relaxation (inelastic scattering) and a dramatic 413 kHz (71%) is due to pure dephasing (T_2') as a result of elastic scattering processes. Finally an OFID (optical free induction decay) was observed in the molecular beam whose decay indicated that $T_2 = 2T_1$. Therefore, in a collisionless environment, the only dephasing process for iodine is spontaneous emission (i.e., no intramolecular dephasing processes exist).

The optical transition that was studied in pentacene ($^1A_{1g} \rightarrow ^1B_{2u}$) exhibits four sites in a p-terphenyl host. The lowest energy site at $16,887 \text{ cm}^{-1}$ has the following characteristics at 1.8°K :

$$T_1 = 24.9 \pm 2 \text{ nsec}; T_2 = 44 \pm 2 \text{ nsec}, \text{ and } \mu = 0.7 \pm 0.1 \text{ Debye}.$$

Experiments in this system are categorized into two time regimes for theoretical analysis: a transient coherence regime where the observed decay is comparable with $(\hbar/\mu \cdot \epsilon)$ and T_2 , and a steady-state coherence regime where transient dephasing is complete and the off-diagonal elements of the density matrix have decayed to their steady-state values in the presence of the laser field. The Wilcox-Lamb method is used to derive rate equations (T_2 dependent) from the density matrix equations of motion. These equations describe the population dynamics in the pentacene level structure ($|0\rangle$ = ground state, $|p\rangle$ = excited singlet state and $\{|l\rangle\}$ = triplet manifold) and upon averaging them over the inhomogeneous linewidth of the transition and then using them to fit

experimental decay curves one obtains:

$$T_{1p0} = 24.9 \pm 2 \text{ nsec} \quad \text{and} \quad T_{1pl} = 15.7 \mu\text{sec} ,$$

the time constants for spontaneous emission to $|0\rangle$ and crossing into $|l\rangle$, respectively. OFID and nutation expressions are presented for the pentacene level structure and when appropriate averaging is done over both the inhomogeneous linewidth and the laser beam spatial profile, good fits can be obtained for the experimental transients. At 1.8°K it was determined that $T_2 = 2T_1$. Therefore, as in iodine at zero pressure, spontaneous emission is the only dephasing process in pentacene at low temperature. At higher temperature, however, a strongly temperature dependent dephasing process takes place with an onset at 3.7°K . A theoretical treatment of the various dephasing channels is presented that explains the observed temperature dependence of T_2 in pentacene and attributes pure dephasing to an anisotropy in the scattering amplitudes between the ground and excited states. Optical site selection of the pentacene transitions has been observed and is related to vibrational relaxation and homogeneous and inhomogeneous broadening in this system. Studies of the homogeneous broadening of the vibronic line 267 cm^{-1} above the lowest energy site indicate that vibrational relaxation is fast (psec) in the excited singlet manifold of pentacene. Finally from more than ten independent experiments including narrow and broad band excitation, on- and off-resonance scattering, Zeeman effect measurements and the transient decay as a function of excess energy in the molecule, a more complete picture of the pentacene level structure

is given. It is proposed that the slow decay ($\sim 15 \mu\text{sec}$) observed during narrowband excitation represents intersystem crossing to nearby triplet manifolds after the transient coherence of the "two-level" system ($0 \leftrightarrow p$) has decayed. Furthermore, the decay of the primary state prepared in these experiments is not sensitive to the bandwidth or the coherence properties of the excitation source.

TABLE OF CONTENTS

	Page
Introduction	1
Chapter I: Theoretical Background: Optical Coherence	13
Chapter II: Experimental	30
A. Apparatus	31
B. Techniques	34
C. Procedures	60
Chapter III: Applications of New Coherent Non-Linear Optical Spectroscopic Techniques	70
A. Incoherent Resonance Decay and Coherent Optical Ringing From Coherently Prepared Electronic States: A New Technique For Probing Phase Memory and Radiationless Relaxation in Gases and Solids	71
B. Optical Dephasing of Small and Large Molecules: Coherent Oscillations of Emitting Molecules	92
C. Spontaneously Detected Photon Echoes in Excited Molecular Ensembles: A Probe Pulse Laser Technique for the Detection of Optical Coherence of Inhomogeneously Broadened Electronic Transitions	109
D. High-Resolution Time-Resolved Spectroscopy of Collisionless Molecular Beams: Optical T_1 and T_2	127
E. Measurements of Molecular Dephasing and Radiationless Decay by Laser-Acoustic Diffraction Spectroscopy	148
Chapter IV: Radiationless Relaxation and Optical Dephasing of Molecules Excited by Wide- and Narrow-band Lasers: II. Pentacene in Low-Temperature Mixed Crystals	169
Appendix I Fourier Transforms of the Laser Pulses Used in This Work	323

	Page
Appendix II Approximate Solutions for Integrals Important for Inhomogeneous Linewidth Averaging	329
Appendix III An Approach to Show that r_1 is an Odd Function of the Off-Resonance Parameter, Δ	332
Propositions	334
I Measurements of Vibrational Lifetimes and Spin-Orbit Relaxation Rates in Matrix Isolated NO	335
II Measurement of the Intersystem Crossing (ISC) Rates in Excited Electronic States of 3,4- Benzopyrene Using A Triplet-Tripled Absorption Technique	347
III Study Photosensitized Redox Reactions At Semiconductor Surfaces	358
IV Synthesize New Substituted Styrenes by Alkylating Group V Heterobenzenes Using Vinyl Triflates .	381
V Study Dephasing Processes in Molecules Capable of Forming Intramolecular Exciplexes Using Picosecond Laser Excitation and the Three- Pulse Photon Echo Method	390

INTRODUCTION

The preparation and decay of excited electronic states in isolated molecules and in the condensed phase has received considerable theoretical and experimental attention over the past several decades. In 1930, Weisskopf and Wigner¹ provided a phenomenological understanding of the decay of excited states due to spontaneous emission by adding a damping matrix to the Schrödinger equation. The resulting excited state has an exponential decay which provides a Lorentzian resonance when Fourier transformed. If these Lorentzian resonances (which will be referred to as homogeneously broadened transitions) can be observed experimentally, then information about the intrinsic dynamics of the system can be obtained. However, in real situations, these Lorentzians are hidden under a Gaussian (origin of inhomogeneous broadening) that completely masks the dynamics. Thus, in analogy with NMR spectroscopy, one can define two distinct types of macroscopic relaxation processes: T_1 processes which refer to longitudinal relaxation and which represent population loss in the system, and T_2 processes which refer to transverse relaxation and which represent phase destroying events in the homogeneous system. In addition, one needs to consider T_2^* processes which correspond to dephasing events in the inhomogeneous system, i.e., $T_2^* = (\pi\Delta\omega_I)^{-1}$ where $\Delta\omega_I$ represents the width of the inhomogeneous line. In the optical regime, T_2 reflects the actual dephasing time (i.e., the time it takes the molecules in the homogeneous system to lose their phase coherence) while T_1 is the spontaneous emission time due to radiative and nonradiative decay. This T_2 which

determines the linewidth of the homogeneously broadened transition cannot be obtained from conventional spectroscopic methods and the dephasing processes it represents originate from different mechanisms depending upon whether the system is a gas, solid, or a molecular beam.

In gases, molecular resonances are inhomogeneously broadened due to the distribution of molecular velocities relative to the experimenter making a measurement of the transition frequency. This Doppler resonance therefore is a weighted statistical distribution for the population among the homogeneous systems. To characterize the dynamics of the excited states one must determine the resonance width of the homogeneous system in addition to the significance of pressure broadening due to collision-induced phase interruptions (elastic) and velocity changes (inelastic).

In solids, the problem is similar. Individual molecules experience different crystal fields and thus have slightly different energies. This inhomogeneity which reflects a distribution of sites in the solid introduces complications due to elastic and inelastic phonon scattering processes which may vary considerably among sites.

In molecular beams, collisional broadening is eliminated; however, intramolecular relaxation processes can destroy the phase coherence of the system. Thus, the homogeneous width of the resonance may still differ from the width due to spontaneous emission.

The objectives of this thesis are (a) to develop new high-resolution (± 3 MHz) techniques for measuring dephasing (T_1 and T_2) in large and small molecules and (b) to show that coherent nonlinear optical

spectroscopy provides important new information about molecular dynamics in gases, solids and molecular beams.

The thesis is comprised of four chapters beginning in Chapter I with a theoretical background of optical coherence. The interaction between the radiation field and the molecule, represented as a two-level quantum system, is treated semiclassically. Using density-matrix formalism² and the Feynman-Vernon-Hellwirth (FVH) representation,³ the problem is cast into a torque equation (Eq. 10, Chapter I) involving a pseudospin vector \vec{R} precessing about an effective field \vec{E}_{eff} . This is done to show the equivalence⁴ of the oscillatory motion of electric dipole moments in the presence of decay and finite phase coherence with the corresponding motion of magnetic moments in spin resonance theory described by the Bloch equation.⁵

Phenomenological relaxation terms T_1 and T_2 introduced into the equation of motion to represent the decay of the system are identified with the decay of the diagonal and off-diagonal density matrix elements, respectively.

The diagonal elements of the density matrix represent the population in the system. Since spontaneous emission can not be neglected for electronic transitions, the decay of the ground and excited levels is not the same usually and so T_1 need not represent a single decay rate as it does in NMR.

As shown in Eq. (9), Chapter I, the magnitude of the macroscopic dipole moment and thus the induced polarization generated by the coherent superposition of the ground and excited states (of the system)

in the presence of a strong field is determined by the off-diagonal density matrix elements. Therefore, these elements of the density matrix determine the coherence in the system. Coherence in the system will be lost by any process that disrupts the phases of the individual dipoles. Thus, relaxation (T_1) as well as pure (elastic) dephasing (T_2') terms must appear (Eq. 17, Chapter I) in the expression for the decay of the off-diagonal elements.

Using the induced polarization given by Eq. (21), Chapter I, as a source term in Maxwell's wave equation, one can calculate the observed signal field (Eq. 26, Chapter I). It is this field that provides the coherent optical transients (i. e., nutation, free induction decay and photon echoes) that are discussed in Chapters III and IV. Since this field is proportional to the magnitude of the off-diagonal density matrix elements, it decays by T_1 and T_2 and thus leads to a characterization of the decay processes of the two level system selected by the laser. Details of the solution of the density matrix equations of motion that describe the time evolution of the field appear in Chapter IV.

Chapter II describes the techniques developed in this thesis. These methods are used to examine the decay and dephasing of small molecules (I_2) and large molecules (pentacene). Iodine was studied in the gas phase and in a molecular beam. This small molecule has been studied extensively in the past and much is known about its conventional spectroscopy.⁶⁻¹⁰ It was used therefore to demonstrate the new techniques developed¹¹ in addition to probing some of the nonradiative relaxation and dephasing processes important in small molecules. For experiments in the condensed phase, single crystals of pentacene in

p-terphenyl were studied to obtain information about the nature of radiationless transitions and dephasing processes important in this large molecule. This system was chosen for several reasons. First, the electronic absorption and emission spectra for pentacene in p-terphenyl at low temperatures ($\leq 4.2^\circ\text{K}$) consist of sharp lines ($\approx 1\text{ cm}^{-1}$) and thus "clean" excitation is possible. Second, previous work¹² indicated that these lines were still significantly inhomogeneously broadened such that optical coherence experiments utilizing the single mode frequency switching technique were feasible. Finally, the lowest allowed transition occurs at the gain peak of the single-mode laser (Rhodamine 6G) such that the possibility of observing optical nutation in solids for the first time existed. Armed now with the molecules and the reasons for their study, the experimental methods are introduced.

Chapter II begins with a description of the coherent and incoherent excitation sources, cryogenics and other apparatus used in the experiments. It then discusses the frequency-switching technique and LADS (for Laser Acoustic Diffraction Spectroscopy). These methods of obtaining nanosecond time resolution with the CW single mode laser allow one to observe coherent transients by rapidly switching the frequency of the laser or by turning it off. As a group of molecules is brought into resonance with the laser, an optical nutation can occur as population is coherently driven between the ground and excited states (absorption and emission) at the Rabi frequency ($\mu \cdot \epsilon / \hbar$, where μ is the transition dipole moment and ϵ in the laser field amplitude). As a group of molecules is switched off resonance, an optical free induction decay can occur as the individual molecules coherently emit and decay. These transients are damped due to dephasing

processes which destroy the phase relationship among the individual molecular dipoles.

In the frequency switching (EO) method an electro-optic crystal is used inside the laser cavity and the transients are observed as heterodyne signals on a detector monitoring the laser beam. The LADS technique utilizes an acousto-optic modulator outside the cavity to diffract the single mode beam into the sample for the duration of an RF pulse supplied to the modulator. Thus, with this technique, one is able to do coherence experiments with narrowband laser pulses since in LADS, the laser is effectively turned off instead of being switched off-resonance as it is in the EO method mentioned above. Therefore, interpretation of the results is simpler because transients from off-resonance molecules are absent.

Some of the techniques developed in this thesis utilize spontaneous emission at right angles to the exciting beam for detection of the transients rather than monitoring the coherence in the forward direction (along the laser beam). The incoherent resonance decay (IRD) method involves monitoring the emission during an excitation pulse supplied by either the EO or LADS technique. This method provides the excited state lifetime (T_1) and in certain circumstances T_2 (as shown in Section B of Chapter III).

A more direct method for measuring T_2 is the photon echo. This echo which is the analog of the spin echo is usually observed by monitoring the signal in the direction of the laser beam following two laser pulses. When performed in this manner, however, the experiment suffers

from many problems. First, high power pulsed lasers are used typically which have appreciable intensity fluctuations between pulses. Second, the weak echo signal follows an intense laser pulse and detectors must be gated to prevent overloading. Finally, since one is monitoring the laser beam, samples must have good optical properties (low scattering) which can be difficult to achieve in solids. For these reasons, a new method was developed using three laser pulses such that the optical polarization induced by the laser is converted into a change in population of the system. In this manner, one can obtain the coherence in the system by monitoring the spontaneous emission at right angles to the exciting beam. There are several advantages to this method. First, since one is detecting an emission signal with no background exciting light, high sensitivity detectors can be used. Second, no demands are made on the optical quality of the sample, and so the technique is simpler and more generally applicable to different kinds of systems. Third, when combined with the IRD using one pulse, one can obtain both T_1 and T_2 directly. Finally, echoes can now be detected on given vibronic bands by resolving the emission from the sample using a spectrometer. The usefulness of the photon echo method lies in the fact that the decay of the echo provides T_2 directly from which the homogeneous linewidth ($1/\pi T_2$) of the optical transition is obtained.

Also described in Chapter II is an apparatus for observing coherent transients in molecular beams. A simple effusive source is employed. The design easily allows one to monitor both the spontaneous emission (IRD) at right angles to the exciting beam and the coherent

transients (nutaton, OFID) along the laser beam. With this apparatus, it is possible to probe the nature of dephasing mechanisms for systems in a collisionless environment.

The rest of Chapter II is devoted to a description of sample preparation, detection equipment, calibration techniques and procedures used to obtain the results and then summarizes the computer analyses utilized for data reduction.

Chapter III presents some of the results on iodine, pentacene and the molecular beam. It contains five papers which investigate the nature of radiationless relaxations and dephasing processes in small and large molecules using the techniques described in Chapter II. Emphasis is placed upon characterizing the contribution of these processes to line broadening in molecules.

Section A introduces the IRD method. It was used to measure the spontaneous emission lifetime in iodine following narrowband (± 3 MHz) excitation into the $B^3\Pi_{0+u}$ state. The lifetime obtained agreed with that found (at the same I_2 pressure) using a broadband incoherent source.⁶ Furthermore, the nonradiative collisional quenching cross section obtained from Stern-Volmer experiments (Section D) with the IRD method was identical to that obtained using broadband excitation.⁷⁻⁹ Therefore, it appears that state preparation (i. e., broadband or narrowband) does not influence T_1 in small molecules. Section A also presents a direct measurement of the transition dipole moment μ , for the $(X^1\Sigma_g^+ \rightarrow B^3\Pi_{0+u})$ transition in iodine from the Rabi frequency of the optical nutation.

Section B discusses the relationship between the preparation of excited states and intramolecular and intermolecular dephasing processes

and shows how these dephasing processes may be distinguished. It also presents the observation of a coherent (oscillatory) transient on the spontaneous emission decay of iodine at low pressure using the IRD method. From this oscillation, T_2 and the Rabi frequency were extracted as well as T_1 from the overall decay. Thus, the IRD method, which monitors the spontaneous emission, can provide the coherence in the system.

Section C introduces the 3-pulse photon echo using laser pulses provided by the EO method. With this technique, an echo was observed on the spontaneous emission of iodine at low pressure. Beating, at the switching frequency, was superimposed on the echo envelope. Since the laser is switched between two groups of molecules with the EO method, the beating is thought to be due to interference between the two groups. From the decay of the echo a homogeneous linewidth ($1/\pi T_2$) of 579 KHz was obtained for the ($X^1\Sigma_g^+ \rightarrow B^3\Pi_{0+u}$) transition. This is almost a thousand times smaller than the inhomogeneous width (≈ 400 MHz) of the transition. Using the IRD method to measure T_1 , it was also determined that 128 KHz (22%) of the homogeneous width was due to radiative broadening, 38 KHz (6.6%) was due to nonradiative processes (inelastic collisions) and a dramatic 413 KHz (71.4%) was due to dephasing (elastic scattering). Thus, combining the IRD and 3-pulse echo allows one to separate the individual processes contributing to line broadening.

Section D presents the observation of coherent transients (OFID) and the IRD in a collisionless molecular beam of iodine. The measurement of T_1 in the beam provided a radiative lifetime of 128 KHz in

agreement with the Stern-Volmer zero-pressure value obtained from experiments in a gas cell as a function of pressure. The OFID revealed that $T_2 = 2T_1$ for iodine in this environment. Therefore, there are no intramolecular processes that destroy phase coherence in iodine. Dephasing occurs solely by spontaneous emission at zero pressure. The coherent oscillations seen on the IRD as described in Section B were not observed in the beam. This is due to the molecular velocity distribution (relative to the laser beam) and the laser beam transverse spatial profile which drastically smooth the oscillations. These points are part of a comprehensive discussion of coherence in molecular beams investigated in a recent paper by Jones et al.¹³

Section E, which introduces the LADS method, concludes Chapter III. Results are presented for T_1 of iodine that agree with those obtained using the EO method. The 3-pulse photon echo observed using LADS is identical to the corresponding EO result; however, no beating is observed on the echo waveform. This suggests that the beating (at the switching frequency) observed on the echo using the EO method is due to the other group excited during the switching procedure. Section E also presents some work on pentacene. Results are shown indicating that the IRD observed using LADS is dramatically different from the EO result. This anomaly is discussed and related to the optical nutation and OFID results which are presented as well.

Chapter IV resolves the anomaly mentioned above and presents a complete summary of all the work done on pentacene. The origin of optical dephasing and radiationless decay in this large molecule is discussed in

great detail and distinguished from the dephasing and relaxation processes important for small molecules. Included in Chapter IV is a theory of optical dephasing in solids which explains the temperature dependent dephasing process observed in pentacene. This theory is part of a general treatment of optical dephasing from the recent work of Jones and Zewail.¹⁴

Three mathematical appendices conclude the main body of the thesis. Appendix I provides Fourier transforms of the laser pulses used in the experiments and shows that the laser bandwidth becomes transform limited as the pulse width in time decreases. Appendix II presents approximate solutions for integrals important for inhomogeneous linewidth averaging of the equations of motion for the density matrix elements and Appendix III shows how the signal field, ϵ_s , in Eq. (26) of Chapter I, depends on r_2 and not r_1 upon averaging over the inhomogeneous linewidth.

REFERENCES

1. W. Weisskopf and E. Wigner, Z. Physik, 63, 54 (1930).
2. U. Fano, Rev. Mod. Phys., 29, 74 (1957).
3. R. P. Feynman, F. L. Vernon, Jr. and R. W. Hellworth, J. Appl. Phys., 28, 49 (1957).
4. R. H. Dicke, Phys. Rev., 93, 99 (1954).
5. F. Bloch, Phys. Rev., 70, 460 (1946).
6. L. Brewer, R. A. Berg and G. M. Rosenblatt, J. Chem. Phys., 38, 1381 (1963).
7. A. Chutjian, J. K. Link and L. Brewer, J. Chem. Phys., 46, 2666 (1967).
8. J. I. Steinfeld and A. N. Schweid, J. Chem. Phys., 53, 3304 (1970).
9. G. A. Capelle and H. P. Broida, J. Chem. Phys., 58, 4212 (1973).
10. P. F. Williams, D. L. Rousseau and S. H. Dworketsky, Phys. Rev. Lett., 32, 196 (1974).
11. These techniques are introduced separately in the five sections of Chapter III.
12. J. H. Meyling and D. A. Wiersma, Chem. Phys. Lett., 20, 383 (1973).
13. K. E. Jones, A. Nichols and A. H. Zewail, J. Chem. Phys., accepted for publication.
14. K. E. Jones and A. H. Zewail, in: "Advances in Laser Chemistry", A. H. Zewail, editor (Springer-Verlag, Berlin, 1978).

CHAPTER I

THEORETICAL BACKGROUND: OPTICAL COHERENCE

The problem of understanding dephasing processes and their contribution to the observed lifetimes and linewidths of molecular electronic states requires a knowledge of how the coherence effects one observes in the laboratory using laser spectroscopy are related to the density matrix that describes the ensemble of resonances under observation. The diagonal elements of the density matrix represent the population distribution within the system while the off-diagonal elements determine the macroscopic polarization induced in the system by the coherent superposition of the ground and excited states. Therefore, of primary concern is a characterization of the time evolution of the density matrix and how dephasing processes influence it. The procedures utilized here for describing the theoretical aspects of coherent optical phenomena in molecules follow the review article by Zewail *et al.*¹ Emphasis is placed upon relating information obtained experimentally to the detailed microscopic processes responsible for decay and dephasing in molecules.

For a two-level system representing an isolated molecule with zero-order Hamiltonian (1) the wavefunction may be written as a linear combination (2) of the time independent eigenstates of the system:

$$\mathcal{H}_0 = \begin{pmatrix} \frac{\hbar\omega_0}{2} & 0 \\ 0 & -\frac{\hbar\omega_0}{2} \end{pmatrix} \quad (1)$$

$$\psi(t) = a(t) e^{-i\frac{\omega_0}{2}t} |a\rangle + b(t) e^{i\frac{\omega_0}{2}t} |b\rangle \quad (2)$$

Here, ω_0 is the transition frequency between the excited state $|a\rangle$ and the ground state $|b\rangle$. The interaction of this two-level system with a radiation field of the form:

$$E(z, t) = \frac{1}{2} \epsilon(z, t) e^{-i(\omega t - kz)} + \text{c.c.} \quad (3)$$

provides the following total (semiclassical) Hamiltonian for the system:

$$\begin{aligned} \mathcal{H} &= \mathcal{H}_0 + V \\ &= \begin{pmatrix} \frac{\hbar\omega_0}{2} & 0 \\ 0 & -\frac{\hbar\omega_0}{2} \end{pmatrix} + \begin{pmatrix} 0 & -\mu \cdot E(z, t) \\ \text{c.c.} & 0 \end{pmatrix} \end{aligned} \quad (4)$$

Here, only off-diagonal coupling is considered (i.e., states $|a\rangle$ and $|b\rangle$ have definite parity).

Physically significant information about this two-level system can be obtained most easily using density matrix formalism² since the expectation value of any operator A , and thus any observable is given by:

$$\langle A \rangle = \text{Tr} \{ \rho' A \} \quad (5)$$

Furthermore, the solution of the equation of motion (6) for the density matrix describing the system:

$$i\hbar \dot{\rho}'(t) = [\mathcal{H}, \rho'(t)] + (\text{relaxation terms}) \quad (6)$$

provides the population of states $|a\rangle$ and $|b\rangle$ in addition to the polarization induced in the sample by the radiation field.

In the laboratory coordinate frame the density matrix may be written as:

$$\rho' = \begin{pmatrix} \langle aa^* \rangle & \langle ab^* e^{-i\omega_0 t} \rangle \\ \text{c.c.} & \langle bb^* \rangle \end{pmatrix} = \begin{pmatrix} \rho'_{aa} & \rho'_{ab} \\ \rho'_{ba} & \rho'_{bb} \end{pmatrix} \quad (7)$$

where the brackets indicate an N-molecule ensemble average over the density matrix elements for individual molecules which may have different ω_0 's (i.e., inhomogeneous broadening due to crystal field effects in solids and the Doppler effect in gases).

The optical coherence effects one observes in the laboratory result from the creation of an oscillating macroscopic electric dipole moment through the interaction of the field with an ensemble of two-level systems. If the induced dipole moment for one molecule is written as:

$$\begin{aligned} \langle \mu \rangle &= \text{Tr} \{ \mu \rho' \} = \text{Tr} \left\{ \begin{pmatrix} 0 & \mu_{ab} \\ \mu_{ba} & 0 \end{pmatrix} \rho' \right\} \\ &= \mu_{ab} \rho'_{ba} + \mu_{ba} \rho'_{ab} \\ &= \mu (\rho'_{ab} + \rho'_{ba}) \end{aligned} \quad (8)$$

where μ_{ab} is assumed to be real such that $\mu_{ab} = \mu_{ba} = \mu$, then the macroscopic dipole moment per unit volume (which is the polarization induced in the medium) is given by:

$$\begin{aligned}
 P(t) &= N\langle \mu \rangle \\
 &= N\mu(\rho'_{ab} + \rho'_{ba})
 \end{aligned}
 \tag{9}$$

where N represents the molecular density. Eq. (9) applies for optically thin samples in which the incident radiation field is not attenuated appreciably due to the interaction (i. e., the z -dependence of the field $E(z, t) = \frac{1}{2} \epsilon(z, t) e^{-i(\omega t - kz)} + \text{c. c.}$ is ignored).

At this point a digression from the formal treatment will be made in order to obtain a better conceptual understanding of the interaction of a two-level quantum system with a radiation field. Later, the formal treatment involving the solution of the density matrix equations of motion will be presented and related to the geometric model discussed below.

Feynman, Vernon and Hellworth (FVH)³ have shown that a two-level system interacting with a radiation field is equivalent to the classical spin $\frac{1}{2}$ problem in magnetic resonance theory first described by Bloch.⁴ To show this, they rewrote the equation of motion given by (6) as a torque equation for a vector \vec{R} precessing about an effective field \vec{E}_{eff} :

$$\frac{d\vec{R}}{dt} = \vec{E}_{\text{eff}} \times \vec{R}
 \tag{10}$$

In their geometric model, the vector \vec{R} may be considered a fictitious electric spin vector whose components are defined as:

$$R = \begin{pmatrix} R_1 \\ R_2 \\ R_3 \end{pmatrix} \text{ where } \begin{aligned} R_1 &= \rho'_{ab} + \rho'_{ba} \\ R_2 &= i(\rho'_{ab} - \rho'_{ba}) \\ R_3 &= \rho'_{aa} - \rho'_{bb} \end{aligned} \quad (11)$$

and whose time evolution is governed by the Schrödinger equation. Thus, a knowledge of $R(t)$ is equivalent to specifying the two-level system defined by $\psi(t)$. The effective field is given by:

$$\begin{aligned} \mathbf{E}_{\text{eff}} = \begin{pmatrix} E_1 \\ E_2 \\ E_3 \end{pmatrix} &= \hbar^{-1} \begin{pmatrix} -(\mu_{ba} + \mu_{ab}) \cdot \epsilon \cos \omega t \\ -i(\mu_{ab} - \mu_{ba}) \cdot \epsilon \cos \omega t \\ \hbar \omega_0 \end{pmatrix} \\ &= \begin{pmatrix} \frac{-2\mu \cdot \epsilon}{\hbar} \cos \omega t \\ 0 \\ \omega_0 \end{pmatrix} \end{aligned} \quad (12)$$

since μ_{ab} is assumed real. The physical significance of Eq. (10) is seen more easily if a coordinate transformation is made to a rotating frame⁵ (at ω) such that the effective field is a stationary vector about which the fictitious electric spin vector precesses.

In the rotating frame, the torque Eq. (10) is written as:

$$\frac{d\vec{r}}{dt} = \vec{\mathcal{E}}_{\text{eff}} \times \vec{r} \quad (13)$$

$$\text{where } \mathbf{r} = \begin{pmatrix} r_1 \\ r_2 \\ r_3 \end{pmatrix} = \begin{pmatrix} \rho_{ab} + \rho_{ba} \\ i(\rho_{ab} - \rho_{ba}) \\ \rho_{aa} - \rho_{bb} \end{pmatrix} \quad (14)$$

and
$$\mathcal{E}_{\text{eff}} = (\mu \cdot \epsilon / \hbar, 0, \Delta) . \quad (15)$$

Here, Δ gives the off-resonance frequency of the radiation field with respect to the molecular resonance, i.e., $\Delta = \omega_0 - \omega$. At this point, the density matrix in the rotating frame is defined as ρ . Later, it will be obtained explicitly and a relationship between r and R will be established. Now, to illustrate the motion described by Eq. (13) in the rotating frame, the precession of the r -vector about \mathcal{E}_{eff} in a coordinate system (1, 2, 3) rotating at ω about axis 3 is shown in Fig. 1.

Here, the on-resonance case is examined where \mathcal{E}_{eff} lies along axis 1 and $r(t)$ precesses in the 2-3 plane at the Rabi frequency $(\mu \cdot \epsilon / \hbar)$ since $\Delta = 0$ [Eq. (15)]. Physically, this diagram represents the coherent oscillation of population between the ground and excited states (i.e., optical nutation) without any damping. In other words, the period of the coherent interaction $(\hbar / \mu \cdot \epsilon)$ is shorter than the relaxation time of the two-level system.

From the torque Eq. (13), the optical analogs of the Bloch equations can be obtained. Here, they are shown with phenomenological relaxation times T_1 and T_2 .

$$\dot{r}_1 = -\Delta r_2 - \frac{1}{T_2} r_1 \quad (16a)$$

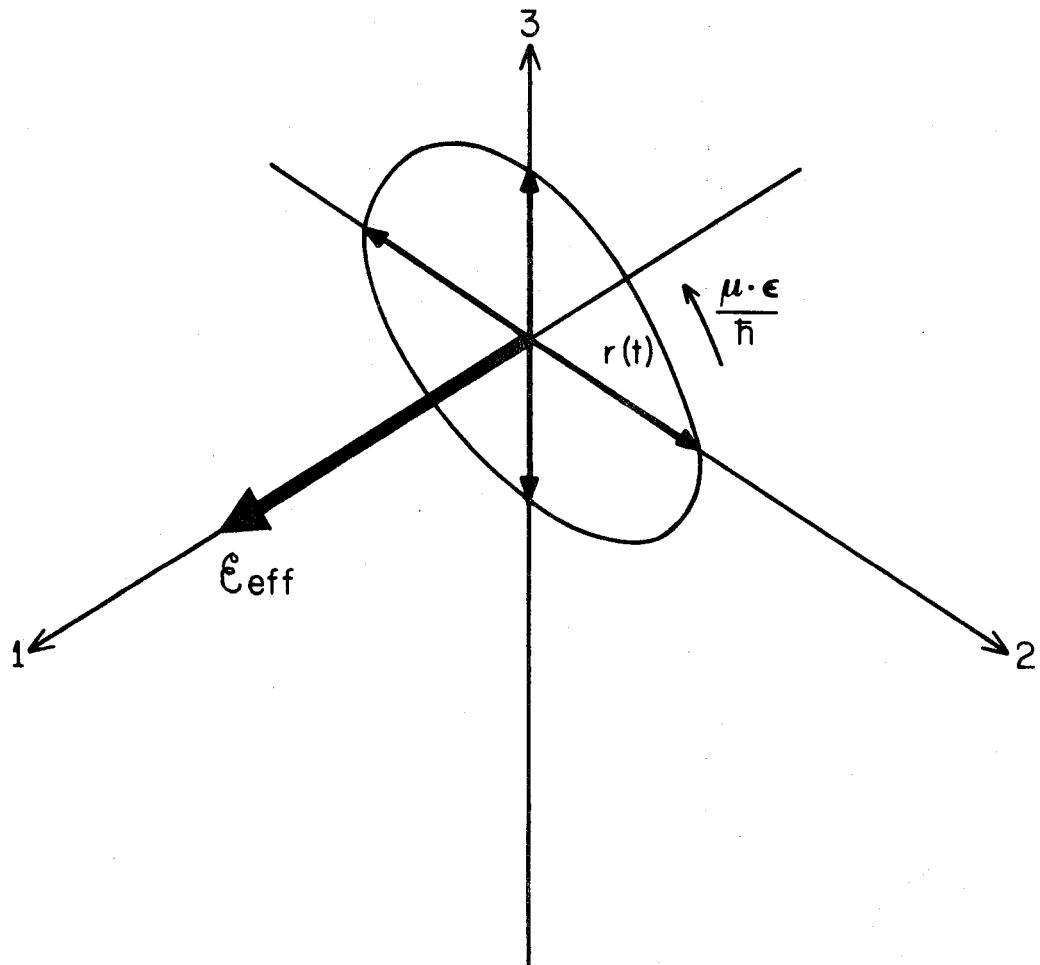
$$\dot{r}_2 = \Delta r_1 - \frac{1}{T_2} r_2 + (\mu \cdot \epsilon / \hbar) r_3 \quad (16b)$$

$$\dot{r}_3 = -\frac{1}{T_1} r_3 - (\mu \cdot \epsilon / \hbar) r_2 \quad (16c)$$

T_2 is the decay time of the off-diagonal density-matrix elements. It corresponds to the transverse relaxation time of magnetic resonance

Figure 1

A geometric representation of the precession of the vector $\mathbf{r}(t)$ about the effective field \mathcal{E}_{eff} in the rotating frame with $\Delta = 0$ (i.e., on resonance). The precession (Rabi) frequency is $\mu \cdot \epsilon / \hbar$. The motion of $\mathbf{r}(t)$ in the 2, 3 plane represents the oscillation of population between the ground and excited states of the two-level system.



theory and is defined as:

$$\frac{1}{T_2} = \frac{1}{T_1} + \frac{1}{T_2'} = \frac{1}{2} \left(\frac{1}{T_{1a}} + \frac{1}{T_{1b}} \right) + \frac{1}{T_2'} \quad (17)$$

Since the off-diagonal density matrix elements determine the polarization, T_2 is the observed dephasing time of the system. T_2' in Eq. (17) is the pure dephasing time resulting from elastic processes such as soft collisions in the gas phase or phonon interactions in the condensed phase which destroy phase coherence but leave the population unchanged. The overall T_2 of course must contain T_1 , the average relaxation time (longitudinal relaxation time in NMR language) for the diagonal elements of the density matrix since all T_1 processes are also T_2 processes.

In the optical Bloch equations shown in (16), r_1 and r_2 are directly related to ρ_{ab} and ρ_{ba} while r_3 is the population difference $\rho_{aa} - \rho_{bb}$, recalling the definitions given in Eq. (14). Thus, on-resonance, the population vector will not only nutate but also dephase. Of course when the field is switched off, r_3 will decay by T_1 . Solutions to the optical Bloch equations, therefore, will provide both the population (r_3) and coherence (r_1, r_2) in the system as a result of the interaction of the two-level system with a radiation field.

Returning now to the formal treatment, one can determine the form of the signal field generated by the induced macroscopic polarization in terms of the components of r and then solve the equation of motion given by (6) to obtain the time-dependence of $r(t)$ and thus a characterization of the signals one observes in the laboratory.

To accomplish this, the density matrix is usually cast in the rotating coordinate frame at ω , the frequency of the radiation field. The significance of this transformation is that in this frame the total Hamiltonian for the system is time-invariant, and thus the time evolution of the density matrix may be determined more easily.

The density matrix in the rotating frame is related to that in the laboratory frame (ρ') by the unitary operator U :

$$\begin{aligned} \rho &= U^{-1} \rho' U = e^{i\frac{\omega}{2} \sigma_3 t} \rho' e^{-i\frac{\omega}{2} \sigma_3 t} \\ &= \begin{pmatrix} \langle aa^* \rangle & \langle ab^* e^{-i\Delta t} \rangle \\ \langle c.c. \rangle & \langle bb^* \rangle \end{pmatrix} = \begin{pmatrix} \rho_{aa} & \rho_{ab} \\ \rho_{ba} & \rho_{bb} \end{pmatrix} \end{aligned} \quad (18)$$

where σ_3 is the Pauli spin matrix $\begin{pmatrix} 1 & 0 \\ 0 & -1 \end{pmatrix}$. From Eqs. (7) and (18) one can see that the off-diagonal density matrix elements in the rotating frame are related to the corresponding elements in the laboratory frame in the following manner:

$$\rho_{ab} = \rho'_{ab} e^{i\omega t} \quad (19a)$$

$$\rho_{ba} = \rho'_{ba} e^{-i\omega t} \quad (19b)$$

Therefore, Eq. (9) for the polarization may now be written as:

$$P(t) = N\mu(\rho_{ab} e^{-i\omega t} + \rho_{ba} e^{i\omega t}) \quad (20)$$

and in terms of r as:

$$\begin{aligned}
P(t) &= \frac{N\mu}{2} (r_1 - ir_2) e^{-i\omega t} + \frac{N\mu}{2} (r_1 + ir_2) e^{i\omega t} \\
&= N\mu (r_1 \cos \omega t - r_2 \sin \omega t)
\end{aligned} \tag{21}$$

From Eq. (21) one can see that r_1 and r_2 are the in-phase (real) and out-of-phase (imaginary) components of the induced polarization, respectively.

The signal field may now be determined using this polarization as a source term in Maxwell's wave equation (MKS units):

$$\vec{\nabla} \times (\vec{\nabla} \times \vec{E}_S) + \mu_0 \sigma \vec{E}_S + \mu_0 \epsilon_0 \ddot{\vec{E}}_S = -\mu_0 \ddot{\vec{P}} \tag{22}$$

where ϵ_0 is the background dielectric constant with η the corresponding index of refraction, μ_0 is the permeability and σ is the conductivity of the medium. For a signal field \vec{E}_S of the form given by Eq. (3) and a polarization \vec{P} written as:

$$\vec{P}(z, t) = \frac{1}{2} \vec{P}(z, t) e^{-i(\omega t - kz)} + \text{c. c.} \tag{23}$$

Equation (22) may be expressed as:

$$\left(\frac{\partial}{\partial z} + \frac{\eta}{c} \frac{\partial}{\partial t} + \kappa \right) \epsilon_S = \frac{-i\omega\eta}{2c\epsilon_0} \vec{P} \tag{24}$$

in the slowly varying envelope approximation (SVEA),⁶ where it is assumed that the amplitudes ϵ_S and \vec{P} vary slowly in time compared to an optical period and slowly in space compared to an optical wavelength. One may safely ignore $\kappa = \sigma\eta/2c\epsilon_0$, the loss per unit length for optically thin samples and experimental conditions can usually be arranged such that $\partial \epsilon_S / \partial z \gg (\partial \epsilon_S / \partial t) \frac{\eta}{c}$ where c is the speed of light. Thus, by integrating

over the interaction path length L , the signal field is given by:

$$\epsilon_s \cong \frac{-i\omega\eta L}{2c\epsilon_0} \vec{P} \quad (25)$$

Now, r_1 and r_2 in the expression for the macroscopic polarization (21) must be averaged over the inhomogeneous linewidth of the transition. For a symmetrical lineshape function with the radiation field frequency ω centered at the peak of the line, the averaging may be performed over Δ , the off-resonance parameter. Because r_2 is an even function of Δ (see Chapter IV and ref. 7) while r_1 is an odd function of Δ (see Appendix III), only the r_2 contribution to the polarization amplitude remains. Eq. (25) may now be expressed as:

$$\epsilon_s = \frac{\omega\eta L}{2c\epsilon_0} N\mu \langle r_2 \rangle = \frac{i\omega\eta L}{c\epsilon_0} N\mu \langle \rho_{ab} \rangle \quad (26)$$

where the brackets denote averaging over the inhomogeneous lineshape. Thus, the polarization induced in the sample produces a signal field that can be detected in the laboratory. The strength of the field depends on the transition moment, μ , the off-resonance frequency, Δ , and the applied field strength. Furthermore, the signal field damps by the optical relaxation constants (T_1, T_2) and therefore measurements of this damping can identify the origin of phase relaxation processes⁸ in the system.

With the signal field expressed as in Eq. (26), what remains is to solve Eq. (6) and obtain the time-dependence of r .

In the rotating frame, the equation of motion for the system is written as:

$$i\hbar\dot{\rho} = [\mathcal{H}_r, \rho] + (\text{relaxation terms}) \quad (27)$$

where the Hamiltonian in the rotating frame is given by:

$$\begin{aligned} \mathcal{H}_r &= U^{-1} \mathcal{H} U - \frac{\hbar\omega}{2} \sigma_3 \\ &\approx \frac{\hbar\Delta}{2} \sigma_3 - \frac{\mu \cdot \epsilon}{2} \sigma_1 \end{aligned} \quad (28)$$

Eq. (28) was obtained using the following identity:¹

$$e^{i\frac{\omega}{2}\sigma_3 t} \sigma_1 e^{-i\frac{\omega}{2}\sigma_3 t} = \sigma_1 \cos \omega t - \sigma_2 \sin \omega t \quad (29)$$

Terms oscillating at 2ω were neglected (rotating wave approximation) and σ_1 , σ_3 are the Pauli spin matrices $\begin{pmatrix} 0 & 1 \\ 1 & 0 \end{pmatrix}$ and $\begin{pmatrix} 1 & 0 \\ 0 & -1 \end{pmatrix}$, respectively.

Given Eqs. (27) and (28) one can show that the equation of motion for ρ can be written, after explicitly including phenomenological relaxation terms, as follows:

$$\dot{\rho}_{aa} = \frac{1}{T_{1a}} \rho_{aa} + \frac{1}{2} i\chi (\rho_{ba} - \rho_{ab}) \quad (30a)$$

$$\dot{\rho}_{bb} = -\frac{1}{T_{1b}} (\rho_{bb} - \rho_{bb}^0) + \frac{1}{T_{1ab}} \rho_{aa} + \frac{1}{2} i\chi (\rho_{ab} - \rho_{ba}) \quad (30b)$$

$$\dot{\rho}_{ba} = \left(-\frac{1}{T_2} + i\Delta\right) \rho_{ba} + \frac{1}{2} i\chi (\rho_{aa} - \rho_{bb}) \quad (30c)$$

Here, T_{1a}^{-1} and T_{1b}^{-1} are the total decay rates for levels $|a\rangle$ and $|b\rangle$, respectively, T_{1ab}^{-1} is the spontaneous emission rate from $|a\rangle$ to $|b\rangle$ which cannot be neglected in the optical region as it usually is in the infrared and microwave regions, $\chi = \mu \cdot \epsilon / \hbar$ and T_2 is defined by Eq. (17).

For all of the experiments on iodine discussed in Chapter III, Eq. (17) is appropriate for describing the observed dephasing rate. In Chapter IV, however, where experiments on pentacene in dilute mixed crystals at low temperature are discussed, Eq. (17) reduces to:

$$\frac{1}{T_2} = \frac{1}{2T_{1po}} + \frac{1}{T_2'} \quad (31)$$

since relaxation from the ground state will be ignored. Here, the level notation $|p\rangle$, $|0\rangle$ replaces $|a\rangle$, $|b\rangle$, respectively.

The solution of the coupled differential equations of motion (30) for the elements of the density matrix can be found using LaPlace transform techniques. From these solutions one obtains expressions to identify T_1 and T_2 from experiment with relaxation and dephasing processes important for both small and large molecules in different environments.

Measurements of T_1 provide information about spontaneous radiative and nonradiative processes occurring within the system. By modifying the environment (i. e., pressure changes in the gas phase or temperature changes in the condensed phase), one can examine the relative magnitudes of the radiative and nonradiative contributions to the observed lifetime. Correlating this information with optical T_2 measurements, which provide the homogeneous linewidth ($1/\pi T_2$), allows one to determine the influence of dephasing processes upon the observed linewidth [using Eq. (17)]. Thus, one can begin to disentangle the individual line-broadening processes and examine each separately in some situations to determine its relative importance. Additional

information is contained in the dephasing time since dephasing processes can be either intra- or inter-molecular. In the latter case, a theory has been worked out⁸ showing that the pure dephasing time (T_2') in Eq. (17) is due to differences in the elastic scattering amplitudes for the ground and excited states. Thus, T_1 and T_2 obtained in optical coherence experiments, can provide useful information in the search for answers to some of the subtle questions in molecular dynamics.

In Chapter III, dephasing and relaxation processes and their effect on the observed linewidth of small molecules (iodine) are examined at low pressure and in a collisionless molecular beam. Chapter IV concentrates on understanding these processes in isolated large molecules (pentacene) at low temperatures.

REFERENCES

1. A. H. Zewail, D. E. Godar, K. E. Jones, T. E. Orlowski, R. R. Shah and A. Nichols, in: "Advances in Laser Spectroscopy I", A. H. Zewail, editor (SPIE Publishing Co., 1977), Vol. 113.
2. U. Fano, Rev. Mod. Phys., 29, 74 (1957).
3. R. P. Feynman, F. L. Vernon, Jr. and R. W. Hellworth, J. Appl. Phys., 28, 49 (1957).
4. F. Bloch, Phys. Rev., 70, 460 (1946).
5. I. I. Rabi, N. F. Ramsey and J. Schwinger, Rev. Mod. Phys., 26, 167 (1954).
6. See, e.g., M. Sargent III, M. Scully and W. E. Lamb, Jr., "Laser Physics", (Addison-Wesley Publishing Co., 1974).
7. A. Schenzle and R. G. Brewer, Phys. Rev. A, 14, 1756 (1976).
8. K. E. Jones and A. H. Zewail, in: "Advances in Laser Chemistry", A. H. Zewail, editor, Springer Series in Chemical Physics (Springer, Berlin, Heidelberg, New York, 1978).

CHAPTER II
EXPERIMENTAL

A. APPARATUS

1. Coherent and Incoherent Excitation Sources

Three different lasers were used as coherent excitation sources for experiments performed in the condensed phase. A pulsed tunable dye laser (Molelectron DL 200) pumped by a nitrogen gas laser (Molelectron UV 400) or a multimode CW dye laser were used for broadband excitation. The N_2 pumped dye laser has a frequency bandwidth of 18 GHz, a peak power of 40 KW, and a pulse duration of 5 nsec. The multimode CW dye laser has a bandwidth of 240 GHz and up to 1 W output power.

For narrowband excitation in the condensed phase and in all of the gas phase experiments, a single-mode tunable jet-stream CW dye laser (Spectra Physics 580A) pumped by an argon ion CW gas laser (Spectra Physics 171) was used. To obtain single mode operation, the dye laser has three intracavity etalons whose free spectral ranges (FSR) are chosen such that the combination is capable of introducing heavy losses to all but one of the modes in the laser cavity. One of the etalons (2 mm air spaced, 75 GHz FSR) is temperature regulated and piezoelectrically tunable. The other two are solid etalons with thicknesses of 0.17 mm (900 GHz FSR) and $\approx 1.7\mu$ (85,000 GHz FSR). The output mirror of the dye laser is mounted on a piezoelectric element such that small changes in the cavity length can be made electronically. To achieve single-mode operation at a particular frequency, a systematic procedure must be followed. First, the laser is carefully aligned and tuned to the frequency of interest using the 1.7μ etalon. At this point the laser is

operating multimode with a bandwidth of approximately 35 GHz. Then, the tunable etalon is installed in the cavity and its mirror spacing is adjusted electronically in conjunction with the cavity end mirror position until laser output is maximized. This occurs when the FSR transmission peaks of the etalon and cavity overlap. With proper alignment the cavity now lases on only two modes (separated by 75 GHz, the tunable etalon FSR). To complete the procedure, the 0.17 mm etalon is installed and tilted until its FSR transmission peak overlaps with just one of the remaining two modes. By adjusting this etalon manually the laser can be tuned by mode hopping to adjacent FSR transmission peaks (900 GHz). Continuous tuning is done electronically by adjusting the tunable etalon mirror spacing and the cavity end mirror position. Ranges of 3 GHz and 18 GHz can be programmed into the electronic controller. Tuning over larger frequency ranges requires manual adjustment of the solid etalons between continuous scanning intervals. It should be emphasized that stable single-mode operation can only be obtained if the FSR transmission peaks of each of the etalons and the cavity have been adjusted properly. Following the above procedure, single-mode operation of the laser (monitored using a scanning confocal etalon) has been maintained for several hours.

For all experiments, Rhodamine 6G is used as the dye gain medium. The maximum power of the linearly polarized single mode is 100 mW in a Gaussian TEM₀₀ beam with a width of 0.62 ± 0.01 mm (see Fig. 3 of Chapter IV) providing a maximum unfocused intensity of 33 W/cm². The transverse intensity profile of the single mode beam was

measured using a photodiode ($50\ \mu$ aperture) mounted on a micrometer controlled translation stage ($4\ \mu$ resolution).

The frequency bandwidth of the single mode laser is determined by jitter and drift due to jet instabilities, temperature fluctuations and vibrations. With a combination of techniques, the long term jitter of the single mode was reduced to ± 3 MHz (measured using a 2 GHz FSR scanning confocal etalon) without active frequency feedback loops. These techniques involved (1) careful regulation of the dye solution temperature using a regulated ($\pm 0.1^\circ\text{C}$) bath; (2) independent air conditioning for the laboratory providing room temperature stability to $\pm 1^\circ\text{C}$; (3) use of a vibration-isolation optical table to mount all laser components; (4) sound-proofing of the dye laser with a tight-fitting enclosure; and (5) amplitude stabilization ($\pm 0.5\%$) of the single mode by a feedback circuit to the pump laser.

Broadband absorption experiments with incoherent sources were performed in the condensed phase using a tungsten (1 KW) or a xenon (0.2 KW) lamp, regulated power supplied and appropriate filters. Most of the experiments with the tungsten lamp were performed with UV (Schott GG-395) and IR (Schott KG-1) blocking filters while the xenon lamp experiments were performed with a UV bandpass filter (Corning 7-54).

2. Cryogenics

Condensed phase experiments were performed with the crystals of pentacene in p-terphenyl suspended directly in a liquid helium filled

glass dewar. Temperatures down to 1.7°K were obtained by pumping on the liquid helium reservoir with a Sargent-Welch (Model 1374) vacuum pump. The temperature was monitored with a calibrated carbon glass resistor (Lakeshore Cryotronics CGR-1-1000) mounted on the sample holder near the crystal and by measuring the vapor pressure of helium with calibrated Wallace and Tiernan pressure gauges.

3. Helmholtz Coils for Magnetic Field Experiments

Several experiments in the condensed phase were performed with samples in the presence of an external magnetic field. Two water-cooled coils were placed around the tail of the dewar at the Helmholtz spacing (R , where R = coil radius) such that the field direction was parallel to the direction of laser polarization (vertical). With a current of 22 amperes (at 60 volts) supplied by a regulated dc power supply, a field strength of 900 Oersted was obtained at the sample using a Bell gaussmeter and a calibrated Hall effect probe. The field was homogeneous at the crystal to better than 1%.

B. TECHNIQUES

1. Electro-Optic Laser Frequency Switching

In an electro-optic (EO) modulator, the application of an electric field causes a change in the refractive index of the crystal and therefore a change in the optical path length through the crystal. If such a modulator is placed within a laser cavity, the field-induced optical path length change will effectively alter the laser cavity length and thus the output laser frequency.¹ This technique allows one to obtain nanosecond time

resolution with the CW narrowband laser and to observe coherent transients by rapidly switching the frequency of the laser from ω_0 (the peak frequency of the optical transition) to a new frequency, ω .

For the laser frequency switching experiments described in Chapters III and IV, a transverse electro-optic modulator of ammonium-dideuterium phosphate (AD*P) with a 45° y-cut orientation (see Fig. 1 and reference 2) was placed inside the cavity of the single mode laser such that the electric field (along the crystal x-axis) was applied normal to the direction of light propagation (\bar{z}).

For a laser cavity modified in this manner, resonances occur at frequencies satisfying the condition:

$$\frac{\omega L}{c} + \frac{\omega n \ell}{c} = m\pi \quad (1)$$

where L is the laser cavity length without the crystal, ℓ is the crystal length, n is the crystal index of refraction and m is the cavity mode number. Solving for ω one obtains:

$$\omega = \frac{cm\pi}{L + n\ell} \quad (2)$$

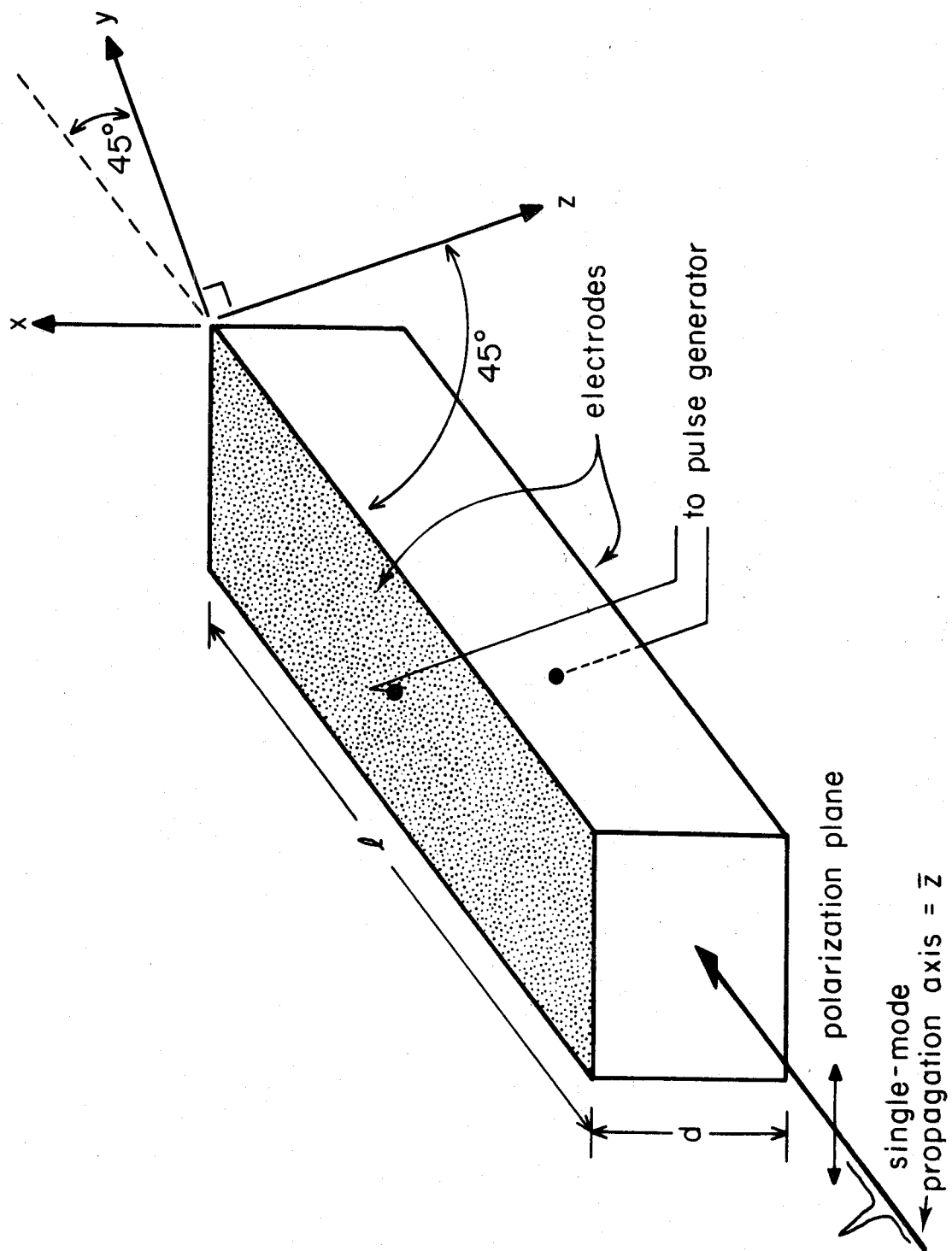
The change in the resonance frequency commensurate with an electric field-induced change in the crystal index of refraction is

$$\Delta\omega = - \frac{cm\pi\ell}{(L + n\ell)^2} \Delta n = - \frac{\omega\ell}{L + n\ell} \Delta n \quad (3)$$

Substituting for Δn an expression² containing crystal properties and applied voltage one obtains

Figure 1

Ammonium dideuterium phosphate (AD*P) electro-optic modulator used for laser frequency switching. The crystal is mounted in a cell placed inside the dye laser cavity. To reduce the loss introduced by the modulator the cell is filled with index matching fluid and its windows are antireflection coated. For alignment purposes an optical mount was designed for the cell to allow horizontal and vertical tilting in addition to rotation about the laser propagation axis. With the modulator in the cavity single-mode output power is reduced approximately 50%.



$$\Delta n = - \frac{n_e^3(\lambda) r_{41} v}{2d} \quad (4)$$

Here, $n_e(\lambda)$ is the extraordinary index of refraction for AD*P, r_{41} is the electro-optic coefficient appropriate for the crystal orientation,² v is the applied voltage and d is the electrode spacing. Now, substituting Eq. (4) into Eq. (3), one can show that the change in laser frequency ($\Delta\omega$) corresponding to an applied voltage v is

$$\Delta\omega = \frac{\omega n_e^3(\lambda) r_{41} v}{2(L + n_e l)} \cdot (l/d) \quad (5)$$

The form of Eq. (5) reveals that for transverse modulation, the frequency switching efficiency is proportional to the ratio of crystal length to electrode spacing. This contrasts markedly with longitudinal modulation where the frequency shift is independent of crystal dimensions and is the primary reason why transverse modulation can occur at low voltages. For a crystal length of 2.5 cm, an electrode spacing of 0.3 cm, and a cavity length of 38.5 cm a frequency switching efficiency of 0.6 MHz/volt was measured for AD*P at 5900 Å consistent with that calculated using Eq. (5) with $r_{41} = 36 \times 10^{-10}$ cm/volt and $n_e = 1.48$.

Although the above steady-state treatment of the frequency switching process first described by Yariv¹ can provide the frequency shift due to a field-induced modulation in the EO crystal's index of refraction, it does not lend much insight into the details of the time-dependent behavior of the switching process.

Recently, Genack and Brewer³ presented a model to describe the dynamics of laser frequency switching and some of their findings

are pertinent here.

Suppose that a standing wave optical field given by:

$$E(\bar{z}, t) = \epsilon_0 \{ e^{i(\omega t - k\bar{z})} + e^{i(\omega t + k\bar{z})} \} + c.c. \quad (6)$$

of angular frequency

$$\omega = \frac{2\pi m}{T} \quad (7)$$

where m is the mode number as before, propagates (along \bar{z}) in a laser cavity of length L such that the cavity round-trip time is given by:

$$T = \frac{2L}{c} . \quad (8)$$

An electro-optic phase modulator which introduces a time-dependent phase change $\phi(t)$ is placed near one end mirror as shown in Fig. 2. Here, \bar{z} is the propagation axis to be consistent with Fig. 1. It should not be confused with the crystal z -axis.

To illustrate the concept of frequency switching consider only one wave from Eq. (6)

$$E(\bar{z}, t) = \epsilon_0 e^{i(\omega t - k\bar{z})} \quad (9)$$

as it passes through the modulator located between $\bar{z} = 0$ and $\bar{z} = \ell$ where ℓ is the crystal thickness and $\ell \ll L$.

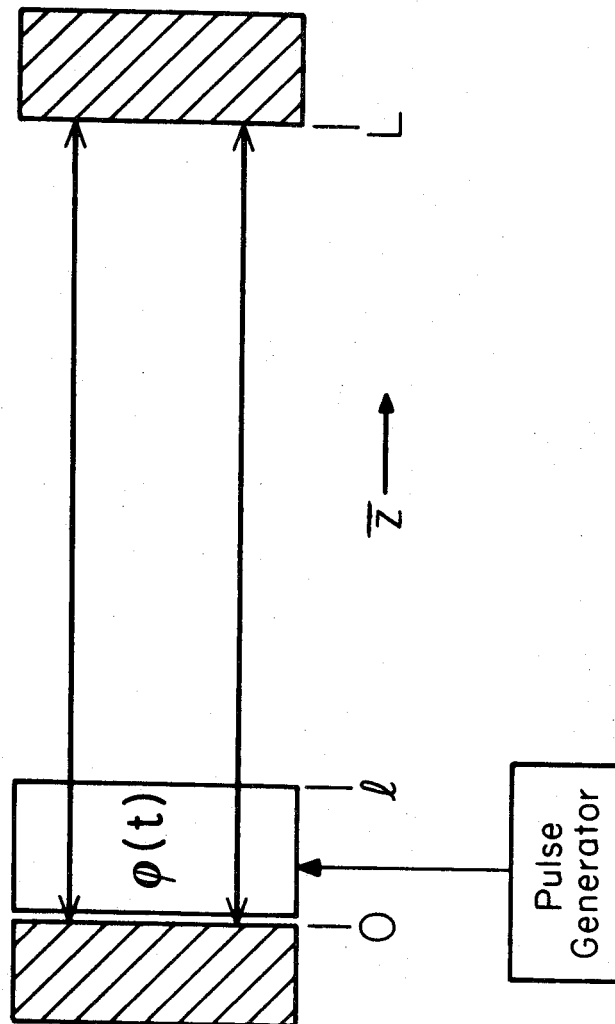
If the phase of this light wave at $\bar{z} = \ell$

$$\phi = k\ell = \frac{\omega}{c} n\ell \quad (10)$$

is modulated by a linear ramp function of the form:

Figure 2

Schematic of a laser cavity of length L containing an electro-optic modulator $\phi(t)$ of thickness ℓ next to one end mirror.



$$\begin{aligned}\phi(t) &= \dot{\phi}(t) & 0 < t < t' \\ \phi(t) &= \dot{\phi}t' & t > t'\end{aligned}\quad (11)$$

then the phase change may be written as:

$$\phi(t) = \dot{\phi}t = 2(\omega/c)n\ell t \quad (12)$$

where n is the index of refraction of the crystal. The factor of 2 in Eq. (12) arises because the phase change involves a double pass through the modulator. Note that the phase time derivative is a constant.

The field at $\bar{z} = \ell$ may now be written as:

$$\begin{aligned}E(\ell, t) &= \epsilon_0 e^{i(\omega - \dot{\phi})t} & 0 < t < t' \\ E(\ell, t) &= \epsilon_0 e^{i\{\omega t - \phi(t')\}} & t' < t < T'\end{aligned}\quad (13)$$

where T' is the new cavity round-trip time and the constant phase factor $e^{-ik\ell}$ has been omitted. Now, for times $t > t'$ the phase change $\phi(t')$ provides an increase in the cavity transit time given by:

$$\Delta T = \frac{\phi(t')}{\omega} = 2(\ell/c)n\dot{\phi}t' \quad (14)$$

each time the wave passes through the modulator twice. Therefore, the light wave propagates in the cavity at the new round-trip time which is:

$$T' = T + \Delta T = \frac{\phi(t')}{\omega} \quad (15)$$

For convenience, let $t' = T'$ such that the modulation function (11) has a final value of $\phi(T') = \dot{\phi}T'$. Eq. (13) for the field at $\bar{z} = \ell$ then becomes:

$$E(l, t) = \epsilon_0 e^{i(\omega - \dot{\phi})t} \quad 0 < t < T' \quad (16)$$

for the first round trip and

$$E(l, t) = \epsilon_0 e^{i\{\omega t - \phi(T')\}} \quad T' < t < 2T' \quad (17)$$

for the second round-trip interval. Successive traversals increase the phase change by an amount $\phi(T')$ due to the increase in cavity transit time ΔT .

Now, let the phase modulated field be written as:

$$E(t) = \epsilon_0 e^{i\{\omega t + \theta(t)\}} \quad (18)$$

where $\theta(t)$ is the resulting phase of the wave at time t , given by:

$$\theta(t) = \theta(t - T') - \phi(t) \quad (19)$$

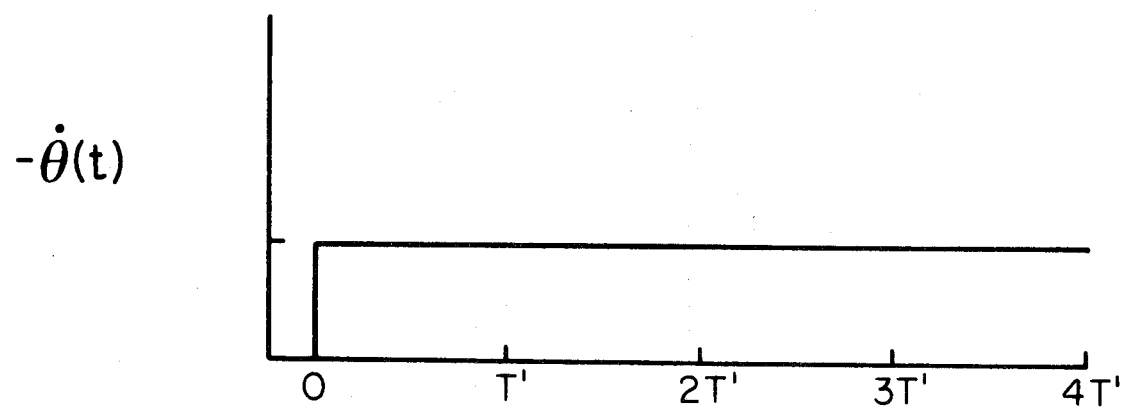
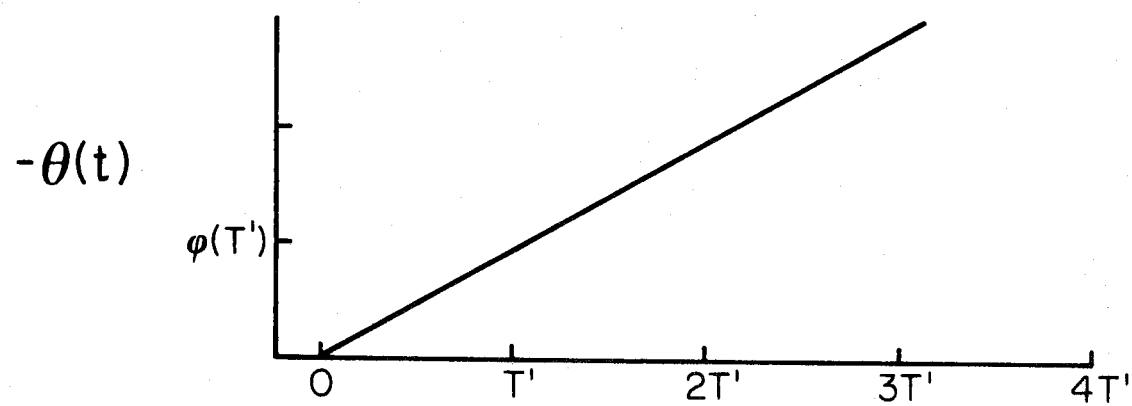
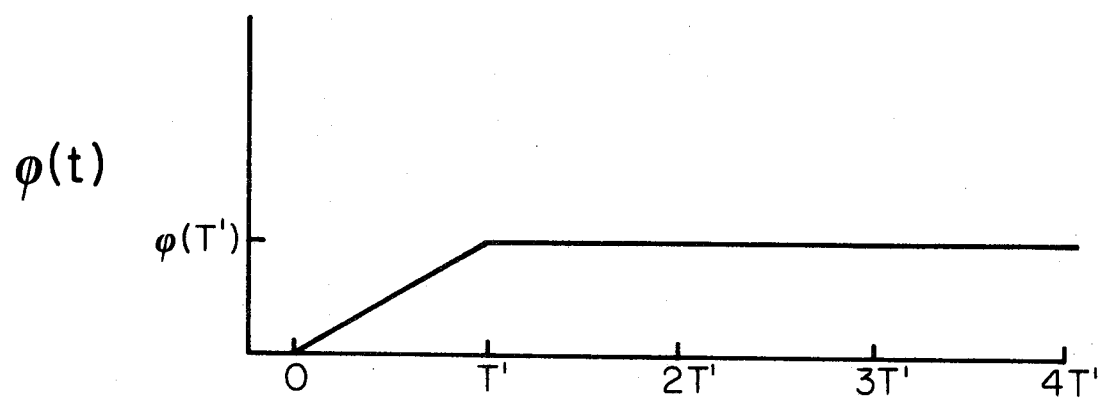
Here, $\theta(t - T')$ is the phase of the wave at time $t - T'$ of the previous traversal and $\phi(t)$ is the phase modulation. Eq. (19) says that the phase of the wave, $\theta(t)$ changes each round trip by a constant amount $\phi(T')$. Therefore, the frequency shift, given by $\dot{\theta}$, is constant following the initial instantaneous change given by (16).

These results are illustrated in Fig. 3 where the phase modulation $\phi(t)$, resulting phase of the wave $\theta(t)$, and $\dot{\theta}(t)$, representing the frequency change, are plotted as functions of time in units of the cavity round-trip time in the presence of modulation, T' .

This model may be extended to modulation functions $\phi(t)$ of different form and for different modulation periods³ but the essential

Figure 3

Graphical representation of the phase modulation process. The top curve shows the phase modulation $\phi(t)$ as a function of time in units of the cavity transit time in the presence of modulation, T' . The middle curve is the resulting phase $\theta(t)$ of the light wave. The bottom curve is the time derivative of the resulting phase $\dot{\theta}(t)$ which represents the frequency shift as a result of the modulation.



features of the dynamics of frequency switching are contained in this simple model.

It should be mentioned at this point that if the modulator were extra-cavity, then the frequency of the wave would still be shifted but only for the duration of the modulation where $\dot{\phi} \neq 0$. When $\dot{\phi} = 0$, the original frequency is recovered.

The EO switching technique was first demonstrated by Kiefer *et al.*⁴ in the IR using a CdTe modulator. Hall⁵ was the first to utilize this technique to observe a coherent transient (OFID) in methane in the IR. Shoemaker and Van Stryland⁶ first discussed the usefulness of this technique for observing optical nutation and thus for measuring electronic transition moments. Brewer and Genack⁷ extended the technique to the visible region and measured transients for an electronic transition in I_2 . Since then, this laser frequency-switching method has allowed one to observe coherent transients in gases (see Chapter III and reference 8), solids (see Chapter IV and references therein) and molecular beams (see Chapter III).

In the experiments described in Chapters III and IV, the voltage pulse supplied to the AD*P crystal had an exponential shape (see Pulse A of Fig. 1 in Appendix I), with a risetime of 12.8 nsec. Since the cavity transit time in the single mode dye laser is 2.6 nsec, the modulation period (time duration over which the crystal index of refraction is changing) spans approximately five cavity round trips. Within the framework of the Genack and Brewer model, this means that the frequency of the laser changes each time the wave makes a double pass through the

modulator until the final frequency is reached at the end of the voltage pulse. However, since the modulation function is an exponential here and not a linear ramp and the modulation period is not exactly an integral multiple of the cavity transit time, the description of the dynamics of the frequency-switching process is much more complicated than that presented above. It is emphasized at this point, however, that for all the experiments discussed in Chapters III and IV, the frequency switching process did not produce transients in the detector when samples were not present.

The EO technique is most useful for observing OFID since extremely sensitive heterodyne detection methods can be employed which exploit the fact that the laser is off-resonance and can beat with the coherent emission from the sample. However, there are limitations on the magnitude of the frequency shift obtainable using the EO technique. Typically, the dispersion of the AD*P crystal provides a 60 MHz frequency shift within the inhomogeneously broadened optical transition for voltage pulses of 100 V. To utilize the EO technique in systems with larger homogeneous linewidths, fast higher voltage pulses are required in order to switch the laser frequency outside the homogeneous linewidth. In practice, these pulses are hard to obtain at high repetition rates and when multiple pulse sequences (e.g., for echo experiments) are desired. Furthermore, the maximum frequency shift attainable while maintaining stable single-mode output is 390 MHz, the cavity mode spacing. To circumvent these limitations when necessary, and also because of many distinct advantages in its own right, the acousto-optic method described in the next section can be utilized.

2. Acousto-Optic Laser Beam Diffraction

Nanosecond time resolution with the CW narrowband laser can also be obtained using an acousto-optic modulator extra-cavity to diffract the single-mode laser beam to and from the sample. This technique referred to as LADS (see Chapter III, Section E) for Laser Acoustic Diffraction Spectroscopy allows one to effectively turn the laser off instead of switching the frequency off-resonance within the inhomogeneous line. LADS relies on the acousto-optic effect⁹ which can be described as follows.

If a photon with energy $\hbar\omega_i$ and momentum $\hbar k_i$ is incident upon an acoustic wave of frequency ω_s and momentum $\hbar k_s$, then the incident photon and a phonon may be annihilated giving rise to a new photon with energy $\hbar\omega_d$ and momentum $\hbar k_d$ consistent with energy and total momentum conservation conditions given by:

$$\begin{aligned}\omega_d &= \omega_i + \omega_s \\ k_d &= k_i + k_s\end{aligned}\quad . \quad (20)$$

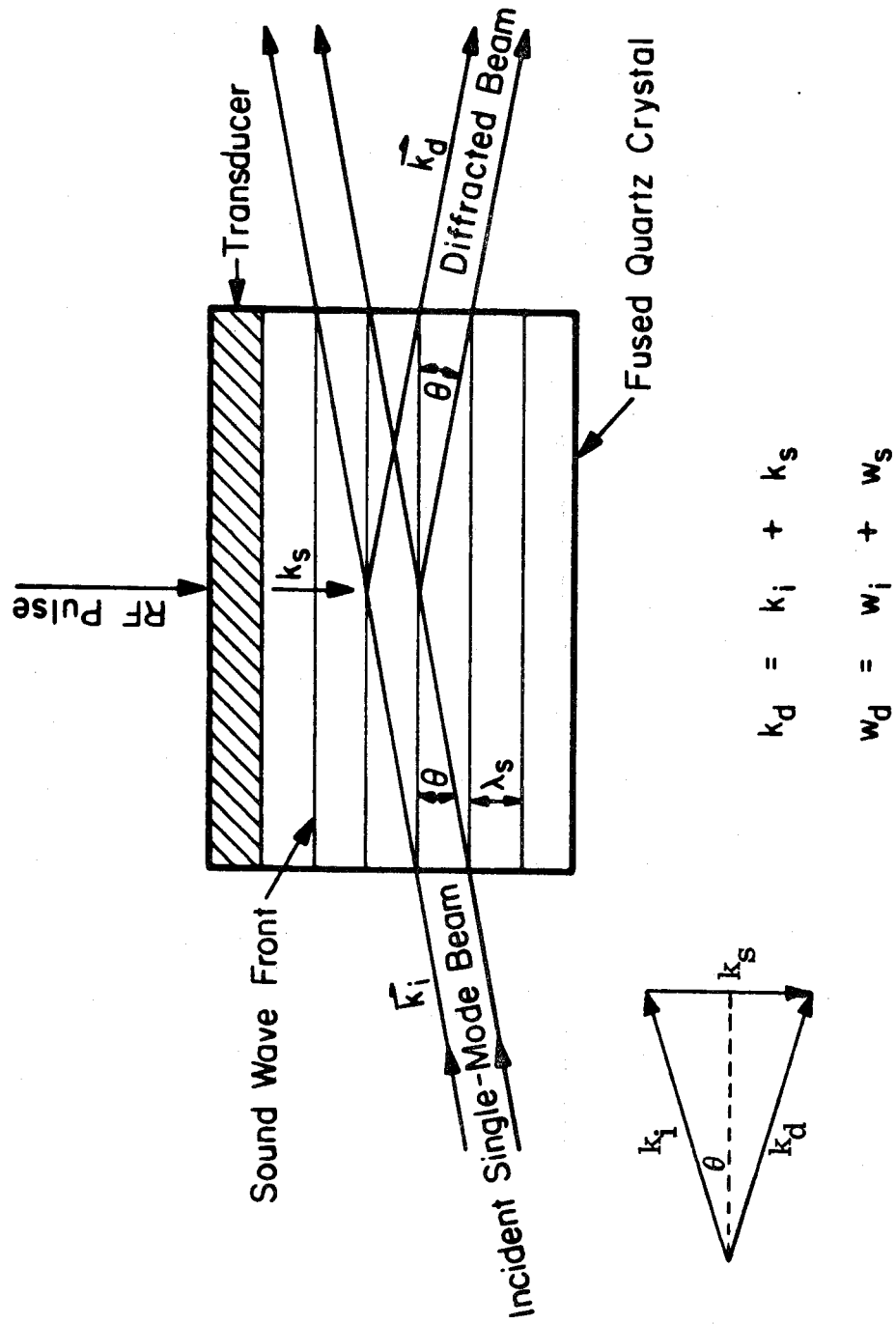
This situation is depicted in the vector diagram shown in Fig. 4. Since $\omega_s \ll \omega_i$, $k_i \approx k_d = k$. If one assumes that the indices of refraction n_i , n_d are approximately equal, then using the relations $k_s = 2\pi/\lambda_s$; $n_i = n_d = n$, and $k = 2\pi n/\lambda$, one obtains the following result:

$$2\lambda_s \sin \theta = \frac{\lambda}{n} \quad . \quad (21)$$

Here, θ corresponds to the Bragg angle since this equation is identical to the first order Bragg equation¹⁰ describing the scattering of X-rays in crystals:

Figure 4

Schematic diagram of an acousto-optic modulator. A traveling acoustic wave is generated in the quartz crystal by a transducer upon receiving an RF pulse. This acoustic wave diffracts an incident light beam such that momentum and energy are conserved as shown in the wave vector diagram.



$$2d \sin \theta = \frac{m\lambda}{n}, \quad m = 1 \quad . \quad (22)$$

The analogy arises because the sound wave front is similar to the atomic planes in a crystal separated by d . Unlike X-ray diffraction, however, there is a frequency shift [Eq. (20)] involved in the acousto-optic effect because the sound wave is traveling with a velocity v_s whereas the atomic planes are stationary.

In the LADS application of the acousto-optic effect, the single-mode laser beam is focused upon a quartz crystal which has a thin film transducer (ZnO) bonded to it as shown in Fig. 4. RF pulses excite phonons in the transducer creating traveling acoustic waves in the crystal which diffract the incident beam at the Bragg angle given by Eq. (21) and shift its frequency by the acoustic phonon frequency (470 MHz in this case). To obtain a laser pulse, the transmitted CW incident beam is blocked and the diffracted beam is allowed to reach the sample.

The characteristics of the laser pulse this technique provides are determined by (1) the RF pulse width and its rise and fall times and (2) the transit time of the acoustic wave across the focused laser beam in the crystal. Laser pulse rise/fall times of 3 nsec ($1/e$ time) have been measured using a 75 mm focal length lens to focus the laser beam into the modulator.

The LADS method has several unique advantages. First, the decay of off-resonance molecules is not superimposed on the build-up transients of on-resonance molecules (which occurs with the EO technique as mentioned previously) because the laser is effectively shut off

except for the duration of the pulse. In large molecules with a high density of excited states this is especially important. The complicated level structure in these systems can make the interpretation of transient spectra difficult. The LADS method removes the influence of off-resonance effects and simplifies the spectra. Secondly, the optical pulses are generated by supplying low-voltage pulses to an RF oscillator instead of the high-voltage pulses that may be required by the EO technique. Finally, one can obtain high sensitivity as with heterodyne techniques by detecting the spontaneous emission at right angles to the exciting laser beam. With the proper pulse sequences, one can directly measure both T_1 and T_2 as shown in Chapter III, Section E.

3. Incoherent Resonance Decay (IRD)

This technique involves measuring the emission intensity (at right angles to the exciting beam) from a sample as the single-mode laser frequency is switched within the inhomogeneous line using the EO method. The superposition of two processes occurring simultaneously is observed. First, molecules originally on resonance decay (by T_1) since they are now off resonance. At the same time, a new group of molecules is brought into resonance being driven coherently (i.e., nutating) by the laser field toward some equilibrium population distribution. Thus, the observed emission signal should show an initial build-up and nutation transient followed by a decay. From this technique one may obtain both optical T_1 and T_2 as shown in Section B of Chapter III.

4. The 3-Pulse Photon Echo

This section presents a geometric description of the photon echo observed by monitoring the spontaneous emission from a sample during a 3-pulse $(\pi/2, \pi, \pi/2)$ sequence of optical excitation. In addition, it presents the techniques required to produce the optical pulse train and to detect the echo.

For a two-level system in the FVH picture, the r -vector rotates in the 2, 3 plane about \mathcal{E}_{eff} at the Rabi frequency $(\mu \cdot \epsilon / \hbar)$ for the on-resonance ($\Delta = 0$) case as shown in Fig. 1 of Chapter I. Before exciting the sample (i. e., $t \leq 0$), each molecule is in its ground state and therefore contributes a vector lying along the -3 axis as shown in Fig. 5a. Thus, $r_1 = r_2 = 0$ and $r_3 = -1$. Now, for an excitation pulse corresponding to $(\mu \cdot \epsilon / \hbar)t = \pi/2$, a rotation of 90° occurs in the position of r in the 2, 3 plane producing a coherent superposition of the ground and excited states for each molecule resulting in a large macroscopic dipole moment. This is shown in Fig. 5b. Following this $\pi/2$ pulse the individual molecules get out of phase with each other due to the distribution of molecular frequencies within the bandwidth of the exciting laser (i. e., inhomogeneous dephasing represented by T_2^*) as shown in Fig. 5c. Homogeneous dephasing represented by T_2 and due to elastic processes as discussed in Chapter I is also occurring. The loss of coherence by homogeneous dephasing processes is irreversible and in the FVH picture is represented by a decrease in the magnitude of the components of the r -vector in the 1, 2 plane. Inhomogeneous dephasing on the other hand is reversible and may be cancelled by applying a π -pulse which reverses the phase of

each vector as shown in Fig. 5d. After a time equal to the separation of the $\pi/2$ and π pulses, the individual vectors will be in-phase again and the echo is formed as shown in Fig. 5e. A $\pi/2$ pulse applied at this time rotates the echo vector from the 1, 2 plane to axis 3 (see Fig. 5f) which, as mentioned before, represents the population difference. Thus, the coherence in the system is determined by burning the spontaneous emission following the phase reversal in the 1, 2 plane. Doing the experiment as a function of the delay time between pulses gives the decay of the homogeneous system which is the optical T_2 . The theoretical details of this probe pulse technique appear in Section C of Chapter III and in reference 8.

Experimentally, an optical pulse train of single-mode laser pulses of variable width and separation is needed to prepare and probe the echo in a sample. These optical pulses may be obtained with the EO method or with LADS. In either case, a sequence of voltage pulses is required to drive the respective modulator.

For the EO method, high level (up to 50 V) pulses with small separations are necessary. It was impossible to satisfy these requirements with a single pulse generator so a technique was devised to provide the desired pulse sequence by combining the outputs of the two pulse generators.

Consider the pulse sequence shown at the top of Fig. 6. Since the first and third pulses are of equal width, they can be provided by one pulse generator (for this application a Rutherford Model B16 was used) operating in double pulse mode (i.e., two identical output pulses

Figure 5

A schematic for the geometric description of the right-angle three pulse photon echo: (a) all the molecules are in the ground state; (b) after a $\pi/2$ pulse; (c) inhomogeneous dephasing; (d) after a π pulse; (e) the echo, (f) termination of the spontaneous emission from the upper level by the third pulse.

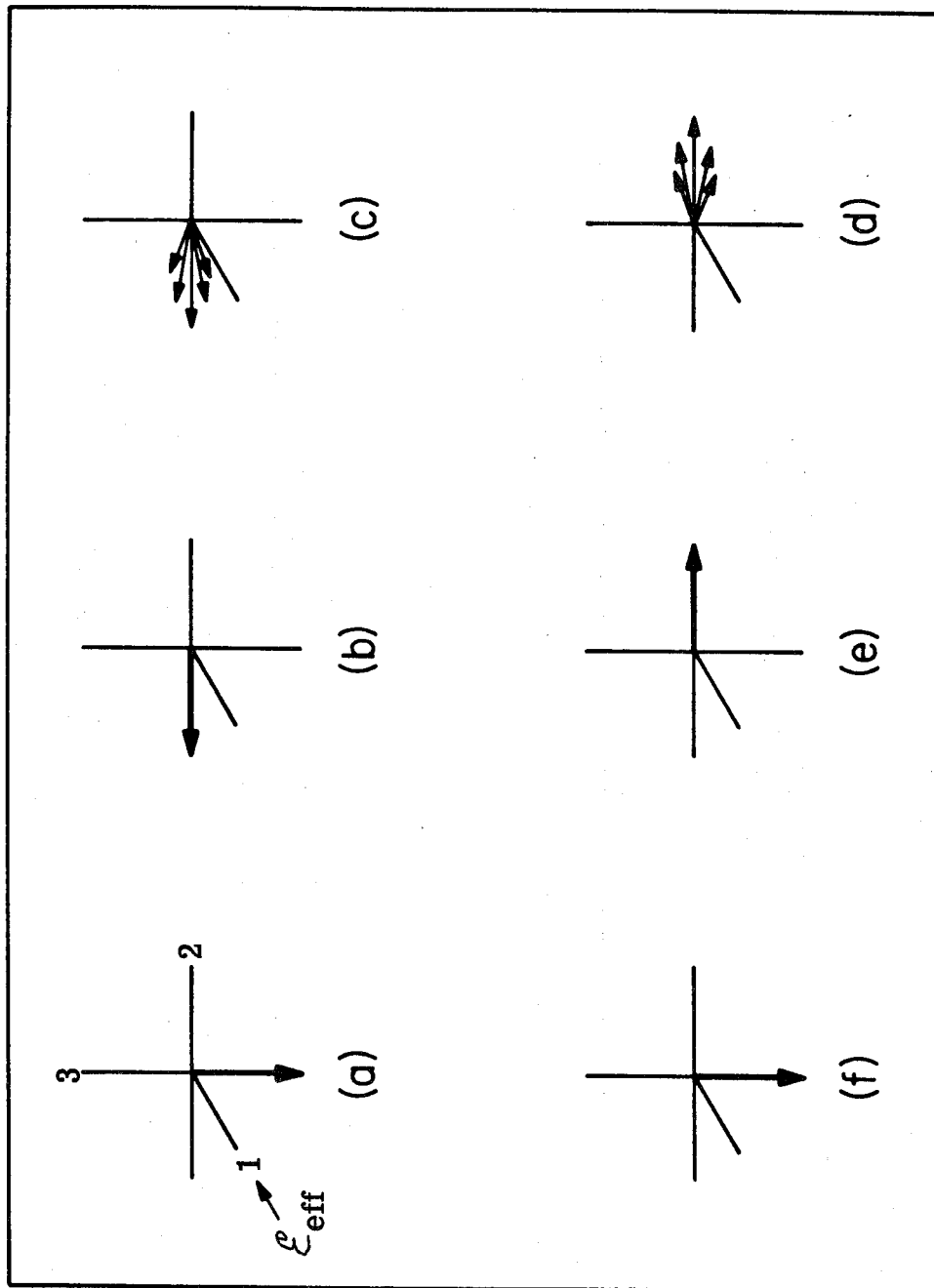
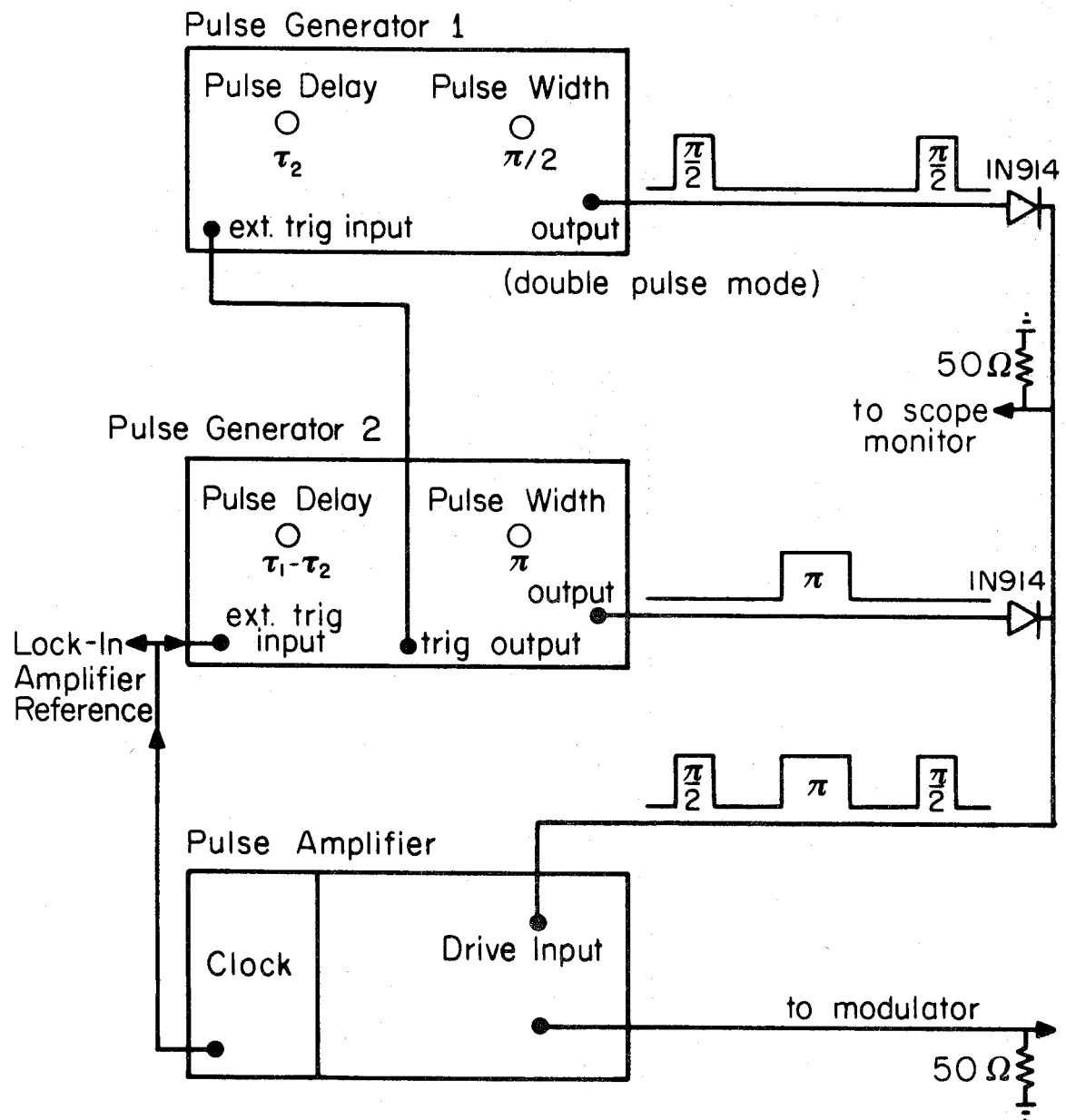
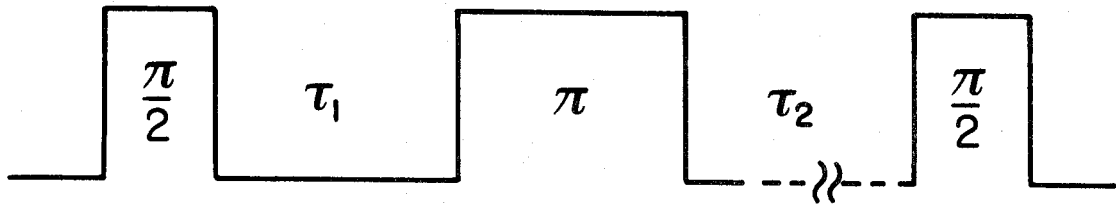


Figure 6

Schematic of the pulse train required for the three-pulse photon echo and the pulse generator network devised to produce it.



of variable width and separation per input trigger pulse). The output of a second pulse generator (Hewlett Packard 214 A) is then combined with the first using fast, high-voltage diodes (1N 914) to prevent pulse reflections. Pulse synchronization and independent control of the delays τ_1 and τ_2 are accomplished by interconnecting the trigger signals as shown in Fig. 6. The combined output of the pulse generators is then amplified (Hewlett Packard 1915 A pulse amplifier) and synchronized with the detection equipment using a clock (Hewlett Packard 1905 A).

This system provides a 3-pulse sequence of up to 50 V in amplitude with no restrictions on the minimum delays or pulse widths and at repetition rates of up to 100 KHz. The output is fed to the AD*P crystal terminated at 50 Ω for the EO method and to the acousto-optic crystal for the LADS method (in this case amplification is unnecessary).

The detection scheme for the photon echo is described as follows. Emission from the sample is collected at right angles to the exciting beam and focused upon a photomultiplier (EMI 9558) which has sharp-cut filters in place to block the exciting wavelength. The output signal is sent to a lock-in amplifier (Hewlett Packard HR-8) operating at a reference frequency determined by the repetition rate of the pulse sequence. In this manner it functions as an integrator for the total emission from the sample due to the pulse train. As one scans the delay τ_2 with τ_1 fixed an echo (minimum in the spontaneous emission signal) is observed at $\tau_1 = \tau_2$. The decay of this echo as a function of pulse delay provides the dephasing time of the homogeneous system and thus the homogeneous linewidth ($1/\pi T_2$) of the optical transition. Details of the

results obtained for iodine at low pressure appear in Sections C and E of Chapter III.

5. Molecular Beam Coherent Transients

To examine coherent transients in a collisionless environment, an apparatus was constructed to generate effusive molecular beams. Shown in Fig. 7 is a schematic of the device. The body is made entirely of glass. A Kovar disc with a horizontal 1.0×0.02 cm slit separates the source chamber from the main pumping chamber. The background pressure in the main chamber is kept at $< 1 \times 10^{-5}$ torr using liquid nitrogen traps and a 2-inch diffusion pump. The source chamber has a set of valves for introducing the sample and can be heated to increase the number of molecules in the beam.

Coherent transients are observed using the EO method by monitoring the single-mode laser after it passes through the molecular beam close to the slit. Emission from the sample at right angles to both the laser and molecular beams is detected at the same time. Using this technique one can obtain both T_1 and T_2 in the absence of collisions and determine therefore, the importance of intramolecular processes as dephasing and relaxation channels for the molecule under study. Results obtained for iodine using this beam apparatus are described in Section D of Chapter III.

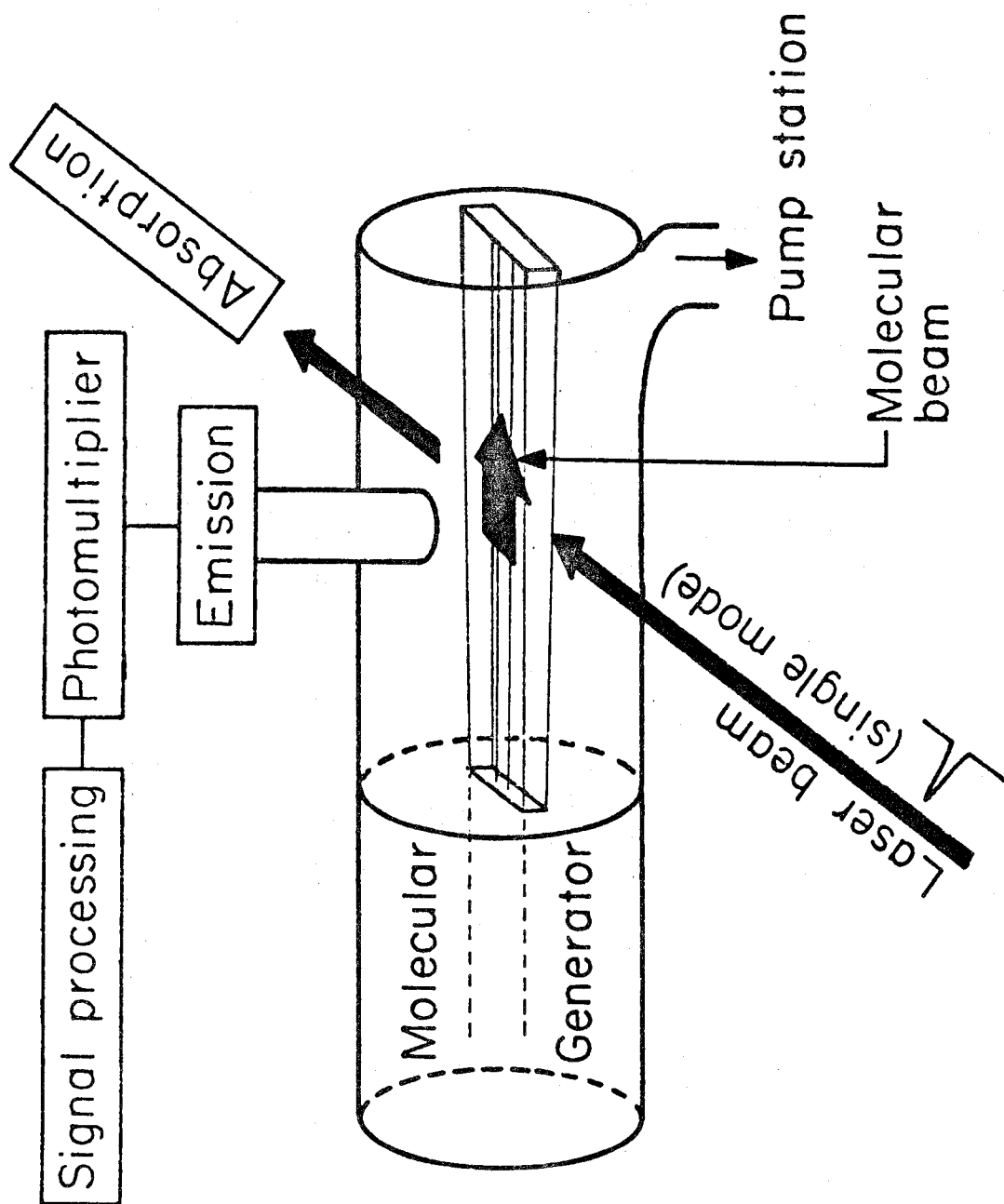
C. PROCEDURES

1. Sample Preparation

A gas cell made of glass with Brewster angle windows and Teflon greaseless stopcocks was used for the experiments on iodine. On a

Figure 7

A schematic of the apparatus for crossed molecular and laser beams studies of coherent transients at zero pressure.



carefully trapped (liquid N₂) vacuum manifold the cell was evacuated and baked out at 100°C for twelve hours to drive off water vapor and adsorbed gases from the cell walls prior to the introduction of I₂.

When the background pressure was reduced to 3×10^{-6} torr, Mallinckrodt analytical reagent grade I₂ was distilled into a cold finger at 0°C attached to the side of the cell. After one hour the distillation arm was sealed off and the cell was then degassed with three cycles to -78°C in a dry ice acetone bath. Finally, the cell was evacuated to 3×10^{-6} torr with the cold finger in liquid nitrogen and sealed off from the vacuum manifold. The above procedure was found to be necessary to avoid contamination which effectively quenches iodine emission resulting in a shorter observed lifetime. The vapor pressure of iodine was controlled by regulating the temperature of the side arm of the cell containing solid iodine with a constant temperature ($\pm 0.1^\circ\text{C}$) bath. Iodine vapor pressure was calculated from the temperature using an equation given by Giaque.¹¹ Results are shown in Table I.

Experiments in the condensed phase were also performed with carefully purified reagents. Scintillation grade p-terphenyl (Eastman Organic Chemicals) was zone-refined for eighty passes before use. Pentacene (Aldrich Chemical Company) was twice vacuum sublimed. Dilute single crystals (10^{-5} - 10^{-7} m/m) of pentacene in p-terphenyl were grown from the melt using standard Bridgman techniques.

2. Measurement of Coherent and Incoherent Transients

The apparatus used for the EO and LADS experiments in the condensed phase is shown schematically in Fig. 2 of Chapter IV. Except

TABLE I. Iodine Vapor Pressure* Versus Temperature

P(mtorr)	T(°C)
10.8	-10.0
13.4	- 8.0
16.6	- 6.0
20.5	- 4.0
25.2	- 2.0
30.9	0.0
37.7	2.0
46.0	4.0
55.9	6.0
67.7	8.0
81.8	10.0
98.5	12.0
118	14.0
142	16.0
170	18.0
202	20.0

*Calculated from the equation¹¹ $\log P(\text{atm}) = - \frac{3512.3}{T(^{\circ}\text{K})} - 2.013 \log T + 13.374.$

for the sample area, experiments in the gas phase and with the molecular beam apparatus were done with the same set-up. In all experiments the output of the single-mode laser was amplitude stabilized and split (8%) to allow continuous monitoring of laser frequency and single-mode operation using a 0.5 m spectrometer and scanning confocal etalon, respectively.

For EO experiments, the switching process can be observed as shown in the insert to Fig. 2 of Chapter IV. This oscilloscope tracing was obtained by synchronizing the scanning confocal etalon with the AD*P pulser.

For LADS experiments, the modulator was placed in the optical path such that the diffracted beam continued on to the sample (after passing through a 2 mm aperture) while the transmitted incident beam was blocked. Thus, the sample was excited only when an RF pulse was supplied to the AO crystal.

Coherent transients along the laser beam were detected using fast (≈ 1 nsec response) Hewlett Packard photo diodes (HP 5082-4203) biased at -15 V or a modified¹² RCA IP28 photomultiplier whose frequency response extended beyond 1 GHz. The signals were amplified using a two-stage Hewlett Packard (Model 8447) amplifier which has an overall gain of 46 dB and a bandwidth of 0.01-1.3 GHz. A Tektronix 1S-1 sampling scope was used to display the results. All ground loops in the detection system were removed to prevent electronic pick-up from interfering with the observed signals.

Emission from the samples was detected at right angles to the exciting beam using a shielded (RF, magnetic, electrostatic) cooled

photomultiplier (EMI 9558). Its output was amplified using a Princeton Applied Research (PAR) Model 115 wideband amplifier (dc-70 MHz) and then averaged using either a scanning-gate boxcar integrator (PAR 162) or a lock-in amplifier (Hewlett Packard HR-8). Hard copy of the data was obtained using a recorder to trace the output of the signal averager. For observing very fast transients on the emission the modified IP 28 photomultiplier was used. In most experiments, a sharp-cut filter was placed in front of the detector to block the exciting wavelength and the total emission from the sample was monitored. However, in several experiments a 0.5 m Jarrel-Ash spectrometer was used to resolve individual vibronic lines. Signals were processed identically in both cases.

3. Absorption Measurements and Calibration Methods

High-resolution absorption measurements were made using a 0.75 m Spex (1-14018) double monochromator equipped with holographic gratings (resolution 0.09 cm^{-1}) in conjunction with a Spex DPC-2 digital photometer. In some experiments, a Burleigh Fabry-Perot interferometer (RC-110) combined with the 0.5 m Jarrell-Ash spectrometer was used for scanning lineshape profiles. Spectrometer wavelength drives were calibrated before each experiment using lines from a Fe-Ne arc lamp.

Laser power was measured using a calibrated Scientech thermopile (Model 360001). Neutral density filters were used to vary laser power after carefully determining their optical densities as a function of wavelength.

4. Data Treatment

Nonlinear least squares regression analyses were used to fit all of the IRD data as well as the optical nutation and OFID for condensed phase experiments. To avoid some of the ambiguities associated with these techniques (e.g., biased initial estimates of parameters which lead to solutions that converge upon only a local minimization of error), most of the data was fit using a two-step procedure.

First, an eigenfunction expansion method developed by Provencher¹³ was utilized to determine the best exponential decay parameters (rate constants and coefficients) for the IRD transients. This method fits data to a function of the general form:

$$y(t) = \sum_{j=0}^{N_{\lambda}} \alpha_j e^{-\lambda_j t} \quad (23)$$

where α_j and λ_j are the coefficients and rate constants of the j^{th} exponential and N_{λ} is the number of exponentials. It requires no initial estimates for the parameters and provides cross-correlation coefficients as well as confidence limits for the best solution. Since no initial guesses are needed, biased results are avoided in most cases. This is a very important consideration with exponentials since their severe nonorthogonality can allow a grossly incorrect solution to reproduce the data satisfactorily.¹⁴ A FORTRAN version of the program was generously provided by Provencher.

For the second step in data reduction, a more conventional procedure for nonlinear least squares regression analysis using an

algorithm developed by Marquardt¹⁵ was used. The initial estimates of parameters required by this method were provided by the best fit values from the first program.

This two-step procedure gave results that converged upon the same values for several different starting points and so, unique solutions could be assumed safely in most cases. Similar procedures were used for lineshape analyses and for treating the results of other transients. Stern-Volmer data from gas phase experiments were analyzed using a linear regression analysis program on a Hewlett Packard Model 65 programmable calculator.

REFERENCES

1. A. Yariv, Proc. IEEE, 52, 719 (1964).
2. D. Anafi, R. Goldstein and J. Machewirth, Laser Focus, 13, 72 (1977).
3. A. Z. Genack and R. G. Brewer, Phys. Rev. A, 17, 1463 (1978).
4. J. E. Kiefer, T. A. Nussmeier and F. E. Goodwin, IEEE J. Quantum Electron. QE-8, 173 (1972).
5. J. L. Hall, "Atomic Physics 3", S. J. Smith, G. K. Walters and L. H. Volsky, eds. (Plenum, New York, 1973), p. 615.
6. R. L. Shoemaker and E. W. Van Stryland, J. Chem. Phys., 64, 1733 (1976).
7. R. G. Brewer and A. Genack, Phys. Rev. Lett., 36, 959 (1976).
8. A. H. Zewail, D. E. Godar, K. E. Jones, T. E. Orlowski, R. R. Shah and A. Nichols, in: "Advances in Laser Spectroscopy I", A. H. Zewail, ed. (SPIE Publishing Co., 1977), Vol. 113, and references therein.
9. R. Adler, IEEE Spectrum, 4, 42 (1967).
10. W. L. Bragg, Proc. Cambridge Phil. Soc., 17, 43 (1913).
11. W. F. Giaque, J. Am. Chem. Soc., 53, 507 (1931).
12. G. Beck, Rev. Sci. Instrum., 47, 537 (1976).
13. S. V. Provencher, J. Chem. Phys., 64, 2772 (1976).
14. S. L. Laiken and M. P. Printz, Biochem., 9, 1547 (1970); C. Lanczos, "Applied Analysis", (Prentice-Hall, Englewood Cliffs, 1956).
15. D. W. Marquardt, J. Soc. Industrial Appl. Math., 11, 431 (1963).

CHAPTER III

APPLICATIONS OF NEW COHERENT NONLINEAR OPTICAL SPECTROSCOPIC TECHNIQUES

INCOHERENT RESONANCE DECAY AND COHERENT
OPTICAL RINGING FROM COHERENTLY PREPARED
ELECTRONIC STATES:

A NEW TECHNIQUE FOR PROBING PHASE
MEMORY AND RADIATIONLESS RELAXATION
IN GASES AND SOLIDS[‡]

A. H. Zewail, T. E. Orlowski and D. R. Dawson
Arthur Amos Noyes Laboratory of Chemical Physics^{‡ ‡},
California Institute of Technology, Pasadena, California 91125

ABSTRACT

A new technique is developed for measuring the incoherent resonance decay (IRD) and the coherent optical ringing of selectively (± 3 MHz) prepared electronic states in solids and gases. The method utilizes electro-optic switching of a single laser mode that is on or off resonance with respect to the homogeneous molecular packets in the excited ensemble. The technique was applied to a variety of systems to give information about their phase memory (optical T_2 processes), radiative and radiationless decay (optical T_1 processes), and to measure directly their optical transition moment between the ground state and the prepared electronic state.

[‡] Chemical Physics Letters, 44, 379 (1976).

^{‡ ‡} Contribution No. 5413

1. INTRODUCTION

Many years of theoretical and experimental work have been devoted to the understanding of the decay and preparation of electronic states in "isolated" molecules and in the condensed phase. The questions that have been usually asked focus on what happens to "primary" states following absorption from the photon field. Green's function techniques have been used¹ successfully to describe the coupling between discrete optical levels and continua of molecular vibrations,¹ lattice phonons,² and the radiative field of photon packets.³ The latter explained theoretically the on-resonance and off-resonance effects of light pulses scattered by molecular states, as demonstrated by the beautiful experiments of Williams et al.⁴ However, to understand fully the many interactions that lead into spectral broadening of the primary states, one is forced not only to consider the radiative and nonradiative decay (T_1 processes) of the state but also the dephasing of molecular dipoles (T_2 processes) in the excited ensemble.

In this letter we show that both the optical coherent (forward) decay and the incoherent (right-angle[†]) decay of the prepared state can be monitored while the system (solid or a gas) is on and off resonance with a single mode (± 3 MHz) of a tunable dye laser. This new IRD technique, which utilizes an electro-optic switching of a specific laser mode between different sub-ensembles of the excited

[†] By right-angle we mean the emission perpendicular to the propagation of the laser beam.

system, is applied to a variety of systems. We believe that much will be learned about the decay (like spontaneous emission, soft and hard collisions, phonon scattering in solids, and dipole dephasing) and the preparation of selective (within 3 MHz) states. The advantage of this technique relies on its simplicity. In contrast to pulsed lasers which span a larger frequency distribution, the utilization of a cw single-mode dye laser stimulates specific molecular packets and provides a continuous tunable source for measuring small anisotropy in the decay channels. Moreover, where it is difficult to obtain coherent absorption, the incoherent resonance decay can be detected using the emission intensity which is very sensitive to the relaxation and the nature of the prepared state.

2. TWO-LEVEL SYSTEM IN A LASER FIELD

The treatment of the interaction between a pulse of radiation (width $t_p < T_1, T_2$) and a two-level system is well-known since 1946 when Bloch⁵ predicted the existence of phase coherence in a spin ensemble. Hahn⁶ in 1950 demonstrated in a classical experiment the dephasing and refocusing of the ensemble moments as a result of finite coherence time that is longer than Rabi's oscillation time in the rotating frame. Hahn's discovery showed clearly that the reversibility of free induction decay exists. The extension of such ideas to the optical region was shown by Kurnit et al.⁷ In their experiments an echo resulted from the in-phase refocusing of the homogeneous optical moments. This discovery has triggered similar experiments⁸ done on other systems. Tang and Statz⁹ were

the first to argue that a step-function light pulse in an amplifying medium would cause the system to nutate at a time determined by the leading edge of the pulse, and to decay with the relaxation time constants. Hocker and Tang⁹ observed an optical nutation in SF_6 gas when a pulse from $10.6 \mu \text{CO}_2$ laser was passed through the cell. Although the modulation was not obviously sinusoidal, it is fair to say that the power level they used in their experiments was in agreement with the theoretical prediction, and that they were the first to point out such an effect which has been recently observed clearly in the elegant experiments of Brewer and his co-workers.¹⁰

As we shall see, in our experiments both the diagonal and off-diagonal elements of the density matrix (ρ) are being monitored in an optically thin sample. Being optically thin ensures that there are no propagation effects, such as self-induced transparency.¹¹ The sample emitting cooperatively resembles Dicke's super-radiance or, more specifically, the linear combination (molecules plus field) of Dicke states.¹² Therefore the coupling between Maxwell's equations of the radiation field and the Schrödinger representation¹³ of the two-level system becomes straightforward.

Defining the total decay time constant for the two levels as T_{1a} and T_{1b} and the energy separation between the two levels as $\Delta E_{ab} = \hbar \omega_0$, one can show that the rate of change of the elements of the density matrix is given by

$$\dot{\rho}_{aa} = -\frac{\rho_{aa}}{T_{1a}} - \rho_{ab} \quad (1a)$$

$$-\dot{\rho}_{bb} = \frac{\rho_{bb}}{T_{1b}} + \rho_{\hat{a}} \quad (1b)$$

$$-\dot{\rho}_{ab} = i\{[\omega_0 + \delta(t)] + [\frac{1}{2}(T_{1a}^{-1} + T_{1b}^{-1})]\} \rho_{ab} - (i/\hbar)V_{ab}(\rho_{aa} - \rho_{bb}) \quad (1c)$$

$$-\rho_{\hat{a}} = (i/\hbar)V_{ab}\rho_{ba} + c.c. \quad (1d)$$

The above equations imply first that there exist differences in the decay if one monitors the diagonal and/or off-diagonal elements, i.e., the polarization component or the population difference between the two levels ($\rho_{aa} - \rho_{bb}$). The latter is, of course, proportional to R_3 in the FVH picture.¹³ Second, the dipole dephasing is incorporated in (1c) as a fluctuating term δ that gives rise to a decay constant $1/T_2$ that can be added to the $1/T_1$ term. This is true if one assumes a simple correlation function for the dephasing process in the gaseous or the solid ensemble when the interaction V ($V = -\mu \cdot E_0 \cos \omega t$) couples the radiation field of frequency ω with the system of moment μ . In our case, the laser field in the optical region couples with the electric dipoles that are generated from the transition between the ground state and a "narrow" optical electronic state. It is this coupling that creates the in-phase and the quadrature components of the polarization which evolves in time as follows:

$$\dot{R}_1 = -\Delta R_2 - \gamma R_1, \quad (2a)$$

$$\dot{R}_2 = \Delta R_1 - \gamma R_2 + (\mu E_0/\hbar) R_3, \quad (2b)$$

$$\dot{R}_3 = (-\gamma_a \rho_{aa} + \gamma_b \rho_{bb}) - (\mu E_0/\hbar) R_2. \quad (2c)$$

γ_a and γ_b are the decay rate constants of levels a and b, respectively, while $\gamma = \frac{\gamma_a + \gamma_b}{2} + 1/T_2$. Δ is the amount off-resonance the single mode of the laser is with respect to the transition frequency of the primary state in the "optical" rotating frame.

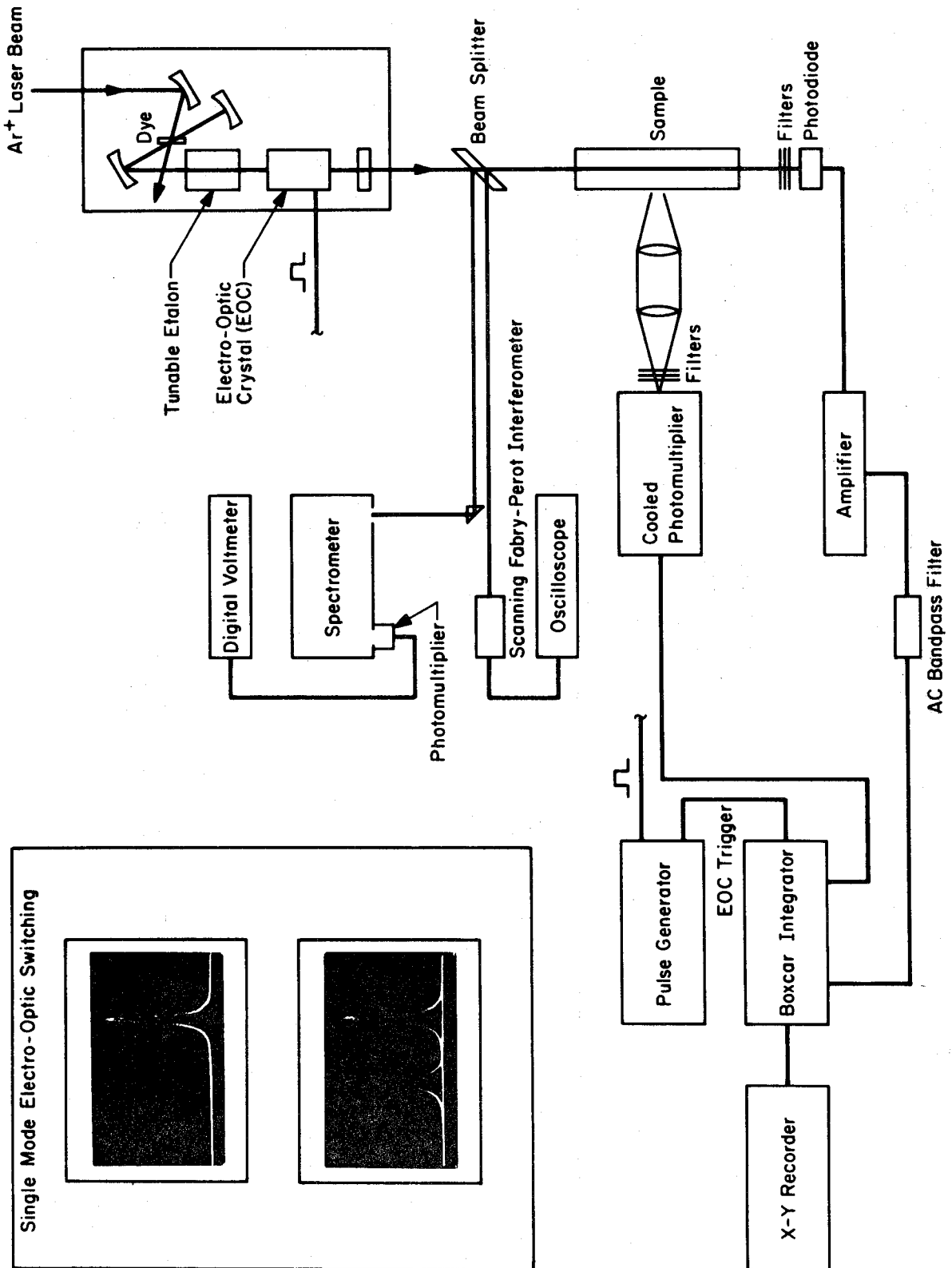
3. THE INCOHERENT RESONANCE DECAY (IRD) EXPERIMENTS

In the IRD experiments, an intense single mode tunable dye laser was used for the excitation. An 18 watt Ar^+ ion laser (Spectra Physics model 170) was used to pump a free jet stream dye laser. The dye solution was rhodamine 6G in ethylene glycol. A modified Spectra Physics (model 580 A) dye laser was used so a single mode could be switched out of the transition resonance frequency by an electro-optic element. Special attention was given to the alignment procedure so the dispersion of the crystal in the electric field was caused by the modulation of the refractive index along the principal axes of the dielectric ellipsoid. The modulation is done transversely and is different from the switching procedure of Telle and Tang¹⁴ used for very rapid tuning of cw dye lasers. The switching is clearly demonstrated in our experiments as shown in fig. 1. From the dispersion frequency we obtained an electro-optic dispersion for the AD*P crystal of 0.6 MHz/V. The net laser power of the single mode is 90 mW and the field is linearly polarized.

The single mode beam was split so both the frequency of the transition and the quality of the single mode can be checked during

Figure 1

A schematic diagram of the experimental setup for the incoherent resonance decay (IRD) and coherent optical resonance (COR) experiments. The insert in the figure shows the single mode of the CW dye laser when the voltage on the electro-optic crystal is nonzero. The mode spectrum was monitored using an interferometer (see text). To minimize the jitter of the mode, the optics and the laser were mounted on an NRC vibration-isolation table.



the experiments (see fig. 1)*. Most of the laser beam intensity was used in the forward direction for the excitation of the sample. For the study of low pressure gases (I_2 and NO_2), a sample tube with flat optical windows was used. A cold finger at the side of the tube was used to control the pressure of the gas. For solid state experiments, the crystal was oriented in a liquid helium dewar that can be pumped to temperatures below the λ -point of liquid helium.

The emission was collimated at a right angle to the exciting beam with lenses of proper f numbers, and focused on a cooled photomultiplier (EMI-9558). The photomultiplier was magnetically and electrostatically shielded. Since noise will be introduced because of the laser light scattering, a sharp cutoff glass filter was placed in front of the phototube. The output of the photomultiplier was terminated in a boxcar integrator (PAR model 162) whose gate width was adjusted between 5 and 50 ns. The photomultiplier was coupled ac into the boxcar and the output was traced on an X-Y recorder.

4. THE COHERENT OPTICAL RESONANCE (COR) EXPERIMENTS

We have observed, for the first time, the coherent ringing** from a coherently prepared homogeneous packet that localizes the optical excitation in solids. The experimental setup for COR is

* The single-mode spectrum was monitored with a Fabry-Perot interferometer that is scanned to allow the observation of on-resonance and off-resonance mode structure of the laser beam.

** The details of this solid state work will be published elsewhere.

identical to IRD except we monitored the laser intensity in the forward direction. Carefully mounted photodiodes were used in combination with filters to obtain the transients. These transients will appear either as coherent absorption and emission, as in the optical nutation (see fig. 2), or as beating with the incident beam, as in the free induction decay (fig. 3) signal*. The output of the biased diode (with constant voltage supply) was amplified and fed into either an oscilloscope or the boxcar integrator. The laser power was measured by a Spectra Physics power meter (model 401 B). Knowing the power of the single mode and the beam diameter gave the radiation density at the sample.

5. OPTICAL T_1 AND T_2 PROCESSES OF EXCITED STATES

Using the above techniques in this series of experiments and in other experiments that will be published elsewhere, we are investigating in a systematic way the optical T_1 and T_2 processes. The small, intermediate, and large molecule limits, both at low pressures and in the solid phase, are examined. The objectives are to obtain information about the incoherent and coherent decays from this new technique and to correlate them with the findings of the many

* Brewer and Genack¹⁰ have reported recently the forward coherent transients in iodine gas. Our results on the coherent decay are in agreement with theirs. We should add that both Dr. Brewer's group and our group are trying the transient coherent experiments on different systems at the same time. So it is fair to say that there is and will be considerable activity in this field.

Figure 2

The boxcar output plots of the on-resonance and off-resonance emission decay when the electro-optic switching pulse is on and off. Also shown in this figure is the optical nutation of iodine at 0°C. The on-resonance emission was taken at 14 MHz switching frequency while the nutation was taken at 4 MHz.

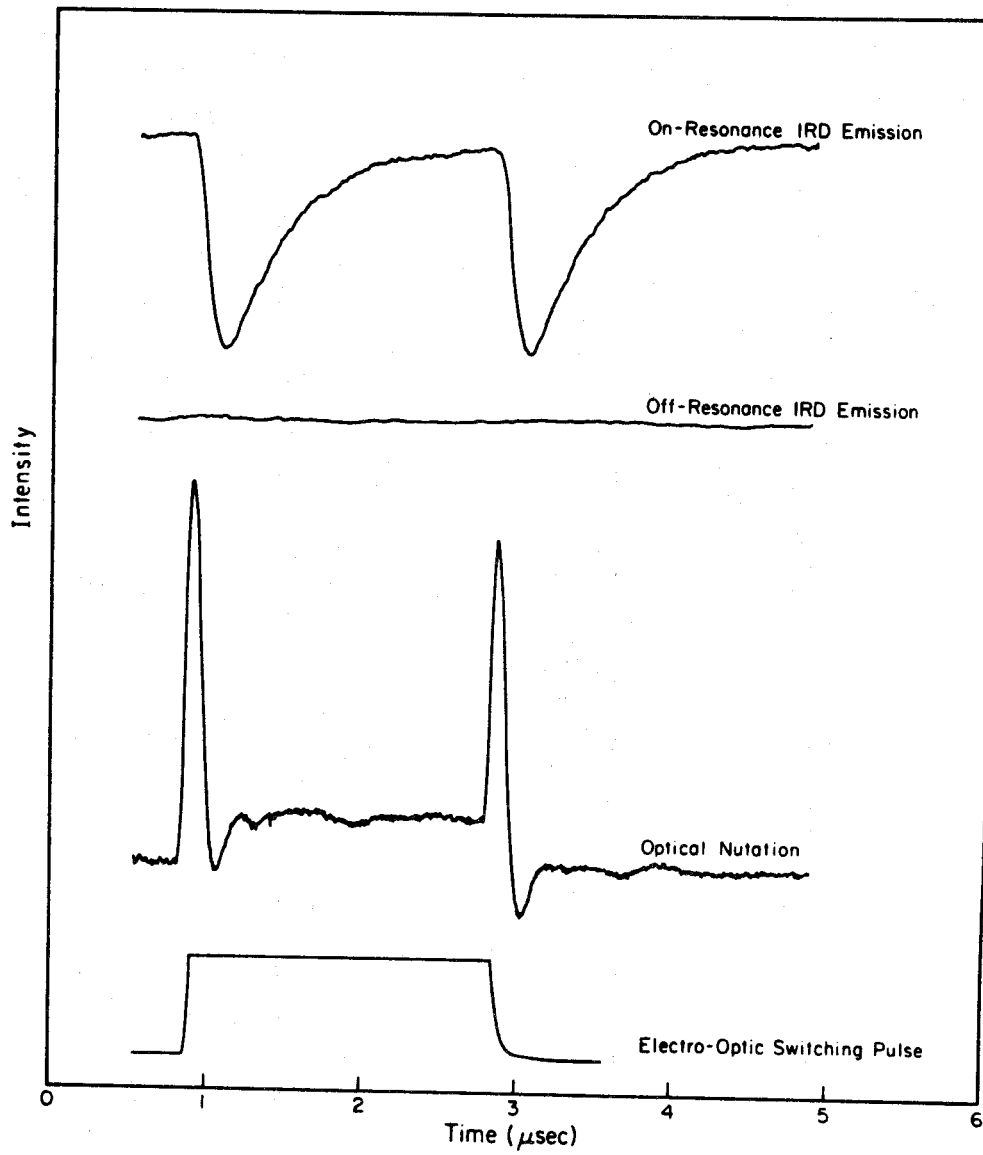
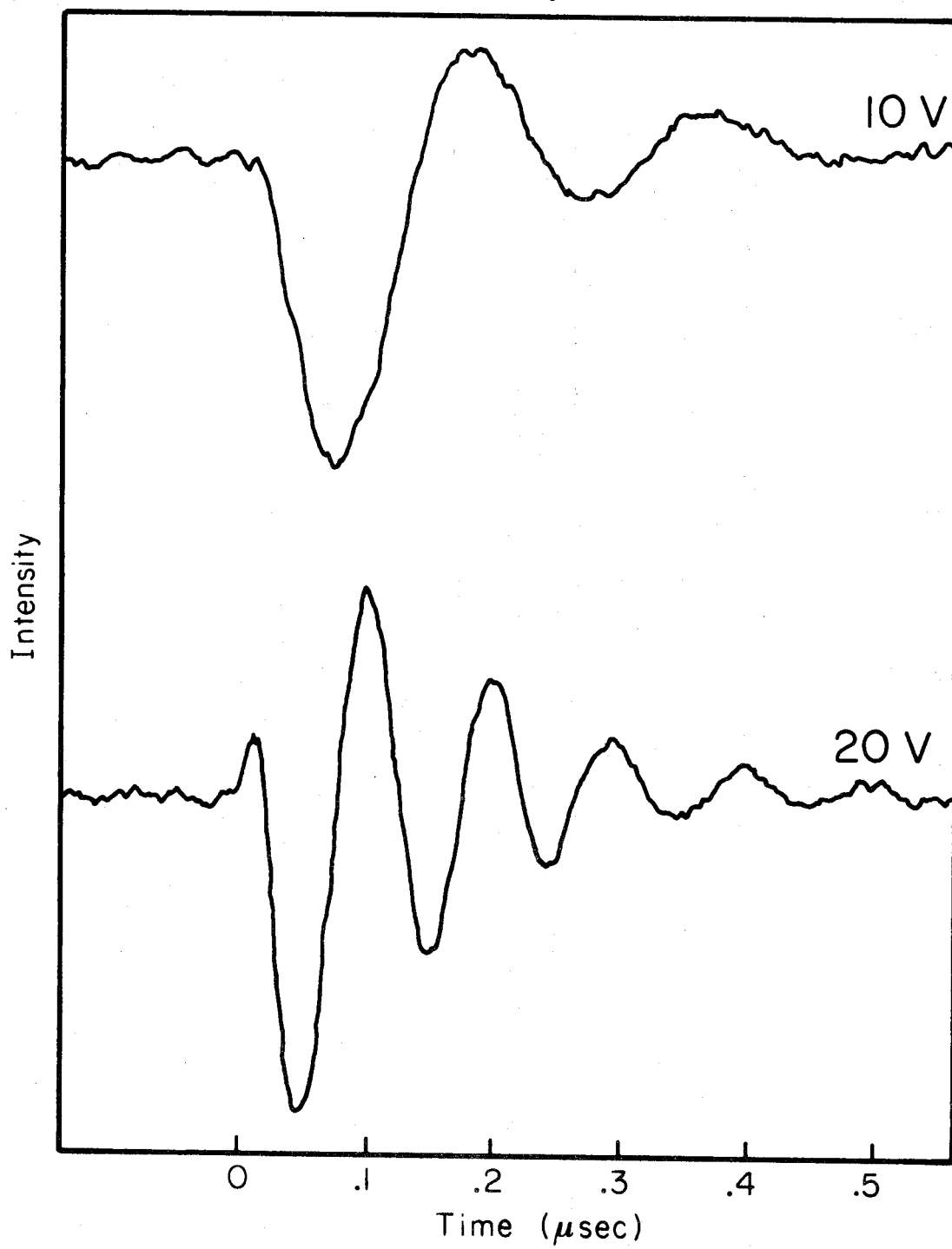


Figure 3

The free induction decay of iodine gas at 0°C coinciding with the leading edge of the EOC pulse. The switching frequency is 5 MHz for the top trace and 10 MHz for the bottom trace. Both transients were obtained at 500 μ W laser power. The singlet-to-triplet transition in resonance with the laser field is $X^1\Sigma_g^+ \rightarrow B^3\Pi_{0_u}^+$. (These data, obtained using improved detectors, replace those shown in the original paper.)

Free Induction Decay: Iodine at 0°C



theories¹⁻³ that already exist about the nature of primary excited states.

We start with the prototype I_2 molecule where we expect a "clean" excitation distribution and minimum vibronic scrambling. Naturally we must consider the Doppler broadening of the transition resonances (T_2^*). Another important system, which certainly is not as simple electronically as iodine, is NO_2 on which decades of work have already been spent to understand its spectroscopy.

The I_2 gas was excited at 5897.5 Å and fig. 2 shows the decay of the iodine on-resonance and off-resonance when the electro-optic switch is modulating the laser beam. The gas pressure was controlled by using different temperature baths at the cold finger. Typically, 30 mtorr was used. At this pressure the IRD was monitored while monitoring the nutation.¹⁰ We also checked the signal at liquid nitrogen temperature and at room temperature and no decay was observed.

5.1 Population Distribution of the Inhomogeneous Ensemble

Two sub-ensembles must be considered in treating the decay and dephasing of the dipoles in the inhomogeneous ensemble. The first group of molecules consists of those that were originally excited by the single mode cw laser. The degree of inversion after long times (compared with relaxation times) can be obtained from eq. (2). On-resonance and if the laser intensity is sufficiently large, $R_3 \sim 0$. Turning the pulse on with $\Delta \gg 1/T_2$, this group of molecules will decay freely while a new group of molecules having

$R_3^0 = -1$, $R_2^0 = R_1^0 = 0$ will be coherently driven. Hence, from eq. (2), one expects the emission intensity, which monitors the diagonal elements of the density matrix, to build up and decay.*

In the iodine case, the IRD fast decay constant was found to be $0.23 \mu\text{s}$ at 105 mtorr. Stern and Volmer¹⁶ have shown that the total decay may be partitioned into a radiative part and another part which measures the number of deactivating collisions. The latter depends on the pressure of the gas and the molecular collision diameter σ . Using our results we obtain a radiative lifetime of $7.5 \times 10^{-7} \text{ s}$ which is in excellent agreement with the results of phase fluorometry¹⁷ done on I_2 gas. By lowering the gas pressure (almost a collisionless gas), the decay time constant gets longer as expected from simple radiationless decay theory. Currently we are investigating the nature of the decay as a function of pressure and laser frequency. This will enable us to establish the relationship between the effective density of states** and the excess rovibronic energy in 3 MHz or less intervals. Hence, the "sparse" intermediate limit¹⁸ (as opposed to the statistical or resonance limits) for the coupling between the prepared state and the rovibronic continua can

*The extension of the formalism to multilevel systems will be reported soon.¹⁵

**The effective density of states here means the product of the actual density of states times the off-diagonal matrix element that connects the primary Born-Oppenheimer state with the continuum.

be clearly identified. The recurrence of the system during the decay is also expected since our switching procedure is, perhaps, fast enough to give the appropriate time resolution. As mentioned before, the IRD experiments were also tried at 77 K and at room temperature (where a very strong emission was seen) and no signal was detected.

For NO_2 the situation is different from iodine. The density of vibrational ground states that are quasi-resonant with the excited level is higher. Moreover, these nonlinear molecules undergo relatively large geometrical changes when excited. This results in a large vibrational Franck-Condon factor which makes the vibronic coupling matrix elements rather large and hence a short decay time is expected. At room temperature the Doppler width of NO_2 near 4880 \AA is $\approx 1 \text{ GHz}$. In our experiments the laser excites NO_2 at 5935.7 \AA where the absorption and fluorescence (0.1 mtorr) at low resolution is known.¹⁹ The coherent decay at relatively high pressure is very fast ($\leq 65 \text{ ns}$) and again disappears at low temperatures. We hope to report soon on the complete study of NO_2 decay characteristics at different pressures and excitation energies.

5.2 Coherent Pumping and the Optical Transition Moment

As we described before [see eq. (2)], in the rotating frame and on-resonance the macroscopic moment will nutate optically at Rabi's frequency.²⁰ Hence, if we know the transition rate for the coherent pumping and the electric field strength at the sample we can compute the transition moment quite easily:

$$(\mu \cdot E_0 / \hbar) = \text{oscillation frequency.} \quad (3)$$

Knowing the laser intensity and measuring the beam diameter in the iodine cell gave $E_0 = 105 \text{ V/cm}$. These preliminary results therefore give $\mu = 0.05$ debye for the resonance transition. To our knowledge this is the first time that this quantity has been measured directly for an electronic transition.

The coherent pumping rate on-resonance can also be used to obtain information about the dipole dephasing processes. From the results of iodine near 0° C , we obtained a pumping rate of $2.1 \times 10^6 \text{ c/s}$ for the molecular packets that are driven on resonance. This value gave a T_2 that predicts a free induction decay time constant of $\approx 0.5 \text{ } \mu\text{s}$ since

$$\frac{1}{\tau} = T_2^{-1} + [T_1 T_2^{-1} \left(\frac{\mu \cdot E_0}{\hbar} \right) + T_2^{-2}]^{\frac{1}{2}}. \quad (4)$$

This is indeed in good agreement with our results (see fig. 3), thus ensuring the self-consistency and showing that this simple technique can be used for examining optical phase coherence and decay processes in excited states.

The coherent ringing and the IRD of pentacene in p-terphenyl clearly indicate that the dephasing of molecular dipoles depends on the phonon population. This was evident from the disappearance of the ringing ($\approx 65 \text{ ns}$) and the decay at high temperatures. We are currently extending the technique to other systems in order to investigate the nature of optical phase coherence in the delocalized states of solids.

ACKNOWLEDGEMENT

One of us (AHZ) would like to thank Kevin Jones for fruitful discussions. The help of Duane Smith and Roy Mead is greatly appreciated. We would like to acknowledge the partial support of the NSF under grant number MPS 73-04613.

REFERENCES

1. R. A. Harris, J. Chem. Phys. 39 (1963) 978; C. A. Langhoff and G. W. Robinson, Mol. Phys. 26 (1973) 249; A. Nitzan, J. Jortner and P. M. Rentzepis, Mol. Phys. 26 (1973) 281.
2. A. Nitzan and J. Jortner, Mol. Phys. 25 (1973) 713; A. Nitzan, S. Mukamel and J. Jortner, J. Chem. Phys. 60 (1974) 3921, and references therein.
3. J. O. Berg, C. A. Langhoff and G. W. Robinson, Chem. Phys. Letters 29 (1974) 305; J. M. Friedman and R. M. Hochstrasser, Chem. Phys. 6 (1974) 155; S. Mukamel and J. Jortner, J. Chem. Phys. 62 (1975) 3609.
4. P. F. Williams, D. L. Rousseau and S. H. Dworketsky, Phys. Rev. Letters 32 (1974) 196.
5. F. Bloch, Phys. Rev. 70 (1946) 460.
6. E. L. Hahn, Phys. Rev. 77 (1950) 297.
7. N. A. Kurnit, I. D. Abella and S. R. Hartmann, Phys. Rev. Letters 13 (1964) 567.
8. N. Takeuchi and A. Szabo, Phys. Letters 50A (1974) 361; T. Aartsma and D. A. Wiersma, Phys. Rev. Letters 36 (1976) 1360.
9. C. L. Tang and H. Statz, Appl. Phys. Letters 20 (1968) 145; G. B. Hocker and C. L. Tang, Phys. Rev. Letters 21 (1969) 591.
10. R. G. Brewer and R. L. Shoemaker, Phys. Rev. A 6 (1972) 2001; R. G. Brewer and A. Genack, Phys. Rev. Letters 36 (1976) 959.

11. S. L. McCall and E. L. Hahn, Phys. Rev. Letters 18 (1967) 908.
12. R. H. Dicke, Phys. Rev. 93 (1954) 99.
13. R. P. Feynman, F. L. Vernon Jr. and R. W. Hellworth,
J. Appl. Phys. 28 (1957) 49.
14. J. Telle and C. L. Tang, Appl. Phys. Letters 24 (1974) 85;
26 (1975) 572.
15. A. H. Zewail, K. Jones and T. E. Orlowski, Phys. Rev., to be
published.
16. O. Stern and M. Volmer, Z. Physik 20 (1919) 183.
17. L. Brewer, R. Berg and G. Rosenblatt, J. Chem. Phys. 38
(1963) 1381.
18. G. W. Robinson and R. P. Frosch, J. Chem. Phys. 38 (1963)
1187; M. Bixon and J. Jortner, J. Chem. Phys. 48 (1968) 715;
D. Chock, J. Jortner and S. A. Rice, J. Chem. Phys. 49 (1968)
610.
19. C. G. Stevens, M. W. Swagel, R. Wallace and R. N. Zare,
Chem. Phys. Letters 18 (1973) 465.
20. R. L. Shoemaker and E. W. van Stryland, J. Chem. Phys. 64
(1976) 1733.

OPTICAL DEPHASING OF SMALL AND LARGE MOLECULES:
COHERENT OSCILLATIONS OF EMITTING MOLECULES *

T. E. Orlowski, K. E. Jones and A. H. Zewail
Arthur Amos Noyes Laboratory of Chemical Physics **,
California Institute of Technology
Pasadena, California 91125

ABSTRACT

We describe the conditions under which large and small molecules may undergo optical dephasing. The relationship between the coherent preparation of excited states and the intramolecular and intermolecular processes are discussed and related to the recent measurements of optical T_1 and T_2 . Finally, we report on the observation of a coherent (oscillatory) transient on the spontaneous emission of iodine gas.

*Chemical Physics Letters, 50, 45 (1977).

**Contribution No. 5585.

1. INTRODUCTION

Recent experiments^{1, 2} have shown that the true molecular eigenstates and the Born-Oppenheimer states of large* molecules (pentacene) can be prepared if the system is excited by narrow or wide band lasers that have well-defined coherence length. It was also found that the optical dephasing time (optical T_2) of the molecular eigenstates in the solid (1.7 K) is almost three orders of magnitude shorter than the spontaneous decay time (optical T_1). This means that the random phase distribution of the excitation (i. e., the analogue of the ergodic limit[†]) is reached much before the system completes its spontaneous decay. Now that we know which state is prepared, one would like to ask the following general questions:

- (1) Does dephasing of homogeneous states occur because of the inhomogeneity of the environment (intermolecular), or does it proceed by intramolecular⁴⁻⁷ radiationless decay, or both?
- (2) How does the preparation of excited states influence the observed optical dephasing?

In this paper we outline the different limits for optical dephasing which depend on whether we prepare the true molecular eigenstates or the Born-Oppenheimer states. It will also be shown that the optical

*Large usually refers to molecules with more than 2 (or 3) atoms.

More precisely, it means that $\hbar\rho/\tau \gg 1$ where τ is the decay time of the zeroth order levels (density ρ) that are located at the energy of the singlet level.

[†]For an excellent review, see ref. 3.

coherence can be monitored directly by monitoring the spontaneous emission of the coherently prepared state. Emission detection of optical coherence (nutration, photon echoes, etc.) can provide T_1 , T_2 and the Rabi frequency ($\mu \cdot \epsilon / \hbar$). In this manner it is easy to distinguish between the coherent oscillations that are due to either the coherent driving of the excited and ground states or to genuine intramolecular dephasing.

2. OPTICAL COHERENCE OF SMALL AND LARGE MOLECULES

Consider a molecule with a state $|s\rangle$ that carries most of the oscillator strength from the ground state $|0\rangle$, and that is imbedded in a manifold of $\{\ell\}$ states. The $\{\ell\}$ states (triplet or hot singlet levels) essentially do not couple radiatively to the ground state. If there were no intramolecular interactions, $v_{s\ell}$, the states, i , are characterized by T_{1i} and T_{2i} . These decay times represent the dephasing times of the levels (T_2 's) and the spontaneous decay times (T_1 's) which contain the radiative and nonradiative (say, the coupling to hot vibrational levels of the ground state) contributions:

$$1/T_1 = 1/T_1^{(r)} + 1/T_1^{(nr)}, \quad 1/T_2 = 1/T_2' + 1/T_1 \quad (1)$$

The total dephasing time contains both the pure dephasing term and the spontaneous loss for the levels involved. Under these conditions, the electric field of the laser (ϵ) couples with the transition moment of the Born-Oppenheimer (BO) state, μ_{0s} , thus recovering the classical two-by-two Rabi limit:

$$\rho = \begin{pmatrix} |0\rangle & & |s\rangle & & \{l\} \\ |c_0|^2 e^{-t/T_{10}} & c_0 c_s^* e^{-i\Delta E_{0s}t} e^{-\frac{1}{2}(\frac{1}{T_{10}} + \frac{1}{T_{1s}})t} e^{-t/T_2'} & 0 \\ \text{c.c.} & |c_s|^2 e^{-t/T_{1s}} & 0 \\ 0 & 0 & 0 \end{pmatrix} \quad (2)$$

where ρ is the density matrix and $|c_i|^2$ is the probability of finding the system in state $|i\rangle$. Note that the diagonal elements are the same as those derived by the effective Hamiltonian method^{4, 7} for isolated molecules with no correlation among the decay channels, e.g.,

$$E_s = \epsilon_s - \frac{1}{2} i/T_1^r - \frac{1}{2} i/T_1^{nr} \quad (3)$$

Therefore in this no coupling limit the system decays by T_1 and dephases by T_2' of the ground and excited ensemble.

Turning v_{sl} on produces the true eigenstates which diagonalize the molecular Hamiltonian⁸:

$$\psi_m = \alpha_{ms} |s\rangle + \beta_{ml} \{ |l\rangle \} \quad (4)$$

Now, if we prepare⁹⁻¹¹ the ψ_m states, we have the same situation as before. The difference, however, will be the change in the transition moment which is now smaller due to the dilution of μ_s amongst the effective $\{l\}$ manifold. Therefore, one expects the Rabi frequency to change to

$$\omega_R^{(m)} = (\alpha_{ms}\mu_{os} + \beta_{ml}\mu_{ol}) \cdot \epsilon/\hbar . \quad (5)$$

The density matrix contains the information about all the levels involved in the coupling and the exact time evolution of it is given by ($\hbar = 1$):

$$i\partial\rho/\partial t = [\mathcal{H}_{BO} + v(s|\ell) - \mu \cdot \epsilon \cos \omega t, \rho] - i\mathcal{R} \cdot \rho , \quad (6)$$

where \mathcal{R} is Redfield's superoperator¹² and contains T_1 and T_2 terms. The intermolecular dephasing of the true molecular eigenstates (TME) can therefore be handled if we assume a large phonon reservoir in solids² or a large reservoir of optically inactive molecules in gases.¹³ As pointed out before, the total rate of dephasing at any temperature T in a solid is given by²

$$\begin{aligned} \Gamma_{\text{total}}(T) = & \frac{1}{2} \left(\frac{1}{T_{1m}} + \frac{1}{T_{10}} \right) T + \frac{\pi}{\hbar} \sum_{p, p'} n_T(p) \\ & \times |\langle m, p' | T | m, p \rangle - \langle 0, p' | T | 0, p \rangle|^2 \delta(E_p - E_{p'}) , \end{aligned} \quad (7)$$

where $|0\rangle$ and $|m\rangle$ are the two states involved and the T_1 terms have a temperature dependence similar to the T_2 terms. This expression which contains the T matrix and the phonon temperature function, n , brings a subtle point about the dephasing of $|m\rangle$ states by the phonons p, p' . If the two levels pumped by the laser have the same scattering amplitude, no loss of coherence is expected by any phase interruption mechanism; only the spontaneous decay will destroy the correlation of the excited ensemble. This implies that electronic dephasing will be faster than IR dephasing and that pure singlet states might have different dephasing rates from those of pure triplet states.

To relate the dephasing of these TME to the original BO states, one uses eq. (7) and the properties of $\mathcal{R}_{f,i',fi}$ between the final and initial states. For example, armed by eq. (7) and using eqs. (4) and (6), one concludes that the intermolecular T_1 dephasing rate is:*

$$\left(\frac{1}{T_1}\right)_{\text{TME}}^m = \left(\frac{1}{T_1}\right)_{\text{BO}}^s \frac{v_{s\ell}^2}{(E_m - E_s)^2 + (\pi v_{s\ell}^2 \rho_i)^2 + v_{s\ell}^2} \quad (8)$$

Eq. (8), which contains the intramolecular density of states ρ_i , gives a Lorentzian distribution for the decay of TME. It is interesting to note that the radiative decay of TME also scales by the same mechanism [see eq. (5)]. Similarly, one obtains expressions for T_2 , which contains the cross terms of α and β .

The preparation of the BO state by broad band excitation^{1, 2} results in an additional channel for the loss of optical coherence. This is because

$$|\langle s | G_m(t) | s \rangle|^2 = \left| \sum_m |\langle m | s \rangle|^2 e^{-iE_m t/\hbar} \right|^2, \quad (9)$$

*In deriving this equation, we have assumed equal level spacing and that the phonon-induced relaxation in the triplet manifold is slower than in the singlet. This is because the energy gap between the excited singlet and triplet states is much smaller than the excitation energy. With this sparse level structure, phonons with a certain frequency spectrum are needed in order to open the vibrational relaxation channels. This, of course, might not be the case in many systems, nevertheless eqs. (7) and (8) point out that the relationship between T_1 and T_2 of the BO and TME states can be obtained using this information.

where G is the molecular propagator; $\exp(-i\mathcal{H}_m t)$. At short times the Fourier integral will therefore give:

$$|\langle s | G_m(t) | s \rangle|^2 = e^{-2\pi v_{sl}^2 \rho_i t}, \quad (10)$$

which is the intramolecular decay that destroys the optical coherence of the BO state that is in quasi-resonance with many states. At longer time the system decays by the radiative lifetime of the state and exhibits oscillations when considering the radiation field in and the Fourier sum of eq. (9). Note that the oscillations depend on the phase angle between $|m\rangle$ and $|m'\rangle$ states. The conclusion of this section indicates therefore that the narrow and wide band excitation of molecules in condensed phases^{1, 2} and in beams^{14, 15} distinguishes¹⁶ the different dephasing processes described above.

3. EXPERIMENTAL

Single modes of a tunable dye laser were used for the high-resolution (better than one part in 10^8) excitation. The incoherent resonance decay (IRD) observed at right-angles to the exciting beam was detected by using a combination of lenses, spectrometer and a photomultiplier, whose output was processed to improve the signal-to-noise ratio. The laser was tuned into or out of resonance by an electro-optical switch.^{17, 18} One pulse and three pulse trains were used to obtain the direct spontaneous decay and the spontaneously detected photon-echo. The details can be found in refs. 18 and 19. The results reported here were obtained from I_2 gas at different pressures, and compared with previous experimental results done on pentacene in p-terphenyl at low temperatures.

4. EMISSION DETECTION OF OPTICAL COHERENCE^{18, 19}

To measure optical dephasing, one must know T_1 and T_2 of the excited ensemble. These relaxation times can be obtained utilizing the optical analogue of coherent NMR spectroscopy. In these experiments, the system is subjected to an intense pulse which forms the coherent superposition of the ground and excited states. The state then decays depending on T_1 and T_2 . This was first done by Hartmann's group who observed photon echoes from ruby at low temperatures.²⁰ The echo which "rides" on a large laser signal is difficult to isolate. Hartmann's pulse sequence was also applied to ionic²¹ and molecular²² systems to obtain T_2 . CW laser excitation¹⁷ has eliminated some of these problems and resulted in the observation of coherent transients in gases,^{17, 18} solids^{23, 24} and molecular beams.^{14, 15} In all these experiments, one monitors the coherent forward signal on the top of the laser.

Recently, we have observed¹⁸ photon echoes on the spontaneous emission of molecules. The system is subjected to three pulses rather than two such that when the echo is formed molecules are burned (into the ground state) leaving a hole in the emission of specific vibrational origin. The three-pulse technique detects as few as 10^6 molecules and does not make demands on the optical quality of the material. The decay of the echo monitored using the diagonal elements of the density matrix (ρ_{ii}) gives T_2 directly. The one-pulse emission, which is also given by ρ_{ii} , gives T_1 of the upper level. However, because the laser is switched into a new group of molecules, the population is driven coherently at the Rabi frequency. This is demonstrated experimentally in figs. 1 and 2 for iodine. Therefore, using the IRD

Figure 1

Top: The observed IRD signal for I_2 at 12 mtorr. The single-mode laser power at 5897.5 \AA was 35 mW and the electro-optic switching frequency was 18 MHz. Bottom: A least squares computer fit for the IRD signal. The fit is excellent and gives a decay time (T_1) of $1.20 \pm 0.02 \text{ } \mu\text{s}$.

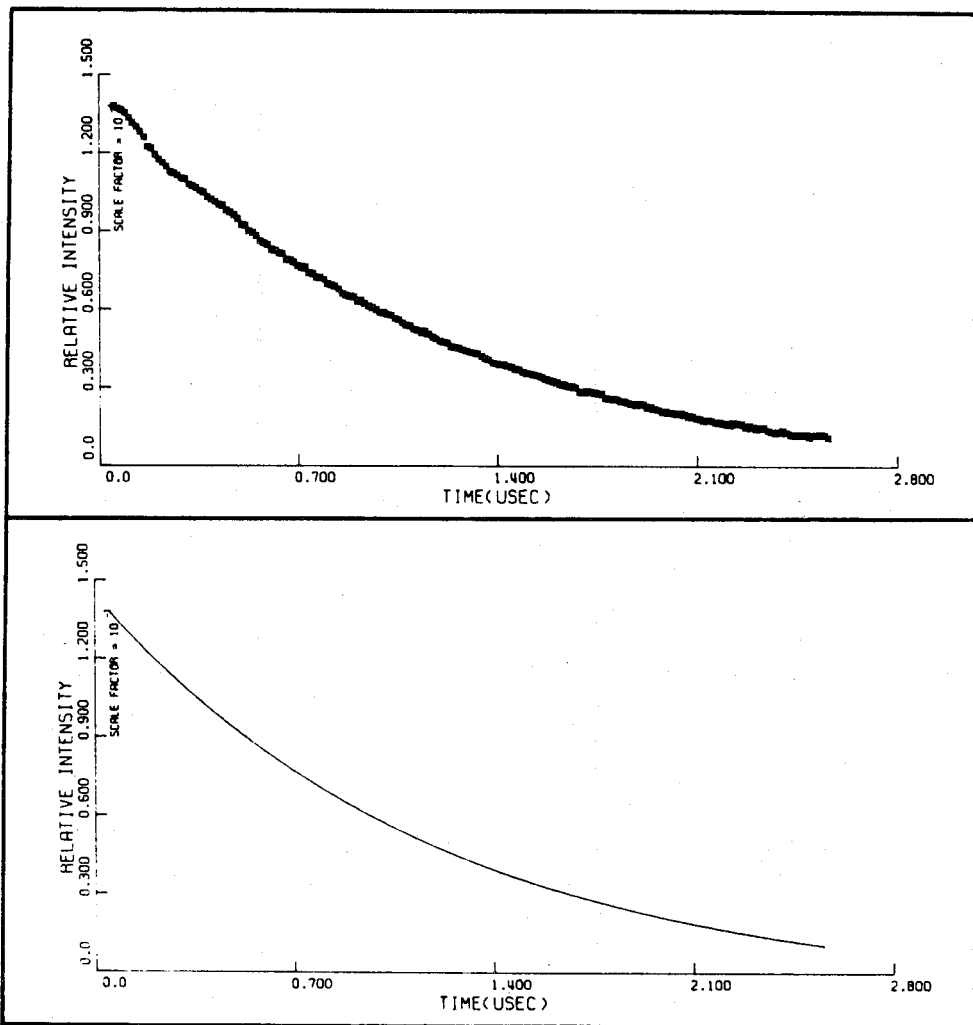
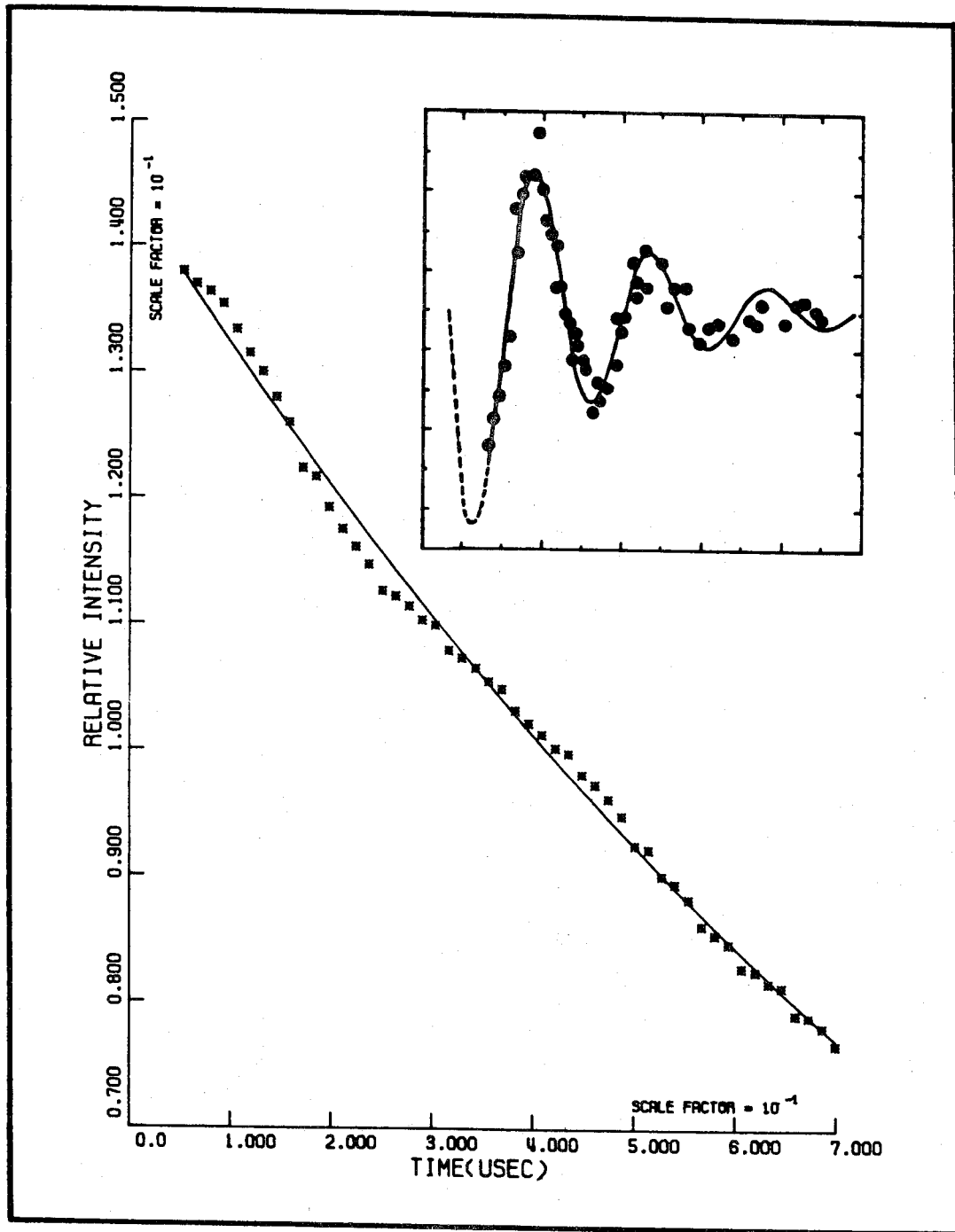


Figure 2

An expanded plot of the IRD signal at short times. The data points clearly show an oscillation pattern while the solid line is the least squares fit for the observed decay. Insert: An enlarged view of the difference spectrum obtained by computer subtraction of the actual data points from the corresponding computer fit (T_1) values. The oscillation frequency is 16.5 ± 1.5 MHz and the damping time is 0.44 ± 0.06 μ s.



technique one can measure $\mu \cdot \epsilon$, the spontaneous decay (T_1) and optical dephasing (T_2) of the transition.

The solution^{14, 15, 25, 26} for eq. (6) including the spontaneous decay ($T_1 \neq T_2$) gives:

$$\begin{aligned} \rho_{ee}(t) &= -\frac{1}{2} \frac{T_1 T_2 (\mu \cdot \epsilon)^2}{1 + T_1 T_2 (\mu \cdot \epsilon)^2} \left[\left(\cos \Omega t + \frac{\sin \Omega t}{\Omega T} \right) e^{-t/T} - e^{-t/T_1} - 1 \right] \\ \Omega &= \left[(\mu \cdot \epsilon)^2 - \frac{1}{4} \left(\frac{1}{T_1} - \frac{1}{T_2} \right)^2 \right]^{\frac{1}{2}} \\ \frac{1}{T} &= \frac{1}{2} \left(\frac{1}{T_1} + \frac{1}{T_2} \right) \end{aligned} \quad (11)$$

which indicates that in addition to the usual T_1 decay, one expects the emission to exhibit a damped oscillatory function that is nutating at the frequency Ω , on resonance. This expression is derived for the cases where the ground state relaxes with the same $1/T_1$ rate as the excited state, a situation that describes the iodine system¹⁷ in these low pressure experiments.

5. COHERENT OSCILLATIONS OF EMITTING MOLECULES

Two distinct kinds of beats are expected on the decay of molecules. The first kind is a genuine intramolecular beating among the molecular levels. As discussed before, this is expected in large molecules when the laser excitation prepares the BO state. In pentacene, however, the IRD did not exhibit this prediction perhaps due to the limited time resolution (≈ 5 ns) of our apparatus. Currently

we are investigating this process using picosecond pulses. The second kind of coherent oscillation on the emission is due to the optical nutation of a homogeneous packet.

Fig. 1 depicts the decay of iodine at 12 mtorr. Shown in this figure is the computer fit for all the data points. The match is excellent and gives $T_1 = 1.20 \pm 0.02 \mu s$. The decay is due to the true molecular eigenstates which have the Rabi frequency of eq. (5). It is also different from the decay that has Zeeman quantum beats due to hyperfine couplings.²⁷ Fig. 2 depicts the short-time region of the decay together with a computer plot for the theoretical curve of ρ_{ee} . The procedure is as follows. The entire experimental curve was fed into the computer to give the best T_1 fit. The computer then subtracted the T_1 curve from the experimental points to give the beat pattern shown in the insert. This pattern gives both the decay of the coherent oscillations and the beating frequency:

$$\Omega = 16.5 \pm 1.5 \text{ MHz}, \quad T = 0.44 \pm 0.06 \mu s . \quad (12)$$

These results, when compared with the dephasing time ($0.55 \mu s$) obtained from the photon echo experiments,¹⁹ indicate that the decay is not totally due to dephasing* and that the oscillation frequency is in excellent agreement with that observed in the nutation of the forward

*In ref. 15 we pointed out the reason behind the mismatch between the value of this decay and that of $\frac{1}{2}(1/T_1 + 1/T_2)$. Basically, the inhomogeneity of the laser and the Doppler averaging are the sources of the inhomogeneous decay which is faster than the intrinsic decay of the coherently excited two level system.

direction at the same laser power density. Moreover, these oscillations describe the true molecular eigenstates and are not due to intramolecular radiationless processes.

6. CONCLUSIONS

This paper emphasizes the different mechanisms for optical dephasing in large and small molecules. Connections with radiationless transition theory were made to describe the relationship between excited state preparation and observed coherent effects. Finally, we reported on the observation of a coherent (oscillatory) transient on the emission of molecular iodine in the gas phase. We believe that these techniques of spontaneously detected coherent optical transients will be useful in probing electronic relaxation processes, and in learning about the origin of energy randomization (dephasing) in molecules.

ACKNOWLEDGMENT

Acknowledgment is made to the donors of the Petroleum Research Fund, administered by the ACS, for partial support of this research. This work was also supported in part by the Research Corporation. We would like to thank J. Jortner for the critical reading of the manuscript and for very stimulating discussions.

REFERENCES

1. A. H. Zewail, T. E. Orlowski and K. E. Jones, Proc. Natl. Acad. Sci. US, 74, 1310 (1977).
2. A. H. Zewail, K. E. Jones and T. E. Orlowski, Spectry. Lett., 10, 115 (1977).
3. R. A. Marcus, Ber. Bunsenges. Physik. Chem., 81, 190 (1977).
4. J. Jortner and S. Mukamel, in "The World of Quantum Chemistry" eds. R. Daudel and B. Pullman (Reidel, Dordrecht, 1974).
5. G. W. Robinson, in "Excited States" (Academic Press, New York, 1974), Vol. 1, p. 1.
6. S. A. Rice, in "Excited States" (Academic Press, New York, 1975), Vol. 2, p. 111.
7. K. F. Freed, Topics Appl. Phys., 15, 23 (1976).
8. M. Bixon and J. Jortner, J. Chem. Phys., 50, 4061 (1969).
9. W. Rhodes, B. R. Henry and M. Kasha, Proc. Natl. Acad. Sci. US, 63, 31 (1969).
10. J. M. Delory and C. Tric, Chem. Phys., 3, 54 (1974).
11. S. Mukamel and J. Jortner, in "Excited States" (Academic Press, New York, 1977), Vol. 3, to be published.
12. A. G. Redfield, Advan. Magn. Reson., 1, 1 (1965).
13. W.-K. Liu and R. A. Marcus, J. Chem. Phys., 63, 272 (1975).
14. A. H. Zewail, Proceedings of the 5th Conference on Chemical and Molecular Lasers; Single-Mode Laser Spectroscopy of Molecules and Molecular Beams, 1977, p. 75.
15. A. H. Zewail, T. E. Orlowski, R. R. Shah and K. E. Jones, Chem. Phys. Lett., 49, 520 (1977).

16. A. H. Zewail, Bull. Am. Phys. Soc., 22, 411 (1977).
17. R. G. Brewer and A. Genack, Phys. Rev. Lett., 37, 959 (1976).
18. A. H. Zewail, T. E. Orlowski and D. R. Dawson, Chem. Phys. Lett., 44, 379 (1976).
19. A. H. Zewail, T. E. Orlowski, K. E. Jones and D. Godar, Chem. Phys. Lett., 48, 256 (1977).
20. N. A. Kurnit, I. D. Abella and S. R. Hartmann, Phys. Rev. Lett., 13, 567 (1964).
21. N. Takeuchi and A. Szabo, Phys. Lett., 50A, 361 (1974).
22. T. Aartsma and D. A. Wiersma, Phys. Rev. Lett., 36, 1360 (1976).
23. A. H. Zewail and T. E. Orlowski, Chem. Phys. Lett., 45, 399 (1977).
24. A. Genack, R. Macfarlane and R. Brewer, Phys. Rev. Lett., 37 1078 (1976).
25. H. C. Torrey, Phys. Rev., 76, 1059 (1949).
26. A. Schenzle and R. G. Brewer, Phys. Rev., A14, 1756 (1976).
27. R. Wallenstein, J. A. Paisner and A. L. Schawlow, Phys. Rev. Lett., 32, 1333 (1974).

SPONTANEOUSLY DETECTED PHOTON ECHOES IN EXCITED
MOLECULAR ENSEMBLES: A PROBE PULSE LASER
TECHNIQUE FOR THE DETECTION OF OPTICAL COHERENCE
OF INHOMOGENEOUSLY BROADENED
ELECTRONIC TRANSITIONS[†]

A. H. Zewail, T. E. Orlowski, K. E. Jones and D. E. Godar

Arthur Amos Noyes Laboratory of Chemical Physics^{††}

California Institute of Technology, Pasadena, California 91125

ABSTRACT

We present a simple and versatile laser technique for the detection of photon echoes in molecular excited ensembles. The method utilizes two optical pulses followed by a third probe pulse which converts the optical polarization induced by the laser into a change in excited population that gives rise to spontaneous emission. This way the photon echo burns the spontaneous emission and does not ride on the top of a large laser signal. The observation thus allows one to untangle the inhomogeneous electronic transitions by monitoring the emission into any vibrational level. The technique is capable of measuring as few as 10^6 molecules and should be applicable to a wide variety of problems in gases and solids that echo on the nanosecond (or perhaps picosecond) time scale.

[†]Chemical Physics Letters, 48, 256 (1977).

^{††}Contribution No. 5509.

1. INTRODUCTION

The discovery¹ of photon echoes, the optical analogue of spin echoes,² has shown that in an inhomogeneous two-level ensemble it is possible to refocus the electric dipole moment that is created by a burst of light capable of tilting the moment ninety degrees into the xy plane of the rotating frame. This is an extremely powerful method for the untangling of inhomogeneous electronic resonances since the photon echo decay time (T_2) provides the homogeneous width directly. The conventional detection of the echo following the two pulse ($\pi/2$ and π) excitation is not that simple, however, because the echo "rides" on the top of an intense light pulse that can overload the detector. Furthermore, the laser beam must traverse optically clear samples, a situation that is not usually encountered especially in studying solid state systems.

In this letter we wish to report on the first observation of photon echoes using a probe pulse technique that is capable of monitoring the in-plane refocusing of the microscopic moments as light emission at right angles to the exciting laser beam. The method utilizes three pulses ($\pi/2, \pi, \pi/2$) rather than two ($\pi/2, \pi$), and exploits the spontaneous emission (not absorption) which can usually be obtained from electronically excited systems in a straightforward manner. The third pulse simply tilts the formed echo from the xy plane to the z-axis. This $\pi/2$ tilting is similar to that done in the detection of spin echoes in excited states.³ The photon echo of the optically pumped two levels can therefore be monitored by detecting the excited state population (diagonal element of the density matrix) which emits

photons in proportion to the magnitude of the echo. The technique offers several advantages. First, the echo can be obtained easily since the total spontaneous emission at right angles to the exciting beam is detected on no background exciting radiation. Because of this high sensitivity, as few as 10^6 molecules can be detected. Second, the technique provides an easy way for detecting the optical coherence (i.e., dephasing and spontaneous processes) in excited ensembles without demands on the "quality" of the material (e.g., solids that do not have good optical properties at low temperatures). Third, this three-pulse photon echo method together with the incoherent resonance decay⁴ (IRD) method, which utilizes only the first $\pi/2$ pulse, give both optical T_1 (radiative and nonradiative) and T_2 (dephasing due to scattering processes) of excited ensembles directly. Finally, photon echoes can now be detected on a given vibronic band of the molecular spectra by monitoring the spontaneous emission which is made sensitive to the laser-induced polarization by the probe pulse.

2. EXPERIMENTAL

Three linearly polarized optical pulses were obtained by driving an intracavity electro-optic crystal (AD*P; dispersion 0.6 MHz/V) with a $\pi/2, \pi, \pi/2$ sequence of voltage pulses. The electro-optic element modulates⁵ the frequency of the single mode of the tunable dye laser according to the voltage applied, without introducing cavity transients.⁶ An intracavity cw laser switching technique⁷ was introduced recently to observe the coherent transients in iodine gas. The method has proven powerful in observing the free induction decay,

photon echoes, and the optical nutation of iodine,⁷ the incoherent resonance decay of gases and solids,⁴ the optical nutation of molecular solids,^{4,8} the free induction decay of ionic crystals,⁹ and free induction decay and IRD in collisionless molecular beams.¹⁰ Our probe pulse technique reported here on iodine gas is done by switching a three pulse train between the homogeneous packets of the Doppler envelope (ca. 400 MHz) using the electro-optic crystal.

The modulated laser beam traverses the iodine cell which has two optical windows at the Brewster angle. The absorption of the forward direction was continuously displayed on an oscilloscope using a p-i-n photodiode while the emission at right angles was monitored by an electrostatically and magnetically shielded photomultiplier (EMI 9558). This is done in order to compare the photon echo decay using the "forward" and "right angle" methods. In all of these experiments, the frequency of the transition at 16951.6 cm^{-1} was monitored using a high resolution spectrometer. The single mode spectrum was seen using a Fabry-Perot interferometer, and its power was measured using a thermopile (Scientech Model 360001). Because the beam has an excellent transverse gaussian profile (measured fwhm = 0.05 cm), the incident power density used in these experiments was up to 18 W/cm^2 .

3. THEORY

Inhomogeneously broadened electronic transitions contain information about both intra- and intermolecular processes. The question of course is how to find and untangle these resonances by

simple optical methods that give both the spontaneous decay and the collision induced dephasing caused by the elastic and inelastic scatterings in gases or solids. In contrast to conventional techniques, the field of nonlinear optical spectroscopy is indeed capable of locating¹¹ very weak transitions and time resolving^{4,7-10} these radiative and nonradiative processes in selectively excited levels. The photon echo decay provides the total dephasing time (T_2) while the incoherent resonance decay gives the optical T_1 directly.

In what follows, we shall discuss the theoretical development necessary to describe the detection of photon echoes with a probe pulse. Although the third pulse makes the physics different, the mathematical approach is that of photon echo theory¹ which closely resembles the conventional theory of spin echoes.²

The description of the echo is simple. For a selective laser excitation between the $|g\rangle$ and excited vibronic level $|v\rangle$ only the two-level polarization and the population difference need to be considered in describing the coherent coupling. The total wavefunction and dipole matrix element of the system can be written as follows:

$$|\psi(r, t)\rangle = a(t)e^{-i\omega_g t} |\psi_g(r)\rangle + b(t)e^{-i\omega_v t} |\psi_v(r)\rangle \quad (1)$$

$$\langle \mu \rangle = \mu_{ab} a(t)b^*(t)e^{+i\Delta\omega t} + \text{c.c.} \quad (2)$$

where $\omega_g = E_g/\hbar$ and $\Delta\omega_t$ is the transition frequency. The cross terms are saying that there is finite polarization induced by the laser even between states of no permanent dipole moment. The response of the system to the first $\pi/2$ pulse turned on at $t = 0$ is to form a

coherent superposition of the ground and vibronic levels which result in a large dipole moment:

$$|\psi(r, 0)\rangle = \frac{1}{\sqrt{2}} [|\psi_g(r)\rangle + i|\psi_v(r)\rangle] \quad (3)$$

Following the π pulse which occurs at say $t = \tau$, the wavefunction of the system becomes

$$|\psi(r, \tau)\rangle = \frac{1}{\sqrt{2}} [e^{-i\omega_v \tau} |\psi_g(r)\rangle + e^{-i\omega_g \tau} |\psi_v(r)\rangle] \quad (4)$$

Now that we reversed the phases, the system continues to develop with the initial characteristics of eq. (1) so that at any time τ' , the wavefunction becomes:

$$|\psi(r, \tau + \tau')\rangle = \frac{1}{\sqrt{2}} [e^{-i\omega_v \tau} e^{-i\omega_g \tau'} |\psi_g(r)\rangle + e^{-i\omega_g \tau} e^{-i\omega_v \tau'} |\psi_v(r)\rangle] \quad (5)$$

This state gives an oscillating polarization (see eq. (2)) which has a maximum value when $\tau = \tau'$ (the echo!) if the transition resonance is inhomogeneous due to Doppler broadening in gases or crystal field effects in solids. The beauty of the echo technique is that the functionality of the decay is independent of these inhomogeneous effects. To give a clear geometrical picture of what happens, let us say that when the system is in the ground state, before turning the $\pi/2$ pulse on, the 2-level molecules will each contribute a vector lying along the $-z$ -axis. In the Feynman-Vernon-Hellworth picture¹² applied to "thin" samples,¹³ this means that R_3 (the population difference which is $bb^* - aa^*$ of eq. (1)) is -1 . The $\pi/2$ pulse will then tilt these "packets" into the xy plane, thus producing the coherent

state (or the super-radiant state¹⁴) described before in eq. (3) using the Schrödinger picture and assuming intense short pulses. Due to the inhomogeneity of the ensemble the system dephases and then rephases after the π pulse. After waiting for the same time it took the system to dephase the echo will be formed since all the packets will be in-phase again. Doing the experiment as a function of waiting period will give the decay of the homogeneous system which is the optical T_2 .

Physically, the probe pulse technique changes the formed echo vector from the xy plane into a vector on the z-axis which, as mentioned before, is proportional to the population difference. It is precisely this action that leads into the detection of the echo by burning the spontaneous emission following the time reversal in the xy plane. Theoretically one must consider the propagation of the polarization as the third probe pulse scans the echo. Defining the duration of the first $\pi/2$ pulse as 0 to t_1 and the π pulse as t_2 to t_3 , the population difference and the laser induced polarization (R_1 , R_2 and R_3 in FVH picture) can be written as:

$$R(t) = \underset{\approx}{G_{t_3}}(E) \underset{\approx}{G_{32}}(\pi) \underset{\approx}{G_{21}}(D) \underset{\approx}{G_{10}}(\pi/2) R(0) \quad (6)$$

where the operation starts with the $\pi/2$ propagator from time 0 to time t_1 . All these operations are 3×3 matrices which describe the pulses, the decay (D) and the echo formation (E) as the polarization evolves in time. Notice the probe pulse will operate on the net component of the polarization to produce R_3 which is related to the population N and the radiative decay of the system.

Because we are switching the laser between two sub-ensembles, the echo shape as a function of the separation τ_2 between the π and probe pulses can be obtained from eq. (6), since every propagator has different boundary conditions. As usual we assume that t_{01} , t_{23} , $t_{\text{pro.}} \ll T_2$, T_1 , and that the molecules that contribute to the formation of the echo see only $\pi/2$ and π pulses.¹⁵ Since the laser pumps a fraction of the inhomogeneous resonance at ω_L the echo shape signal is simply given by

$$S(\Delta, \tau_2, \tau_1) = A e^{-|\tau_2 - \tau_1|/\sigma} e^{-(\tau_2 + \tau_1)/T_2} \cos \Delta(\tau_2 - \tau_1) \quad (7)$$

where Δ is the off-resonance frequency and σ is the echo width in time for a Lorentzian distribution of molecules that are excited by the laser. The constant A is determined by the inhomogeneous resonance shape. This result resembles that obtained for the field created by a polarization in free induction decay theory.¹⁶ One notes that (a) beating at frequency Δ is expected, (b) the maximum of the echo is at $\tau_1 = \tau_2$, (c) the echo shape is essentially a modulated envelope since $T_2 > \sigma$, and (d) the decay of the normalized photon echo signal is independent of the more rapid inhomogeneous dephasing encountered in free induction decay, i. e. ,

$$E(\tau_1 = \tau_2 = \tau) = e^{-2\tau/T_2} \quad (8)$$

4. RESULTS AND DISCUSSION

Fig. 1 depicts the spontaneously detected photon echo in iodine as the probe pulse is swept through the echo position at $\tau_1 = \tau_2 = 180$ ns. As predicted by eq. (7), the beat pattern is clearly seen. At longer

Figure 1

Spontaneously detected photon echo in iodine at 10 mtorr pressure using a three-pulse sequence. Here, $\tau_1 = 180$ ns and τ_2 was scanned to locate the echo. Note the maximum amplitude is at $\tau_2 = 180$ ns where the photon echo burns the spontaneous emission. The switching frequency was determined from the free induction decay monitored in the forward direction. The insert is a least squares fit of the amplitude of the photon echo (at $\tau_1 = \tau_2$) as a function of pulse separation. Note that the echo occurs at τ_2 that is not delayed from τ_1 by $t_1/2$ as in the forward echo case of fig. 2 (see text).

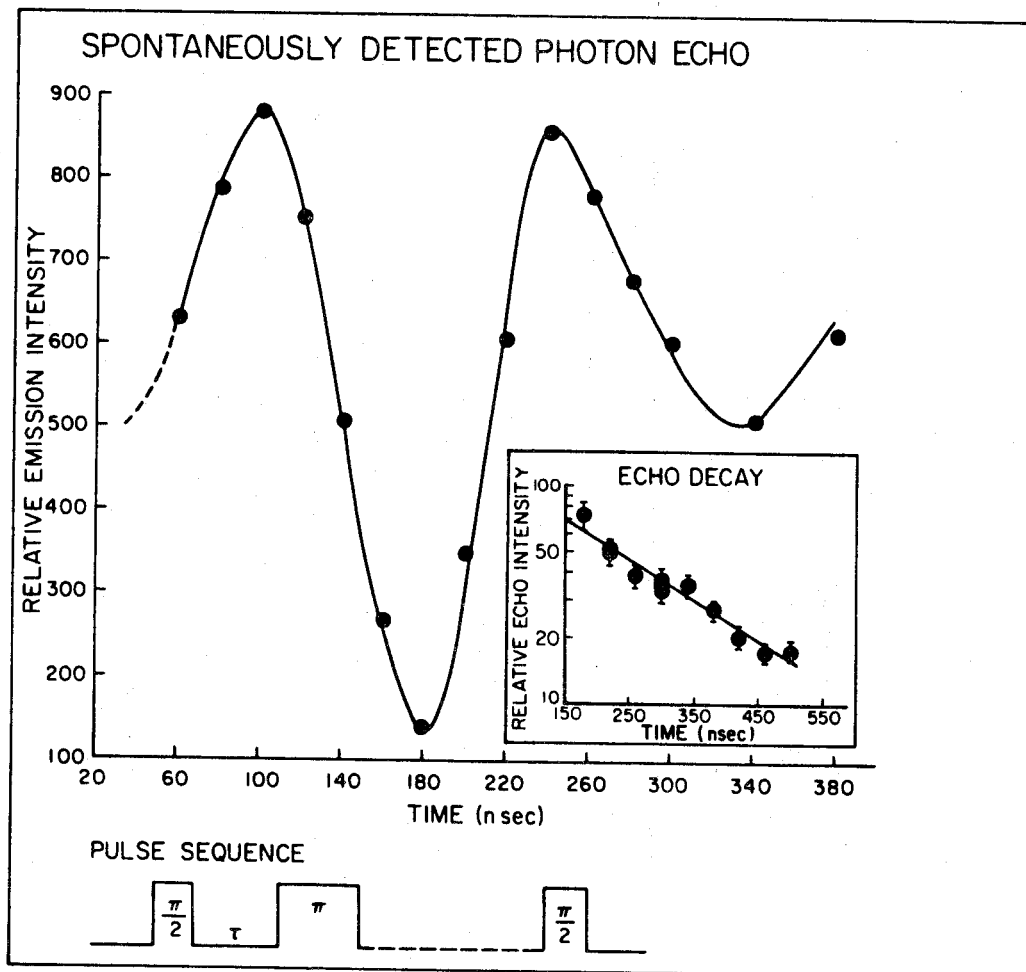
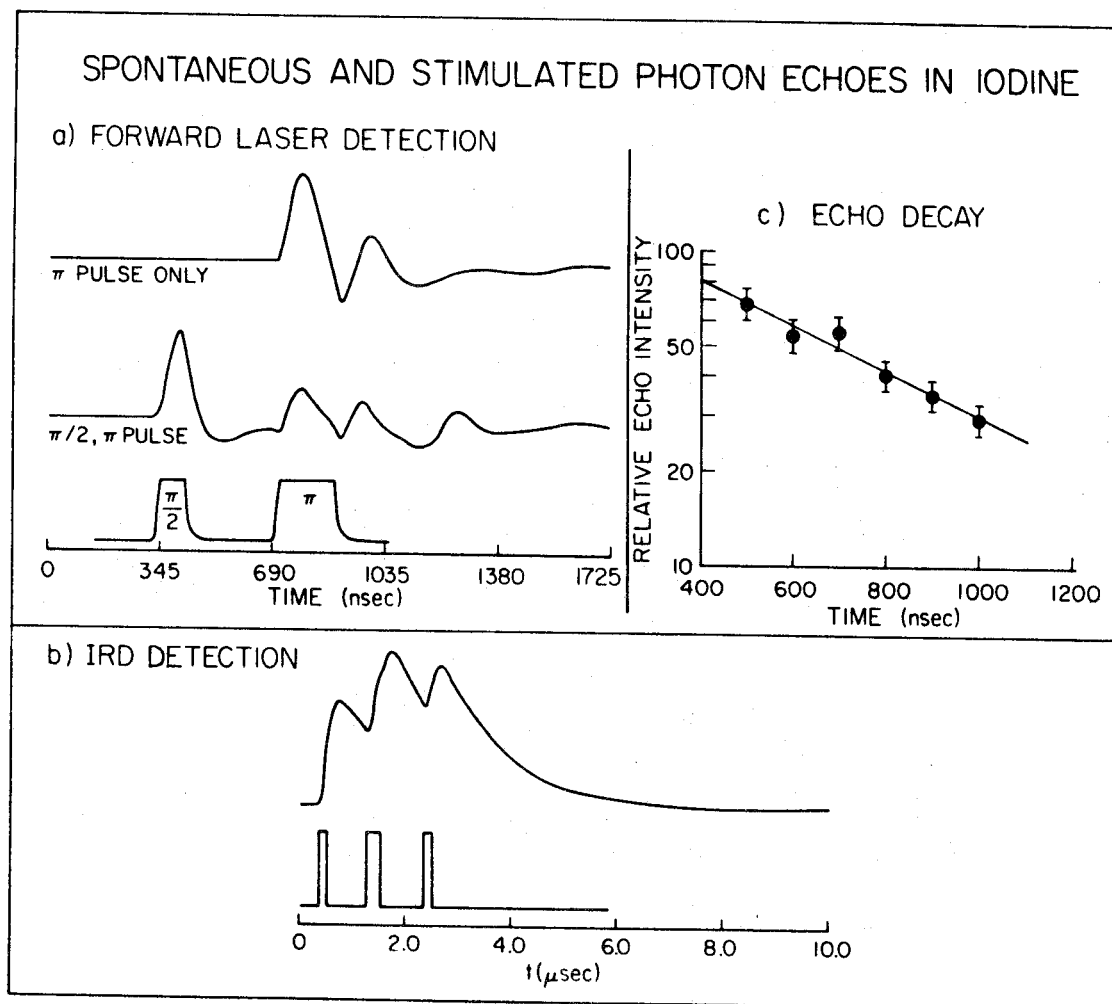


Figure 2

(a) The photon echo in iodine monitored in the forward direction using a two-pulse sequence.⁷ Note the absence of the echo when the $\pi/2$ pulse is eliminated. (b) The three-pulse incoherent resonance decay monitored at 90° to the exciting laser beam. (c) The photon echo decay in the "forward" direction. It should be mentioned that the traces in this figure are raw data.



times τ and large Δ , up to eight oscillations have been observed. The decay of the echo follows eq. (8) (see fig. 1) and at 10 mtorr gas pressure we found that $T_2 = 500 \pm 50$ ns. The time resolved three-pulse IRD together with the photon echo observed in the forward direction by only two pulses is shown in fig. 2. The decay of the "forward" echo gives T_2 which is in agreement with previous work⁷ and with the probe pulse results.* Because the laser is pumping two levels (excited, e, and ground, g) T_2 is the sum of the pure phase interruptions ($1/T'_2$) and the spontaneous decay terms, i.e.,

$$\frac{1}{T_2} = \frac{1}{T'_2} + \frac{1}{2} \left(\frac{1}{T_{1e}} + \frac{1}{T_{1g}} \right) \quad (9)$$

Using one pulse the IRD gives $T_{1e} = 1.08 \mu s$ at 10 mtorr for the transition which has a dipole of ca. 0.05 D.⁴ Recent molecular beam and bulb results¹⁰ indicate that in the collisionless regime $T_{1e} = 1.24 \mu s$. Since the ground state radiative decay rate is essentially zero the echo decay is

* The decay of the echo in the forward direction at this pressure gives $T_2 = 0.6 \pm 0.1 \mu s$ which compares with that obtained from the IRD. The relatively large error in these results is caused by the choice of the base line which is sensitive to the beat pattern of the echo.

given by*

$$\left(\frac{1}{T_2}\right)_{\text{echo}} = \frac{1}{\tau_{\text{coll}}} + \frac{1}{2} \frac{1}{T_{1e}(r)} \quad (10)$$

where the rate of collision-induced decay is simply $\tau_{\text{coll}}^{-1} = \gamma_{\text{coll}} = \gamma_d + \frac{1}{2}(\gamma_{1e}^{\text{nr}} + \gamma_{1g}^{\text{nr}})$. Therefore the radiative and nonradiative broadenings of the homogeneous resonance ($X^1\Sigma_g^+ \rightarrow B^3\Pi_{0+}^+$) in iodine are 128 kHz and 451 kHz, respectively. This total homogeneous width of 579 kHz is much smaller than the ca. 400 MHz inhomogeneous width which corresponds to a dephasing time of 796 ps. Furthermore, if we assume that at this low pressure the excited state nonradiative decay due to quantum jumps into radiative levels is small and that the ground state nonradiative decay time is relatively long, one concludes that the broadening due to pure dephasing and nonradiative processes is 413 kHz and 38 kHz, respectively. This means that 71% of the width is due to dephasing. Note that the echo measurements of T_2 should not be sensitive to effects due to power broadening as in CW frequency scan techniques. The overall elastic scattering which leads to phase interruptions is determined by the microscopic anisotropy of the scattering events in the ground and excited states. On the other hand, the inelastic loss is due to collision-induced radiationless deactivation.

*The spontaneous radiative decay of the $\nu = 2$ rovibronic level into other levels is much smaller than that of the electronic level at 16951.6 cm^{-1} because in the optical region the density of states in the radiation field is much higher.

As expected, therefore, the echo amplitude must decrease when the gas pressure increases, as confirmed experimentally* by the three-pulse echo (see fig. 1).

The echo position in all our measurements is in good agreement (to within $\approx 3\%$) with the predicted value**. The duration of the echo σ is also consistent with the theory. Several features of the echo are noteworthy. First, we have demonstrated that the echo disappears when the probe pulse is not in the train. This is because the detector at right-angles to the laser beam cannot see the in-plane polarization. Second, the echo amplitude decreases when the pulse width and/or the optical field E_0 is changed from optimum values. This is due to the change in the areas of the $\pi/2$ and π pulses which is given by $(2\pi/\hbar) \int_{-\infty}^{\infty} E_0 dt$. Finally, the quantum beats seen on the echo shape, as predicted by eq. (7), follow the beats of the free induction decay that we observed in the forward direction of the laser. This beating among the packets (which may or may not have hyperfine sub-structure) suggests that the technique can be used to obtain optical Fourier transform spectroscopy in excited states, since the different subgroups

* The echo amplitude was decreased by approximately a factor of 3 when the pressure in the cell increased by a factor of 3.

** Because the off-resonant packets have their effective field (FVH picture) tilted from that of the on-resonance packet, one can show that the delay caused by the first $\pi/2$ is cancelled by the last $\pi/2$ pulse. Thus the echo does not occur at $t_3 + t_2 - t_1 + (\approx t_1/2)$.¹⁷

after the first $\pi/2$ pulse will essentially go in and out of phase with each other (in the xy plane) at a rate determined by the difference in Larmor frequencies.¹⁸

Finally, a wide variety of experiments using this spontaneous detection of photon echoes are now in progress. These include forced transitory precession, rotary echoes and multiple pulse trains which will be valuable in resolving intra- and intermolecular radiationless processes that may or may not care about phase coherence. The technique will obviously be extended to solids which echo on the nanosecond time scale. Furthermore, we believe that the method is extremely powerful for observing coherent transients on the picosecond time scale. We are currently investigating the feasibility of the measurement using tunable picosecond lasers.¹⁹

ACKNOWLEDGEMENT

This work is supported in part by the Research Corporation, The United States Energy Research and Development Administration, and the Sloan Fund. We would like to thank D. Smith and R. Mead for their help in these experiments.

REFERENCES

1. N. A. Kurnit, I. D. Abella and S. R. Hartmann, Phys. Rev. Letters 13 (1964) 567; Phys. Rev. 141 (1966) 391.
2. E. L. Hahn, Phys. Rev. 80 (1950) 580.
3. W. G. Breiland, C. B. Harris and A. Pines, Phys. Rev. Letters 30 (1974) 158.
4. A. H. Zewail, T. E. Orlowski and D. R. Dawson, Chem. Phys. Letters 44 (1976) 379.
5. J. Telle and C. L. Tang, Appl. Phys. Letters 24 (1974) 85; 27 (1975) 572.
6. A. Yariv, Proc. IEEE 52 (1964) 6.
7. R. G. Brewer and A. Genack, Phys. Rev. Letters 37 (1976) 959.
8. A. H. Zewail and T. E. Orlowski, Chem. Phys. Letters 45 (1977) 399; A. H. Zewail, Proc. SPIE, Unconventional Spectroscopy 82 (1976) 43.
9. A. Genack, R. M. Mcfarlane and R. G. Brewer, Phys. Rev. Letters 37 (1976) 1078.
10. A. H. Zewail, T. E. Orlowski, R. R. Shah and K. E. Jones, Chem. Phys. Letters, submitted for publication; Phys. Rev. Letters, submitted for publication.
11. R. L. Swofford, M. E. Long and A. C. Albrecht, J. Chem. Phys. 65 (1976) 179, R. M. Hochstrasser, H. N. Sung and J. E. Wessel, J. Chem. Phys. 58 (1973) 4694; P. R. Monson and W. M. McClain, J. Chem. Phys. 53 (1970) 29.
12. R. P. Feynman, F. L. Vernon Jr. and R. W. Hellworth, J. Appl. Phys. 28 (1957) 49.

13. S. L. McCall and E. L. Hahn, Phys. Rev. Letters 18 (1967) 908.
14. R. H. Dicke, Phys. Rev. 93 (1954) 99.
15. J. C. Mc Gurk, T. G. Schmalz and W. H. Flygare, Advan. Chem. Phys. 25 (1974), and references therein.
16. R. G. Brewer and R. L. Shoemaker, Phys. Rev. A 6 (1972) 2001; F. A. Hopf, R. F. Shea and M. O. Scully, Phys. Rev. A 7 (1973) 2105.
17. A. L. Bloom, Phys. Rev. 98 (1955) 1105; S. Fernbach and W. G. Proctor, J. Appl. Phys. 26 (1955) 170.
18. W. B. Mims, Phys. Rev. B 5 (1972) 2409; L. G. Rowan, E. L. Hahn and W. B. Mims, Phys. Rev. 137 (1965) A61.
19. C. V. Shank and E. P. Ippen, Appl. Phys. Letters 24 (1974) 373.

HIGH-RESOLUTION TIME RESOLVED SPECTROSCOPY OF
COLLISIONLESS MOLECULAR BEAMS:
OPTICAL T_1 AND T_2 [‡]

A. H. Zewail, T. E. Orlowski, R. R. Shah and K. E. Jones
Arthur Amos Noyes Laboratory of Chemical Physics^{†‡},
California Institute of Technology, Pasadena, California 91125

ABSTRACT

We report on the observation of the coherent and incoherent transients of collisionless molecular beams using single-mode laser spectroscopy. The technique offers a resolution of one part in 10^8 , and resolves the spectra on the time scale of nanoseconds. The method is demonstrated on an effusive beam of iodine. Since the beam is collisionless the optical dephasing of the selectively excited (10^{-4} cm^{-1}) molecular packet can be directly related to the zero-pressure optical T_1 obtained from the Stern-Volmer relationship of iodine gas in a bulb. Finally, the cross section for the radiationless and radiative deactivation are reported and related to the free-induction decay (FID) of the coherently excited molecular beam.

[‡]Chemical Physics Letters, 49, 520 (1977).

^{†‡}Contribution Number 5500.

1. INTRODUCTION

Molecules that are driven by an intense laser field undergo the well-known Rabi oscillations. This means that the system visits the ground and the excited state at a frequency determined by the dipole moment (μ) of the transition and the electric field amplitude of the laser (E_0). Damping of this coherent transient depends on both the optical spontaneous (T_1) and the dephasing (T_2) processes.

These optical relaxation rates, T_1 and T_2 , are macroscopic and represent the contribution of many different effects such as the natural broadening due to the finite lifetime of the state,¹ the Lorentz² broadening due to collisions in mixed ensembles, the Holtsmark³ broadening due to collisions among the molecules of the same kind and finally the broadening due to collisions with ions and electrons (Stark effect). In addition to the homogeneous processes which are caused by hard and/or soft collisions, one must consider two effects that contribute to the measurement of ensemble coherence, the laser coherence and the inhomogeneous Doppler effect.

Molecular beam techniques,⁴⁻¹⁰ on the other hand, eliminate many of the broadening mechanisms described above. Specifically, the pressure broadening and the pressure induced energy shifts are absent in collisionless molecular beams. This means that the destruction of optical phase coherence in beams will result only from the spontaneous decay of the system and the intramolecular processes that cause phase interruptions. However, Doppler dephasing in beams, which is not as large as in bulbs, is still finite especially in nozzle

jet sources. The Doppler width in the bulb $\Delta\nu_D = 2\nu_0 (2\ln 2kT/mc^2)^{\frac{1}{2}}$ is reduced in an effusive beam to

$$\delta\nu = \nu \alpha \frac{\bar{v}}{c} \quad (1)$$

where $\delta\nu$ is the residual Doppler broadening and \bar{v} is the average velocity of the beam. The angular aperture α depends on the geometry of the beam apparatus (collimation ratio, etc.).

Conventional laser excitation of the Doppler components in the beam yields the spontaneous decay rates but not the rates for the loss of phase coherence. Furthermore, in "large molecule" spectroscopy the preparation¹¹ of excited states and the laser coherence are very important in determining the decay characteristics of the state. In fact, the high resolution and low resolution excitation of pentacene gave totally different emission rates to the ground state. Thus, in order to separate the intra- and intermolecular decay channels, one would like to investigate the decay behavior of collisionless beams by (a) preparing the true eigenstates and not a mixture, and (b) examining the optical coherence of the molecular beam.

In this paper we will present a method for obtaining the high-resolution time resolved spectra of molecular beams using single mode laser excitation. Because of the sensitivity of the technique, we were able to observe, for the first time, the optical free induction decay in molecular beams. The time-resolved spectra (nanoseconds) which manifest the optical coherence and the incoherent decay can be obtained following the selective (one part

in 10^8) excitation by the laser. We demonstrate the method on an effusive beam of iodine and compare the results with the decay in the bulb which gives the cross section for the radiationless quenching of excited states. Furthermore, it will be shown that the phase coherence and the spontaneous decay times are related because the beam is collisionless.

2. OPTICAL COHERENCE OF MOLECULAR BEAMS

Consider a two level system of a molecular packet in a beam. The state $|a\rangle$ and the excited state $|b\rangle$ are coupled by the laser to form the following coherent superposition of states:

$$\psi(t) = c_a e^{-i\omega_a t} |a\rangle + c_b e^{-i\omega_b t} |b\rangle \quad (2)$$

The time evolution of the electron density is therefore infinite and only depends on the energy difference between the ground and the excited states $E_0/\hbar = \omega_0$. The two relaxation rates (T_1 and T_2) are usually added to the formalism by (a) using the Weisskopf-Wigner¹² approximation for the damping of the diagonal elements of the density matrix (population density), and (b) incorporating the dephasing processes T_2 as a frequency fluctuating term on the off-diagonal elements of the density matrix ρ . In what follows we will use the rotating wave approximation and the Feynman-Vernon-Hellworth (FVH)¹³ picture which defines the following \underline{r} vector in terms of the elements of ρ :

$$\underline{\underline{r}} = \begin{bmatrix} r_1 \\ r_2 \\ r_3 \end{bmatrix} = \begin{bmatrix} \rho_{ba} + \rho_{ab} \\ i(\rho_{ba} - \rho_{ab}) \\ \rho_{bb} - \rho_{aa} \end{bmatrix} \quad (3)$$

The component r_3 is the population difference between the two levels while r_1 and r_2 are the components of the laser induced polarization in the medium. Considering "thin" samples where the propagation effects are negligible, the time evolution of ρ is given by $[\hbar = 1]$

$$i \frac{\partial}{\partial t} \rho = [(\mathcal{H}_0 - \underline{\underline{\mu}} \cdot \underline{\underline{E}}_0 \cos \omega t), \rho] - i \mathcal{R} \cdot \rho \quad (4)$$

where \mathcal{R} is the relaxation super-operator (Redfield's relaxation matrix),¹⁴ and ω is the frequency of the laser.

In a collisionless molecular beam, $T_2 = 2T_1$ for any specific laser excitation. With the optical resolution we have with the single-mode of the laser, eq. (4) can easily be solved.¹⁵ In the beam we assume that the ground state feeding rate and the excited state loss rate are equal when the ground state is fed by direct spontaneous decay or by new molecules entering the laser beam with certain velocities. Furthermore, we assume that the equilibrium population value for the $|b\rangle$ level is zero. This is certainly the case in the optical frequency range since the thermal population of $|b\rangle$ is negligible.

The method we describe in this paper monitors two sub-ensembles, α, β ; those which are on-resonance with the laser field, i.e., $\omega = \omega_0$, and those which are off-resonance, i.e., $\omega - \omega_0 > 1/T_2$. Therefore, using eq. (4), the complete solution for the density matrix of both α and β is:

$$\rho_{bb}^{\alpha}(t) + \rho_{bb}^{\beta}(t) = - \frac{\Omega'^2 T_1^2}{1 + 2\Omega'^2 T_1^2} \left[\left(\cos \Omega t + \frac{\sin \Omega t}{\Omega t} \right) e^{-t/T} - e^{-t/T_1} - 1 \right] \quad (5)$$

where $T = \frac{2}{3} T_2$ and $\Omega' = (\mu \cdot E_0)$, and $\Omega = [\Omega'^2 - \frac{1}{4} T_2^{-2}]^{\frac{1}{2}}$ on resonance.

The above results indicate that the emission decay of the beam will give the natural width of the resonance and also the dipole moment of the transition. The modulation depth of the decay, however, does not only depend on Ω but also on the averaging¹⁶ over the inhomogeneity of the laser and the Doppler spread as in the case of optical nutation. It should be added that the boundary conditions invoked in deriving eq. (5) are $r_3^0 = -1$, $r_2^0 = r_1^0 = 0$ for the sub-ensemble that is unexcited (off-resonance), while the pumped sub-ensemble has the steady state value of r .

3. THE IRD METHOD¹⁷ IN BEAMS AND BULBS

The coherent transients of I_2 molecules in a bulb were recently observed by the laser switching method.¹⁸ The technique allows one to detect the optical transients in the forward direction of the laser beam. This resulted in the first observation of optical nutation^{17,19} and the free induction decay²⁰ in solids. The incoherent resonance decay method is different. The IRD technique¹⁷ monitors the emission at right angles (not absorption) to the exciting laser beam whose single-mode frequency can be tuned on or off-resonance with the homogeneous packet of the excited ensemble. This way one obtains T_1 and T_2 directly.²⁸

The tunable dye laser excites the beam molecules at right angles to the generation axis. The beam is effusive with an average

velocity of 1.6×10^4 cm/s. The intracavity electro-optic²¹ switching of the laser single mode (6 MHz) is done by an AD*P crystal. When the laser is on resonance a steady state emission is observed. Switching the laser off-resonance gives the absorption of the newly driven molecules and the decay of the now off-resonant molecules. The emission and absorption of the beam following the laser switching is monitored by an electrostatically shielded photomultiplier and a photodiode, respectively. The output signal is then processed to improve the signal-to-noise ratio. For more details see refs. 17, 22. Typical results are shown for the I₂ beam and bulb in figs. 1-3.

3.1 Bulb Experiments

In these experiments the clean iodine bulb with greaseless teflon stopcocks is evacuated to 3×10^{-6} torr. The cell is heated to 100° C for twelve hours to drive off water and adsorbed gases from the cell walls. Mallinckrodt analytical reagent grade I₂ is then distilled into the cell cold finger which is cooled in an ice bath. After one hour the distillation arm is sealed off and the cell cold finger is then cooled to -78° C in a dry ice acetone bath. Finally, the cell is evacuated to 3×10^{-6} torr and sealed off from the vacuum manifold. The pressure is regulated by controlling the temperature of the side arm of the bulb. The above treatment is carried out to avoid contamination which causes unwanted quenching of iodine and results in a shorter IRD.¹⁷

The IRD in the bulb is analyzed at each temperature. The results shown in fig. 1 give the standard deviation of the least

Figure 1

The resonance decay and optical free induction decay of the coherently excited I_2 beam. The top two traces were taken with an electro-optic voltage of 50 and 0.2. The bottom trace was taken when the laser was off-resonance with the beam. The background pressure during all these measurements was 3×10^{-6} torr. The insert in this figure shows the optical free induction decay signal. As expected, the beat signals which disappeared in the absence of I_2 follow the electro-optic switching frequency. Of course, the signal disappears when the laser is blocked. The least squares fitting of all the data points gave a single exponential whose time constant is determined by T_2 and the Rabi frequency. The Rabi frequency in the beam was computed by measuring the nutation frequency of the bulb and scaling it by the square root of the power density ratio (beam-to-bulb).

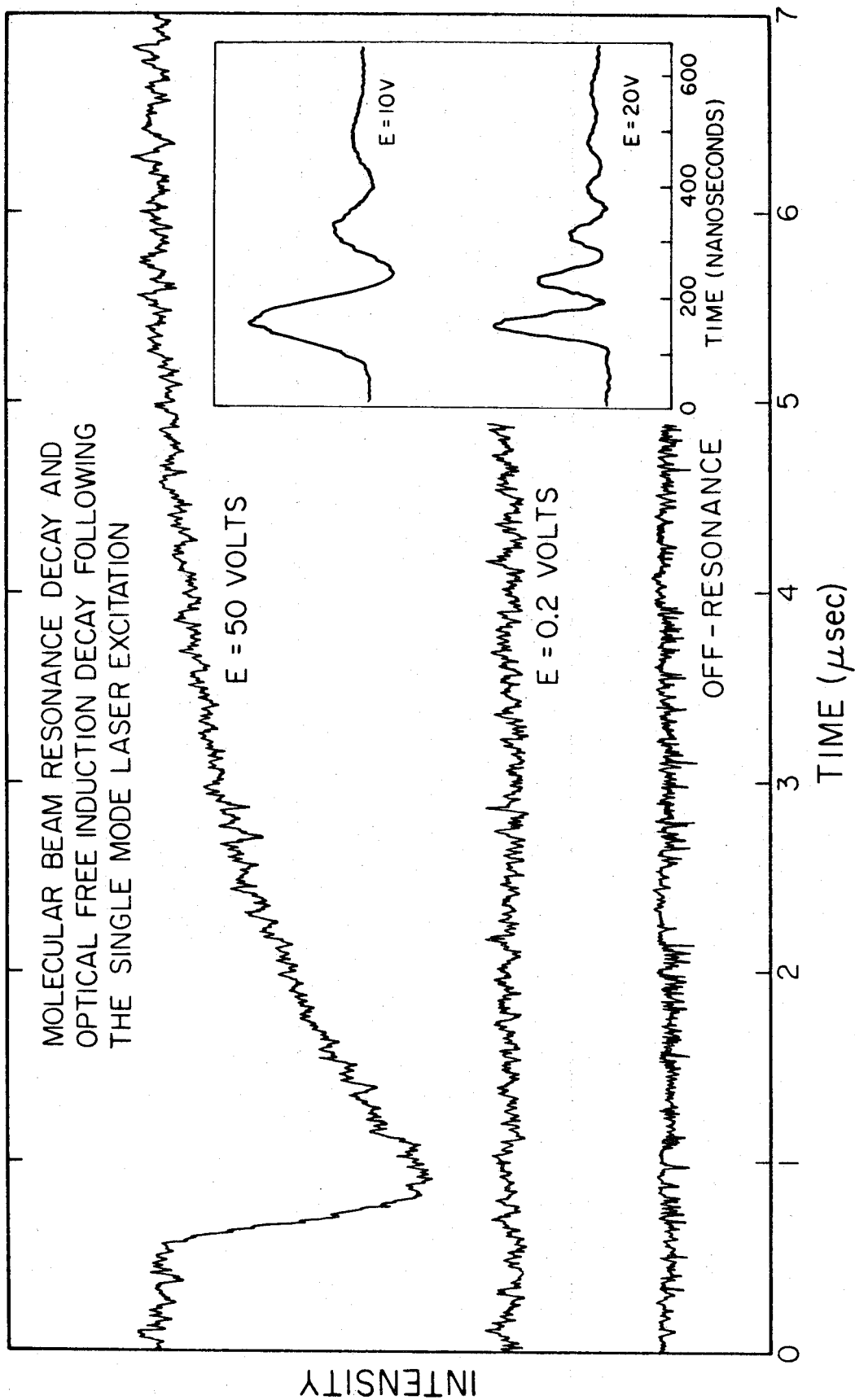


Figure 2

Stern-Volmer plot of the incoherent resonance decay in an iodine bulb. The least squares fit at each reported pressure gives the standard deviation (error bars). The value of T_1 at zero pressure was obtained after least squares fitting of all the data points.

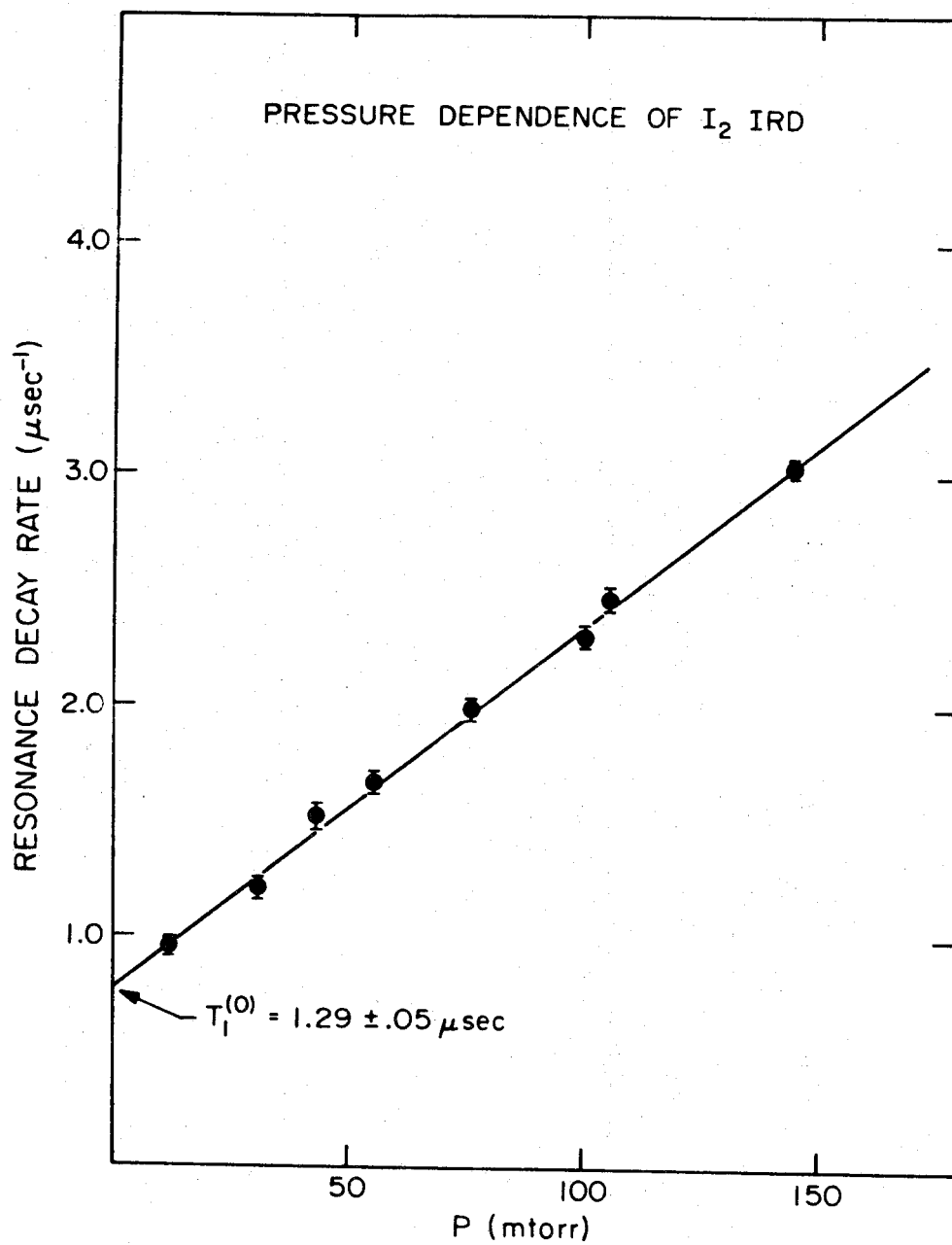
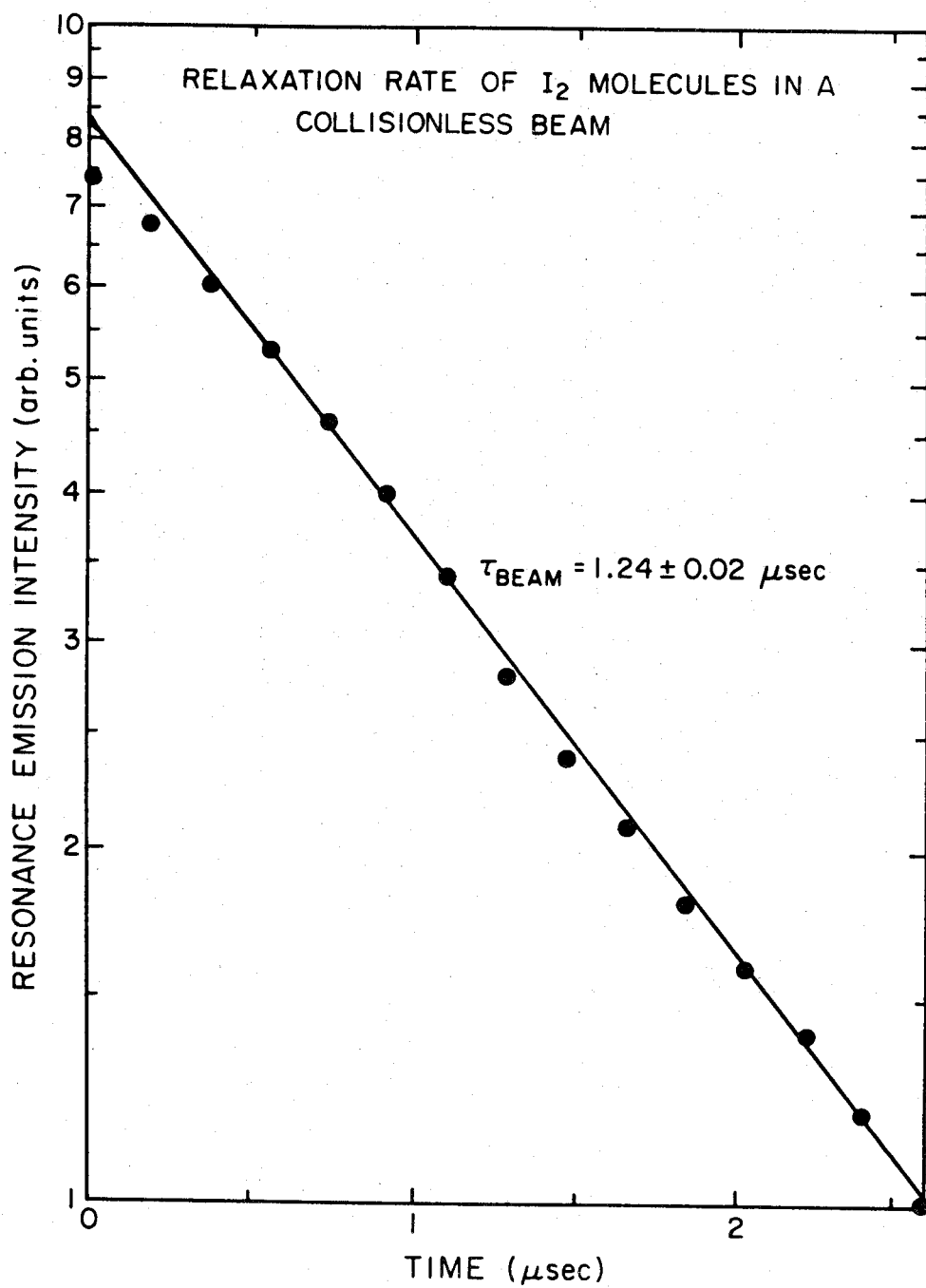


Figure 3

The transient decay of iodine in a molecular beam. The reported decay constant is obtained by least square fitting the data points of the entire wave form. Comparison of this result with the bulb result indicates that the beam is collisionless in nature. It should be mentioned, however, that soft collisions might not influence T_1 but change T_2 .



squares fit at each pressure, and show that

$$\frac{1}{T_1} (\mu\text{sec}^{-1}) = 0.775 \pm 0.029 + (0.0158 \pm 0.0004)P \quad (6)$$

where P is in millitorr. Two observations can be made from these results. First, the natural radiative decay time of the selectively excited state is $1.29 \pm 0.5 \mu\text{s}$ which gives a homogeneous linewidth of $123 \pm 5 \text{ kHz}$. Secondly, the quenching cross section for the pressure induced broadening is $\sigma^2 = 70 \pm 2 \text{ \AA}^2$. Knowing the exact radiative lifetime from the Stern-Volmer plot and the beam experiments, we concluded that Q' (specific quenching rate times the radiation lifetime) is 3.6×10^5 liter/mole. This means that the collision efficiency is 1.1 considering the long-range energy correction to the hard sphere cross section of the Lennard-Jones potential.

3.2 Beam Experiments

The transient following the electro-optic switching of the laser out of the transition frequency of the beam is shown in fig. 1. The IRD signal is not seen when the switching frequency is below 0.3 MHz which is close to the width of the homogeneous resonance. Fig. 1 also depicts the absence of the signal when the laser is off-resonance. The on- and off-resonance conditions are also checked by observing the emission of I_2 in the bulb.

Since $\mu \cdot E_0$ (laser power is up to 100 mW) is much larger than T^{-1} , eq. (5) predicts a fast build up for the absorption which reaches the saturation limit, and a decay determined by T_1 . The coherent oscillation seen²³ on the IRD of clean iodine samples is not observed in the beam because the depth of these oscillations is very small (due

to the power and Doppler averaging) and a high S/N waveform is therefore needed. As in the optical nutation, the averaging of eq. (4) must be taken into consideration. To illustrate the point we solve this equation analytically for the case of $T_1 = T_2 = T$. Knowing that our laser beam has an excellent transverse gaussian profile, i.e., $E_0(R) = \epsilon_0 \exp(-R^2/w)$, the averaged diagonal elements of $|b\rangle$ in the beam are given by:

$$\langle \rho_{bb}^{\alpha}(t, E_0(R)) + \rho_{bb}^{\beta}(t, E_0(R)) \rangle_R = \left\{ a_1 \left[\frac{\sin x_1 t}{t} - \frac{\sin x_2 t}{t} \right] + a_2 \left[\text{Si}(X) \right] \frac{x_1 t}{x_2 t} + a_3 \right\} e^{-t/T} \quad (7)$$

where a_1 , a_2 and a_3 are constants and the function $\text{Si}(X)$ is the sine integral whose argument depends on $x_1 (= \mu\epsilon_0 + \beta^{-1})$, $x_2 (= \beta^{-1})$ and the time t . The important point is that the spatial averaging drastically smooths the oscillatory character of eq. (5) which describes the IRD pattern. This is because the sine integral behaves like a damped sinusoid,^{*24} and because the first term in the above equation damps as $1/t$. The nutation frequency is slightly modified by the very small value of β^{-1} . It should be noted, however, that even in the presence of the oscillations, the overall decay will still give T_1 . We therefore conclude that for I_2 in a collisionless beam

$$T_1 = 1.24 \pm 0.01 \mu s. \quad (8)$$

* The solution of eq. (7) was obtained by approximating the Lorentzian $(1 + T^2\Gamma^2)^{-1}$ by $(1 + \beta\Gamma)^{-1}$. The dc terms are not given.

The above results show that (a) the beam decay is in excellent agreement with the zero-pressure value of I_2 in the bulb (see figs. 2 and 3); and (b) the IRD of the beam is different from the decay following the 5145 Å excitation done by Ezekiel and Weiss.⁹ The reported lifetime is $3 \pm 0.5 \mu\text{s}$. These differences in lifetimes could be due to the presence of resonant states in the repulsive potential well that causes the lifetime to be shorter. To find the cause, we plan to do these high resolution experiments as a function of the excitation wavelength. Finally, the natural width of the selectively excited $X^1\Sigma_g^+ \rightarrow B^3\Pi_{0_u}^+$ rovibronic state at 5897.5 Å is $128 \pm 2 \text{ kHz}$, which to our knowledge has not been quoted accurately perhaps because of power broadening problems in cw experiments or in pulse deconvolution analysis in the conventional time resolved experiments.

The bulb result which is in agreement with the beam IRD result gives a nonradiative quenching similar to previous emission measurements^{25, 26} which utilize broad band excitation. Thus the influence of state preparation, on T_1 decay encountered in large molecules,¹¹ is not important. The results, however, give a cross section that is different from those measured by absorption techniques.¹⁸ It was pointed out before¹⁸ that this difference is because inelastic processes between the pumped level and neighboring levels will not necessarily produce a non-radiative decay into the ground state. In other words, the IRD gives the overall nonradiative cross section of the excited states population to the ground state. However, recent calculation²⁷ has yielded a cross-

section of 64 \AA^2 for cross relaxation and phase shifts. This point needs further study.

4. OPTICAL FREE INDUCTION DECAY IN BEAMS

To obtain the optical dephasing in the beam, the forward coherent signal which rides on top of the laser was detected. This way we observed the optical free induction decay (optical analogue of NMR free induction decay) in the effusive beam of iodine following the coherent excitation by the laser. The heterodyne signal which shows beats between the emitted light and the switched laser frequency is depicted in fig. 1. The results demonstrate that coherent optical transients in molecular beams can be observed even if the density is low. The beat frequency follows the electro-optical switching frequency while the decay is consistent with the conclusion that $2T_1 \approx T_2$ in the collisionless beam, considering the above mentioned approximations. This is an important conclusion because it says that in molecules like iodine there are essentially no intramolecular relaxations that destroy the phase coherence, and that the spontaneous loss is responsible for the optical dephasing at zero pressure. In large molecules (e.g. pentacene) and in molecules like NO_2 , where one expects intramolecular decay processes, the optical dephasing in the beam should not necessarily relate to T_1 at zero pressure.

5. CONCLUSIONS

This paper presents the first observation of the coherent and incoherent time-resolved spectra of molecular beams with very high resolution (10^{-4} cm^{-1}). Beam techniques are very valuable because

of (a) the absence of collisions, (b) reduction of Doppler dephasing, and (c) the possibilities of space and time resolution along the beam. These advantages together with this high resolution capability are useful in probing nonradiative processes in molecules and the coherence of internal energy distribution in beam reactions. With this in mind, we are currently exploring these ideas on large molecules in the effusive and nozzle beams.

ACKNOWLEDGEMENT

This work was supported in part by the Research Corporation and in part by the Energy Research and Development Administration. We would like to thank the referee for the careful reading of the manuscript and for the constructive comments.

REFERENCES

1. E. Merzbacher, Quantum mechanics (Wiley, New York, 1967).
2. H. A. Lorentz, Proc. Amst. Acad. 18 (1915) 134.
3. J. Holtsmark, Z. Physik. 77 (1932) 459.
4. N. F. Ramsey, Molecular beams (Oxford Univ. Press, London, 1956); P. Kusch and V. W. Hughes, in: Handbuch der Physik, Vol. 37, Part 1 (Springer, Berlin, 1959); T. C. English and J. C. Zorn, in: Methods of experimental physics, Vol. 3 (Academic Press, New York, 1974) p. 669.
5. D. R. Herschbach, Advan. Chem. Phys. 10 (1966) 135;
R. A. Larsen, S. K. Neoh and D. R. Herschbach, Rev. Sci. Instr. 45 (1974) 1511.
6. J. B. Anderson, R. P. Andres and J. B. Fenn, Advan. Chem. Phys. 10 (1966) 275.
7. J. M. Farrar and Y. T. Lee, Ann. Rev. Phys. Chem. 25 (1974) 357.
8. R. N. Zare and P. J. Dagdigian, Science 185 (1974) 739.
9. T. J. Ryan, D. G. Youmans, L. A. Hackel and S. Ezekiel, Appl. Phys. Letters 21 (1972) 320; S. Ezekiel and R. Weiss, Phys. Rev. Letters 20 (1968) 91.
10. R. E. Smalley, B. L. Ramakrishna, D. H. Levy and L. Wharton, J. Chem. Phys. 61 (1974) 4363.
11. A. H. Zewail, T. E. Orlowski and K. E. Jones, Proc. Natl. Acad. Sci. US 74 (1977) 1310; A. H. Zewail, K. E. Jones and T. E. Orlowski, Spectry. Letters 10 (1977) 2; T. E. Orlowski,

- K. E. Jones and A. H. Zewail, Bull. Am. Phys. Soc. 21 (1976) 1284.
12. W. Weisskopf and E. Wigner, Z. Physik 63 (1930) 54.
 13. R. P. Feynman, F. L. Vernon Jr. and R. W. Hellworth, J. Appl. Phys. 28 (1957) 49.
 14. A. G. Redfield, Advan. Magn. Reson. 1 (1965) 1.
 15. H. C. Torrey, Phys. Rev. 76 (1949) 1059.
 16. C. L. Tang and B. D. Silverman, in: Physics of quantum electronics, eds. P. Kelley, B. Lax and P. Tannenwald (McGraw-Hill, New York, 1966) p. 280; R. L. Shoemaker and E. W. van Stryland, J. Chem. Phys. 64 (1976) 1733.
 17. A. H. Zewail, T. E. Orlowski and D. R. Dawson, Chem. Phys. Letters 44 (1976) 379.
 18. R. G. Brewer and A. Genack, Phys. Rev. Letters 37 (1976) 959.
 19. A. H. Zewail, SPIE 82 (1976) 26; A. H. Zewail and T. E. Orlowski, Chem. Phys. Letters 45 (1977) 399.
 20. A. Genack, R. M. Macfarlane and R. G. Brewer, Phys. Rev. Letters 37 (1976) 1078.
 21. J. Telle and C. L. Tang, Appl. Phys. Letters 24 (1974) 85; 26 (1975) 572; A. Yariv, Proc. of IEEE 52 (1964) No. 6.
 22. A. H. Zewail, T. E. Orlowski, R. R. Shah and K. E. Jones, Phys. Rev. Letters, submitted for publication.
 23. T. E. Orlowski, K. E. Jones and A. H. Zewail, Chem. Phys. Letters 50 (1977) 45.

24. M. Abramowitz and I. A. Stegun, eds., Handbook of mathematical functions (Dover, New York, 1965).
25. G. A. Capelle and H. P. Broida, J. Chem. Phys. 58 (1973) 4212;
J. I. Steinfeld and A. N. Schweid, J. Chem. Phys. 53 (1970) 3304;
R. Brown and W. Klemperer, J. Chem. Phys. 41 (1965)
3072; 42 (1965) 3475; R. B. Kurzel and J. O. Steinfeld, J. Chem.
Phys. 53 (1970) 3293; 44 (1966) 2740.
26. A. Chutjian, J. K. Link and L. Brewer, J. Chem. Phys. 46
(1967) 2666.
27. S. Mukamel, A. Ben Reuven and J. Jortner, J. Chem. Phys.
64 (1976) 3971.
28. A. H. Zewail, T. E. Orlowski, K. E. Jones and D. Godar,
Chem. Phys. Letters 48 (1977) 256.

E

MEASUREMENTS OF MOLECULAR DEPHASING AND
RADIATIONLESS DECAY BY LASER-ACOUSTIC
DIFFRACTION SPECTROSCOPY[†]

T. E. Orlowski, K. E. Jones and A. H. Zewail
Arthur Amos Noyes Laboratory of Chemical Physics^{††},
California Institute of Technology
Pasadena, California 91125

ABSTRACT

In this paper we present a method for the measurements of molecular dephasing and radiationless decay in gases and solids. The technique utilizes a single-mode of a tunable dye laser and an extra-cavity acousto-optic element. The latter diffracts the laser beam into or out of the sample for finite times when a train of radio frequency pulses is fed into the transducer. Using this laser-acoustic diffraction spectroscopy (LADS) we report some new results on iodine gas, and pentacene in a p-terphenyl host at 1.8 K. Combining these new results of LADS on pentacene and our earlier findings using the frequency switching method we present an analysis for the effect of laser bandwidth on the decay of the prepared excited states.

[†]Chemical Physics Letters, 54, 197 (1978).

^{††}Contribution Number 5702.

Recently we have reported¹ on the measurements of electronic dephasing (T_2) and radiationless decay (T_1) in molecules using emission spectroscopy as a probe. Basically the method can be described as follows. The molecules in the ensemble are optically excited in-phase by a well defined ($\pi/2$) pulse similar to that done in NMR spectroscopy² and its optical analogue.³ The induced macroscopic moment (i.e., the sum of all molecular moments) from all excited molecules dephases as a result of the ensemble inhomogeneity. Rephasing of the moments with a π -pulse gives a superradiant state that can usually be detected in the forward direction of the laser. In our method, however, this superradiant "moment" is changed into ground state population (by a $\pi/2$ pulse) resulting therefore in the loss of the emission from the molecules. Thus the photon echo whose decay gives T_2 directly appears as a temporal hole in the emission that is detected at right-angles to the exciting laser beam.

The right-angle photon echo¹ utilizes a single mode of a narrow-band ($\approx 10^{-4} \text{ cm}^{-1}$) cw dye laser and an intracavity electro-optic (EO) element that modulates the frequency of the laser. Applying voltage pulses into the EO crystal switches the laser frequency from ω_0 (the peak frequency of the transition resonance) into another frequency ω . This switching⁴ procedure allows one to observe coherent transients in gases,^{4,1} solids⁵⁻⁷ and molecular beams.⁸ Typically the dispersion of the nonlinear EO crystal (e.g., AD*P) gives a 60 MHz frequency shift within the inhomogeneous resonance of the optical transition (width \approx GHz or larger). Therefore, to switch the laser frequency further, one

must use high voltage signals that are usually hard to obtain especially for multiple pulse experiments. Secondly, there is a limit on the frequency shift which is conditioned by a mode spacing ($C/2L$; C is the speed of light and L is the cavity length) of the cavity. Thirdly, because the laser is switched into a new group of molecules some complications may arise in interpreting the transient spectra especially in large molecules. This is because in large molecules the density of excited states is high and thus the build-up transients of ω -molecules (which could be complex) will be superimposed on the decay of ω_0 -molecules. Finally, off-resonance effects (e.g., beats) between the molecules at frequency ω and ω_0 cannot be avoided.

In this paper we present a laser-acoustic diffraction spectroscopic technique that resolves the above mentioned problems and provides optical T_2 and T_1 directly. Using LADS we show new results concerning the dephasing and the decay in small (iodine) and large (pentacene) molecules in the gas and condensed phases.

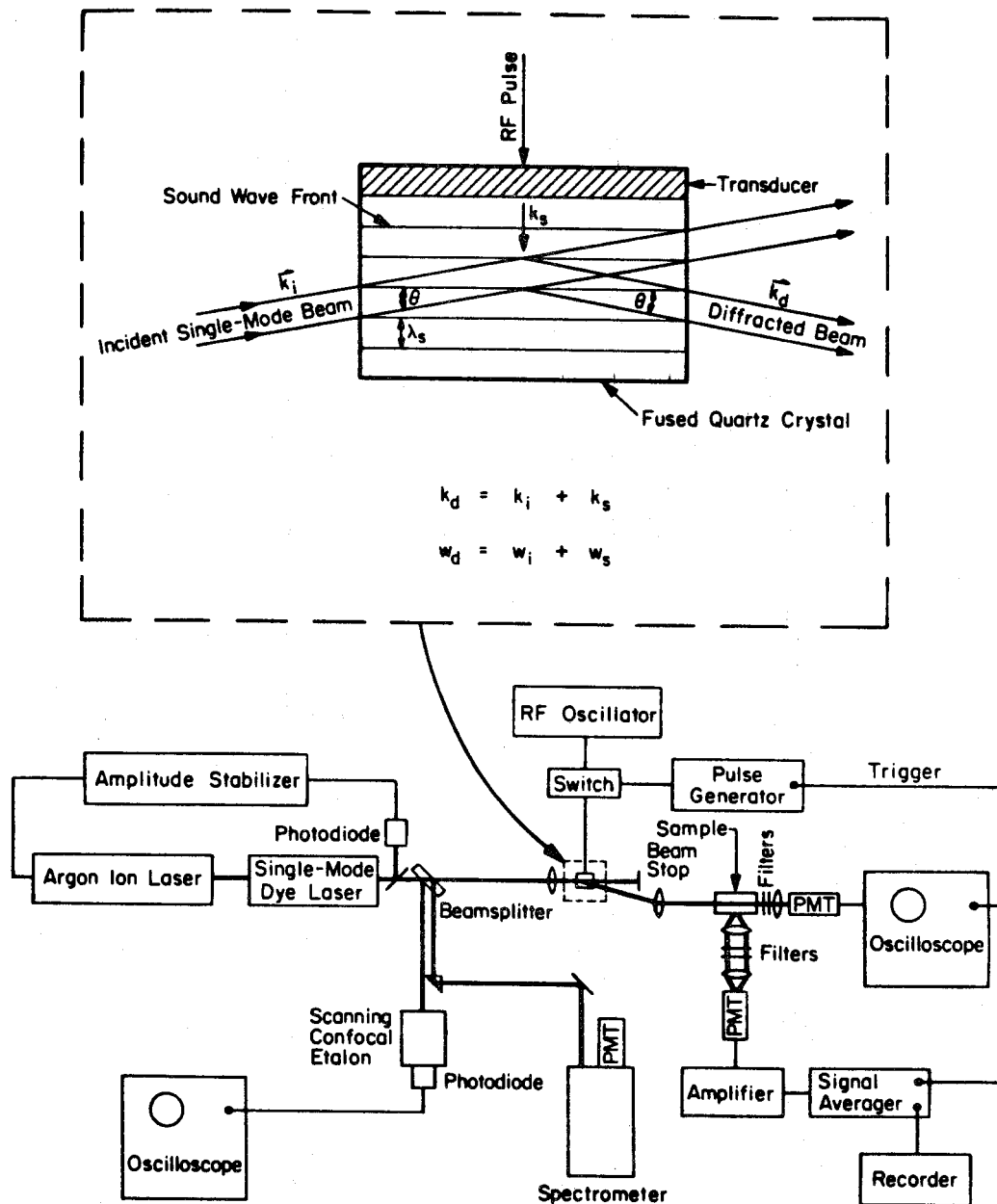
To measure the rate of electronic dephasing the single-mode of the cw dye laser was diffracted by an extracavity acousto-optic element. The sample sees optical pulses of finite duration only when an rf pulse train (e.g., $\pi/2, \pi, \pi/2$) is fed into the transducer which provides acoustic waves that diffract the light. By feeding the rf pulse train at a certain repetition rate the system (gas or solid) is excited coherently at this repetition rate and at ω_0 without pumping other molecules in the inhomogeneous frequency distribution of the optical transition. This simple method for measurement of optical T_2 and T_1 relies on the well-known acousto-optic effect⁹ that has been used before for the measurement of fluorescence kinetics,¹⁰ and is different from the techniques of gating cw lasers by Pockels cells.¹¹

The advantages of LADS are: (a) Gating procedures for separating the laser from the signal are not needed since the coherence of the ensemble is monitored by the emission at right-angles to the exciting laser beam. For nonemitting molecules, heterodyne detection can also be done. (b) The pulses that give optical transients are radio frequency and can be generated by switching an rf oscillator on and off using low-voltage pulse trains (e.g., from home-made TTL devices). (c) One rf pulse will give the T_1 decay while a three-pulse train will provide optical T_2 directly. And finally (d) LADS is especially useful for studying large molecules because the off-resonance effects inherent in the EO switching method are nontrivial to separate.

The apparatus used for these LADS experiments is shown schematically in fig. 1. An argon ion laser pumps a cw single-mode jet stream dye laser. The amplitude stabilized single-mode beam is split (8%) to allow continuous monitoring of laser frequency and single-mode operation using a 0.5 m spectrometer and a Fabry-Pérot scanning confocal etalon. The linearly polarized beam (80 mW) is then focused upon a quartz crystal which has a thin film transducer bonded to it. Phonons injected by the transducer (switched on and off with any desired pulse sequence by a pulse generator) create acoustic waves in the crystal which diffract up to 50% of the incident light at the Bragg angle (θ , see insert in fig. 1). This diffraction beam, shifted in frequency by the acoustic phonon frequency (470 MHz) is deflected into the sample for the duration of the rf pulse. Thus, the acousto-optic modulator acts as a fast shutter. The characteristics of the laser pulse this technique

Figure 1

A schematic diagram of the experimental setup for LADS. The insert in the figure shows the single mode of the cw dye laser interacting with the phonon grating injected into the crystal by the transducer. To minimize the jitter of the mode, the acousto-optic element and the laser were mounted on an NRC vibration-isolation table. To minimize amplitude fluctuations in the laser we inserted a stabilizer on the output of the dye laser.



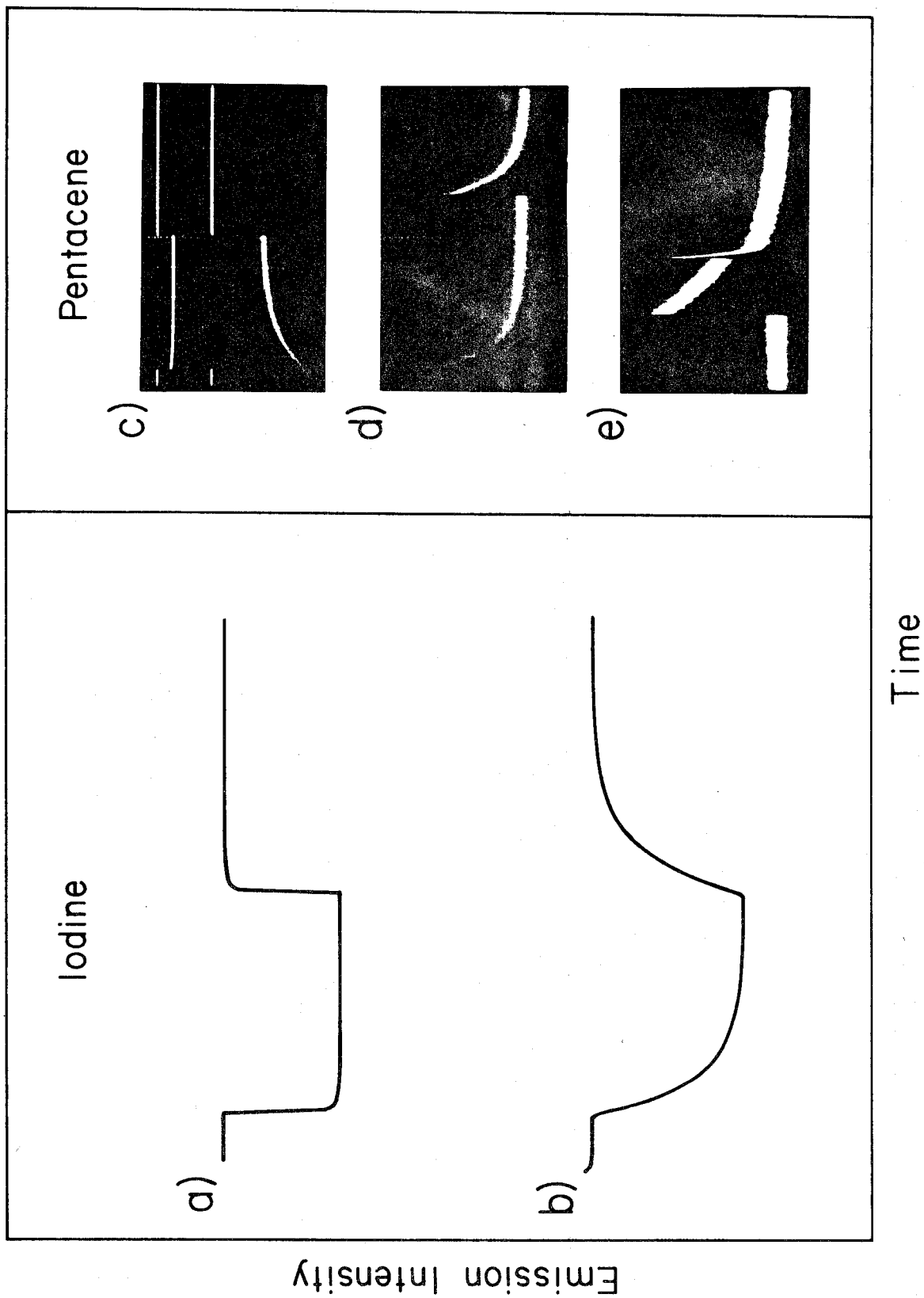
provides are determined by (1) the rf pulse width and its rise/fall times, and (2) the transit time of the acoustic wave across the focused laser beam in the crystal. We have measured laser pulse rise/fall times of 3 ns (1/e time) using a 75 mm focal length lens to focus the laser beam into the crystal. Analogous with our frequency-switching emission experiments¹ the emission intensity from the sample is monitored at right-angles to the exciting beam while the laser pulse characteristics are monitored by a fast photomultiplier in the forward direction (see fig. 1). For lifetime measurements, a single pulse is used and the emission waveform detected by a cooled shielded photomultiplier (EMI 9558) is amplified and then averaged using a scanning gate box car signal integrator (PAR model 162). In the photon echo experiments a three-pulse sequence is used. Signal integration is accomplished using a phase-sensitive detector which monitors changes in the emission intensity as the separation between pulses is varied. The signal is then processed and recorded.

Mixed crystals of pentacene in p-terphenyl were grown by Bridgman techniques. All the measurements were done on relatively dilute crystals ($\approx 10^{-5}$ - 10^{-7} M/M) at temperatures below the λ -point of liquid helium. For the iodine experiments, the gas cell was treated carefully to avoid quenching. Details of the treatment and the setup can be found in ref. 8.

Fig. 2 shows the transient spectrum of iodine gas, and pentacene in p-terphenyl at 1.8 K. In iodine when the rf pulse is turned on (i.e., the laser beam is diffracted to the sample) the population builds

Figure 2

The laser excitation of iodine gas and pentacene in p-terphenyl at 1.8 K using LADS and EO methods: a is the light pulse generated by the rf pulse (width = $3.4 \mu\text{s}$) and b is the iodine response (raw data). Note the decay on the falling edge of the pulse and the build up on the leading edge. c is the LADS signal from pentacene ($10 \mu\text{s}/\text{div}$). d ($20 \mu\text{s}/\text{div}$) and e ($5 \mu\text{s}/\text{div}$) are the signals of pentacene when excited with long and short EO pulses, respectively. (d and e are inverted emission signals.) Note that in e on the leading edge the system is excited by a long pulse while on the falling edge the system is excited only by $\approx 10 \mu\text{s}$ pulse.



up in the state at 5897.5 Å. When the rf is terminated the beam is deflected away from the sample and the molecules decay freely. We have studied the pressure and laser power dependence of the build up and the decay. At lower pressure the build up in emission intensity is biexponential and is sensitive to the laser power. On the other hand, the decay on the falling edge of the pulse gives T_1 which depends on the pressure according to the Stern-Volmer relationship. This linear relationship gives

$$\frac{1}{T_1} = (0.783 \pm 0.032) + (0.0143 \pm 0.0005)P, \quad (1)$$

where T_1 is in μs and P is the pressure in mtorr. One notices that:

(a) the results of LADS are in very good agreement with those obtained using the frequency switching technique;⁸ (b) the cross section for quenching (pressure dependent T_1 processes) is the same when the laser is switched into a new group of molecules in the Doppler resonance or completely turned off (LADS method); and finally (c) the extrapolated zero pressure value of T_1 ($1.28 \pm 0.05 \mu\text{s}$) is in excellent agreement with our earlier results for an iodine molecular beam.⁸ In the pentacene case the situation is different.⁶

Recently we have reported on a decay signal in pentacene ($\approx 15 \mu\text{s}$) using narrow band excitation^{6, 12} of the lowest excited singlet state (O_1 site). The signal (fig. 2) has the following characteristics: (a) the decay signal is absent when the molecule is excited above the electronic origin at $16,887 \text{ cm}^{-1}$; (b) the decay time does not change when the power level of the laser is reduced; (c) the decay is exponential and

changes as we scan the narrow-banded laser in the manifold of the origin; (d) the signal gets stronger at higher switching frequency; (e) there is a magnetic field effect on the decay; (f) the decay changes from 15 μ s to 25 ns when the laser effective width changes from 6 MHz to 18 GHz; and finally (g) the signal disappears at high temperatures. These observations forced us to conclude that the 15 μ s decay is due to a state which is a mixture of the Born-Oppenheimer (BO) singlet state and some triplets (or hot singlets) that are in quasi-resonance with the BO state.*

Figure 3 shows both the optical nutation and the free induction decay observed for the O_1 origin in the mixed crystal. The nutation was taken at 20 mW laser power and a switching frequency of 30 MHz.[†] To observe the optical free induction decay of fig. 3 we used 400 μ W of laser power on a 2.5 mm thick crystal. The laser propagation direction was perpendicular to the cleavage plane of the crystal. Clearly the free induction decay, which provides the dephasing time (T_2) at low powers, gives a T_2 (45 ns) that is much shorter than 15 μ s, and very close to the results of the photon echo.¹⁴ This led us to conclude that either there is a special mechanism for dephasing that is mediated by phonons or that the laser bandwidth is very important in determining the decay characteristics. To resolve this problem, we therefore studied the decay signal

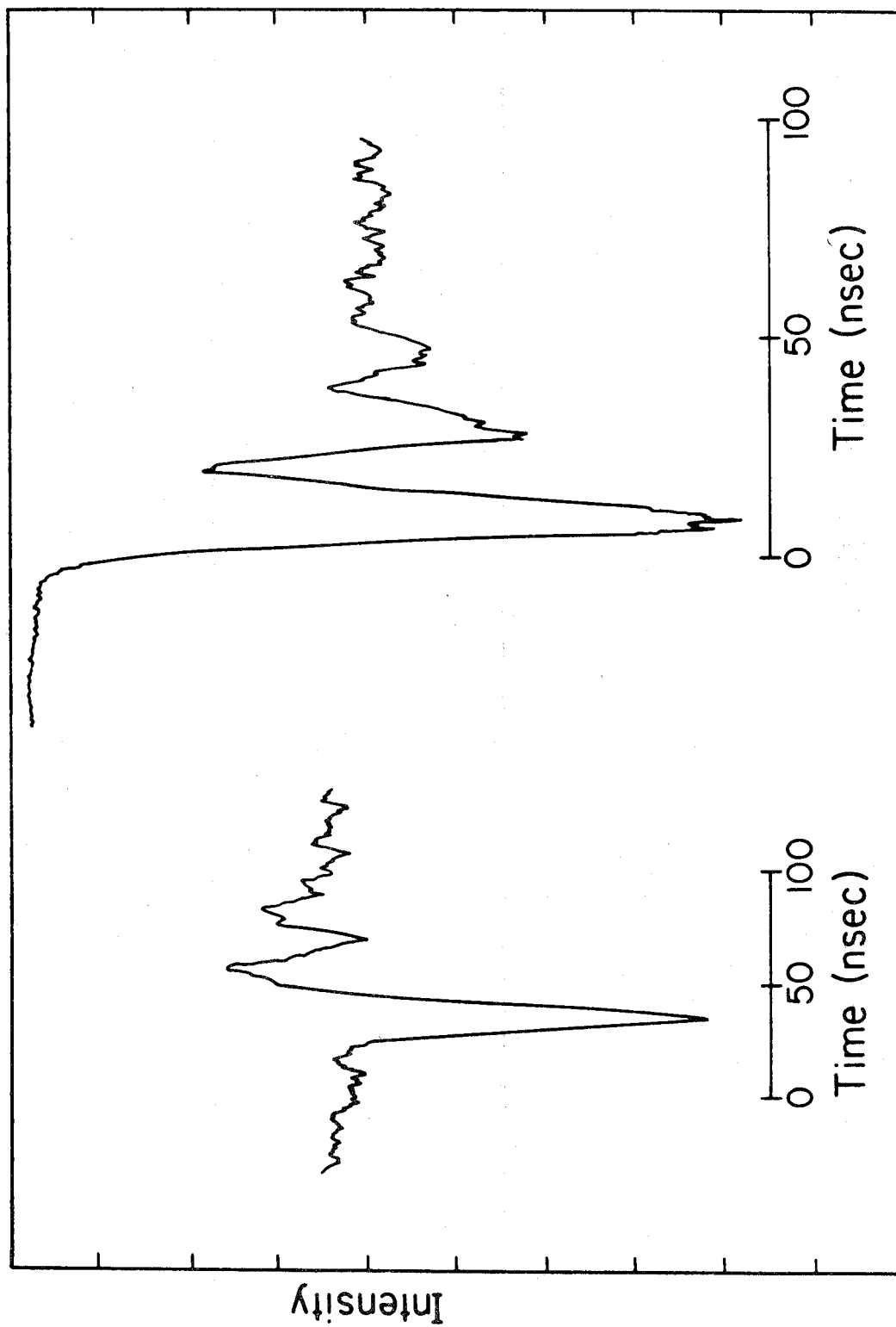
*For a review on radiationless transitions in large molecules, see ref. 13.

[†]The free induction decay was also observed by Wiersma *et al.* (presentation of some of the results was made at the VIIIth Molecular Crystal Symposium in Santa Barbara, California).

Figure 3

Optical free induction decay (right) and nutation (left) of pentacene in p-terphenyl at 1.8 K. The beats of the nutation give $\mu\epsilon/\hbar$, see text, and the beats of the free induction decay give the switching frequency of the EO crystal.

Optical Free Induction Decay and Nutation in Pentacene at 1.8°K



as a function of the EO pulse width (d and e of fig. 2). Couched in the thoughts of the EO experiments one can explain these transients (figs. 2d and 2e). When the pulse is narrow the Fourier transform of it brackets many eigenstates of the molecule, thus producing the BO decay followed by a long decay component. A wide pulse excitation, on the other hand, prepares only the molecular eigenstates which give the long decay on the leading and falling edges of the pulse. However, from the LADS experiments (fig. 2c) there is no long decay when the laser is turned off, suggesting that the state prepared by the narrow band laser is mostly singlet and the long decay observed using LADS is due to cross-relaxation between the prepared state and the nearby slowly decaying levels (e.g., long-lived triplets). The kinetic analysis⁶ of the data is consistent with the transient patterns shown in fig. 2, and shows that the long decay time can be explained provided the laser is not exciting a two-level system.* The prepared state has a moment of ≈ 1.5 Debye as calculated from the spectra in fig. 3. Note that the beat frequency of

*Drs. P. Grigolini and A. Lami (private communication) have shown that nonradiative decay in large molecules excited by an intense laser field can be described using a "reduced" molecular system formalism which includes the coherence of excited levels. Their findings predict an effective three-level description for the excitation process among the complex many levels interacting with the radiation field. We are now testing these predictions in more detail.

the nutation gives $\mu \epsilon / \hbar$, where μ is the transition dipole moment and ϵ is the laser amplitude. Also the free induction decay at finite powers depends on $\mu \epsilon / \hbar$, and T_1 and T_2 .¹⁵ Thus by knowing ϵ one estimates μ from the nutation and then cross checks the free induction decay results since T_1 and T_2 are known.

In addition to the T_1 measurements reported above we have observed the photon echo of I_2 gas using LADS. The emission at right-angles to the exciting beam was detected while the separation between the second and the third rf pulse of the three-pulse train was changed. This way instead of switching the frequency of the laser as we did before,¹ the laser is completely switched off following the pulses. At 7 mtorr and using three pulses ($\pi/2, \pi, \pi/2$) an echo was seen on the emission (fig. 4). Two pulses ($\pi/2$ and π), on the other hand gave no echo on the emission and only a sloping base line was observed. This base line is similar to that observed on the three-pulse echo and we used it to obtain the actual shape of the echo. The result, which shows the dependence of the emission intensity on the separation of the second and third pulse, is depicted in fig. 4.

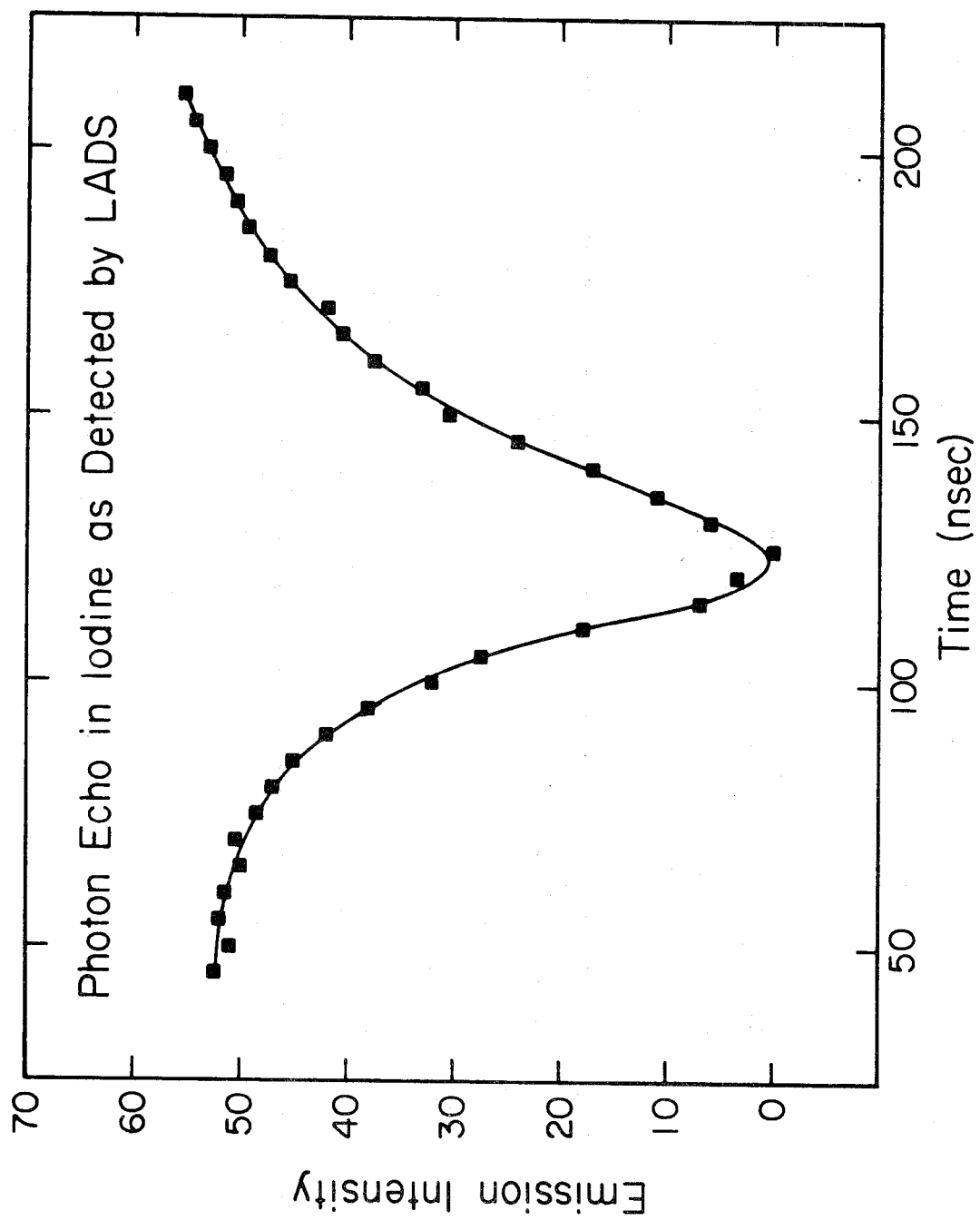
The photon echo observed in fig. 4 by LADS does not show the beat pattern observed using the EO switching method.¹ As has been shown before, the echo shape signal, I , detected on the emission spectrum is given by⁶

$$I(\tau_2) = -A e^{-(\tau_1 + \tau_2)/T_2} e^{-|\tau_2 - \tau_1|/\sigma}, \quad (2)$$

where A is a constant and σ is the echo width in time for a Lorentzian distribution of molecules that are excited by the laser. Eq. (2) was

Figure 4

The observed photon echo in iodine using LADS at 7mtorr gas pressure. The separation between the first $\pi/2$ and π pulse is 120 ± 5 ns. The separation between the π and the last $\pi/2$ pulse is varied.



derived for the case where the laser is turned off during τ_1 (separation between first $\pi/2$ and π pulses) and τ_2 (separation between π and last $\pi/2$ pulse) periods. This is true for the LADS case (see fig. 4) but not for the EO switching case of ref. 1. The width σ^{-1} depends on the intrinsic line width of the laser, the Fourier transform width of the $\pi/2$ pulse and the power broadening term. The former is negligible relative to the last two. In fact, when we lowered the laser power by a factor of two, the echo decreased in intensity and the time width became larger indicating the presence of some power broadening contribution to σ . The decrease in the echo amplitude when ϵ was decreased is due to the change in the areas of the $\pi/2$ and π pulses which is given by

$$(2\pi/\hbar) \int_{-\infty}^{\infty} \epsilon \, dt \quad .$$

The decay of the echo gives directly the dephasing time.

Scanning the separation between pulses synchronously (i. e., $\tau = \tau_1 = \tau_2$) while monitoring the emission showed that the echo amplitude decreases at long τ 's. The decay gives $T_2 = 0.5 \pm 0.15 \, \mu\text{s}$ at 7 mtorr. There is a large uncertainty in the result due to the base line on the echo shape. This problem will be eliminated in the future by interfacing the signal detector into a computer and gating the emission at the desired time portion of the spectrum.* The dephasing time is close to that obtained previously by the frequency switching method, and gives a homogeneous

*At longer τ_2 , there appears to be a "beat" on the emission near the actual echo. However, at these long times we need to improve the S/N in order to investigate this point further.

line broadening (≈ 636 kHz) similar to that reported before for iodine.^{1, 8}

In conclusion, with the help of LADS we have presented a method for measuring molecular dephasing. The method is especially suitable for large molecules where T_1 and T_2 processes are not necessarily as simple to understand as in small molecules. We believe that because the acousto-optical element is extracavity the technique is relatively simple and could become useful for investigating the coherent and incoherent time resolved spectroscopy of molecules excited by high resolution single-mode lasers.

ACKNOWLEDGMENTS

This work was supported in part by the Research Corporation and in part by the Energy Research and Development Administration. Acknowledgment is also made to the donors of the Petroleum Research Fund, administered by the ACS, for partial support of this research. One of us (AHZ) would like to acknowledge a fruitful discussion with M. Levenson of USC regarding the possible connections between the observation of the beats in the echo experiment and Ramsey's fringes.

REFERENCES

1. A. H. Zewail, T. E. Orlowski, K. E. Jones and D. E. Godar, Chem. Phys. Lett., 48, 256 (1977); A. H. Zewail, T. E. Orlowski and D. R. Dawson, Chem. Phys. Lett., 44, 379 (1976); T. E. Orlowski, K. E. Jones and A. H. Zewail, Chem. Phys. Lett., 50, 45 (1977).
2. E. L. Hahn, Phys. Rev., 80, 580 (1950).
3. N. A. Kurnit, I. D. Abella and S. R. Hartmann, Phys. Rev. Lett., 13, 567 (1964); ibid., 141, 391 (1966).
4. R. G. Brewer and A. Genack, Phys. Rev. Lett., 37, 959 (1976).
5. A. H. Zewail and T. E. Orlowski, Chem. Phys. Lett., 45, 399 (1977).
6. A. H. Zewail, D. E. Godar, K. E. Jones, T. E. Orlowski, R. R. Shah and A. Nichols in: "Advances in Laser Spectroscopy I" A. H. Zewail, ed. (SPIE Publishing Company, 1977) Vol. 113, p. 42.
7. A. Genack, R. M. Mcfarlane and R. G. Brewer, Phys. Rev. Lett., 37, 1078 (1976).
8. A. H. Zewail, T. E. Orlowski, R. R. Shah and K. E. Jones, Chem. Phys. Lett., 49, 520 (1977).
9. R. Alder, IEEE Spectrum, 4, 42 (1967).
10. R. Z. Bachrach, Rev. Sci. Instr., 43, 734 (1972).
11. P. F. Liao, R. Leigh, P. Hu and S. R. Hartmann, Phys. Lett., 41A, 285 (1972).
12. A. H. Zewail, T. E. Orlowski and K. E. Jones. Proc. Natl. Acad. Sci. US, 74, 1310 (1977).

13. S. A. Rice, in: "Excited States" (Academic Press, New York, 1975) Vol. 2, p. 111; G. W. Robinson, in: "Excited States" (Academic Press, New York, 1974), Vol. 1, p. 1; S. Mukamel, in: "The World of Quantum Chemistry", R. Daudel and B. Pullman, eds. (Reidel, Dordrecht, 1974); K. F. Freed, Topics Appl. Phys., 15, 23 (1976).
14. J. B. W. Morsink, T. J. Aartsma and D. A. Wiersma, Chem. Phys. Lett., 49, 34 (1977).
15. R. G. Brewer and R. L. Shoemaker, Phys. Rev., A6, 2001; (1972); F. A. Hopf, R. F. Shea and M. O. Scully, Phys. Rev., A7, 2105 (1973).

CHAPTER IV

RADIATIONLESS RELAXATION AND OPTICAL DEPHASING OF
MOLECULES EXCITED BY WIDE- AND NARROW-BAND
LASERS: II. PENTACENE IN LOW-TEMPERATURE
MIXED CRYSTALS*

T. E. Orlowski and A. H. Zewail**

Contribution No. 5790 from the Arthur Amos Noyes Laboratory of
Chemical Physics, California Institute of Technology, Pasadena,
California 91125

*Submitted to J. Chem. Phys.

**Alfred P. Sloan Fellow

ABSTRACT

One purpose of this paper is to present new studies on the effect of bandwidth and the coherence properties of the excitation source on the decay and the dephasing of isolated large molecules. A detailed study of the system pentacene in a p-terphenyl matrix is presented utilizing three different excitation sources: a single mode dye laser (60 KHz - 6 MHz bandwidth depending on the time scale of the experiment); a multimode dye laser (240 GHz bandwidth), and an incoherent N₂ flash lamp. Optical T₁ (the longitudinal relaxation time) and T₂ (the transverse relaxation time) are measured from the coherent and incoherent transients observed either in the forward direction of the laser or at right-angles to the exciting beam. At 1.8°K, the optical transition (¹A_{1g} → ¹B_{2u}) of pentacene in p-terphenyl exhibits four sites, the lowest of which at 16,887 cm⁻¹ has the following parameters:

$$T_2 = 44 \pm 2 \text{ nsec}; T_1 = 24.9 \pm 2 \text{ nsec}, \text{ and } \mu = 0.7 \pm 0.1 \text{ Debye.}$$

The transition moment, μ , is obtained directly from the optical nutation, which exhibits a Rabi nutation time ($\hbar/\mu \cdot \epsilon$) of 27.3 nsec, and is corrected for the effect of the Lorentz local field inside the terphenyl crystal. The experiments presented here are categorized into two time regimes for theoretical analysis; a transient coherence regime where the observed decay is comparable with ($\hbar/\mu \cdot \epsilon$) and T₂, and a steady-state coherence regime where transient dephasing is complete and the off-diagonal elements of the density matrix have decayed to their steady-state values in the presence of the field of amplitude ϵ . Using the Wilcox-Lamb method, rate equations (with T₂ expressions) describing

the population flow in the "complete" level structure of pentacene (ground $|0\rangle$, singlet $|p\rangle$, and triplet $\{|l\rangle\}$) are derived from the density matrix equations of motion. When these equations are averaged over the inhomogeneous width of the optical transition and the measured Gaussian transverse profile of our laser we obtain $T_{1p0} = 24.9 \pm 2$ nsec and $T_{1pl} = 15.7$ μ sec, the time constants by which pentacene spontaneously decays to $|0\rangle$ or crosses over into l , as well as the averaged population at time t . In an effort to be complete, attention is placed upon the relationship between theory and the experimental findings. First, expressions for the OFID and nutation in the solid are presented for the pentacene case in order to relate T_1 , T_2 , and μ to the level structure. Second, at low temperatures (1.8°K), the origin of dephasing is identified as spontaneous emission from $p \rightarrow 0$ since experimentally $T_2 \approx 2T_1$. At higher temperature, however, a strongly temperature dependent dephasing process with an onset at 3.7°K takes place. Armed with these observations we present a theoretical treatment of these distinct dephasing channels and their temperature dependences. A discussion regarding the influence of "accepting" phonon modes (either optical or acoustic) on optical dephasing is also given. The results indicate that the treatment of Jones et al.⁷² can (1) explain the observed temperature dependence of T_2 in pentacene; (2) distinguish dephasing as a result of scattering by acoustic phonons from that due to resonance or quasi-localized phonons with clear connections to gas and liquid state theories, but without invoking the binary collision approximation; (3) explain both the level shift and linewidth changes as a result of "conventional" dephasing

or dephasing by exchange mechanisms, and (4) relate the pure dephasing term to an anisotropy in the scattering amplitudes (between the ground and excited states in the system) which contribute largely to the homogeneous width of the transition. Optical site selection of these transitions is also reported and discussed in relation to vibrational relaxation and to both homogeneous and inhomogeneous broadenings. The studies of the homogeneous broadening of the vibronic origin (267 cm^{-1}) indicate that vibrational relaxation is fast (psec) in the excited singlet manifold of pentacene. Finally from more than ten independent experiments including single and multimode excitation, on- and off-resonance scattering, Zeeman effect and the transient decay as a function of excess energy in the molecule, a more complete picture of the pentacene level structure $\{|\ell\rangle\}$ is given. With this in mind, the influence of the laser bandwidth and coherence properties on state preparation and subsequent dephasing and decay is concluded. It is proposed that the slow decay, ($\sim 15\text{ }\mu\text{sec}$) observed during the narrow-band excitation represents intersystem crossing to nearby triplet manifolds after the transient coherence of the $0 \rightarrow p$ subsystem is decayed. In addition, the decay of the primary state prepared in these experiments is not sensitive to the bandwidth or the correlation time of our excitation sources.

I. INTRODUCTION

Radiationless relaxation processes in large molecules have been under examination ever since their discovery and especially whenever new theoretical or experimental tools are made available. In these large molecules, where the density of vibrational modes at the optical excitation energy is very large, one usually finds that the lifetime of the excited state is shorter than the radiative lifetime (obtained from oscillator strength measurements) and the quantum yield is less than one,¹ contrary to the behavior in small molecules discussed by Douglas.² This paradox originates from a radiationless decay within the molecule, and was resolved by incorporating different coupling mechanisms among the so-called Born-Oppenheimer (BO) singlet and triplet states.³

In the theory³⁻⁵ of radiationless transitions, the molecule has a primary or doorway state (e.g., a singlet state which carries most of the oscillator strength) $|p\rangle$ which may or may not couple to many isoenergetic vibronic levels $\{|l\rangle\}$ from the ground singlet state or nearby triplet manifolds. The coupling matrix elements v_{pl} and the density of states will determine the routes of the nonradiative decay. In many ways this scheme resembles Fano's description⁶ of the auto-ionization of helium. However in molecules, irreversible vibronic relaxation and radiative decay (optical T_1 processes; the longitudinal relaxation time) deactivate the excited level with no ionization or bond breakage. This irreversibility which has been discussed by Freed⁷ and others³ requires that the vibrational levels in quasi-resonance with

$|p\rangle$ form an effective continuum. Under simple coupling conditions the line shape of the $|p\rangle$ state becomes Lorentzian in the energy domain. Thus if one prepares the $|p\rangle$ state, the homogeneous linewidth will be given by the sum of the radiative and nonradiative T_1 contributions.

The question that was first raised by Rhodes et al.,⁸ and Langhoff and Robinson⁹ is: Do we really prepare the $|p\rangle$ state under all excitation conditions? This question has stimulated several theoretical investigations,³ and from them have emerged the conditions under which one may excite the BO singlet state or the molecular eigenstates ψ_m which are linear combinations of the singlet and triplet (or hot ground singlet) states.

If the molecular eigenstates are prepared, then the radiative decay of these states will be different from the radiative decay of the BO singlet state according to the following relationships:

$$|\psi_m\rangle = \alpha_{pm}|p\rangle + \sum_{\ell} \beta_{\ell m}|\ell\rangle \quad (1)$$

and

$$[T_{1r}^m]^{-1} = \alpha_{pm}\alpha_{pm}^*[T_{1r}^p]^{-1} + (\approx 0) \quad (2)$$

Hence, the radiative lifetime (T_{1r}) of the molecular eigenstates will be "scaled" according to the coefficients α 's which in turn depend on $v_{p\ell}$ and the energy difference between $|p\rangle$ and $\{|\ell\rangle\}$. It is precisely this coupling to the radiation field which makes the energy of the state $|m\rangle$ imaginary. Strictly speaking the states $\{|m\rangle\}$ therefore do not represent the true molecular eigenstates which diagonalize the following Hamiltonian:

$$\mathcal{H} = \mathcal{H}(\text{singlet}) + \mathcal{H}(\text{triplets or hot singlets}) + \mathcal{H}(\text{interaction}) \quad (3)$$

In other words, the above semi-classical description says that because $|m\rangle$ couples to the radiation field continuum (or the nonradiative continuum), the monochromatic preparation makes the state evolve in time not only by the quantum mechanical stationary state characteristics but also by the Weisskopf-Wigner¹⁰ damping term; i. e.,

$$\begin{aligned} \langle m | m(t) \rangle &= \langle m | e^{-i\mathcal{H}t/\hbar} | m \rangle \\ &= \text{Exp} \left[-\frac{i}{\hbar} \{ E_m - \frac{i}{2} (T_{1r}^m)^{-1} - \frac{i}{2} (T_{1nr}^m)^{-1} \} t \right] \end{aligned} \quad (4)$$

where T_{1nr} is the nonradiative T_1 decay time and E_m is the real energy of state $|m\rangle$. (At this point we would like to emphasize that our use of the term "molecular eigenstate" is not rigorous because of the above reasons. Nevertheless, we shall use it to describe the states which are mixtures of the singlet $|p\rangle$ and $\{|\ell\rangle\}$.) The spacing between $|m\rangle$'s and their homogeneous linewidth will determine whether or not these states can be prepared in the laboratory, and whether or not the above theoretical description is adequate.

Experimentally, the first attempt to excite a large molecule with a narrow band (MHz) laser was made on pentacene about two years ago (henceforth referred to as I¹¹). The experiments were performed hoping to answer the following questions:

- (1) Do radiationless transitions depend on the nature of the exciting field?
- (2) What is the exact nature of the state we excite?

- (3) What is the influence of the ensemble optical coherence on the time evolution of the prepared state?
- (4) To what extent does the correlation time of the light source influence the decay of the prepared state?
- (5) Is there a threshold for an "ergodic" behavior in large molecules?

Our preliminary experiments on pentacene in a p-terphenyl host naturally did not answer all of these questions but they did shed some light on the effect of narrow band excitation on the observed (short and long) time resolved spectra. Furthermore, they provided the dephasing time (optical T_2 ; transverse relaxation time) following the narrow-band coherent excitation.

In this paper we provide a full account of our studies of the narrow and wide band laser excitation done on pentacene in p-terphenyl at 1.7°K and above. A description of the effect of magnetic field, temperature, laser power and frequency on the observed decay patterns is given and new results regarding the coherent transients are presented. We then relate these findings to the origin of optical pure dephasing (i.e., the process by which the prepared state loses its phase coherence) and radiationless decay in the solid at different temperatures. Finally, from more than ten independent experiments we present a more complete picture (different from I) for the excitation pathways in pentacene following the narrow- and wide-band excitation. This picture (a) does not support the preparation of a molecular eigenstate, (b) explains the origin of optical dephasing (T_2) and optical T_1 , and (c) indicates that there are more than two states involved even in the narrow-band laser excitation process.



The paper is outlined as follows. Section II presents the methodology and the physical description of the different transients (optical nutation, free induction decay, etc.) that are obtained from the coherent narrow band excitation, and will be used throughout the entire paper. Section III gives the experimental procedures and data analysis. Section IV presents the relevant theory of dephasing for pentacene. Section V gives results and analysis of the observed coherent and incoherent transients. Finally, Section VI gives summary and conclusions and Table I presents some nomenclature used by us and others.

II. OBJECTIVES AND METHODOLOGY

The objectives of these experiments are to measure the decay (T_1) and the dephasing (T_2) of selectively prepared vibronic states of a large molecule like pentacene using broad (coherent and incoherent) and narrow band excitation sources, and to determine the environmental effects as well as the effects of excess vibrational energy upon optical T_1 and T_2 processes important for large molecules. Pentacene was chosen because (a) it suits our single-mode laser which has an effective band width of 60 KHz-10 MHz depending on the time scale of the experiment, and (b) it has a level structure which might favor the formation of the states of Eq. (1) since triplet manifolds are close-by the singlet state (see reference 13 and Table II).

To better understand what is meant by selectively prepared states one can refer to Fig. 1 where we show an inhomogeneously broadened optical transition represented as a Gaussian distribution of homogeneous groups each having a Lorentzian lineshape whose width is

TABLE I. Some nomenclature and definitions

Term	Meaning
BO states	Born-Oppenheimer states
T_1	optical longitudinal relaxation time
T_2	optical transverse relaxation time
T_2'	optical pure dephasing time ^a
OFID	optical free induction decay
IRD	incoherent resonance decay
EO	electro-optic
AO	acousto-optic
LADS	laser-acoustic diffraction spectroscopy
p-terphenyl	para-terphenyl: 
pentacene	
ISC	intersystem crossing

^aSome authors refer to this as T_2^* .

TABLE II. Pentacene optical properties^a

Phase	State	Origin (cm ⁻¹)	Extinction Coefficient × 10 ⁻³	Oscillator Strength	Lifetime (nsec)	Assignment	Ref.
vapor(580°K)	S ₀					¹ A _{1g} ⁻	b
	S ₁	18,900			6.1 ⁱ	¹ B _{2u} ⁺	c
solution(n-heptane)		17,100	12	0.08			b
solid(p-terphenyl) (1.8°K)	S ₁	$\left\{ \begin{array}{l} 17,065 \\ 17,006 \\ 16,887 \\ 16,883 \end{array} \right\}^d \left\{ \begin{array}{l} 17,069 \\ 17,009 \\ 16,891 \\ 16,887 \end{array} \right\}^m$			9.7 ^j	O ₄	
					9.7 ^j	O ₃	
					25.7 ^j	O ₂	
					25.7, ^j 23.5, ^k 24.5 ^l	O ₁	
solution(n-heptane)	S ₂	24,000	0.6			¹ B _{3u} ⁻	b
solution(n-heptane)	S ₃	32,300	300	2.2		¹ B _{3u} ⁺	b
calculation	T ₁ [†]	6,400, 7,800			(vapor) 33,000 ^c (solution) 70,000 ^g	³ B _{2u} ⁺	e, f
solid(tetracene)	T ₁ [†]	6,500					h
calculation	T ₂ [†]	17,000, 21,700				³ B _{3u} ⁺ , ³ B _{3u} ⁻	f
solution(benzene) (323°K)	T ₃	T ₁ + 19,820	120	0.7		³ B _{1g} ⁻	g
vapor(580°K)	T ₃	T ₁ + 21,500					c
solution(benzene) (323°K)	T ₄	T ₁ + 25,500	3	< 0.005		³ A _{1g} ⁻	g

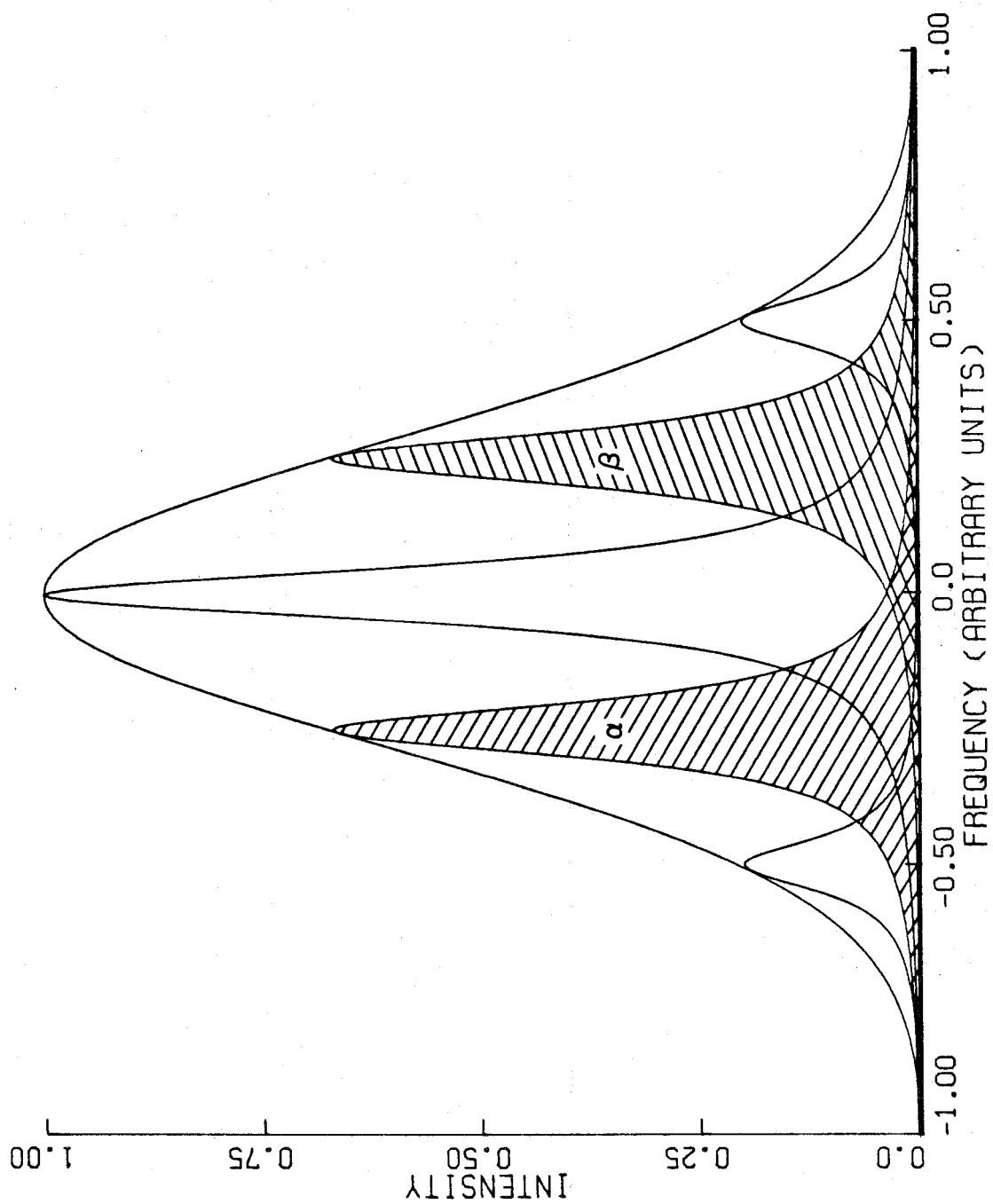
TABLE II. (Continued)

- ^aThe axis system adopted here is: x - long axis, y - short axis, and z is the out of plane axis.
- ^bE. Clar, Aromatische Kohlenwasserstoffe (Verlag, Julius Springer, Berlin, 1941); H. B. Klevens and J. R. Platt, *J. Chem. Phys.* **17**, 470 (1949).
- ^cB. Soep, *Chem. Phys. Lett.* **33**, 108 (1975).
- ^dJ. H. Meyling and D. A. Wiersma, *Chem. Phys. Lett.* **20**, 383 (1973).
- ^eR. Pariser, *J. Chem. Phys.* **24**, 250 (1956).
- ^fD. R. Kearns, *J. Chem. Phys.* **36**, 1608 (1962).
- ^gC. Hellner, L. Lindquist, and P. C. Roberge, *Faraday Trans. II*, **68**, 1128 (1972).
- ^hN. E. Geacintor, J. Burgos, M. Pope, and C. Strom, *Chem. Phys. Lett.* **11**, 504 (1971).
- ⁱS. Okajima and E. C. Lim, *Chem. Phys. Lett.* **37**, 403 (1976).
- ^jN. J. Bridge, University of Kent, private communication (T = 4.2°K).
- ^kT. J. Aartsma, J. Morsink, and D. A. Wiersma, *Chem. Phys. Lett.* **47**, 425 (1977); T = 1.8°K.
- ^lOur measurement (LADS) was independent of temperature in the region 1.8 → 4.2°K.
- ^mThis work (see Fig. 13 and the text).
- ⁿA. P. Marchetti, W. C. McColgin, and J. H. Eberly, *Phys. Rev. Lett.* **35**, 387 (1975).
- [†]These T₁ and T₂ refer to the first and second triplet states of pentacene, and should not be confused with T₁ and T₂ relaxation times.

Figure 1

Inhomogeneous broadening of an optical transition in a solid. Shown is a Gaussian distribution of homogeneously broadened molecular groups; each having a Lorentzian lineshape. The shaded areas, α and β , refer to distinct groups of molecules selected in the narrowband coherence experiments.

HOMOGENEOUS AND INHOMOGENEOUS BROADENING



given by $(\pi T_2)^{-1}$. For pentacene in a p-terphenyl host the inhomogeneous broadening is probably due to crystal field irregularities caused by strain and lattice defects. The homogeneous broadening on the other hand contains both the spontaneous decay (T_1 contribution) and the contribution due to pure dephasing (T_2'). For the latter case the population of the state is unchanged and the "scattering," say by phonons, is elastic in nature.

Our experiments focus on unraveling the details of line-broadening mechanisms in pentacene by separating experimentally the contribution to the total homogeneous linewidth of the various T_1 relaxation processes from the T_2' processes. In this manner we can relate the measurements to the question raised earlier, namely, the effect of excitation bandwidth on the decay and dephasing of the prepared state. To obtain optical T_1 and T_2 following narrow-band excitation we have used the coherent transient methods or the method of emission detection of optical coherence. It is therefore important to understand the various phenomena that occur when large molecules interact with strong coherent fields, and to examine how the dynamics of the interaction provide the detailed molecular information we seek.

Before proceeding into a detailed discussion of our experiments and the theory required to understand the processes of interest, it is perhaps useful to make use of a general description that provides a physical explanation of the somewhat complicated and different terminology used throughout the paper for describing coherence experiments done by monitoring the laser¹⁴ or the spontaneous emission.¹⁵

A. Optical nutation

When a group of molecules (say, α of Fig. 1) is brought into resonance with a strong coherent optical field the population can be completely driven from the ground state to the excited state in an oscillatory fashion as molecules alternately absorb and re-emit radiation coherently. This process known as optical nutation¹⁶ has an oscillation frequency (Rabi frequency) determined by $\bar{\mu}$, the transition dipole moment and $\bar{\epsilon}$ the laser field amplitude. A nutation is damped due to inhomogeneous broadening and the nonuniform spatial intensity distribution of the laser as well as the molecular dephasing processes. From this coherent transient which occurs at the leading edge of the laser pulse one can determine μ and estimate T_2 . Under certain conditions in solids, T_2 can be determined.

B. Optical free induction decay (OFID)

As a group of molecules initially on resonance with a coherent field (not necessarily a strong field) is suddenly switched off resonance they will emit initially in phase.¹⁷ If, as shown in Fig. 1, the laser frequency is switched from being on resonance with the homogeneous group α to group β , then the molecules emitting coherently (from α) can beat against the new laser frequency (ω_β) if a square-law detector is used for monitoring the transmitted laser beam. The beat pattern will decay as the molecules dephase and as with the optical nutation, the FID contains contributions from inhomogeneous and power broadening processes. Extrapolated to zero laser power the decay time gives T_2 directly.

Now, since the laser is brought into resonance with group β an optical nutation can occur (at ω_β) at the same time but if the laser power is low enough only the OFID pattern from α will be observed.

C. Incoherent resonance decay

Up to this point we have discussed coherent absorption and coherent emission processes which are usually observed along the laser beam. One can also observe these coherent signals utilizing the incoherent (spontaneous) emission¹⁵ at right angles to the exciting beam and from it obtain optical T_1 and T_2 .

If the emission intensity is measured as the single mode laser frequency rapidly changes from α to β then one should see the superposition of two processes occurring simultaneously. First, α molecules will decay (by T_1) since they are now off resonance. At the same time, β molecules are being driven coherently (i.e., nutating) by the laser field toward some equilibrium population distribution. Thus, the observed signal should show an initial rapid build-up and nutation transient (due to β molecules) and a decay (due to α molecules). We have used IRD to denote the process of incoherent resonance decay.

III. EXPERIMENTAL

A. Sample preparation

p-Terphenyl (scintillation grade) was purchased from Eastman Organic Chemicals and zone-refined for eighty passes. Pentacene (Aldrich Chemical Company) was twice vacuum sublimed. Dilute single crystals (10^{-5} - 10^{-7} m/m) of pentacene in p-terphenyl were grown from

the melt using standard Bridgman techniques. Crystals (1-3 mm thick) were cut parallel to the ab cleavage plane and mounted in most experiments with the crystal b-axis parallel to the polarization direction of the exciting laser.

B. Cryogenics

The crystals were suspended directly in a liquid helium filled glass Dewar. Temperatures down to 1.7°K were obtained by pumping on the helium reservoir with a Sargent-Welch (Model 1374) vacuum pump. The temperature was monitored with a calibrated carbon glass resistor (Lakeshore Cryotronics CGR-1-1000) mounted on the sample holder near the crystal and by measuring the vapor pressure of helium with calibrated Wallace and Tiernan pressure gauges.

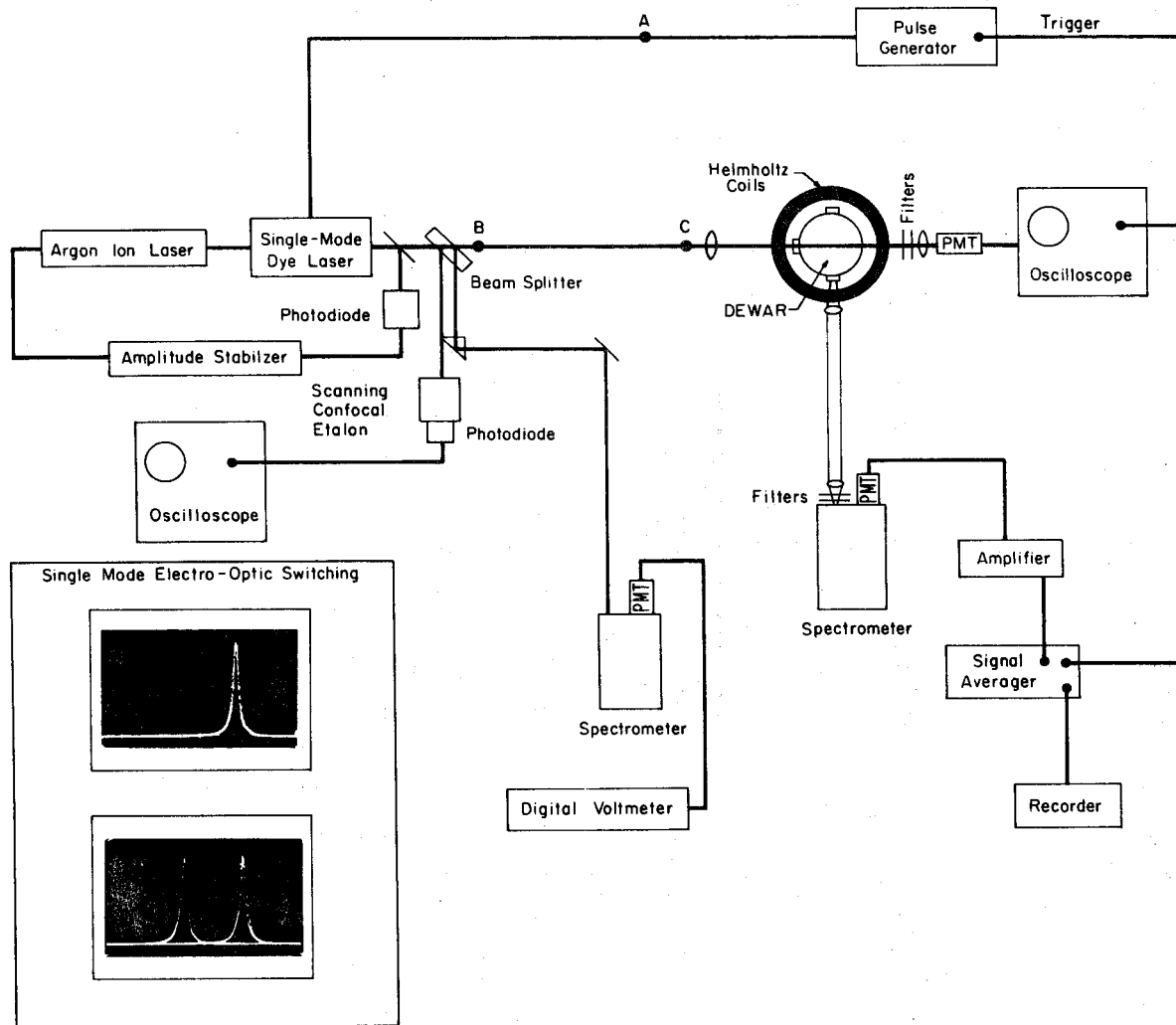
C. Laser excitation sources

Three different laser sources were used for the excitation of pentacene in p-terphenyl. For broad band excitation, a pulsed tunable dye laser (Molelectron DL 200) pumped by a nitrogen gas laser (Molelectron UV 400), or a multi-mode CW dye laser were used. The N₂ pumped dye laser has a frequency bandwidth of 18 GHz, a peak power of 40 KW, and a pulse duration of 5 nsec. The multimode CW dye laser has a bandwidth of 240 GHz and up to 1 W output power.

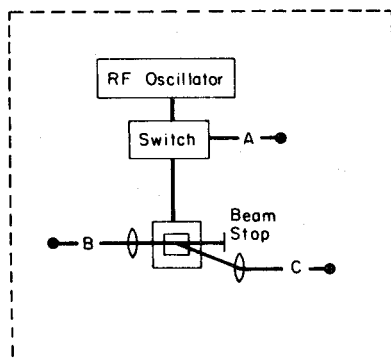
For narrow band excitation (see Fig. 2) we used a single-mode tunable jet-stream CW dye laser (Spectra Physics 580A) pumped by an argon ion CW gas laser (Spectra Physics 171). To obtain single-mode operation, the dye laser has three intracavity etalons with different free spectral ranges (FSR). One of the etalons (2 mm air spaced) is

Figure 2

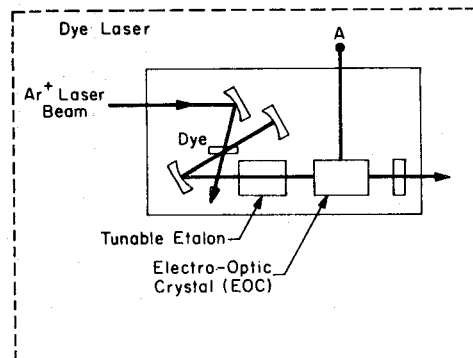
A schematic diagram of the experimental arrangements used for EO and LADS experiments. All laser components are mounted on a vibration-isolation optical table. The electro-optic switching process shown in the insert is monitored by synchronizing the scanning confocal etalon with the voltage pulse supplied to the AD*P crystal. The other insert depicts the method of LADS.



LADS METHOD



EO METHOD



temperature regulated and piezoelectrically tunable. The other two are solid etalons of 0.17 mm and $\approx 1.7 \mu$ thickness, respectively.

For all of these experiments Rhodamine 6G is used. The maximum laser power of the linearly polarized single mode is 100 mW in a Gaussian beam (Fig. 3) with a half-width ($1/e$) of 0.31 ± 0.01 mm providing a maximum intensity (unfocused) of 33 W/cm^2 . The transverse field profile of the single mode beam was measured using a photodiode mounted on a micrometer controlled translation stage (4μ resolution). Slits ($\approx 50 \mu$) were attached to the photodiode thus limiting its aperture. The results in Fig. 3 were obtained by scanning the photodiode across the beam. The Gaussian profile seen here is what one expects for a TEM_{00} beam.

The frequency bandwidth is determined by jitter and drift due to jet instabilities, temperature fluctuations and vibrations. With a combination of techniques we were able to reduce the jitter (long term) of the single mode to ± 3 MHz without active frequency feedback loops. These techniques involved (1) careful control of the dye solution temperature using a regulated bath; (2) independent air conditioning for the lab providing room temperature stability to $\pm 1^\circ\text{C}$; (3) use of a vibration isolation optical table to mount all laser components; (4) sound-proofing of the dye laser with a tight fitting enclosure, and (5) amplitude stabilization of the single mode by a feedback circuit.

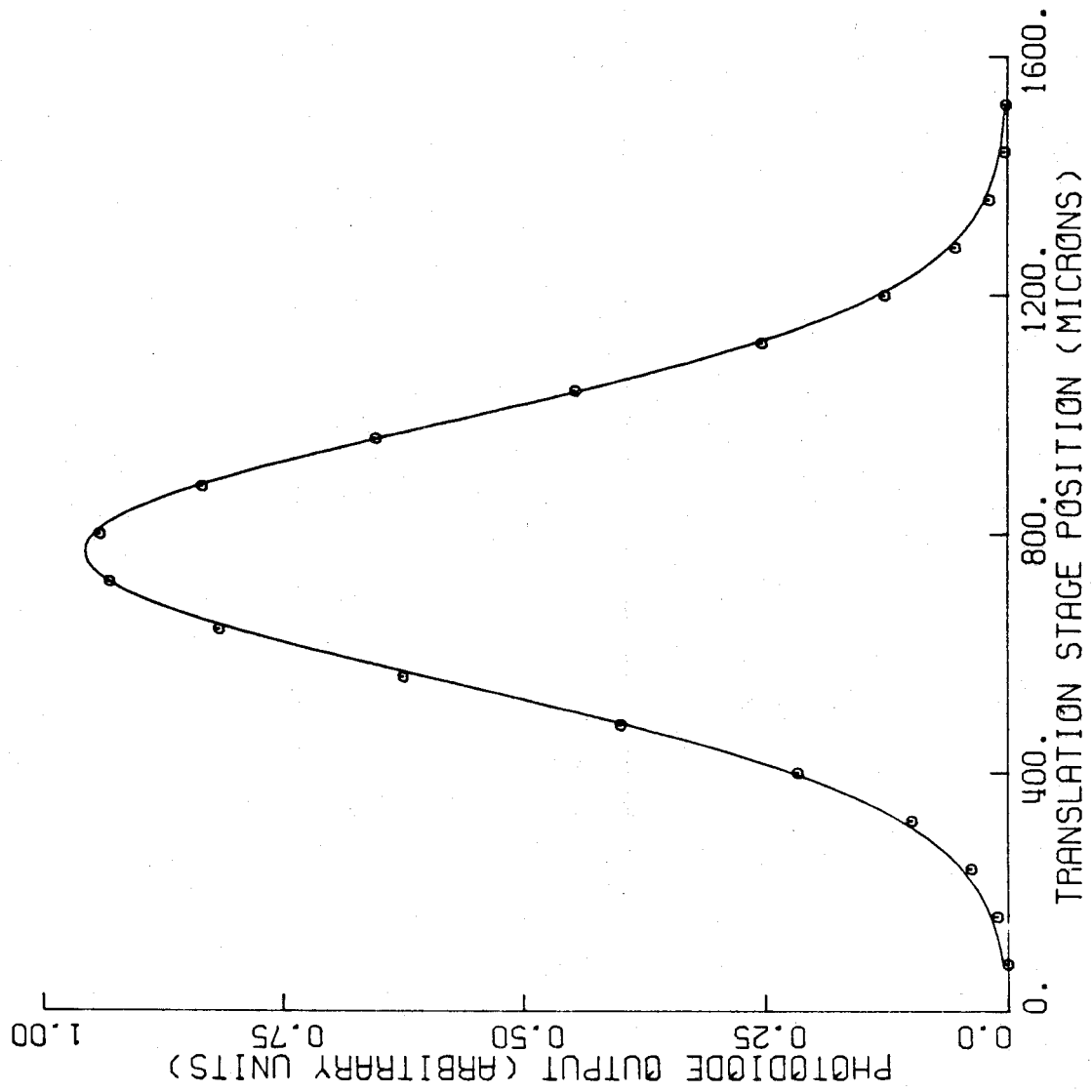
D. The laser frequency switching and laser-acoustic diffraction techniques

To obtain nanosecond time resolution with the CW narrow band laser we employ either electro-optic (EO) frequency modulation or laser

Figure 3

The transverse beam profile of the single-mode laser. Experimental data (circles) obtained by scanning a carefully apertured ($50\ \mu$) photodiode across the laser beam are fit to a Gaussian whose $1/e$ halfwidth is 0.31 ± 0.01 mm. The excellent fit to a Gaussian profile confirms the TEM_{00} nature of the laser beam. This will be important for obtaining the transition moment from optical nutation experiments (see text).

SINGLE-MODE LASER TRANSVERSE BEAM PROFILE



acoustic diffraction. (We call the latter technique LADS¹⁸ for Laser Acoustic Diffraction Spectroscopy to avoid confusion with another technique: opto-acoustic spectroscopy developed by Harshbarger and Robin.¹⁹) For EO frequency modulation we modified the laser cavity to accept an AD*P crystal. Frequency switching is accomplished by supplying voltage pulses to the EO crystal which alter its index of refraction and the optical path length. Thus, for the duration of the voltage pulse, the frequency of the laser can be changed from ω_0 (the peak frequency of the transition resonance) to a new frequency ω . This EO switching technique was first described by Yariv²⁰ and later by Kiefer et al.²¹ for CdTe modulators. Hall²² was the first to demonstrate the frequency switching technique to observe a coherent transient (FID) in methane in the IR. He used a LiNbO₃ modulator to frequency switch a He-Ne laser operating at 3.39 μ . Shoemaker and Van Stryland²³ first discussed how this technique would be useful for observing the nutation and thus for measuring transition moments. Brewer and Genack²⁴ were successful in extending the technique to the visible region and measured transients in I₂. Since then this laser frequency-switching method has allowed one to observe coherent transients in gases,^{24, 15} solids,^{25, 26} and molecular beams.²⁷ In addition to the above-mentioned technique we have utilized the IRD¹⁵ method to monitor the coherence of the ensemble excited by a narrow-band laser. In this method, the EO crystal is also intracavity.

Typically, the dispersion of the nonlinear EO crystal gives a 60 MHz frequency shift within the inhomogeneous resonance of the optical transition (width > GHz) for voltage pulses of 100 V. To switch

the laser frequency further (which would be necessary in systems with larger homogeneous linewidths), fast high-voltage pulses are required. In practice, these pulses are hard to obtain--especially at high repetition rates and when multiple pulse (photon echo) experiments are desired. Furthermore, there is a limit on the maximum frequency shift possible (maintaining stable single-mode output) which is determined by the cavity mode spacing (~ 400 MHz). When one finds it difficult to switch out of the homogeneous linewidth (i. e., off-resonance) with the EO method, then one can utilize the LADS method.

The LADS technique for observing coherent transients was reported recently by Orłowski *et al.*¹⁸ An extra cavity acousto-optic modulator is used to diffract the laser beam to and from the sample. Thus, instead of switching the frequency of the single-mode laser off resonance within the inhomogeneous line we effectively turn the laser "off." This technique relies on the acousto-optic effect²⁸ and can be described as follows. The single mode beam is focused upon a quartz crystal which has a thin film transducer bonded to it. RF pulses excite phonons in the transducer creating traveling acoustic waves in the crystal which diffract the incident beam (up to 50%) at the Bragg angle and shift its frequency by the acoustic phonon frequency (470 MHz). Thus, the diffracted beam is deflected into the sample for the duration of the RF pulse. The characteristics of the laser pulse this technique provides are determined by (1) the RF pulse width and its rise/fall times and (2) the transit time of the acoustic wave across the focused laser beam in the crystal. We have measured laser pulse rise/fall

times of 3 nsec ($1/e$ time) using a 75 mm focal length lens to focus the laser beam into the crystal.

There are advantages to both of the techniques described above. The EO technique is most useful for observing OFID since extremely sensitive heterodyne detection techniques can be employed which exploit the fact that the laser is off-resonance and can beat with the coherent emission from the sample. The LADS method offers the following advantages. First, the decay of off-resonance molecules is not superimposed on the build-up transients of on-resonance molecules (which occurs with the EO technique) because the laser is effectively shut off except for the duration of the pulse. This is especially important for large molecules with a high density of excited states. In these systems the complicated level structure can make the interpretation of transient spectra difficult. The LADS method removes the influence of off-resonance effects and thus simplifies the spectra. Secondly, the optical pulses are generated by supplying low-voltage (TTL level) pulse trains to an RF oscillator instead of the high-voltage pulses that may be required by the EO technique. Finally, one can obtain high sensitivity as with heterodyne techniques by detecting the spontaneous emission at right angles to the exciting laser beam. With the proper pulse sequences, one can directly measure both T_1 and T_2 .¹⁸

E. Magnetic field experiments

Several experiments were performed with samples in the presence of an external magnetic field. Two coils were placed around the tail of the Dewar at the Helmholtz spacing such that the field direction

was parallel to the direction of laser polarization. With 22 amps of current supplied by a regulated dc power supply we measured a field strength of 900 Oersted at the sample using a Bell gaussmeter and a calibrated Hall effect probe. The field was homogeneous at the crystal to better than 1%.

F. Experimental procedure

The apparatus used for the EO and LADS experiments is shown schematically in Fig. 2. The output of the single mode laser is amplitude stabilized and split (8%) to allow continuous monitoring of laser frequency and single-mode operation using a 0.5 m spectrometer and a scanning confocal etalon, respectively.

For LADS experiments the modulator was placed in the optical path such that the diffracted beam continues on to the sample while the transmitted beam was blocked. Thus, the sample was excited only when an RF pulse was supplied to the AO crystal.

Coherent transient along the laser beam was detected using fast biased photodiodes (HP 5082-4203) and/or a modified RCA IP 28 photomultiplier.²⁹ In some experiments (OFID) polarizers were used on either side of the Dewar to ensure that only light polarized with the laser reached the detector.

For some experiments the transients were displayed directly on a sampling scope; however, signal averaging was also done using a scanning-gate boxcar integrator (PAR Model 162).

Emission from the sample was detected at right angles to the exciting beam using a shielded (RF, magnetic, electrostatic), cooled

photomultiplier (EMI 9558). For detecting very fast transients on the emission we used the modified IP28 photomultiplier which has a bandwidth greater than 1 GHz. Sharp-cut glass filters were used to block the exciting wavelength. In most experiments the total emission from the sample was monitored; however, several experiments were performed using a 0.5 m (or 0.75 m) spectrometer to resolve individual vibronic lines. The output of the PMT was amplified and fed to the boxcar integrator for signal averaging.

Absorption experiments were performed by using a tungsten (1000 W) or a xenon (200 W) lamp, together with the appropriate filters. For high-resolution measurements a Spex (1-14018) double monochromator equipped with holographic gratings (resolution = 0.09 cm^{-1}) was used. In some experiments, a Fabry-Perot interferometer (Burleigh RC 110) in front of a 0.5 m Jarrell-Ash spectrometer was used for scanning the line shape profile.

G. Data treatment

1. Temperature-dependence measurements

The temperature dependence of the optical nutation signal (initial amplitude) and the IRD signal was determined using the following carefully controlled procedure. For the optical nutation experiment the d.c. signal and the transient initial amplitude were monitored at each temperature. Detector linearity was checked using calibrated neutral density filters. As the temperature rose above the λ point of liquid helium and boiling started, the d.c. signal decreased one order of magnitude due to scattering from helium bubbles. Amplifier gain was

increased at this point. All data were corrected for the d. c. signal strength which appeared to decrease slightly as the temperature was raised. Since the transients observed in our experiments were insensitive to temperature until $\approx 3^\circ\text{K}$ the λ point (2.17°K) does not represent a problem in determining the onset of the temperature effect.

For the IRD experiments, the entire decay signal was measured at each temperature. The PMT current (d. c.) was kept constant (within the detector's linear region) throughout the range of temperatures studied. We observed an increase in the d. c. emission intensity (factor of three) when the temperature was increased from 2.17 to 4.2°K . Similar temperature dependences were obtained for both the optical nutation and IRD experiments.

2. Zeeman measurements

IRD experiments performed with external magnetic fields of up to 900 Oersted were compared very carefully with their zero-field counterparts using the following procedure. First, an IRD decay and d. c. emission intensity were measured at zero field. Then, the field was turned on and another decay (and intensity) were recorded. Finally, we immediately repeated the zero field experiment to insure reproducibility. Because the magnetic field effect on the observed decay was small ($\approx 15\%$) we repeated this cycle more than twenty times with several different crystals, concentrations, and orientations. In all experiments which utilize a shielded photomultiplier reproducibility was excellent; however, the magnitude of the effect was very sensitive to slight changes (one cavity mode [390 MHz] or less) in laser frequency.

One should note that the effect of a small d.c. magnetic field on the photomultiplier current might result in small changes in the d.c. signal level but will not affect the dynamic response of the tube. More discussion of the Zeeman experiments will be presented later.

3. Computer fitting procedures

Computer assisted nonlinear least squares regression analyses were performed to fit all of the IRD data as well as the optical nutation and the OFID. To avoid some of the ambiguities associated with these techniques (e.g., making initial estimates of parameters which may be biased or which may lead to only a local minimization of error) most of the data was fit in a two-step procedure. First, we utilized an eigenfunction expansion method developed by Provencher³⁰ for determining the best exponential decay parameters (rate constants and coefficients) for the IRD transients [discussed later in Eqs. (43) and (46)]. This method requires no initial guesses and provides cross correlation coefficients as well as confidence limits. From the values of the coefficients of the exponentials we were able to make good initial guesses for the rate constants needed in the steady-state coherence model of Section IVB. Then, we used a more conventional (and more general) procedure for nonlinear least squares regression analysis using an algorithm developed by Marquardt.³¹ Although our program handles up to 50 parameters, only two parameters were simultaneously varied (for the IRD fits) to get solutions that converged upon the same values for several different starting points. Thus, unique solutions can be assumed safely in most cases. Similar procedures were adopted for treating the results of other

transients, and thus the program, which is stored in the Caltech computer library, was used routinely for analyzing all the data reported in this paper.

IV. THEORY OF DEPHASING IN PENTACENE

Pentacene, which vibrates in 102 different modes, has approximately 3×10^{14} vibrational levels per wavenumber near the energy of the $|p\rangle$ state.³² This implies that the molecule belongs to the "statistical limit" in the sense that the levels interacting with $|p\rangle$ form essentially a continuum. However, the presence of a nearby triplet manifold might make the interaction between the sparse levels of the triplet state and the $|p\rangle$ state a discrete one, thus resulting in the formation of $|m\rangle$ states. Furthermore, not every state out of the 10^{14} levels has the appropriate Franck-Condon and/or symmetry properties for coupling with $|p\rangle$. If this coupling between $|p\rangle$ and quasi-resonant levels is operative and the homogeneous linewidth of the resulting states is less than their spacing, we expect to locate $|m\rangle$'s which as mentioned before have different T_1 decay times from that of the $|p\rangle$ state.

In the statistical limit,⁵ it has been shown^{3, 33} that following the excitation into $|p\rangle$, the decay will exhibit a fast component with a rate of $(2\pi/\hbar) v_{pl}^2 \rho(E_p)$ and a slow component (T_{1m}^{-1}) in addition to a complicated beat pattern due to interference effects³⁴ similar to those of quantum beat phenomena. In the sparse limit the situation is different and depends on how many $|m\rangle$ states the light source spans as well as the correlation time of the source.

If $|m\rangle$ is excited say by a coherent narrow band source, then the description of dephasing at any time t is that of a two-level system provided there are no cross relaxations among $\{|m\rangle\}$. The treatment for the interaction between coherent light and such two-level systems is a standard one and can be found in several articles and textbooks.³⁵ If, on the other hand, $|p\rangle$ is prepared as depicted in Fig. 4, then we have more than two levels to treat, and the description of the time evolution of the excited state crucially depends on the time scale of the experiment.

As we shall see from the experiments done on pentacene, the picture shown in Fig. 4 can be simplified considerably if one knows optical T_1 , T_2 , and the Rabi frequency. Of course, the definitions of T_1 and T_2 in such a complex level structure require some care since a genuine dephasing mechanism might be washed out by changing representations or conversely an artificial dephasing process may be introduced by changing the number of degrees of freedom!

For the pentacene case, we define the following rates for the different pathways:

$$\Gamma_{p0} = T_{1p0}^{-1} = \text{total decay rate of } |p\rangle \text{ to } |0\rangle$$

$$\Gamma_{pl} = T_{1pl}^{-1} = \text{total decay rate of } |p\rangle \text{ to } \{|l\rangle\}$$

$$T_{1p}^{-1} = T_{1pl}^{-1} + T_{1p0}^{-1} = \text{total rate for the depletion of } |p\rangle \text{ population}$$

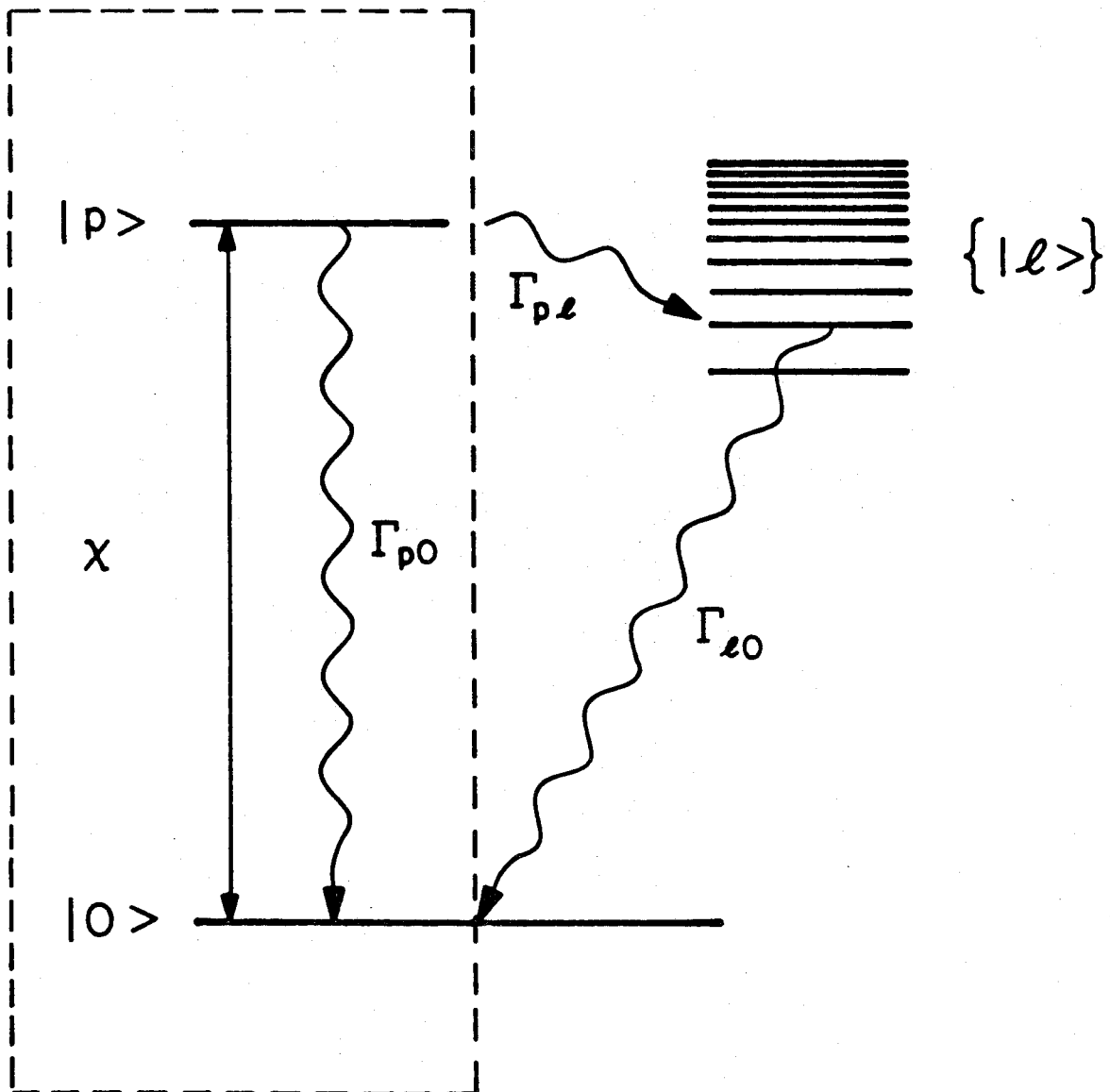
$$\Gamma_{l0} = T_{1l0}^{-1} = \text{total decay rate of } l \text{ into } |0\rangle$$

$$T_{10}^{-1} = T_{1p0}^{-1} + T_{1l0}^{-1} = \text{total feeding rate to } |0\rangle$$

$$\chi = \text{"pump" rate}$$

Figure 4

A schematic diagram of the level structure in pentacene showing important decay channels. The levels $|0\rangle$ and $|p\rangle$ refer to the ground and first excited electronic states, respectively, while $\{|\ell\rangle\}$ is a manifold of effective levels that interacts with the two-level system enclosed in dashed lines. The nature of the $\{|\ell\rangle\}$ manifold is unspecified and all the rate constants are defined in the text (see Section IV).



$\Gamma = T_2^{-1}$ = total dephasing rate of the two levels $|p\rangle$ and $|0\rangle$

$T_2'^{-1}$ = rate of pure dephasing (with no T_1 terms) of the two levels $|p\rangle$ and $|0\rangle$.

In what follows we provide the theoretical analysis that will be used later in all of the experiments done on pentacene. These experiments span different time regimes, and effectively probe the excited population either in the $|0\rangle$ and $|p\rangle$ levels (the levels in the dashed rectangle of Fig. 4) or in the entire (statistically closed) level structure after the phase coherence of $|0\rangle$ and $|p\rangle$ achieves a steady state. Thus we have two extreme limits which we will term the transient coherence and steady-state coherence regimes, respectively. If the observed transient decay time τ_0 (observed say by monitoring the population of $|p\rangle$) is much longer than $(\hbar/\mu \cdot \epsilon)$ and T_2 , then the steady-state coherence regime can be used assuming that on the τ_0 time scale all correlations among $\{|l\rangle\}$ do not exist, otherwise one may use the decoupling scheme of Grigolini and Lami.³⁶ On the other hand, if τ_0 is comparable to $(\hbar/\mu \cdot \epsilon)$ the transient coherence coupling regime will be recovered.

A. Transient coherence regime: $\tau_0 \approx T_2$

In this limit the rate of optical pumping (χ) is very large and the dephasing is reaching a steady state value before the channel to $\{|l\rangle\}$ is opened. In effect the two levels are therefore decoupled from the rest of the (many) molecular levels. To describe the dephasing of the two-levels on such time scales, we shall follow the standard procedure of using the density matrix and the representation of Feynman, Vernon, and Hellworth (FVH).³⁷

First, we write the complete Hamiltonian for the system as a sum of the zero-order Hamiltonian and an interaction term signifying the coupling of the two molecular states by the field:

$$\mathcal{H} = \frac{\hbar\omega_0}{2} \sigma_3 - \mu \cdot \epsilon \sigma_1 \cos \omega t \quad (5)$$

Here σ_1 and σ_3 are the Pauli matrices, and ω_0 and ω are the transition and laser frequency, respectively. In the laboratory frame, the equation of motion for the system is therefore given by

$$i\hbar\dot{\rho}' = [\mathcal{H}, \rho'] \quad (6)$$

where ρ' is the density matrix and the prime is used to designate the laboratory frame representation.

By going into a rotating frame of reference (at ω) one obtains

$$i\hbar\dot{\rho} = [\mathcal{H}_r, \rho] \quad (7)$$

where

$$\mathcal{H}_r = U^{-1} \mathcal{H} U \approx \frac{\hbar\omega}{2} \sigma_3 \approx \frac{\hbar\Delta}{2} \sigma_3 - \frac{\mu \cdot \epsilon}{2} \sigma_1 \quad (8)$$

Eq. (8) was obtained using the unitary transformation $U = e^{-i\frac{\omega}{2}\sigma_3 t}$ and the following identity:

$$e^{i\omega\sigma_3 t/2} \sigma_1 e^{-i\omega\sigma_3 t/2} = \sigma_1 \cos \omega t - \sigma_2 \sin \omega t \quad (9)$$

Terms oscillating at 2ω were neglected and Δ is defined as $\omega_0 - \omega$.

Given Eqs. (7) and (8) one can easily show that the equation of motion for ρ can be written, after adding phenomenological relaxations terms for pentacene, as:

$$\dot{\rho}_{00} = \frac{1}{T_{1p0}} \rho_{pp} + \frac{1}{2} i \chi (\rho_{p0} - \rho_{0p}) \quad (10a)$$

$$\dot{\rho}_{pp} = \frac{-1}{T_{1p0}} \rho_{pp} + \frac{1}{2} i \chi (\rho_{0p} - \rho_{p0}) \quad (10b)$$

$$\dot{\rho}_{0p} = (-\frac{1}{T_2} + i\Delta) \rho_{0p} + \frac{1}{2} i \chi (\rho_{pp} - \rho_{00}) \quad (10c)$$

Here T_{1p0} is the spontaneous emission lifetime of the upper level,

$\chi = \frac{\mu \cdot \epsilon}{\hbar}$ and

$$\frac{1}{T_2} = \frac{1}{2T_{1p0}} + \frac{1}{T_2'} = \frac{1}{2T_1} + \frac{1}{T_2'} \quad (11)$$

The quantity $(T_2')^{-1}$, the pure dephasing rate, represents elastic interactions with phonons in the solid which at very low temperatures approaches zero. Thus, $T_2 = 2T_{1p0}$ in the absence of dephasing processes in the system and only when the level structure³⁸ is similar to that discussed here for pentacene.

The solution of the coupled differential equations of motion (10) for the elements of the density matrix must be found to interpret the coherent transients one sees in the laboratory. Effects due to inhomogeneous broadening and the nonuniform spatial distribution in ϵ of the laser must also be treated. We shall deal with each transient separately and focus our attention only upon those that we have observed in pentacene.

1. Optical nutation

Optical nutation has been observed recently in solids by Zewail and Orłowski.²⁵ To describe these nutation signals one must

determine the time dependence of the off-diagonal elements of the density matrix because these elements of ρ are related to the polarization P (amplitude \bar{P}) induced by the laser in an ensemble density of N molecules according to the following expression:

$$\begin{aligned} P(t) &= N\mu(\rho_{0p} e^{-i\omega t} + \rho_{p0} e^{i\omega t}) \\ &= N\mu(r_1 \cos \omega t - r_2 \sin \omega t) \end{aligned} \quad (12)$$

where from the FVH picture:

$$\begin{pmatrix} r_1 \\ r_2 \\ r_3 \end{pmatrix} = \begin{pmatrix} \rho_{0p} + \rho_{p0} \\ i(\rho_{p0} - \rho_{0p}) \\ \rho_{pp} - \rho_{00} \end{pmatrix} \quad (13)$$

Thus the polarization acts as a source term in Maxwell's equation and provides a field amplitude ϵ_s in the solid (optically thin) that is given by

$$\epsilon_s \simeq -i \frac{\omega L \eta}{2c\epsilon_0} \bar{P} \quad (14a)$$

where L is the crystal thickness, ϵ_0 the background dielectric constant, η the corresponding refractive index and c the speed of light.

Since the macroscopic polarization is given by r_1 and r_2 averaged over the inhomogeneous lineshape, and because r_1 is an odd function of Δ while r_2 is an even function of Δ , we can write ϵ_s as follows (see Eq. 12):

$$\epsilon_s = \frac{\omega L \eta}{2c\epsilon_0} N\mu \langle r_2 \rangle = \frac{i\omega L \eta}{c\epsilon_0} N\mu \langle \rho_{p0} \rangle \quad (14b)$$

Therefore, to obtain $\langle r_2 \rangle$ or $\langle \rho_{p0} \rangle$, Eq. (10) must be solved. Using

Laplace transformation techniques, Schenzle and Brewer³⁹ solved Eq. (10) and we show their result for r_2 in the high power limit (i. e., $\chi \gg \frac{1}{T_1}, \frac{1}{T_2}$) which applies in our case:

$$r_2 = \chi \exp \left[- \left(\frac{1}{T_2} + \frac{1}{2T} \frac{\chi^2}{\chi_1^2} \right) t \right] \frac{\sin \chi_1 t}{\chi_1} \quad (15)$$

Here $\frac{1}{T} = \frac{1}{T_{1p0}} - \frac{1}{T_2}$, and $\chi_1^2 = \Delta^2 + \chi^2$.

Eq. (15) must now be averaged over the inhomogeneous line shape $g(\omega)$ of the solid. We assume a Gaussian lineshape function (normalized area) of the form:

$$g(\Delta) = \frac{1}{\sqrt{\pi} \delta \omega_I} e^{-\Delta^2 / \delta \omega_I^2} \quad (16)$$

where $\delta \omega_I$ is the width of the inhomogeneous line centered at $\omega = \omega_0$.

For pentacene and for many other solids in the optical region $\chi \ll \delta \omega_I$, and therefore the averaged value of r_2 can be written in the following way [see Appendix II]:

$$\langle r_2(t) \rangle \simeq \chi e^{-t/T_2} \left\langle \exp \left[-\frac{1}{2T} \left(\frac{\chi^2}{\Delta^2} \right) t \right] \right\rangle \left\langle \frac{\sin \chi_1 t}{\chi_1} \right\rangle \quad (17)$$

This factorization of the averaging is valid especially at short times and has been checked numerically.³⁹ The first integral can be evaluated analytically while the second integral has been approximated by the usual Bessel function description for optical nutation;¹⁶ i. e.,

$$\langle r_2(t) \rangle \simeq \chi \frac{\sqrt{\pi}}{\delta \omega_I} \exp \left[-\frac{t}{T_2} - \frac{\chi}{\delta \omega_I} \left(\frac{2t}{T} \right)^{\frac{1}{2}} \right] J_0(\chi t) \quad (18)$$

This solution is valid except near $t = 0$ because of the approximations made to evaluate the integrals. Later we will correct Eq. (18) so that it will be valid for all times. Now, since $\delta\omega_I \gg \chi$ we can simplify Eq. (18) even further:

$$\langle r_2(t) \rangle \simeq \chi \frac{\sqrt{\pi}}{\delta\omega_I} J_0(\chi t) e^{-t/T_2} \quad (19)$$

To complete our calculation we must average Eq. (19) over the measured transverse profile of the TEM_{00} Gaussian beam of our laser (Fig. 3) since individual molecules will see different field strengths along the width of the beam and will therefore have different χ 's. This will smear out the Bessel function causing more rapid damping of the transient.

First, let us consider the signal at the detector. As a square-law device, it will see an intensity $I(t)$ given by:

$$I(t) = c\mathcal{E}_0 \langle [\epsilon \cos \omega t + \epsilon_s \cos \omega t]^2 \rangle_t \quad (20)$$

The time average simply yields

$$I(t) = c\mathcal{E}_0 \left(\frac{\epsilon^2}{2} + \epsilon_s \epsilon + \frac{\epsilon_s^2}{2} \right) \quad (21)$$

We may assume for optically thin samples that $\epsilon_s \ll \epsilon$. Defining $I_0 = \frac{1}{2} c\mathcal{E}_0 \epsilon^2$ the total signal at any time t is:

$$I(t) = I_0 + c\mathcal{E}_0 \epsilon \epsilon_s(t) \quad (22)$$

Eq. (22) reveals the amplification of the signal field by the laser field, similar to the heterodyne detection scheme. Combining Eqs. (14, (19), and (22) we have:

$$I(t) = I_0 - A\chi^2 J_0(\chi t) e^{-t/T_2} \quad (23)$$

where A is a constant: $A = (\sqrt{\pi}/2)\hbar\omega_L N/\delta\omega_I$ and $\eta = 1$.

If we replace ϵ by $\epsilon e^{-R^2/2B_L^2}$, where B_L is the laser beam halfwidth ($1/e$) of the intensity profile (not field), and integrate over the surface area of the detector, which is larger than the beam diameter, our total signal is:

$$I_T(t) = 2\pi \int_0^\infty I(t) R dR \quad (24)$$

If we make the substitution

$$\chi' = \chi t \exp [-R^2/(2B_L^2)] \quad (25)$$

Eq. (24) can be solved easily to yield

$$\begin{aligned} I_T(t) &= \pi B_L^2 \left\{ I_0 - \frac{2A}{t^2} e^{-t/T_2} \int_0^{\chi t} \chi' J_0(\chi') d\chi' \right\} \\ &= \pi B_L^2 \left\{ I_0 - 2A \left(\frac{\chi}{t} \right) J_1(\chi t) e^{-t/T_2} \right\} \end{aligned} \quad (26)$$

Shoemaker and Van Stryland²³ obtained results similar to Eq. (26) when dealing with gases in the IR region, except for the exponential term containing T_2 . In their approach they assumed an infinitely long relaxation time $T_1 = T_2$ (which is reasonable in the IR) and thus the nutation essentially damps by the preexponential terms of Eq. (26). However, in our case (optical) T_2 is short enough so that the transient decay is given by the full expression (26). Because of this the nutation signal when treated properly can give T_2 . We see that averaging over the laser beam causes the transient to damp faster than the result of Eq. (23) which describes only the inhomogeneous averaging. However, the

oscillation frequency is essentially unchanged. This point is illustrated with the computer simulation of Eqs. (23) and (26) shown in Fig. 5, and will be clearly demonstrated when we fit the nutation data of pentacene.

Although $J_1(\chi t)$ goes to zero at $t = 0$, the factor of $1/t$ in the expression for the nutation obtained by averaging over the laser beam causes Eq. (26) to be invalid near $t = 0$ ($\chi t < 1$). We can correct this behavior with an error function similar to that used by Tang and Silverman¹⁶ in their discussion of the nutation effect. Since the limiting form of $J_1(\chi t)$ for small arguments is:

$$J_1(\chi t) \big|_{\text{short times}} \approx \frac{\chi t}{4}, \quad (27)$$

an error function of the form:

$$\text{erf}\left(\frac{\chi t}{2}\right) = \frac{2}{\sqrt{\pi}} \int_0^{\frac{\chi t}{2}} e^{-\alpha^2} d\alpha \quad (28)$$

will correct the behavior of Eq. (26) and provide a result valid for all t , within the framework of the above mentioned approximations. Thus we have

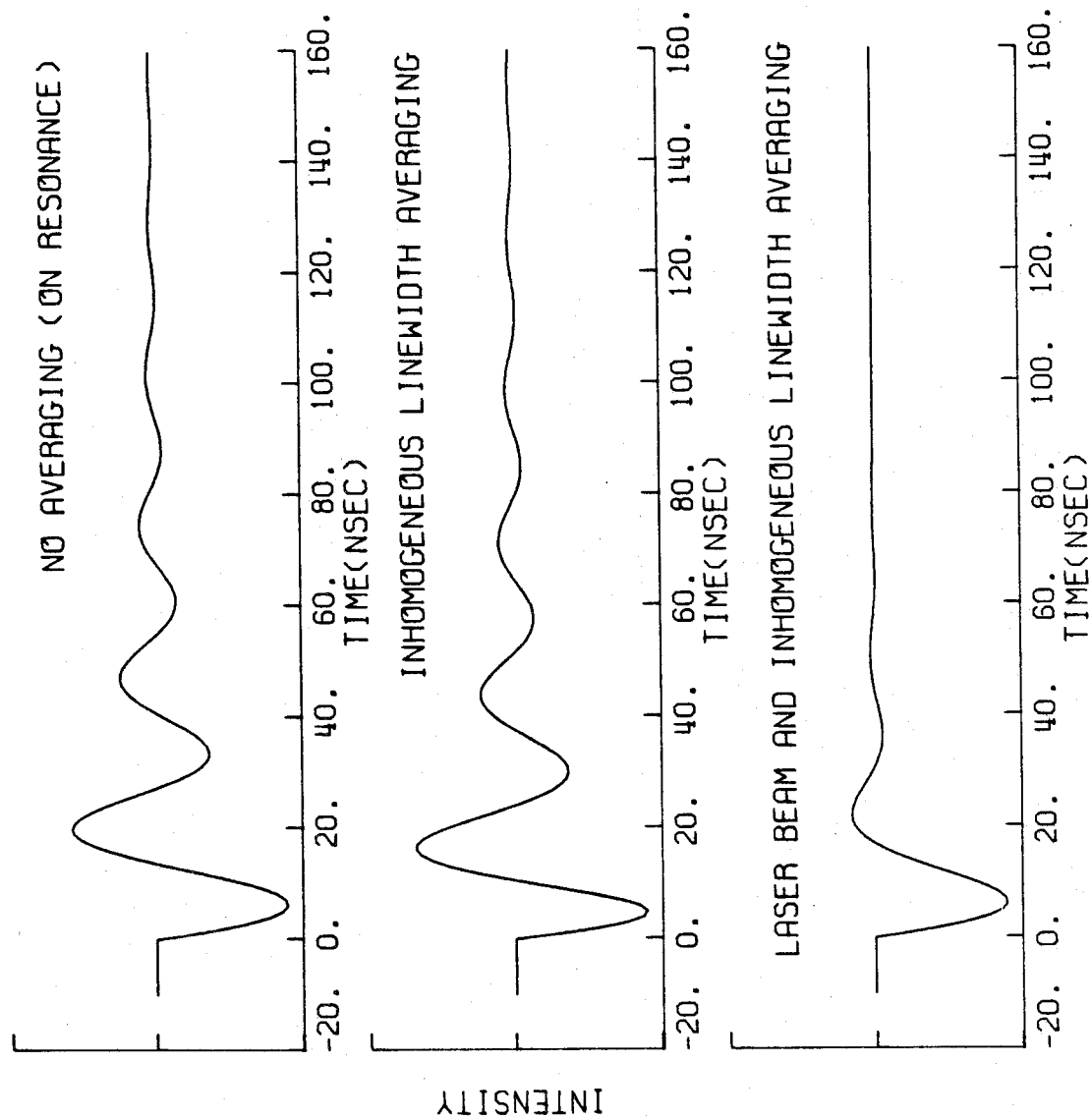
$$I_T(t) = \pi B_L^2 \{ I_0 - 2A \left(\frac{\chi}{t}\right) \text{erf}\left(\frac{\chi t}{2}\right) J_1(\chi t) e^{-t/T_2} \} \quad (29)$$

This result (a) reveals the importance of averaging over the laser beam if one is interested in relating the observed decay (see Fig. 5) of the transient to T_2 and (b) shows that an accurate value of the transition dipole moment can be obtained by fitting the observed transient since the oscillation of the signal is still given by the Rabi frequency χ .

Figure 5

Shown at the top is a plot of the expression [Eq. (15)] for the optical nutation in pentacene without averaging (on resonance case). In the middle is shown the result of averaging over the inhomogeneous linewidth [Eq. (19)]. Here Eq. (19) is multiplied by the error function shown in Eq. (28) for proper behavior at $t = 0$. Finally, at the bottom, is shown a plot of Eq. (29) which considers averaging over both the inhomogeneous lineshape and the laser beam spatial profile. In all three graphs, the Rabi frequency (36.6 ± 0.6 MHz) is the same; only the amplitude and transient decay time are affected by the averaging process. Results obtained in Fig. 3 were used in the averaging over the laser beam.

OPTICAL NUTATION: PENTACENE AT 1.8K



2. Incoherent resonance decay

The initial jump in emission intensity seen on the IRD for pentacene is due to the coherent driving of a new group of molecules (β of Fig. 1) brought into resonance with the switched laser frequency. For short times, we may use the solution of Eq. (10b) to predict the jump in emission intensity and from it characterize the temperature dependence of the IRD obtained experimentally.

We will present the complete solution for $\rho_{pp}(t)$ obtained using Laplace transform techniques and the perturbative expansion approach used by Schenzle and Brewer.³⁹ This solution has not been presented before and is generally applicable for solids at low temperatures.

Using Eq. (10b) and solving for the diagonal elements of ρ we have:

$$\begin{aligned} \rho_{pp}(t) = & \frac{-\frac{1}{2}\chi^2}{(\lambda_1 - \lambda_2)^2} \left\{ \left(1 + \frac{1}{\lambda_1 T_2}\right) e^{\lambda_1 t} \right. \\ & \left. + e^{\lambda_2 t} \left(A \cos \chi_1 t + \frac{B \sin \chi_1 t}{\chi_1} \right) \right\} \\ & + \frac{1}{2} \frac{\chi^2}{T_2 \lambda_1 (\lambda_2^2 + \chi_1^2)} \end{aligned} \quad (30a)$$

where

$$\lambda_1 = \frac{-1}{T_{1p0}} + \frac{\chi^2 T}{1 + T^2 \chi_1^2} \quad (30b)$$

$$\lambda_2 = -\frac{1}{T_2} - \frac{\chi^2 T}{2[1 + T^2 \chi_1^2]} \quad (30c)$$

$$A = \frac{(\lambda_1 - 2\lambda_2)}{T_2(\lambda_2^2 + \chi_1^2)} - 1 \quad (30d)$$

and

$$B = (\lambda_2 - \lambda_1) + \frac{\lambda_2(\lambda_2 - \lambda_1) - \chi_1^2}{T_2(\lambda_2^2 + \chi_1^2)} \quad (30e)$$

We should emphasize that the above solution is for the level structure described earlier for pentacene. In the case where the T_1 's of the excited and ground states are equal the solution is not the same as (30a) but yields identical results to Eq. (5) of reference 27.

Now, Eq. (30) represents the time dependence of the emission intensity for the group of molecules on resonance with the laser. Off-resonance molecules provide the transient decay. For the initial jump in emission intensity which relates to T_2 we will ignore the contribution from the decay of the group switched off-resonance. This is equivalent to saying that we are in the high power limit where $\chi \gg \frac{1}{T_1}, \frac{1}{T_2}$. The oscillations predicted by Eq. (30) have been observed experimentally⁴⁰ but due to the drastic smoothing that takes place when averaging Eq. (30) over the laser beam intensity profile and the inhomogeneous linewidth, one will not observe them easily without subtracting the background resulting from the off-resonance decaying molecules.

In the high power limit and at short times, Eq. (30) reduces to:

$$\rho_{pp}(t) \simeq -\frac{1}{2} e^{\lambda_2 t} B \sin \frac{\chi_1 t}{\chi_1} \quad (31)$$

where B is now $\approx -\frac{1}{2}(\frac{1}{T_{1p0}} + \frac{1}{T_2})$ and the steady state term has been ignored. Thus, we recover a function very similar to that found for the nutation [Eq. (15)]. Averaging (31) over the inhomogeneous linewidth

and making the previous approximation (i. e., $\chi \ll \delta\omega_I$) we obtain the solution:

$$\langle \rho_{pp}(t) \rangle = \frac{1}{4} \left(\frac{1}{T_{1p0}} + \frac{1}{T_2} \right) \frac{\sqrt{\pi}}{\delta\omega_I} J_0(\chi t) e^{-t/T_2} \quad (32)$$

As we shall see later, this result will be valid for examining the temperature dependence of the initial jump in the IRD. If we measure the relative amplitude of Eq. (32) at fixed t near the peak for various values of T_2 (see Fig. 6), averaging over the laser beam (which introduces a faster damping rate and decreased absolute intensity) is unnecessary since we are making a relative intensity measurement at fixed t when examining this T_2 dependence in Eq. (32). Note that to obtain the "exact" functional form for $\langle \rho_{pp}(t) \rangle$ we must follow the procedure done in the nutation section.

3. Optical free induction decay

When a group of molecules initially on resonance (under steady state conditions) is allowed to freely radiate by rapidly switching the frequency of the laser off-resonance, the solution for the off-diagonal density matrix element (and thus the polarization) is from Eq. (10) with $\chi = 0$:

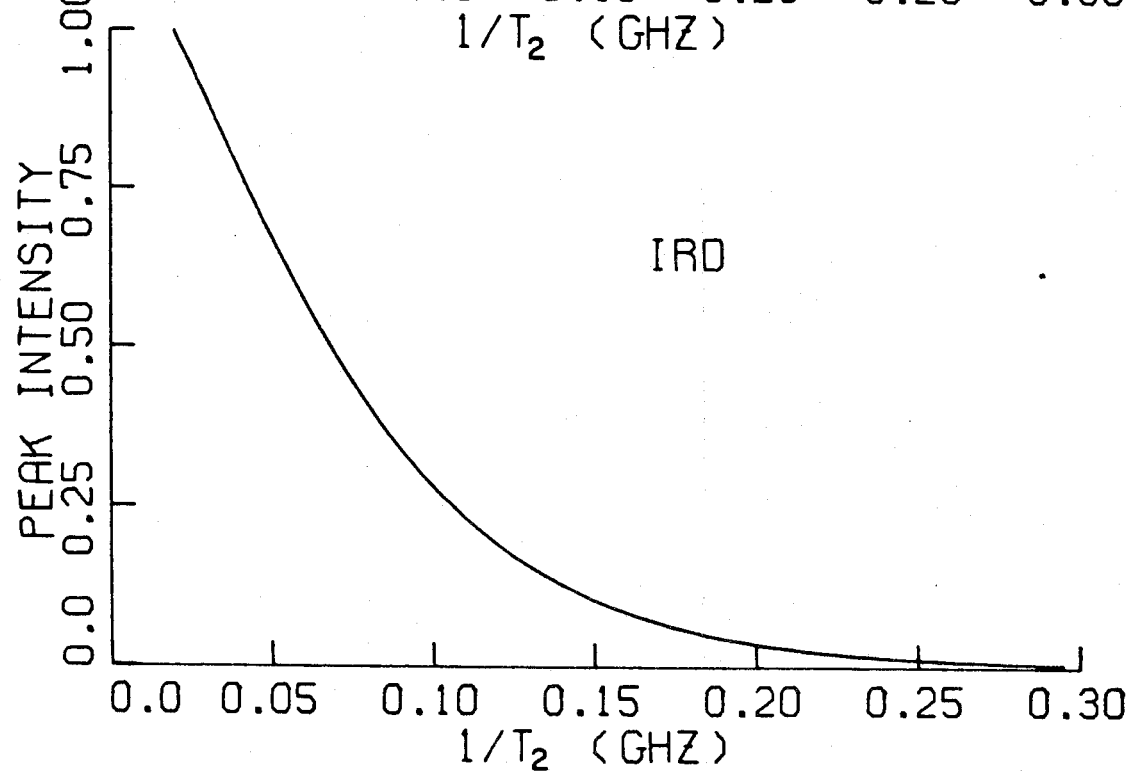
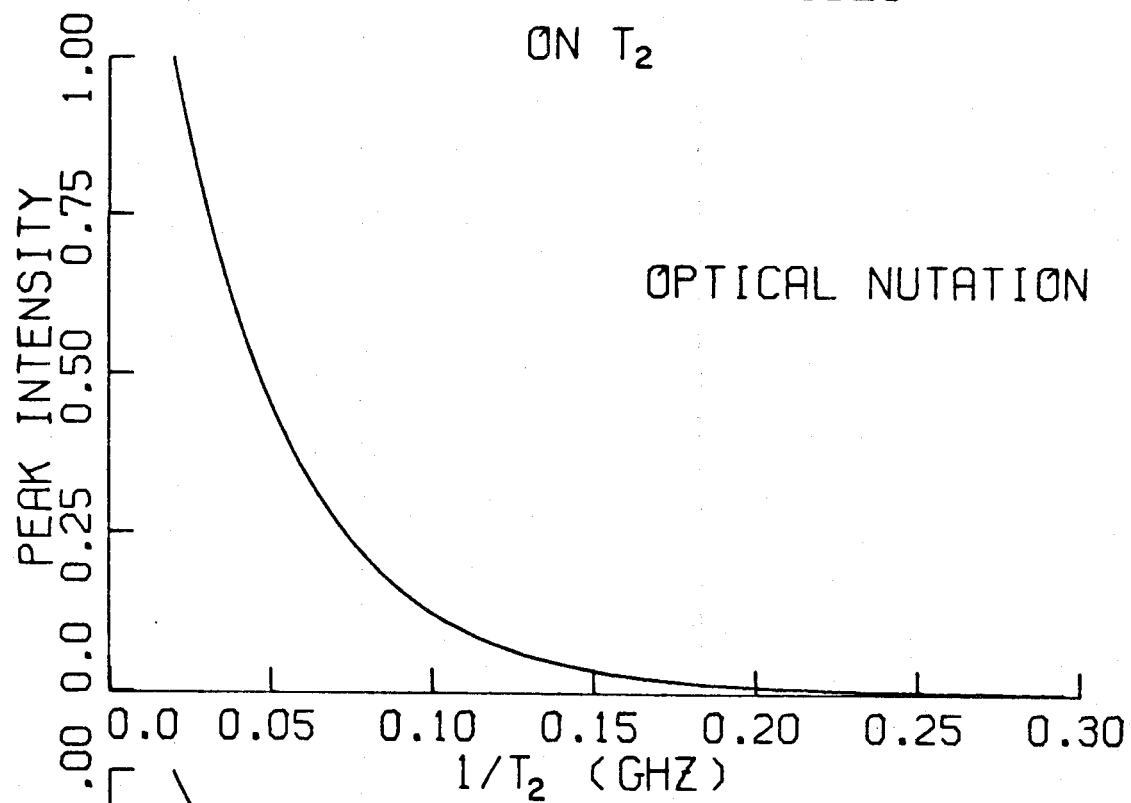
$$\rho_{0p}(t) = \rho_{0p}^{(\infty)} e^{(-\frac{1}{T_2} + i\Delta)t} \quad (33)$$

For the pentacene case we obtained the following result:

Figure 6

The dependence of the (relative) optical nutation and IRD peak amplitudes on T_2 from Eqs. (29) and (32), respectively. In the nutation expression the d.c. term $\pi B_L^2 I_0$ is ignored. In the IRD expression, a factor of T_2^{-1} appears in the pre-exponential factor which causes the amplitude to "decay" slower than the nutation.

DEPENDENCE OF OPTICAL NUTATION
AND IRD PEAK AMPLITUDES
ON T_2



$$\rho_{0p}(t) = -\frac{\chi}{2} \rho_{00}(0) \frac{\left(\frac{i}{T_2} - \Delta\right) e^{\left(-\frac{1}{T_2} + i\Delta\right)t}}{\Delta^2 + \left[\left(\frac{1}{T_2}\right)^2 + \frac{\chi^2}{2} \frac{T_{1p0}}{T_2}\right]} \quad (34)$$

Averaging this result over the inhomogeneous linewidth one has:^{17, 39}

$$\langle \rho_{0p}(t) \rangle \simeq \frac{i\chi\sqrt{\pi}}{\delta\omega_I} \left(1 - \left\{ \frac{\frac{1}{T_2}}{\left[\left(\frac{1}{T_2}\right)^2 + \frac{\chi^2}{2} \frac{T_{1p0}}{T_2}\right]^{\frac{1}{2}}}} \right\} \right) \times \exp \left\{ - \left[\frac{1}{T_2} + \left(\frac{1}{T_2^2} + \frac{\chi^2}{2} \frac{T_{1p0}}{T_2} \right)^{\frac{1}{2}} \right] t \right\} \quad (35)$$

To obtain the signal field ϵ_s we use Eq. (14) and (35) ($\eta = 1$):

$$\epsilon_s(t) \simeq \frac{\omega L N \mu}{c \epsilon_0} \frac{\chi \sqrt{\pi}}{\delta\omega_I} \left(1 - \frac{1}{\left[1 + \frac{\chi^2}{2} T_{1p0} T_2 \right]^{1/2}} \right) \times \exp \left\{ - \left[\frac{1}{T_2} + \left(\frac{1}{T_2^2} + \frac{\chi^2}{2} \frac{T_{1p0}}{T_2} \right)^{\frac{1}{2}} \right] t \right\} \quad (36)$$

In the OFID experiment the signal at the detector [different from (20)] is:

$$I_T(t) = c \mathcal{E}_0 \langle [\epsilon \cos \omega t + \epsilon_s \cos \omega_s t]^2 \rangle_t \quad (37)$$

which for optically thin samples, ignoring the high frequency $(\omega + \omega_s)$ component, is

$$I(t) = I_0 + 2c \mathcal{E}_0 \epsilon \epsilon_s(t) \cos (\omega - \omega_s)t \quad (38)$$

Thus, one should see heterodyne beating at $(\omega - \omega_s)$ superimposed on a

power dependent exponential decay. As one can see from Eq. (36), in the low power regime (i.e., $\chi \ll \frac{1}{T_1}, \frac{1}{T_2}$) the FID gives T_2 directly, and this is verified from our pentacene results. The dependence of the decay rate on χ is depicted in Fig. 7. It should be mentioned that the above treatment is only valid for the case where the population remains in the two level system. If, however, the system is statistically open with net population loss then the treatment of Jones *et al.*⁴¹ must be used. The closed two-level system theory describes our pentacene solid state results quite well.

B. Steady-state coherence regime: application of Wilcox-Lamb method to pentacene

In this limit, τ_0 , the observed transient decay time is much longer than $(\hbar/\mu \cdot \epsilon)$ and T_2 . Thus, if $\tau_0 \sim 10 \mu\text{sec}$ and T_2 is in the nanosecond range as in pentacene, we can assume that transient dephasing is complete and that the off-diagonal density matrix elements connecting levels $|0\rangle$ and $|p\rangle$ have decayed to their steady-state values in the presence of the laser field.

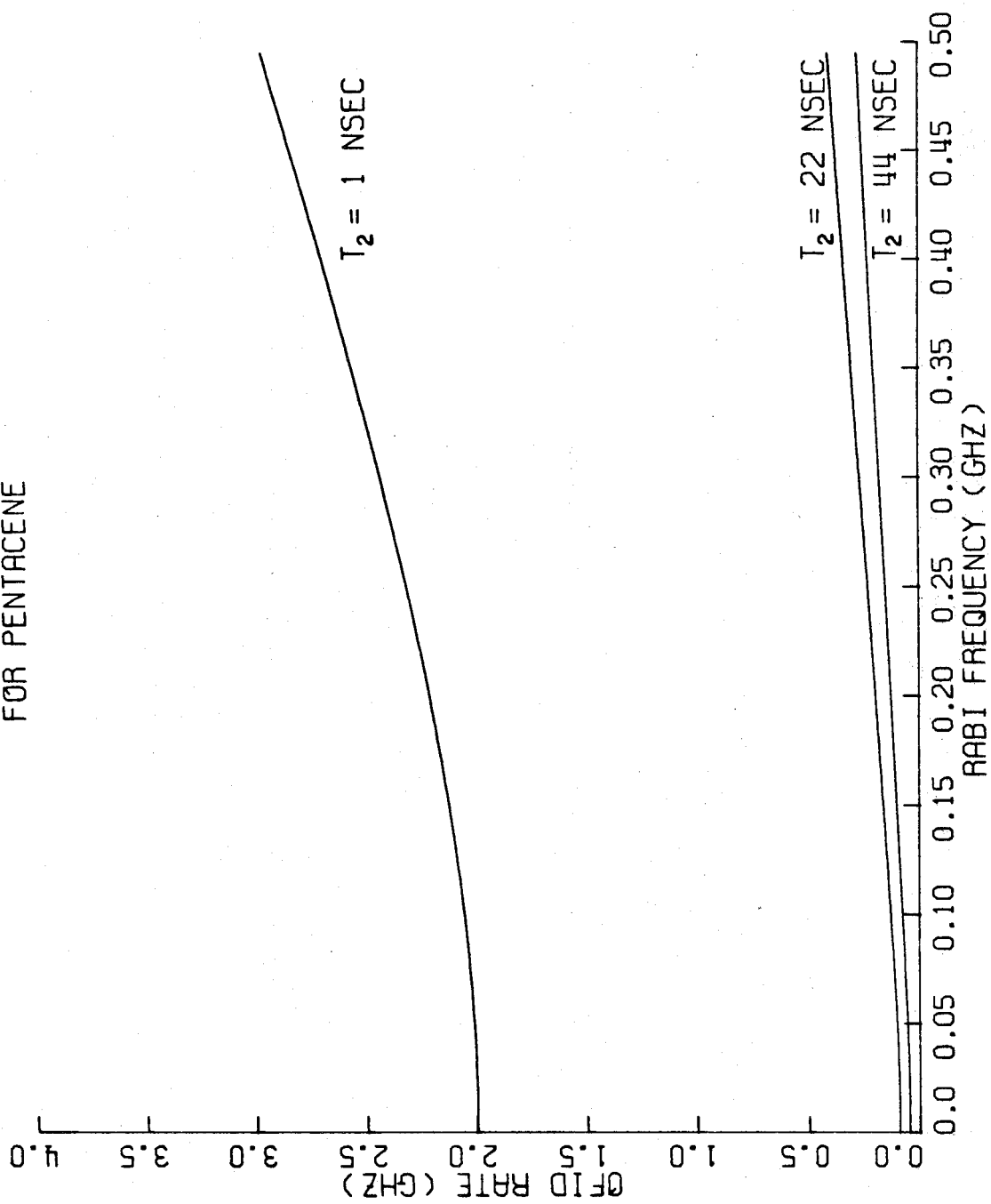
We may smoothly enter this regime using the Wilcox-Lamb method⁴² for deriving density matrix equations from the original Bloch equations. This method has been used to show in several cases⁴³ that rate equations yield solutions equivalent to the time-averaged (i.e., the usual transient solution "without" coherent oscillations) Bloch solutions for describing population flow in multi-level systems.

For the pentacene case, we shall first modify Eq. (10) to include relaxation terms to and from the $\{|\ell\rangle\}$ manifold, and then

Figure 7

Shown here are graphs of the OFID rate dependence on the Rabi frequency in pentacene for various values of T_2 . T_1 has been fixed at 23.5 nsec. Extrapolated to $\chi = 0$, these plots allow one to obtain T_2 (intercept = $T_2/2$) for the optical transition. As shown in the graph, the power broadening term in Eq. (36) dominates the expression at high laser power and the observed decay becomes linear in χ .

DEPENDENCE OF OFID RATE ON RABI FREQUENCY
FOR PENTACENE



provide analytical solutions for the EO and LADS experiments which involve entirely different descriptions. With this in mind, Eq. (10) can now take the form:

$$\dot{\rho}_{00} = \Gamma_{p0}\rho_{pp} + \Gamma_{\ell 0}\rho_{\ell\ell} + \frac{1}{2}i\chi(\rho_{p0} - \rho_{0p}) \quad (39a)$$

$$\dot{\rho}_{pp} = -(\Gamma_{p0} + \Gamma_{p\ell})\rho_{pp} + \frac{1}{2}i\chi(\rho_{0p} - \rho_{p0}) \quad (39b)$$

$$\dot{\rho}_{\ell\ell} = \Gamma_{p\ell}\rho_{pp} - \Gamma_{\ell 0}\rho_{\ell\ell} \quad (39c)$$

$$\dot{\rho}_{0p} = (-\Gamma + i\Delta)\rho_{0p} + \frac{1}{2}i\chi(\rho_{pp} - \rho_{00}) \quad (39d)$$

We note that the structure of $\{|\ell\rangle\}$ is unspecified and therefore the Γ 's which describe the feeding into and the decay from ℓ represent an average quantity. We will come back later to this point. Now, the first step in the Wilcox-Lamb method involves setting the time-derivatives of the off-diagonal density matrix elements to zero. This step is based on the condition that the off-diagonal elements dephase quickly to their steady state values. Expressing our result for Eq. (39d) in terms of r_2 and r_3 (see Eq. (13)) we obtain:

$$r_2 = \left(\frac{\chi\Gamma}{\Gamma^2 + \Delta^2} \right) r_3 \quad (40)$$

Substituting (40) into the differential equations for the diagonal density matrix elements of (39) and assuming a statistically closed system (i.e., $\rho_{00} + \rho_{pp} + \rho_{\ell\ell} = 1$) we obtain the following rate equations for the on-resonance case:

$$\dot{\rho}_{pp} + (\Gamma_{p0} + \Gamma_{pl} + \frac{1}{2} \chi^2 T_2) \rho_{pp} - \frac{1}{2} \chi^2 T_2 \rho_{00} = 0 \quad (41)$$

$$\dot{\rho}_{00} + (\frac{1}{2} \chi^2 T_2 + \Gamma_{l0}) \rho_{00} - (\frac{1}{2} \chi^2 T_2 + \Gamma_{p0} - \Gamma_{l0}) \rho_{pp} = \Gamma_{l0} \quad (42)$$

We now consider the solution appropriate for the two different experiments (EO and LADS) done on pentacene, and consider off-resonance effects later.

1. LADS experiments

We can solve the above set of differential equations analytically using Laplace transform methods and Cramer's Rule. The solution presented here for ρ_{pp} provides us with the parameter directly related to our experimental observable: emission intensity. Under the above mentioned conditions, and provided that the laser is turned on at $t = 0$ (i. e., $\chi = 0$ when $t < 0$), the solution is given by:

$$\rho_{pp}(t) = \frac{R_p}{\lambda_+ - \lambda_-} \left[\left\{ \frac{\Gamma_{l0} + \rho_{00}(0)\lambda_+}{\lambda_+} \right\} e^{\lambda_+ t} - \left\{ \frac{\Gamma_{l0} + \rho_{00}(0)\lambda_-}{\lambda_-} \right\} e^{\lambda_- t} \right] + \frac{R_p}{\lambda_+ \lambda_-} \Gamma_{l0} \quad (43)$$

Here $\rho_{00}(0)$ is the population of $|0\rangle$ at $t = 0$, and $R_p = \frac{1}{2} \chi^2 T_2$. For most experiments we set $\rho_{00}(0) = 1$, although the extension for other cases (e. g., when describing ρ_{00} at the end of short laser pulses) where $\rho_{00}(0) \neq 1$ is straightforward and will be discussed later. The arguments of the exponentials, λ_{\pm} , satisfy the following quadratic equation:

$$2\lambda_{\pm} = - (2R_p + \Gamma_{l0} + \Gamma_{p0} + \Gamma_{pl}) \pm [(2R_p - \Gamma_{l0} + \Gamma_{p0} + \Gamma_{pl})^2 - 4R_p\Gamma_{pl}]^{1/2} \quad (44)$$

Eq. (43) provides a function that rapidly builds up at $t = 0$ to a peak value ($t = t_p$) and then decays by essentially a single exponential ($e^{\lambda-t} \approx 0$ for $t > t_p$) to an equilibrium value $\rho_{pp}(t_{eq})$. The decay time τ_0 and the equilibrium value are determined by $\Gamma_{p\ell}$ and $\Gamma_{\ell 0}$. In our experiments the laser does not turn on instantly so we have modified the pumping rate in Eq. (43) to account for the finite rise time Γ_L^{-1} of our laser pulse. To do this we simply replace R_p by

$$R_p(t) = (1 - e^{-\Gamma_L t}) R_p(\max) \quad (45)$$

where $R_p(\max)$ is the maximum value for the pumping rate, and the laser pulse has been given an exponential build-up which was measured and verified experimentally. Eq. (43) gives the population of the emitting level as a function of time when the laser is on-resonance. The off-resonance solution (i. e., $R_p = 0$; $t > t'$) for ρ_{pp} can be written as

$$\rho_{pp}(t > t') = \rho_{pp}(t = t') e^{-t/T_{1p}} \quad (46)$$

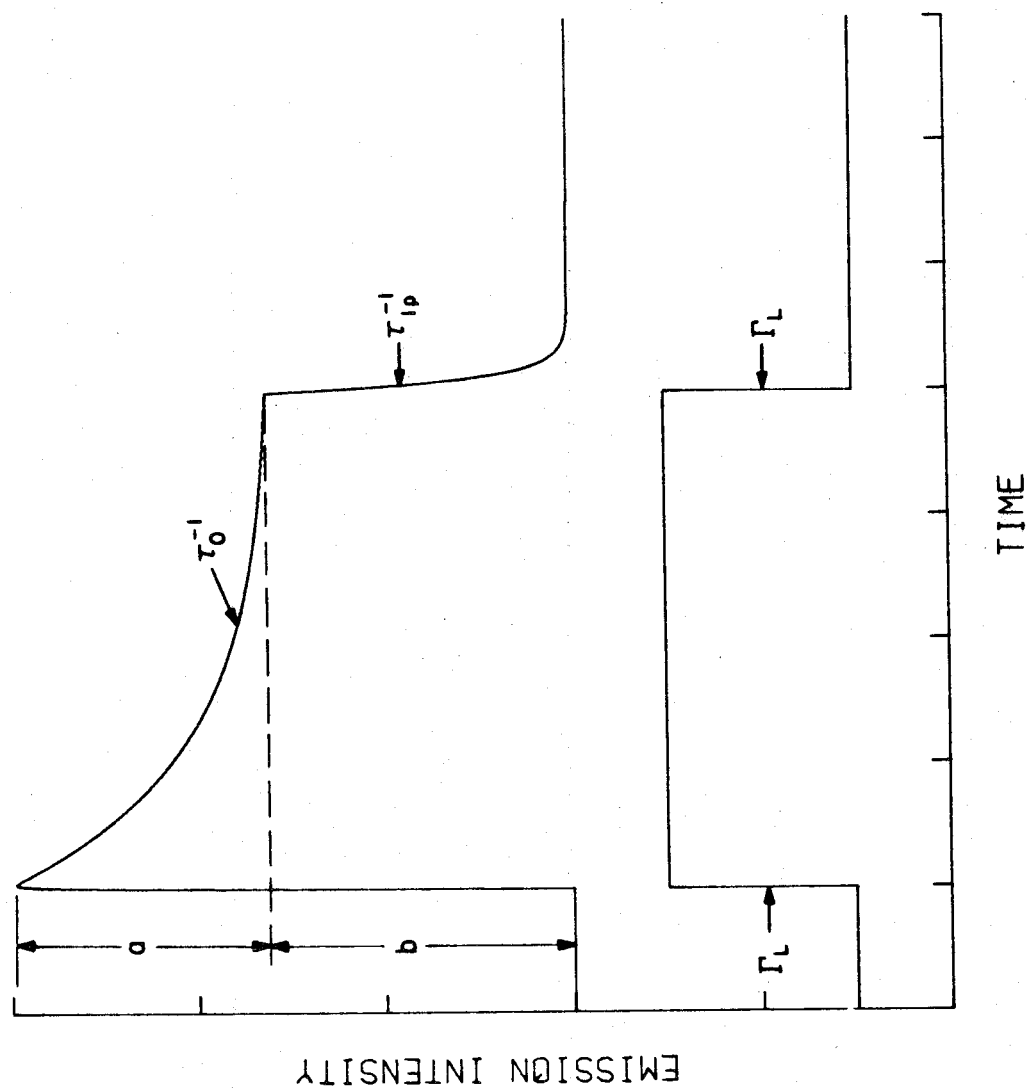
Here, t' is the time at which the laser pulse ends and so Eq. (46) is simply an exponential decay of population from the primary level. The initial value $\rho_{pp}(t')$ equals the equilibrium value on resonance if the laser pulse width is long enough.

Using Eqs. (43)-(46) one can generate the curve shown in Fig. 8 which, as we shall show later, fits our results quite well. In the same figure the pulse used in the excitation into $|p\rangle$ is also depicted.

Figure 8

Plotted here are the theoretical transients obtained from Eqs. (43) and (46) for describing LADS emission experiments (top) and the excited pulse (bottom). The slow decay during the pulse is labelled τ_0^{-1} and the fast decay at the falling edge of the pulse is τ_{1p}^{-1} , the observed emission rate of the prepared state $|p\rangle$ convoluted by the pulse decay, Γ_L . The quantity, a , is the magnitude of the "overshoot" in emission intensity observed before reaching a final steady-state value, b . The ratio $\gamma = a/b$ will be referred to in later figures.

EMISSION INTENSITY VS. TIME FOR STEADY-STATE
COHERENCE IN PENTACENE LEVEL STRUCTURE



Physically, the model can be explained in the following manner. As the population builds up in $|p\rangle$ some of it gets trapped in the slow decay channel involving $|\ell\rangle$ before returning to $|0\rangle$. Following the fast initial build-up, population is redistributed until $\rho_{pp}\Gamma_{p\ell}$ and $\rho_{\ell\ell}\Gamma_{\ell 0}$ are equal and equilibrium results.

Two quantities labeled a and b in Fig. 8 play different roles. The first, a, is the extent to which ρ_{pp} is driven beyond equilibrium; it increases as $\Gamma_{p\ell}$ increases and gives a measure of how much of the total population is "tied up" in the slow decay channel. For long pulses, the second parameter, b, is the equilibrium population of $|p\rangle$. The ratio $\gamma = a/b$ is therefore determined by the ratio $\Gamma_{p\ell}/\Gamma_{\ell 0}$ for fixed R_p . If one simultaneously fixes τ_0 , the observed decay time, then a unique solution exists because only one value of $\Gamma_{\ell 0}$ and the ratio $\Gamma_{p\ell}/\Gamma_{\ell 0}$ can provide both the observed γ and τ_0 . The interrelationship of the parameters and the physical significance of certain trends can be more easily understood by examining Figs. 9 and 10. Here $\Gamma_{\ell 0}$ is fixed as we examine (1) the ratio (γ) versus $\Gamma_{p\ell}/\Gamma_{\ell 0}$ at various pumping rates R_p in Fig. 9; (2) the observed decay time τ_0 versus $\Gamma_{p\ell}/\Gamma_{\ell 0}$ in Fig. 9, and finally (3) the observed decay time τ_0 versus R_p in Fig. 10. From Fig. 9 we see that γ is directly proportional to the ratio $\Gamma_{p\ell}/\Gamma_{\ell 0}$. Physically, this means that more population is trapped in the slow decay channel as $\Gamma_{p\ell}$ increases (with $\Gamma_{\ell 0}$ fixed). If the pumping rate increases, more population should be trapped for any given $\Gamma_{p\ell}/\Gamma_{\ell 0}$ since more population is available in $|p\rangle$. This effect shows up as a change in the slope of the lines of Fig. 9 (bottom). Also, the intercept

Figure 9

The dependence of the slow transient decay time, τ_0 , and $\gamma = a/b$ on the ratio Γ_{pl}/Γ_{l0} [from Eq. (43)]. In these graphs, Γ_{l0} is fixed at the best fit value (0.0266 ± 0.002 MHz) obtained from the EO experiments, $\Gamma_{p0} = 40$ MHz and $R_p = \frac{1}{2} \chi^2 T_2$ is the pumping rate in the steady-state coherence regime. As the ratio Γ_{pl}/Γ_{l0} decreases, both the decay rate τ_0^{-1} , and γ decrease. Thus, a measurement of the decay time at very small values of Γ_{pl}/Γ_{l0} is difficult to make accurately.

DEPENDENCE OF OBSERVED DECAY TIME AND GAMMA ON THE RATIO Γ_{pL}/Γ_{L0}

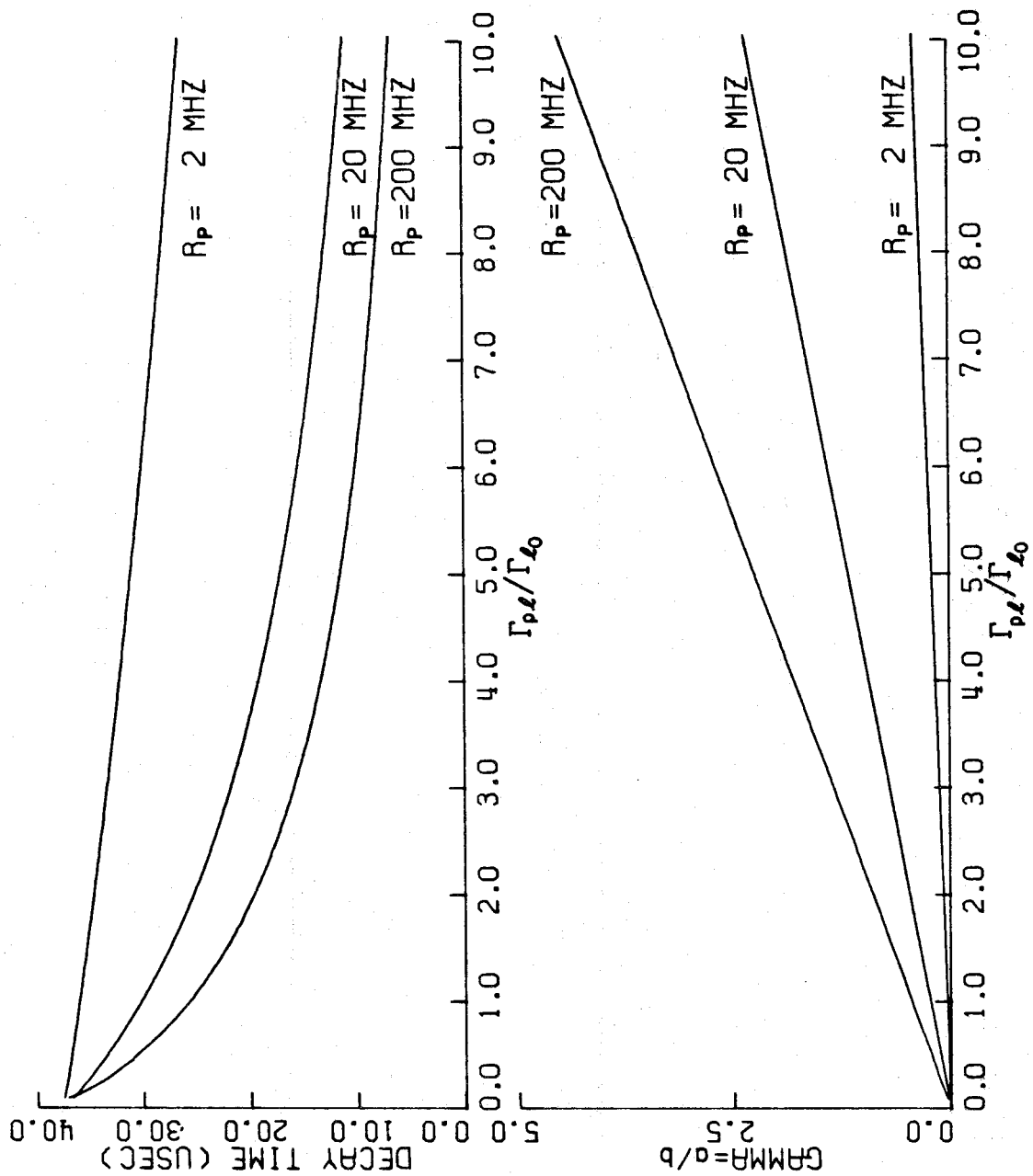
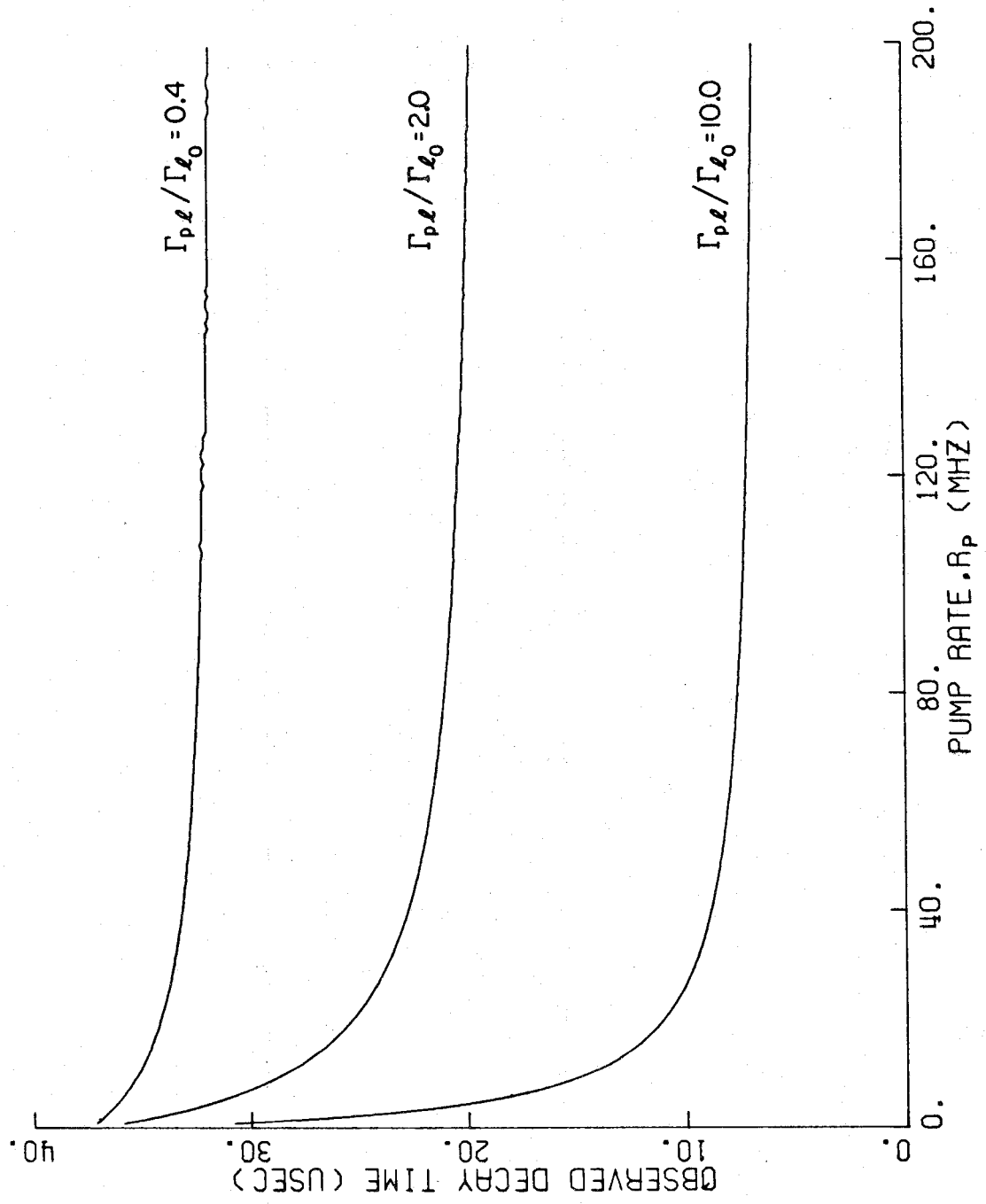


Figure 10

Shown here is the dependence of τ_0 on the pumping rate, R_p obtained from Eq. (43) for various ratios of Γ_{pl}/Γ_{l0} . As in Fig. 9, Γ_{l0} and Γ_{p0} are fixed. At very low pumping rates, the decay time increases but since the overshoot, a , becomes very small also (see Fig. 9), τ_0 cannot easily be measured experimentally. Most of the experiments in pentacene were carried out in the flat portion of the curves. Note that at these higher power densities absorption from p to higher excited states is feasible, although fast relaxation from these states will hinder such processes.

DEPENDENCE OF OBSERVED DECAY TIME ON PUMPING RATE



of this plot is zero which it should be since if the slow decay channel is removed ($\Gamma_{pl} = 0$), ρ_{pp} should approach its equilibrium value (b) with no overshoot. Finally, for fixed γ , the observed τ_0 is constant on this plot (i.e., a horizontal line represents a constant τ_0 decay time). Thus, for a given τ_0 there are different ratios of Γ_{pl}/Γ_{l0} (corresponding to different pumping rates) that provide identical γ values.

Fig. 9 (top) shows a plot of observed decay time τ_0 versus Γ_{pl}/Γ_{l0} . As expected, the decay time increases as Γ_{pl} goes to zero. Careful examination of Fig. 9 indicates that there is only one value of Γ_{pl} and Γ_{l0} that will simultaneously provide (1) the observed decay time and (2) the observed γ for fixed R_p .

Figure 10 depicts a plot of the observed decay time τ_0 versus R_p for various ratios of Γ_{pl}/Γ_{l0} . This plot as well as Fig. 9 show how insensitive the model is to the choice of R_p , especially in the high power limit. In addition, one sees that the observed decay time increases as R_p decreases. This is understandable physically since as the pumping rate decreases it must take longer to achieve equilibrium.

2. EO experiments

For these experiments, the treatment is somewhat more complicated than that described above for LADS, since in EO experiments the laser is switched into resonance with another ensemble instead of being turned off completely. Thus one must keep track of the time-dependent emission characteristics (population) of both groups simultaneously. At the beginning of an EO experiment ($t < 0$) the laser is on-resonance with one group (α of Fig. 1) and this group has reached

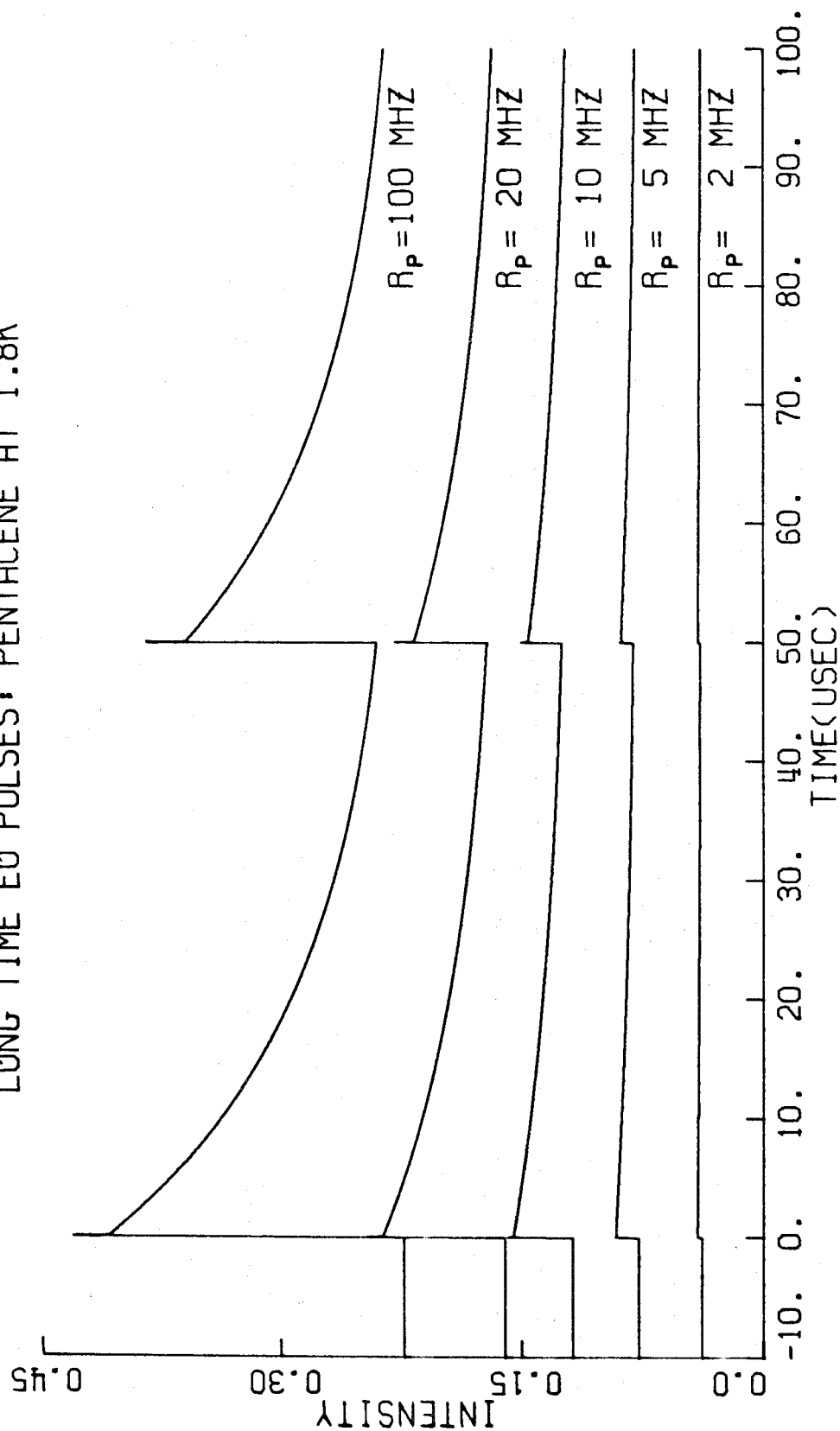
its steady state value $\rho_{pp}^{(\alpha)}(t_{eq.})$. At $t = 0$ the laser is switched into resonance with a new group, β . Eq. (43) can be used to determine the build-up of population ρ_{pp} due to group β while the off-resonance solution, Eq. (46), will provide the decrease in population due to the decay of α molecules. The sum of the two provides the total population $\rho_{pp}^{\alpha} + \rho_{pp}^{\beta}$ and hence the total emission signal. Now, the build-up population rate from β does not usually equal the decay rate from α . Thus, an "overshoot" is expected if the β build up is faster than the α decay and an undershoot for the reverse condition. Whether or not this phenomenon is observed experimentally will be determined by R_p , T_{1p} and, of course, detector response time and the signal averager time resolution. We have observed an overshoot in pentacene (i.e., β build-up $>$ α decay) using a fast photomultiplier (1 GHz) in connection with a sampling scope.

To complete the analysis of the EO experiments we must consider what happens when the laser is switched back to the original frequency. Population in β will decay from the value at $t = t'$ (the switching time) according to Eq. (46) while population in α , ρ_{pp}^{α} , will build-up again according to Eq. (43). If the frequency-switching pulse is long compared to τ_0 , the total population will evolve in time (beginning at t') just as it did at $t = 0$. This is shown in Fig. 11 for various values of the pumping rate, R_p . However, if the pulse is shorter than or comparable with τ_0 , all of the population has not yet returned to $|0\rangle$ for the α group at $t = t'$. Thus, the build-up will not be as large as it is for the long pulses and the net population will decrease at a rate determined by $(1/T_{1p})$. To more fully explain this we must go back to

Figure 11

The dependence of the IRD in pentacene at 1.8°K on the pumping rate for the EO method. Eq. (43) and (46) are used to generate these computer plots considering both the on-resonance and off-resonance molecules (i.e., intensity here refers to $\rho_{pp}^{\alpha}(t) + \rho_{pp}^{\beta}(t)$). The parameters chosen are best fit values from experimental data (see Fig. 18). A transient overshoot (different from the overshoot, a, referred to in Fig. 8) occurs at the leading and trailing edges of the EO pulse. As described in the text, it results from the combination of incoherent emission and coherent pumping of different groups of molecules. The amplitude of the IRD at the end of the EO pulse ($t = 50 \mu\text{sec}$) is smaller than the initial jump. This occurs because the ground state population of the off-resonance molecules has not recovered completely (i.e., population is still tied up in $\{|\ell\rangle\}$).

DEPENDENCE OF THE IRD ON PUMPING RATE FOR
LONG TIME EO PULSES: PENTACENE AT 1.8K



Eq. (43) and realize that $\rho_{00}(0)$ is the population of the ground state when the system is brought into resonance. The boundary condition for $\rho_{00}(0)$ is usually 1 which means the group was initially off-resonance for a long time compared to τ_0 such that all population had adequate time to return to $|0\rangle$. For short switching pulses we need to calculate the off-resonance solution for $\rho_{00}(t)$ and use it to determine the proper initial value of $\rho_{00}(t')$ in Eq. (43).

The solution is found by solving the same differential equations as before (41), (42) with R_p set equal to zero. One obtains

$$\rho_{00}(t) = \rho_{pp}(t_{eq}) \frac{(\Gamma_{p0} - \Gamma_{l0})}{(T_{1p}^{-1} - \Gamma_{l0})} \{e^{-\Gamma_{l0}t} - e^{-t/T_{1p}}\} - [1 - \rho_{00}(t_{eq})] e^{-\Gamma_{l0}t} + 1 \quad (47)$$

To complete the solution for the off-resonance time dependence of $\rho_{00}(t)$ we need to know two initial (boundary) values. These are (1) the equilibrium value of ρ_{pp} on resonance, $\rho_{pp}(t_{eq})$, and (2) the equilibrium value of ρ_{00} on-resonance ($\rho_{00}(t_{eq})$). The first can be obtained from Eq. (43) at long times (compared to τ_0). The second can be obtained from a solution of the differential Eq. (42). The solution ($R_p \neq 0$) is:

$$\begin{aligned} \rho_{00}(t) = & \frac{R_p + T_{1p}^{-1}}{\lambda_+ - \lambda_-} \left[\left\{ \frac{\Gamma_{l0} + \lambda_+}{\lambda_+} \right\} e^{\lambda_+ t} - \left\{ \frac{\Gamma_{l0} + \lambda_-}{\lambda_-} \right\} e^{\lambda_- t} \right] \\ & + \frac{1}{\lambda_+ - \lambda_-} \left[(\lambda_+ + \Gamma_{l0}) e^{\lambda_+ t} - (\lambda_- + \Gamma_{l0}) e^{\lambda_- t} \right] \\ & + \frac{R_p + T_{1p}^{-1}}{\lambda_+ \lambda_-} \Gamma_{l0} \end{aligned} \quad (48)$$

Now $\rho_{00}(t_{eq})$ can be found from Eq. (48) at long times (compared to τ_0). Armed with the results of Eqs. (47) and (48) one can calculate the population of the ground state for any pulse width defined by t' . Then one can use Eq. (43) to calculate the contribution of group α to the total signal as the laser frequency is switched back to the original group. The physical situation can be understood most easily by examining Fig. 12 where the total population $\rho_{pp}^{\alpha}(t) + \rho_{pp}^{\beta}(t)$ is plotted for various frequency switching pulse widths.

For pulse widths long compared to τ_0 the two decay patterns are completely identical as also shown in Fig. 11. As the pulse width decreases, however, one notices that the height of the jump at the falling edge of the pulse is somewhat lower than the initial jump. Further reductions in pulse width make this difference more noticeable until finally the pulse width is short enough so that the increase in emission due to α being switched back into resonance is less than the decrease in emission due to β being switched off-resonance. For these very short pulses where the contribution of α is negligible one can actually measure $1/T_{1p}$ from the decay of population at the falling edge of the pulse. These solutions of the coupled density-matrix equations for the EO and LADS experiments will be shown to fit all our available data on pentacene.

V. RESULTS AND DISCUSSION

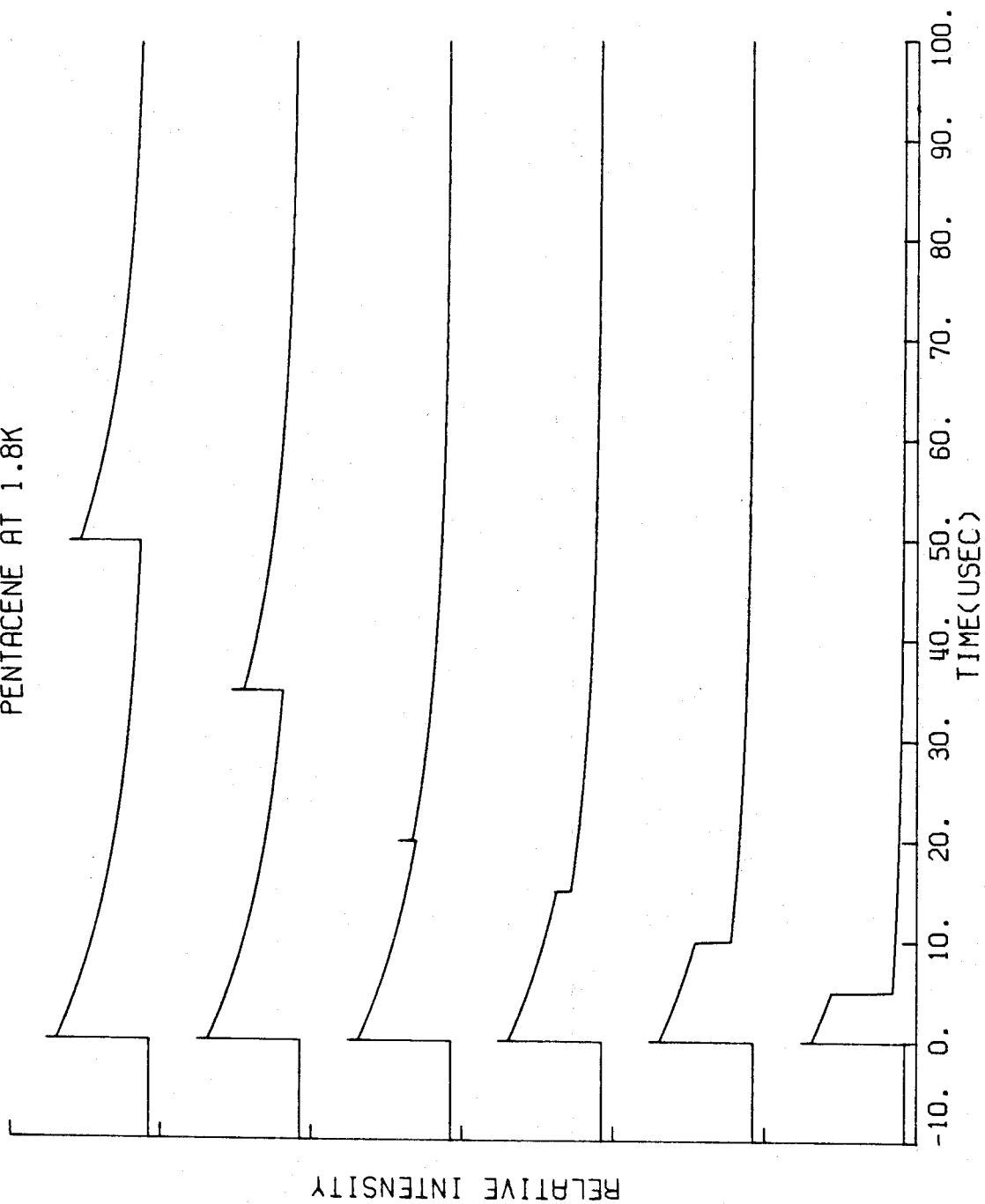
A. Narrow-band excitation: Site selection and vibrational relaxation

At low temperature (1.8°K) mixed crystals of pentacene in p-terphenyl exhibit site splittings; four distinct lattice sites have been

Figure 12

Shown here is the dependence of the IRD on EO pulse width with $R_p = 100$ MHz and all other parameters as in Fig. 11. The lifetimes of the slow decay seen after the leading and falling edges of the pulse are identical, regardless of pulse width. The fast decay seen for short pulses has a lifetime close to that obtained from LADS experiments.

DEPENDENCE OF THE IRD ON EO PULSE WIDTH.
PENTACENE AT 1.8K



observed (see Fig. 13) in our crystals. Each site shows a vibronic progression of "sharp" lines ($1-3 \text{ cm}^{-1}$) both in absorption and emission (Fig. 14). In our work we have used several crystals of varying concentration (10^{-5} - 10^{-7} m/m) and all of them show sites at energies (cm^{-1}): 16,887 (0_1), 16,891 (0_2), 17,009 (0_3) and 17,069 (0_4). These energies which are not vacuum corrected agree with the previous work of Marchetti *et al.*⁴⁴ and Bridge⁴⁵ and are different by approximately $+4 \text{ cm}^{-1}$ with the results of Meyling and Wiersma,⁴⁶ if the spectrum reported in their Fig. 1 is the real spectrum (i. e., without vacuum correction). If, however, their numbers are the corrected values, then all results agree to $\pm 1 \text{ cm}^{-1}$.

A careful study of the spectra was done in order to identify these sites so that it is possible to make a meaningful comparison of our time resolved spectra with all other available work on pentacene in p-terphenyl. Furthermore, these sites must be identified in order to establish whether or not intersite communication exists at these concentrations and temperatures since this process would introduce another dephasing channel, a primary concern of this paper. The optical properties of pentacene obtained in this work as well as a collection of pertinent other spectroscopic data in the gas and liquid phases are summarized in Table II.

To determine whether intersite communication occurs in pentacene isolated in p-terphenyl several experiments were performed at guest concentrations of Ca. $5 \times 10^{-6} \text{ m/m}$ and $5 \times 10^{-7} \text{ m/m}$.

Following narrowband excitation of the origin of site 0_1 we obtained the

Figure 13

Optical site selection in a mixed crystal of pentacene in p-terphenyl (5×10^{-6} m/m). Shown are (a) the emission spectrum of pentacene at 4.2°K with the single-mode laser on resonance with a vibronic line of site 0_1 , 267 cm^{-1} above the origin (see arrow). A very small amount (relative intensity = 0.03) of emission is seen from 0_4 , otherwise narrowband excitation has selected 0_1 molecules exclusively. (b) The emission spectrum of pentacene under identical conditions as in (a) except $T = 1.8^\circ\text{K}$. The phonon sideband at the 0_1 origin is weaker but no other change in the spectrum occurs. (c) The spectrum of pentacene obtained with broadband excitation (Xenon lamp; $2000 \rightarrow 4000 \text{ \AA}$) at 1.8°K . Emission is seen from each site in this case. The spectrometer resolution was 0.7 cm^{-1} for all spectra. Shown on the right of the figure is an energy level scheme that is consistent with the above results.

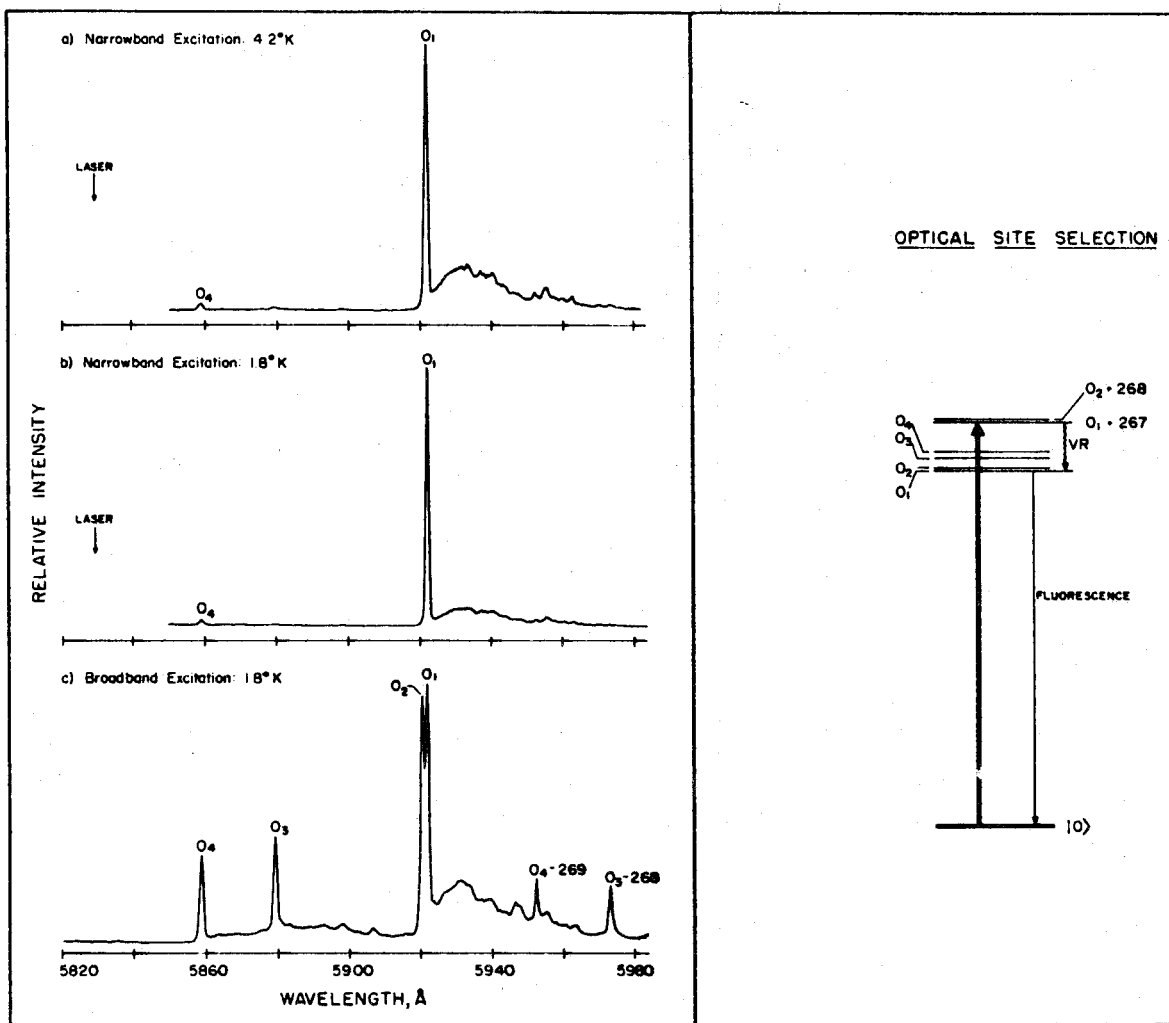
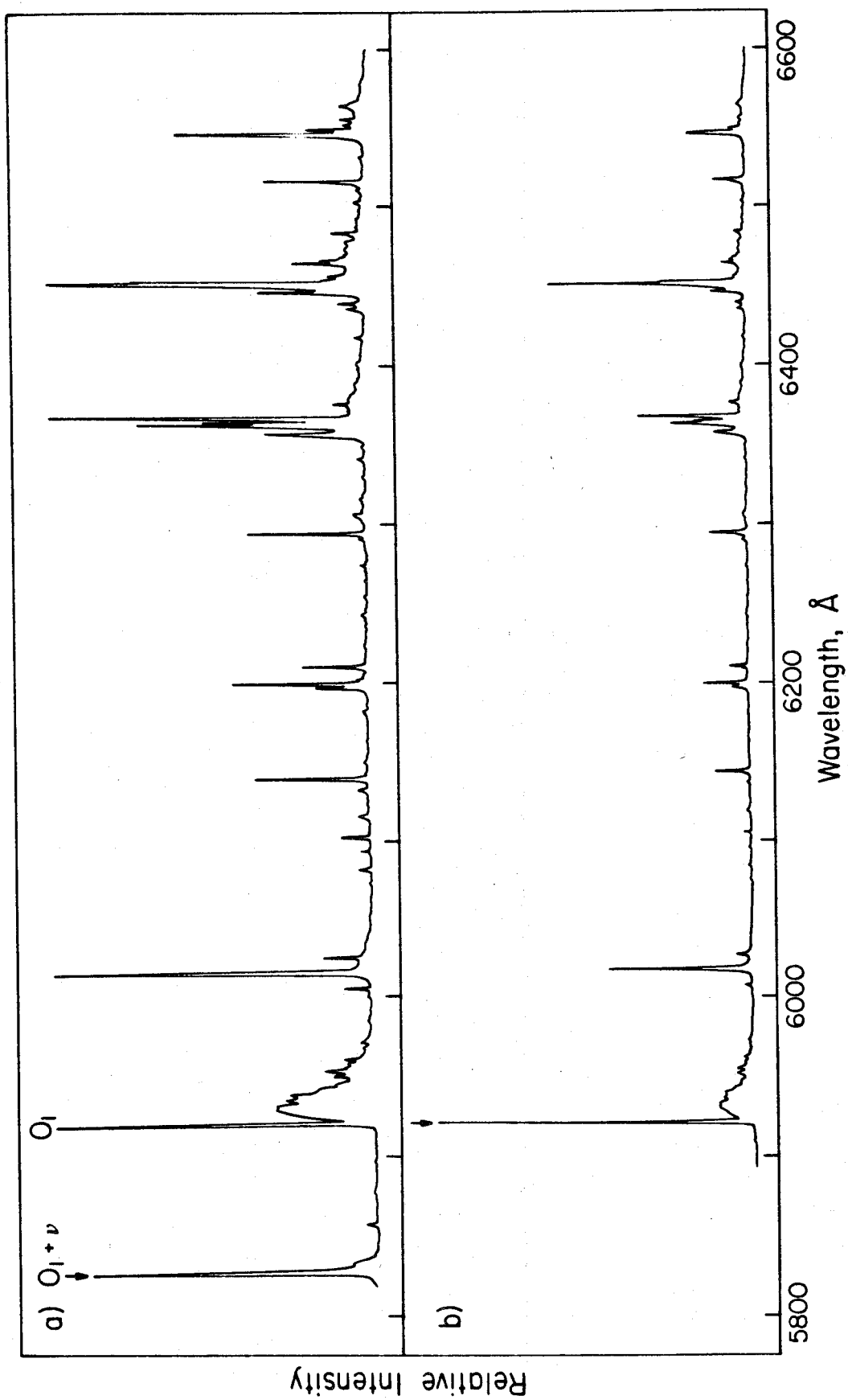


Figure 14

(a) The emission spectrum of pentacene in p-terphenyl with single-mode excitation (arrow) at $0, \nu(267 \text{ cm}^{-1})$ of site 0_1 . (b) The emission spectrum with the laser at $0, 0$ of 0_1 . Both spectra were obtained at 1.8°K and the linewidths shown here are determined by the spectrometer slit-width (1.4 cm^{-1}).



emission spectrum at 1.8°K shown in Fig. 13 for the high concentration sample. An identical spectrum was obtained when we excited (narrow band) at the first vibronic line of O_1 (5829.8 Å), 267 cm^{-1} above the origin. No emission was observed from sites O_2 and O_3 and only very weak emission from O_4 (relative intensity = 0.03) although each origin lies below the vibronic line in energy (see Table II). The spectra for the low concentration sample at 1.8°K and both samples at 4.2°K matched the spectrum mentioned above except that the phonon sideband of the O_1 origin was more intense and showed structure at higher temperature. The weak emission at O_4 also appeared at very low laser power indicating that power broadening of the O_1 vibronic line can not be responsible for the communication observed with O_4 . It is interesting to note that site 4 is the closest in energy to the excitation energy and its appearance may therefore indicate the importance of near resonance energy transfer to O_4 . Although we cannot rule out that the site is due to an impurity, the fact that it has the same vibronic progression⁴⁵ leads one to believe that it is due to pentacene.

Also, the emission spectrum for the high concentration sample at 1.8°K following broadband excitation (Xenon lamp, UV bandpass) was obtained. In this spectrum (see Fig. 13) emission is seen from each site origin and vibronic lines can be identified. Several conclusions can be drawn from these experiments.

First, vibrational relaxation within the lowest excited singlet manifold is fast enough so that emission is observed from the origin only. Second, at these concentrations ($\leq 5 \times 10^{-6}$ m/m) and temperatures ($\leq 4.2^\circ\text{K}$) spectral diffusion processes such as excitation exchange

among sites are not competing effectively with vibrational relaxation because emission is seen from the site 0_1 origin predominantly (with narrowband excitation) although we are exciting above the origins of all the other sites. Although the vibronic line for site 0_2 found at 5827.9 \AA is only 5.6 cm^{-1} above the corresponding vibronic line for 0_1 (excited by the laser), no communication between these two sites occurs. Thus, with narrowband excitation individual sites can be selected and their interaction with the environment can be studied free from complications due to intersite effects. Even though intercommunication between sites may not influence the spectra, it is possible that the T_2' processes involving elastic site communications will be influenced and thus alter the decay rate of coherent transients. Therefore one must be careful about correlating the emission spectra with T_2 -type processes that involve other sites. Finally, there appears to be structure superimposed on the phonon sideband continuum near the origin of 0_1 which may indicate the presence of pseudolocalized or resonance phonon modes in the lattice.^{47, 48} These are not seen in our absorption spectrum or in the spectrum of Aartsma *et al.*⁴⁹ However, there is evidence that phonon structure can be markedly different in absorption and emission in very similar mixed crystals.⁵⁰ These modes can be very important dephasing channels and we will address this point in more detail in a later section.

Because vibrational relaxation is fast enough so that emission following excitation into the vibronic line is seen only from the site origin, we decided to carefully measure the absorption linewidths of

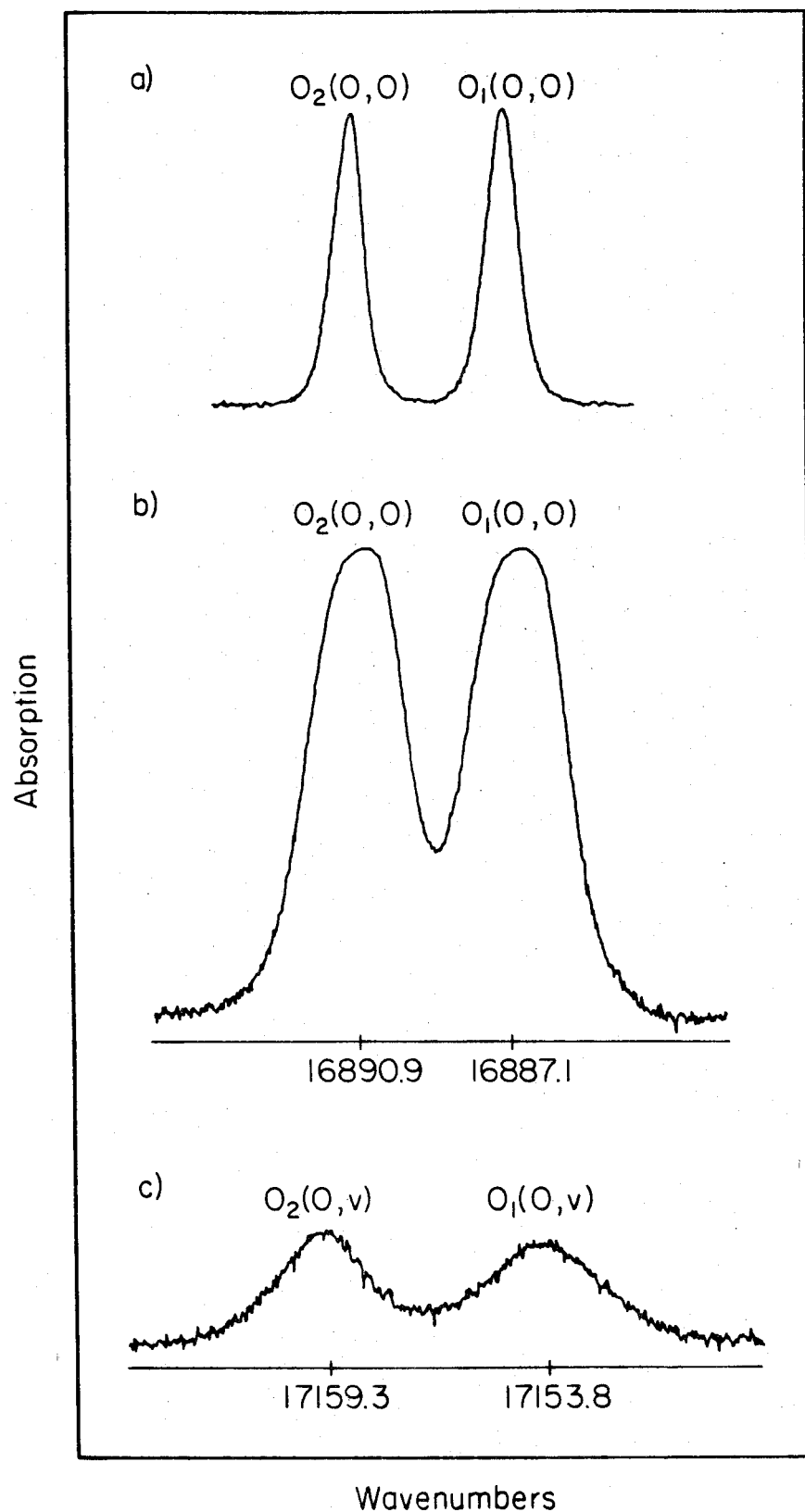
the O_1 origin and its vibronic line 267 cm^{-1} to higher energy. Initial results with spectrometer resolution of 0.8 cm^{-1} revealed that the origin can be fit to a Gaussian whose linewidth increases with sample concentration and temperature. The vibronic line, on the other hand, appeared Lorentzian. Because the absorption at the origin was high ($\approx 90\%$), self-absorption (which makes the observed lifetime longer than the actual lifetime) and scattering effects could introduce artifacts in the measurement.

With very low concentration crystals ($OD \sim 10^{-2}$) we repeated these linewidth measurements using a high resolution spectrometer (Spex double monochromator, 0.75 m , 0.09 cm^{-1} resolution). The results are depicted in Fig. 15 for the $0,0$ and $0,v$ transitions of both O_1 and O_2 . The origins show dramatic broadening as the concentration increases. For the lowest concentration crystal, the linewidths (FWHM) of the O_1 and O_2 origins are $0.7 \pm 0.1\text{ cm}^{-1}$. At the highest concentration used, these widths increase by more than a factor of two. Consistently, we found that the vibronic lines of O_1 and O_2 are broader than the $0,0$ transition. From the coherent transient experiments we know that the broadening of the O_1 origin is inhomogeneous in nature. If the vibronic line is homogeneously broadened, as it appears to be, then we can obtain T_2 directly. We were therefore encouraged to computer fit the data carefully in order to establish whether the lines are Lorentzian or Gaussian. The best fit for the O_2 vibronic line gives a Lorentzian with a width (FWHM) of $1.99 \pm 0.03\text{ cm}^{-1}$. If this width is entirely due to vibrational relaxation, then $T_{1v} = 2.7\text{ psec}$, much different from previous results.⁴⁴ We shall return later to this point in Section VI.

Figure 15

High resolution absorption spectra for pentacene in p-terphenyl at 1.8°K. Shown are (a) 0_1 and 0_2 origins at low concentration ($\approx 1 \times 10^{-6}$ m/m, 1 mm crystal); (b) 0_1 and 0_2 origins at high concentration ($\approx 5 \times 10^{-6}$ m/m, 3 mm crystal); (c) 0_1 and 0_2 vibronic lines at high concentration.

High Resolution Absorption Spectra:
Pentacene / p-terphenyl at 1.8°K



B. Optical dephasing: Nutation and OFID

As discussed earlier, electronic dephasing times (T_2) can be obtained from optical nutation and OFID experiments under the proper conditions. Dilute (10^{-6} m/m) crystals of pentacene in p-terphenyl of good optical quality were used to observe the optical nutation (Fig. 16) and OFID (Fig. 17) at 1.8°K utilizing the EO method of frequency switching.

The data in Fig. 16 were obtained with high (single-mode) laser power (20 mw) exciting the electronic origin 0_1 at $16,887\text{ cm}^{-1}$. The EO switching frequency measured using a scanning confocal etalon was 26 MHz (see Fig. 2). Theoretical curves for the data points were generated (solid lines) using Eq. (19) which considers averaging the result for $r_2(t)$ over only the inhomogeneous linewidth of the transition (top), and using Eq. (29) which considers both inhomogeneous linewidth averaging as well as averaging over the laser field spatial profile (bottom of Fig. 16). It is apparent how important averaging over the laser beam, which essentially causes the transient to damp after the first oscillation, is for fitting the signal adequately. For both plots, the same values of the Rabi frequency ($\chi = \mu \cdot \epsilon / \hbar$) and T_2 were used and the best fit values for the bottom plot are 230 ± 10 MHz (which corresponds to a nutation time of 27.3 nsec) and 45 ± 2 nsec, respectively. Thus, our experimental results verify the assumption of high power ($\chi \gg \frac{1}{T_2}, \frac{1}{T_1}$) which was made to simplify the form of the density matrix solution for r_2 and show that with the appropriate averaging over the laser beam, optical nutation measurements can provide T_2 . This T_2 , as we shall see later, can also be obtained from OFID and echo

Figure 16

Shown here are experimental data points and theoretical curves for the optical nutation in pentacene at 1.8°K . In each plot, the vertical axis corresponds to a relative absorption (arbitrary units) and $t = 0$ is taken to be the switching time of the EO pulse. The top plot considers only inhomogeneous lineshape averaging [Eq. (19) multiplied by the error function shown in Eq. (28)]. The bottom plot considers averaging over both the inhomogeneous lineshape and the laser beam spatial profile (Eq. 29). The fit is quite good in the latter case and provides values of 27.3 ± 1.3 nsec for the nutation time and 45 ± 2 nsec for T_2 .

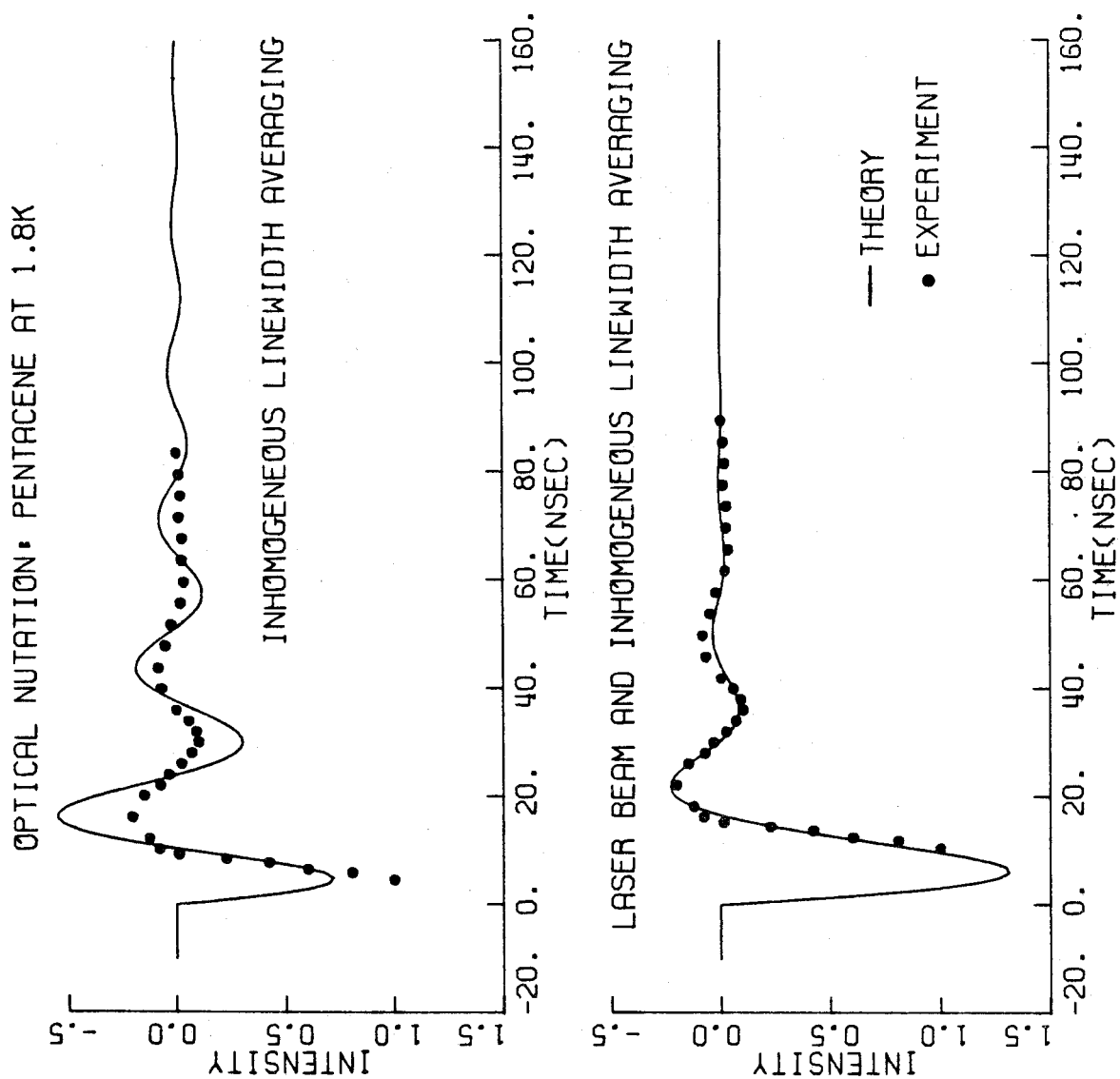
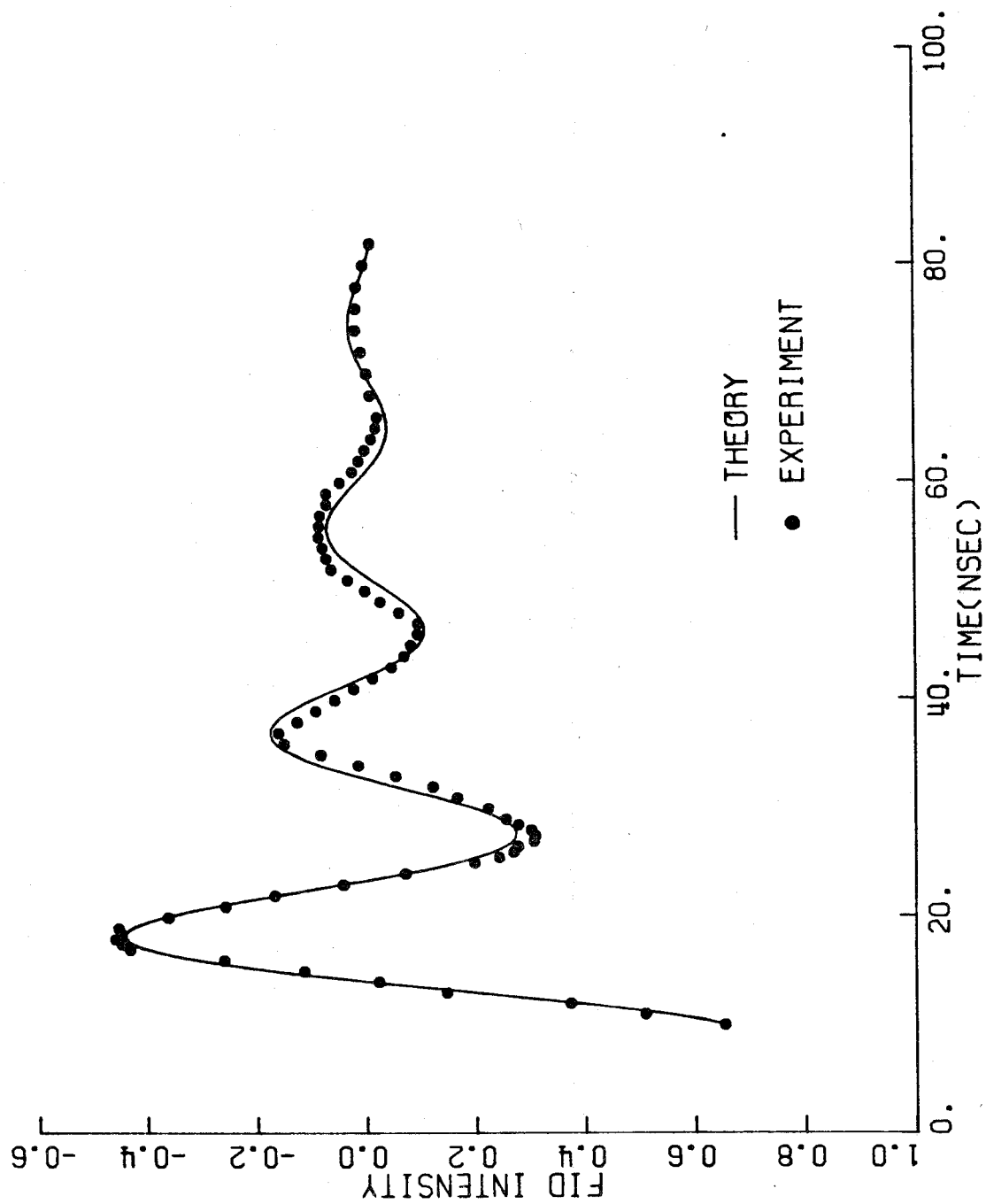


Figure 17

The optical free induction decay observed in pentacene (0_1 origin) at 1.8°K and $400\ \mu\text{W}$ of laser power. Here the experimental data points and theoretical curve (Eq. 38) are in excellent agreement. The power broadening term in Eq. (35) was calculated by scaling the Rabi frequency from the nutation by the square root of the ratio of the laser power used in each experiment. (The nutation and the OFID were taken under identical conditions on the same crystal.) The computer fit then provided a value of $45 \pm 2\ \text{nsec}$ for T_2 from the observed transient decay.

OPTICAL FREE INDUCTION DECAY. PENTACENE AT 1.8K



experiments. Since the spatial profile of the laser has been characterized (Fig. 3) the laser intensity can be determined, and thus the laser field strength. As emphasized by Shoemaker and Van Stryland²³ careful nutation measurements provide the Rabi frequency which allows a direct determination of the transition dipole moment. Knowing the power of the laser P_L in mwatts, the Rabi frequency χ in MHz (10^6 c/sec) and B_L in microns from the laser spatial profile, one obtains the following expression for μ in Debyes:

$$\mu(\text{Debye}) = 4.06 \times 10^{-4} \frac{\chi B_L}{\left(\frac{\eta_b^2 + 2}{3} \right) \sqrt{P_L}} \quad (49)$$

The Rabi frequency χ (in linear units) obtained from Fig. 16 is 36.6 ± 1.6 MHz. The terphenyl b-axis refractive index $\eta_b = 1.687$. We have used the Lorentz local field approximation to obtain the laser field inside the crystal. For a single mode power of 17 ± 1 mwatts at the crystal (after correcting for reflection losses from the optical elements; only 3 mwatt, i.e., total of 15%), and using Eq. (49) we obtain for pentacene in p-terphenyl at 1.8°K , a value for μ of 0.7 ± 0.1 Debye. This value is less than our earlier estimate of 1.5 Debye,¹⁸ where no field correction was made. The T_2 value obtained from the same transient (Fig. 16) agrees with our OFID measurements⁵¹ (described later in detail) and with the results obtained independently by Wiersma.⁵²

We have studied the nutation signal at various EO switching frequencies and have observed an increase in the initial amplitude of

the transient as the frequency is increased. No change in the Rabi frequency ($\mu \cdot \epsilon / \hbar$) could be detected. This is very important since it confirms the absence of complications due to OFID transients from off-resonance molecules which at this power decay extremely rapidly (see Fig. 7). This increase in nutation amplitude can be explained by realizing that at low switching frequency the laser is not "moved" completely off-resonance with the original power-broadened group, allowing it to weakly pump the original molecules. At very low switching frequencies (i. e., within the homogeneous linewidth; 7.1 MHz) no transient is observed, as expected. In addition to this frequency shifting effect on the nutation amplitude, the signal is very sensitive to changes in temperature. This effect will be discussed in a following section where we consider phonon processes as effective dephasing channels.

The data shown in Fig. 17 for the OFID were obtained at very low laser powers (400 μ W) exciting the same electronic origin in the same crystal under identical conditions of temperature and laser frequency as in Fig. 16. Unlike the nutation, the computer fit (solid line) using Eqs. (36) and (38) is very good when we only consider averaging over the inhomogeneous linewidth. Since the OFID transient originates from molecules off-resonance its decay may not be influenced by the laser. To be specific, averaging over the laser profile gives an effective Rabi frequency which affects the decay of transients occurring on-resonance. To obtain the fit in Fig. 17 we fixed T_{1p} at 25 ± 1 nsec (see Table II and Section C) and scaled the Rabi frequency in the power broadening term for the OFID from that obtained in the nutation experiment (done under identical conditions) by the ratio of the square root of

the observed laser intensities in each experiment. The fit then provided a value of 45.3 ± 2 nsec for T_2 consistent with our nutation experiment. Thus, our results show that at 1.8°K , the pure dephasing time T_2' is essentially infinite for pentacene in the terphenyl host since $T_2 = 2T_{1p}$ [see Eq. (11)]. We shall see later that this is no longer true at higher temperature.

In Fig. 17, the heterodyne beat frequency is 53 MHz. It depends linearly on the EO switching voltage (here 100 V) and agrees with the experimentally measured dispersion of the AD*P crystal (0.56 MHz/V) determined using the etalon setup mentioned earlier (Fig. 2). We should mention that a considerable improvement in OFID signal quality was observed when linear polarizers were placed immediately before and after the dewar windows. This is reasonable since slight depolarization can occur from irregularities in the optical surfaces used to direct the laser beam to the sample, and from strain-induced birefringence in the dewar windows themselves.

In these frequency switching experiments, where both off-resonance and on-resonance molecules are observed simultaneously, the dependence of the observed transients on laser power is very dramatic. At low power (< 1 mW) the OFID signal from off-resonance molecules dominates and the optical nutation from molecules switched into resonance provides a weak background absorption whose Rabi frequency $< \frac{1}{T_2}$. On the other hand, at high power (≥ 20 mW) the optical nutation from on-resonance molecules dominates since the power broadening term in the OFID expression (Eq. (36)) causes the observed damping time for the OFID of off-resonance molecules to be much

shorter than T_2 (see Fig. 7). In other words, power broadening allows a larger fraction of the total frequency distribution within the inhomogeneous linewidth to "participate" in the coherent pumping process and this distribution will cause a faster decay of the transient due to inhomogeneous dephasing.

In the OFID experiments at 400 μ W the power broadening term contributes only 10% to the observed decay. However, at 20 mW, the observed decay would be approximately 7 nsec and within the fall time of the switching pulse. Thus, an accurate measurement of T_2 from the OFID requires very low laser power while for the nutation experiment an accurate value can be obtained at high power if averaging over the laser beam spatial profile is carefully done.

The homogeneous linewidth ($1/\pi T_2$) obtained from the nutation and OFID is 7.1 ± 0.4 MHz. This value is over one thousand times smaller than the inhomogeneous linewidth (see Section A). The fact that this homogeneous broadening is very small has turned out to be a valuable result since we can use EO and LADS techniques to study the effects of environment (see Section F) and excess vibrational energy upon radiationless relaxation processes which are important for large molecules like pentacene. If the homogeneous linewidth was a factor of ten larger we would be forced to do these experiments on the picosecond time scale.

The important points about this homogeneous broadening are (1) it is entirely determined by the relaxation rate of the primary level $|p\rangle$ and there is no unusual intramolecular dephasing process at

low temperature (1.8°K) and (2) knowing T_{1p} of sites O_3 and O_4 (Table II) and assuming that $T_2'^{-1}$ is zero (mimicking the O_1 site) the width must be 16.4 MHz, and that is why these sites have relatively weaker transients that decay faster than O_1 .

C. Radiative and radiationless relaxation: IRD

1. Broadband excitation

In the molecular eigenstate picture, broadband excitation prepares a large number of $|m\rangle$ states simultaneously. As mentioned before, the observed decay should have a "fast" component and a slow component whose decay time is essentially characteristic of ψ_m of Eq. (1). If many states are involved in the coupling then the amplitude of the slow component will be insignificant compared to the initial fast decay and the total decay could appear as a single exponential (statistical limit). On the other hand, for a sparse level structure narrowband excitation should select $|m\rangle$ states and their decay will reflect the contribution of the primary level to the molecular eigenstate [Eq. (1)].

Broadband excitation of pentacene in p-terphenyl was performed in three different ways: using a nitrogen laser pumped pulsed dye laser, a nitrogen flash lamp, and a multimode CW dye laser. Using the nitrogen laser pumped dye laser (5nsec pulse) with 18 GHz bandwidth a lifetime (T_{1p}) of 23 ± 3 nsec was measured for pentacene in p-terphenyl exciting the electronic origin O_1 at $16,887 \text{ cm}^{-1}$ at a temperature of 1.8°K. This value agrees with previous measurements yet is a factor of three longer than that found from gas phase experiments (see Table II). Using an N_2 flash lamp ($3650 \pm 50 \text{ Å}$) careful lifetime

measurements were performed by N. J. Bridge⁴⁵ at 4°K for each of the electronic origins of a crystal supplied by us. He found that the two highest energy sites ($0_3, 0_4$) have lifetimes of 9.7 ± 1 nsec while the lower energy sites ($0_1, 0_2$) have lifetimes of 25.7 ± 1 nsec. Within detection limits the decays appear as single exponentials. Also, similar vibrational progressions for each of the sites were observed in the spectra consistent with the spectrum depicted in Fig. 14. The third kind of broadband excitation, which utilized a multimode (240 GHz) CW dye laser and LADS, gave the same T_1 decay time; its importance will be discussed later.

From these T_1 type experiments done with broadband excitation sources, two points can be made: (a) the lifetimes of origins 0_1 and 0_2 are constant from 1.8 to 4.2°K (this will also be shown to be true for the narrowband excitation) and (b) because the observed decay is a single exponential over many lifetimes there is no apparent evidence of the long-lived tail that characterizes the decay of ψ_m following broadband excitation. Point (a) will be important later (Section F) when temperature dependent dephasing processes are discussed.

2. Narrowband excitation: EO and LADS

Our first experiments (I) on pentacene utilizing narrowband excitation (± 3 MHz) and the EO frequency switching method showed a fast build-up in emission intensity followed by a slow decay ($\approx 15 \mu\text{sec}$) occurring at the leading and falling edges of the EO pulse. This decay could be fit to a single exponential over three lifetimes and the transient pattern is characterized by several important observations

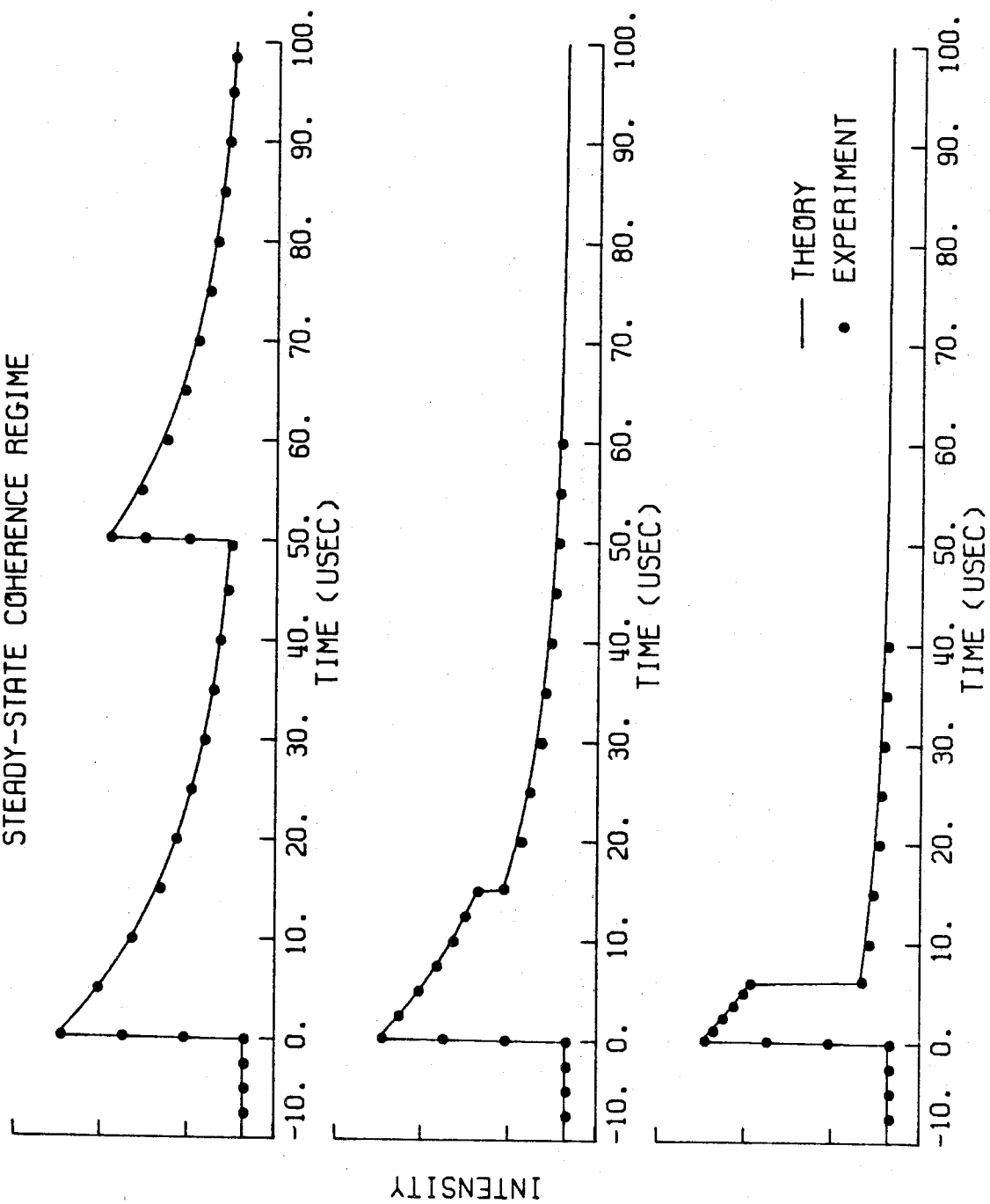
that span the short (transient coherence regime) and the long (steady state coherence regime) time scales. The short time behavior of the pattern manifests the coherence effects discussed previously (Section B) and will be examined later when we discuss the role of temperature. The decay pattern at long times (i.e., $t \gg T_2$) will now be discussed.

The decay at the falling edge of the pulse is very sensitive to pulse width which in this regime is much larger than T_2 . Fig. 18 shows IRD waveforms (data points) and computer fits (solid lines) utilizing Eqs. (43)-(48) from the density matrix solution for $\rho_{pp}(t)$ in the steady-state coherence regime. Here, the data were obtained with a signal averager time resolution of 200 nsec and so the overshoot predicted in Figs. 11 and 12 is averaged out at the leading and falling edges of the EO pulse. This overshoot has been observed using a fast (> 1 GHz bandwidth) photomultiplier and a sampling scope. As the pulse width decreases, the observed decay approaches that found in the broad band experiments. Although this effect has been explained in Section IV, up until this point we have neglected the fact that as the pulse width decreases, its Fourier transform (in frequency) broadens. Therefore, the effective bandwidth of the laser is wider than its CW single-mode value and thus it may span a different energy width in the molecular excitation process. In Appendix I we show Fourier transforms for narrow and wide laser pulses to illustrate the effect. In general, it is therefore not surprising that although one is exciting with a single-mode source, the broad band prepared state may be recovered as the pulse width decreases, especially if the homogeneous width of $|m\rangle$'s is comparable to their separation.

Figure 18

Pentacene IRD experimental data points and theoretical fits as a function of EO pulse width at 1.8°K. The steady-state coherence regime density matrix equations for $\rho_{pp}(t)$, Eqs. (43) and (46), were used to determine the contribution of resonance and off-resonance molecules to the total emission signal. The computer fits provided values of $20.4 \pm 1.5 \mu\text{sec}$ for Γ_{pl}^{-1} and $37.6 \pm 2.6 \mu\text{sec}$ for Γ_{l0}^{-1} with Γ_{p0} fixed at 40 MHz.

PENTACENE IRD AT 1.8K
STEADY-STATE COHERENCE REGIME



From Fig. 18 one can see that the build-up in emission intensity at the falling edge of a long EO pulse does not equal the build-up at the leading edge if the decay has not reached a steady-state value. As explained earlier (Section IV), this effect is due to population not having returned completely to the ground state, $|0\rangle$.

To obtain the fits shown in Fig. 18, only one parameter, T_{1p} , was fixed. All others were optimized by the nonlinear least squares regression analysis program described in Section III. We set T_{1p} , the lifetime of the primary level, equal to 25 ± 1 nsec as obtained from our measurements. The computer fit provided values of 20.4 ± 1.5 μ sec for $\Gamma_{p\ell}^{-1}$ and 37.6 ± 2.6 μ sec for $\Gamma_{\ell 0}^{-1}$. The fit for the observed decay gave a value of $\tau_0 = 19.6 \pm 1.5$ μ sec and this decay was insensitive to the initial estimate of R_p , the pumping rate, if we chose a value large enough (≥ 100 MHz) such that we were in the flat portion of the observed lifetime versus pumping rate curve (Fig. 10). This choice of R_p is consistent with our observation of the decay time being insensitive to laser power. At very small pumping rates where Fig. 10 predicts a longer decay time the overshoot (referred to as "a" in Fig. 8) becomes very small and so the decay time becomes difficult to measure accurately. Over the laser power range that we could measure decay time accurately (1 mW to 50 mW), the decay time did not vary significantly. Considering the value of $\Gamma_{p\ell}/\Gamma_{\ell 0}$ in Fig. 10 the experimental results are consistent with the theoretical predictions.

The rate of population loss from the $\{|\ell\rangle\}$ manifold, $\Gamma_{\ell 0}$ corresponds to a lifetime of 37.6 ± 2.6 μ sec, which is very close to the

lifetime of the lowest triplet state in pentacene measured at low pressures in the gas phase (see Table I). So, it is reasonable to conclude that the $\{|\ell\rangle\}$ manifold does indeed involve triplet states. Of course, it is possible that hot singlets happen to have similar lifetimes.

The rate at which the $\{|\ell\rangle\}$ manifold receives population from the primary level $|p\rangle$ is $\Gamma_{p\ell}$. In the steady state coherence regime it represents an average of all the processes connecting $|p\rangle$ with $\{|\ell\rangle\}$. This average rate, however, does not mean that an indirect mechanism involving an initial fast crossing between $|p\rangle$ and vibrational levels of the $\{|\ell\rangle\}$ manifold isoenergetic with $|p\rangle$ followed by slow relaxation to lower levels in the manifold is indistinguishable from the simple description shown in Fig. 4. In fact, this mechanism would provide a completely different emission transient from the one observed as will be discussed later.

We observed no dependence of the decay of the IRD with EO switching frequency although the initial amplitude varied linearly in most experiments. As discussed earlier for the nutation, the initial amplitude should decrease if one does not switch completely outside of the power-broadened homogeneous linewidth. The observation of no change in decay rate with switching frequency up to the maximum value of 65 MHz is interesting when one considers another observation. As the laser frequency is tuned within the inhomogeneous linewidth (≈ 50 GHz) we measure decay rates that vary in the range 11 to 20 μsec depending on the frequency and the samples used. Thus, with

these two observations there appears to be an anisotropy in the decay channel(s) connecting the primary level $|p\rangle$ to the $\{|l\rangle\}$ manifold that occurs for energy separations outside the range of the frequency switched laser. The inhomogeneous linewidth of the $0 \rightarrow p$ transition reflects a distribution of local environments for the isolated pentacene molecules, but it is not obvious whether the observation of decay rate differences implies an environmental effect on the intramolecular process connecting $|p\rangle$ with $\{|l\rangle\}$ or that the coupling to individual levels is nonuniform even in the absence of any environment (i.e., a completely isolated system). Molecular beam experiments are being planned to clear up this point.

The emission signal seen for pentacene at 1.8°K using LADS excitation (Figs. 19 and 20) differs dramatically from the IRD seen for the EO method (Figs. 18 and 20). In Fig. 19, data points were fit using the density matrix solution for $\rho_{pp}(t)$ in the steady-state coherence regime considering only one ensemble of molecules since the laser is shut off following the slow decay and not switched to a new group of molecules as in the EO experiment. The slow decay is somewhat faster here ($14.7 \pm 1.0 \mu\text{sec}$) but within the range of the EO experiments. When EO and LADS experiments were performed under identical conditions of laser frequency and sample concentration, identical decays were measured (see Fig. 20).

The fast decay on the falling edge of the LADS pulse has a lifetime of $24.5 \pm 2 \text{ nsec}$ which is in excellent agreement with T_{1p} obtained from broadband experiments. This decay at the falling edge is a single

Figure 19

Pentacene IRD experimental data points and the theoretical fit for LADS excitation pulses at 1.8°K. Here $\rho_{pp}(t)$ is calculated using Eqs. (43) and (46) for only the one group of molecules excited by the narrowband laser. The computer fit provides values of $16.3 \pm 1.2 \mu\text{sec}$ for Γ_{pl}^{-1} ; $26.6 \pm 1.5 \mu\text{sec}$ for Γ_{l0}^{-1} and $14.7 \pm 1.0 \mu\text{sec}$ for the observed decay time, τ_0 . The crystal of pentacene in p-terphenyl used in this experiment was different from the one used for the results shown in Fig. 18 but was approximately the same concentration (1×10^{-6} m/m).

PENTACENE LADS EXPERIMENT AT 1.8 K
STEADY-STATE COHERENCE REGIME

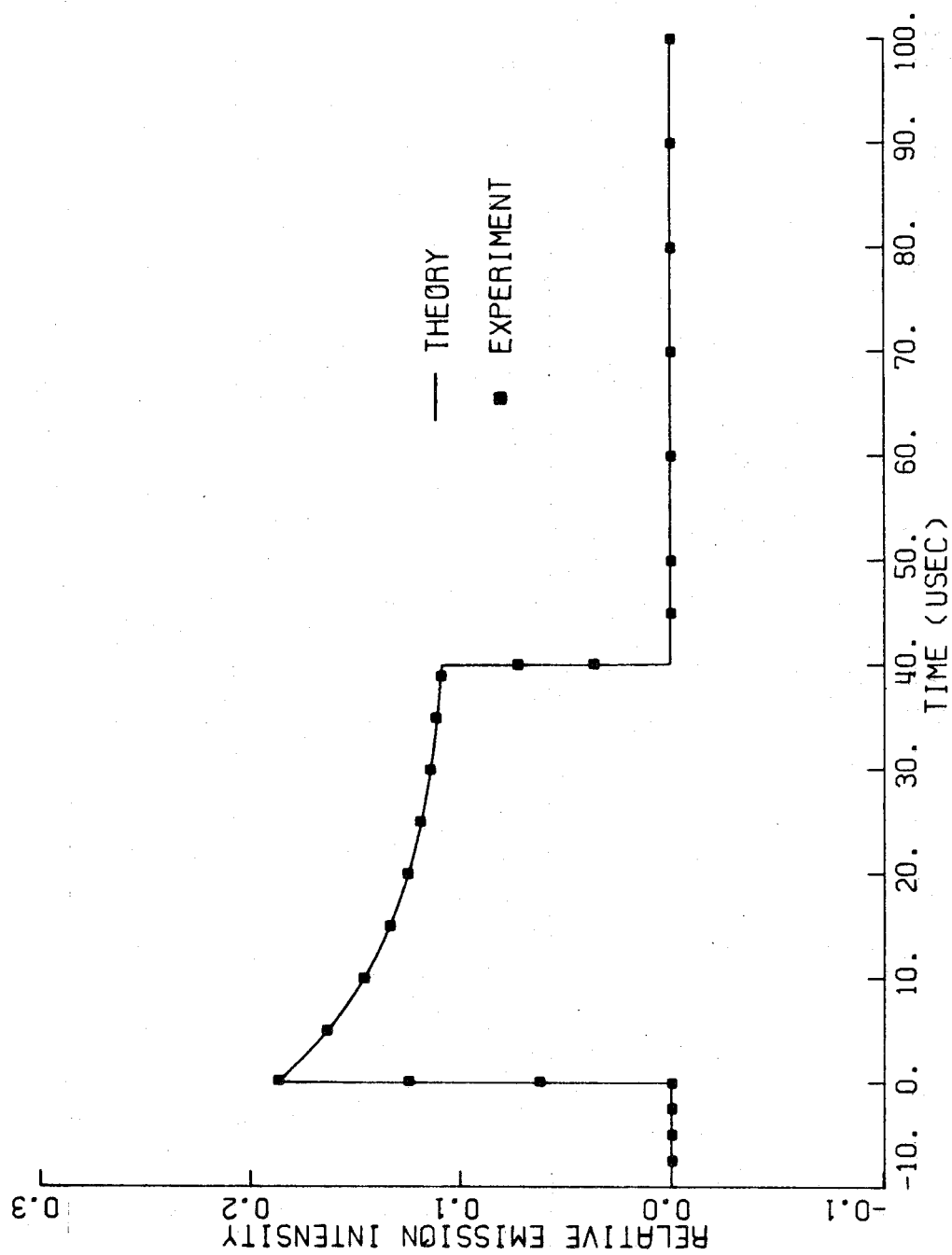
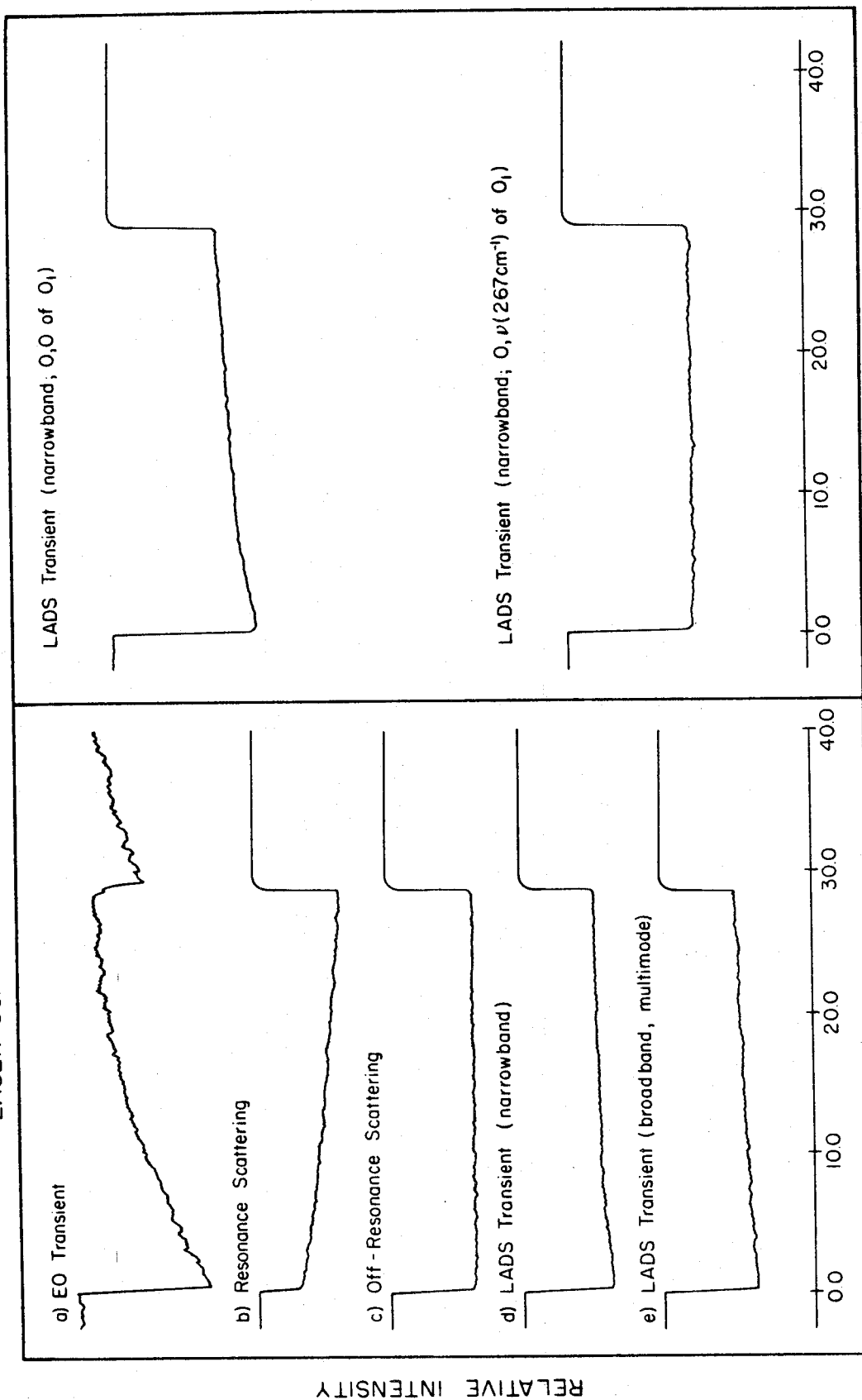


Figure 20

Emission and laser scattering experiments for pentacene at 1.8°K. Shown are (a) The emission transient observed with the EO technique; $\tau_0 = 13.9 \pm 0.4 \mu\text{sec}$. (b) The laser scattering signal (on-resonance) observed with narrow spectrometer slits (0.7 cm^{-1}). Here, the slow build-up time is $13.8 \pm 0.3 \mu\text{sec}$. (c) The laser scattering signal off-resonance (-3.5 cm^{-1}).⁶⁴ (d) The emission transient observed with the LADS technique (single-mode); $\tau_0 = 13.8 \pm 0.4 \mu\text{sec}$. (e) The emission transient observed with multimode (broadband) LADS excitation; $\tau_0 = 15.6 \pm 0.6 \mu\text{sec}$. At the top right of the figure is shown the single-mode LADS emission transient exciting at a different frequency from experiment (d) but still within the inhomogeneous linewidth of the 0_1 site origin; here $\tau_0 = 14.6 \pm 0.5 \mu\text{sec}$. At the bottom right of the figure is shown the LADS emission signal exciting at the 0_1 vibronic line 267 cm^{-1} above the origin.

LASER SCATTERING AND EMISSION EXPERIMENTS: PENTACENE AT 1.8°K



exponential after deconvolution knowing the exact excitation pulse shape. Furthermore, there is no change in the long and short decays (obtained from these LADS experiments) as a function of temperature in the range 1.8-4.2°K: At 1.8°K $\tau_0 = 11.7 \pm 0.3 \mu\text{s}$, $T_{1p} = 24.5 \pm 2$ nsec and at 4.2°K, $\tau_0 = 12.8 \pm 0.5 \mu\text{s}$, $T_{1p} = 25.3 \pm 2$ nsec. In Fig. 21, the temperature dependence of τ_0 , obtained from the EO results of a different crystal, and T_{1p} obtained from LADS are depicted.

Two important conclusions can now be drawn. First, the narrowband (LADS, single-mode) and wideband (incoherent N₂ flash lamp or N₂ pumped dye laser) measurements of T_{1p} give identical results. Second, the narrowband single-mode excitation and multi-mode excitation give the same T_{1p} decay characteristics even though the coherence properties of the laser are different. In other words, in pentacene, the T_1 decay is insensitive to (a) the nature of the light source and (b) the environment in the temperature range studied. This situation is very different from the temperature dependence of T_2 .

D. Zeeman measurements

Several IRD experiments were performed in the presence of a d.c. magnetic field parallel to the laser polarization and up to 900 Oersted in strength. Measurements of the IRD lifetime and d.c. emission intensity were made on several crystals with different concentrations and orientations. A summary of data obtained in over twenty-five individual experiments done on different runs appears in Table III. In all cases, we observed both a decrease in d.c. emission intensity (up to 17%) and a longer IRD lifetime (up to 15%) in the presence of the field.

TABLE III. Zeeman effect on IRD: Pentacene at 1.8°K

Experiment Number	Crystal ^a	B ₀ (Oersted)	Orientation ^b or ⊥	τ ₀ ^c (nsec)	PMT Anode Current(d.c.) (μA)	Average τ ₀ (μsec) ^d
1	A	0		12.5 ± 0.2	100.0	$\langle \tau_0 \rangle_{ }^A (B_0 = 0) = 10.4 \pm 0.2$
2	A	400		14.3 ± 0.3	89.0	
3	A	0		10.1 ± 0.5	100.0	$\langle \tau_0 \rangle_{ }^A (B_0 = 900) = 11.9 \pm 0.6$
4	A	900		12.8 ± 0.5	83.0	
5	A	0		10.4 ± 0.5	100.0	$\langle \tau_0 \rangle_{ }^A (B_0 = 450)$ $= 12.2 \pm 0.1$
6	A	900		11.7 ± 0.5	83.0	
7	A	0		10.8 ± 0.5	100.0	
8	A	450		12.2 ± 0.7	88.0	
9	A	0		10.4 ± 0.5	100.0	
10	A	900		11.7 ± 0.5	83.0	
11	A	0		10.4 ± 0.5	100.0	
12	A	450		12.1 ± 0.5	88.0	
13	A	0		10.2 ± 0.5	100.0	
14	A	900		11.4 ± 0.5	83.0	
15	A	0		10.5 ± 0.5	100.0	

Table III. (continued)

Experiment Number	Crystal ^a	B ₀ (Oersted)	Orientation ^b or ⊥	τ ₀ ^c (nsec)	PMT Anode Current (μA)	Average τ ₀ (μsec) ^d
16	A	0	⊥	10.9 ± 0.5	100.0	$\langle \tau_0 \rangle_{\perp}^A (B_0=0) = 11.9 \pm 0.9$
17	A	550	⊥	13.1 ± 0.8	87.0	
18	A	0	⊥	12.5 ± 0.7	100.0	$\langle \tau_0 \rangle_{\perp}^A (B_0=550) = 13.3 \pm 0.3$
19	A	550	⊥	13.5 ± 0.8	87.00	
20	A	100	⊥	12.1 ± 0.5	95.0	
21	A	0	⊥	12.4 ± 0.5	100.0	
22	B	0		11.2 ± 0.5	100.0	$\langle \tau_0 \rangle_{ }^B (B_0=0) = 12.2 \pm 0.6$
23	B	550		13.9 ± 0.7	88.0	
24	B	0		12.6 ± 0.5	100.0	
25	B	0		12.4 ± 0.5	100.0	
26	B	550		14.0 ± 0.8	88.0	$\langle \tau_0 \rangle_{ }^B (B_0=550) = 14.0 \pm 0.1$
27	B	0		12.2 ± 0.5	100.0	
28	B	0		12.5 ± 0.5	100.0	

^aCrystal A $\approx 1 \times 10^{-5}$ m/m; crystal B $\approx 1 \times 10^{-6}$ m/m.^b|| and ⊥ refer to two distinct (90° to each other) directions of the applied magnetic field, B₀, in the cleavage plane: || direction is close to the b-axis as identified by the growth habit of the crystal.^cThe errors quoted in this column are standard deviations.^dThe errors quoted in this column are standard deviations for the average values of τ₀. Only data obtained on the same day at fixed laser frequency and under identical conditions are averaged.

The IRD waveforms were run at zero field, in the field, and zero-field again in order to ensure that no irreversible effects were occurring (i. e., field induced strain, etc.). The magnitude of the effect is not that sensitive to crystal orientation but it is quite sensitive to small changes in laser frequency (i. e., one cavity mode = 390 MHz or less). Note that because τ_0 changes with the laser frequency one cannot at random correlate the in-field experiments with the out-of-field ones.

Since the magnitude of the effect is quite small a careful measurement of the decay over several lifetimes is necessary to accurately determine the change in lifetime in the presence of the field. Considering an exponential decay of the form $A(t) = A_0 e^{-\Gamma t}$ the maximum change in intensity ΔA corresponding to a change in rate $\Delta \Gamma$ occurs at $t = \tau_0$ and equals $(-\Delta \Gamma / \Gamma) A$. For changes in decay rate of 10-15% this represents a small change in emission intensity and even for excellent S/N waveforms which we were able to obtain (typically 100-1000), several decay lifetimes were followed for all experiments to obtain accurate measurements. Possibly the overall d.c. signal from the detector could change partially due to the influence of a magnetic field on the path that electrons follow through the dynode chain of the photomultiplier. However, the tube is shielded and for the field strengths we used any effect of this nature would be small. Furthermore, a d.c. field will not affect the dynamic (time) response of the detector. The observed decay pattern therefore reflects changes in τ_0 and also will have the largest effect at $t \simeq \tau_0$, as observed in the experiments.

We originally performed these experiments to determine whether the $\{|\ell\rangle\}$ manifold coupled to the primary level $|p\rangle$ consisted

of triplets or hot ground singlets. There should be no magnetic field effect on the IRD lifetime if singlets are involved predominantly. Conversely, the participation of triplet states in the IRD decay can essentially be guaranteed if an effect is observed.

Several discussions of the rates of intersystem crossing for the individual triplet spin sublevels and the effect of external magnetic fields⁵³⁻⁵⁸ have appeared in the literature. It is generally considered, with experimental evidence in some cases, that fluorescence intensity modulation occurs in the presence of a magnetic field due to changes in spin-orbit coupling strength.^{59, 60} There should be differences in the magnitude of the effect however if the field is applied along different principal magnetic axes of the molecule since the Zeeman interaction will mix only the spin sublevels not aligned with the field. Of course, an average effect will usually be observed especially in mixed molecular crystals since different orientations of the guest exist, and the molecule in the site has a very large number of vibronic levels near $|p\rangle$.

In these Zeeman-IRD experiments the effect always resulted in a longer IRD decay time and a slightly lower d.c. emission intensity. The two observations are consistent in that an overall decrease in the average rate of population of $\{|l\rangle\}$ levels would decrease the overall rate of return of population to $|0\rangle$ and, therefore, reduce the d.c. emission intensity. The rate of population return to $|0\rangle$ from $\{|l\rangle\}$ at Γ_{l0} may be affected by the field also. Thus because we do not know the precise nature of the levels near $|p\rangle$ we cannot quantitatively treat the dependence of τ_0 on the orientation and the strength of the magnetic field. Nevertheless, the experiments indicate the positive participation of spin levels in the $\{|l\rangle\}$ manifold.

E. Laser scattering experiments: on- and off-resonance effects

In a real two-level system with homogeneous broadening, the interaction between the molecular ensemble (i.e., a collection of molecules characterized by ground and excited states) and the radiation field gives rise not only to molecular absorption and emission of light but also to the scattering of photons "off the molecule." Clearly, this scattering process depends on T_2 and the off-resonance frequency difference between the molecule and the field. Stimulated by the experimental work of Williams *et al.*⁶¹ on iodine, several investigators have recently addressed this question of resonance emission versus scattering⁶² when the molecule is excited by a weak broadband source.

Narrow-band excitation of such a system may influence the observed decay depending on the relative magnitude of the laser bandwidth and $1/\pi T_2$ of the transition. In the limit where the laser bandwidth is much smaller than $1/\pi T_2$, the scattering pattern will exhibit a decay which is due to the light source. This phenomenon is sometimes referred to as the Heitler effect, and has been discussed in detail by Hochstrasser and his co-workers.⁶²

This effect was of concern to us when we studied the narrow-band transients of pentacene, since $1/\pi T_2 = 7.1$ MHz and the bandwidth of the laser on the time scale of the experiment is ≤ 3 MHz. Considering a Gaussian-shaped laser beam profile and a Lorentzian-shaped molecular resonance, the response function for the interaction between the molecule and the light was calculated as a function of the ratio of the laser bandwidth to $1/\pi T_2$. It was concluded that the Heitler effect is negligible, under weak excitation conditions, when this ratio becomes close to three.⁶³ Indeed, for the narrow band excitation of iodine, this ratio is

larger than three and the decay is molecular⁶³ as is evident from it being purely exponential and obeying²⁷ the Stern-Volmer relationship.

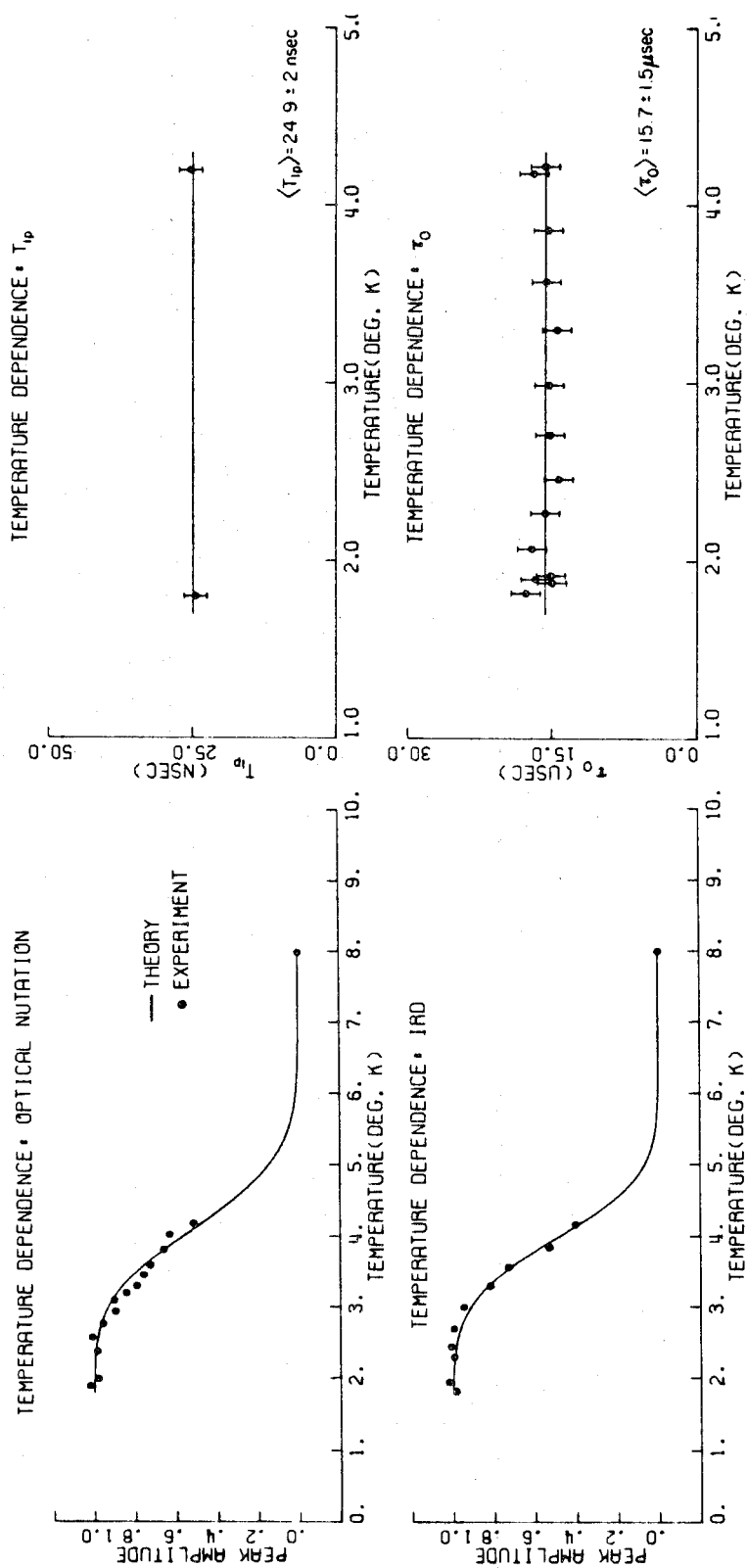
As shown in Appendix I, the effective laser bandwidth in our narrow-band short pulse excitation experiments is not determined by the residual FM jitter (≈ 60 KHz) of the CW single-mode but by the Fourier transform of the pulse (0.1-30 MHz) depending upon the pulse width. Furthermore, as the temperature is increased to 4.2°K, there is no change in the observed decay even though T_2 has changed (see Fig. 21), and consequently the ratio of the linewidth to the laser bandwidth has been altered. Finally the "real" T_1 of the 0_1 origin in these narrow-band excitation experiments is the same as the T_1 observed with broadband excitation. With these facts in mind, together with the Zeeman experiments, we concluded that the effect of narrow-band scattering is not a dominant one in pentacene under our experimental conditions.

Careful investigation of the on- and off-resonance scattering can provide additional valuable information, namely ground state population dynamics. In the pentacene case, this kind of experiment is important because if the ≈ 15 μ sec decay represents a population flow from $|p\rangle$ -to- $\{|l\rangle\}$ -to- $|0\rangle$, then one should observe a slow transient on the scattering signal that characterizes in part the time dependence of the ground state population.

To check the above hypothesis we performed resonance and off-resonance laser scattering experiments in the mixed crystal at 1.8°K. Since $|0\rangle$ receives population from the slow decay channel

Figure 21

The dependence of coherent transient amplitudes and lifetimes on temperature for pentacene in p-terphenyl. Optical nutation data for the peak amplitude fit to Eq. (29) provided values of: $(T_2)_0 = 44 \pm 2$ nsec; $\Gamma_p = 10.4 \pm 0.3$ GHz; and $\Delta = 16.9 \pm 1.1$ cm⁻¹. IRD data for the peak emission intensity fit to Eq. (32) provided values of: $(T_2)_0 = 44 \pm 2$ nsec; $\Gamma_p = 12.0 \pm 0.3$ GHz; and $\Delta = 15.1 \pm 0.9$ cm⁻¹. The lifetimes of both the primary level $|p\rangle$, T_{1p} , and the slow transient decay, τ_0 , were found to be independent of temperature in the range 1.8-4.2°K with narrowband excitation. Average values found were: $\langle T_{1p} \rangle = 24.9 \pm 2$ nsec and $\langle \tau_0 \rangle = 15.7 \pm 1.5$ μ sec. (See the data presented at the top of this figure.)



while $|p\rangle$ loses population to the slow channel, one might naively think at first that the laser scattering transients should provide the recovery time of the ground state and thus show a build-up transient rather than the decay seen in emission (Fig. 19). This is not a correct picture of the population flow within the level structure, however, for light on experiments. In the presence of the laser field, net population is continuously lost from both $|0\rangle$ and $|p\rangle$ (at a rate τ_0^{-1}) to the $\{|l\rangle\}$ manifold until $\Gamma_{pl}\rho_{pp} = \Gamma_{l0}\rho_{ll}$ and equilibrium exists. Thus, true molecular scattering in pentacene should produce a scattering transient that decreases in intensity during the laser pulse, as shown in Fig. 22.

The procedure used in these experiments was as follows. During a single-mode laser pulse (LADS method), scattered laser light from the sample was collected at right angles to the laser beam and was observed through a 0.5 m Jarrel-Ash spectrometer with narrow slits (0.7 cm^{-1}). The experiments were performed with the laser on- and off-resonance with the 0_1 origin. Although the sample emits at the laser frequency, most of the emission (Fig. 14) occurs to upper vibronic levels of the ground state and with narrow slits the scattered laser light signal dominates.

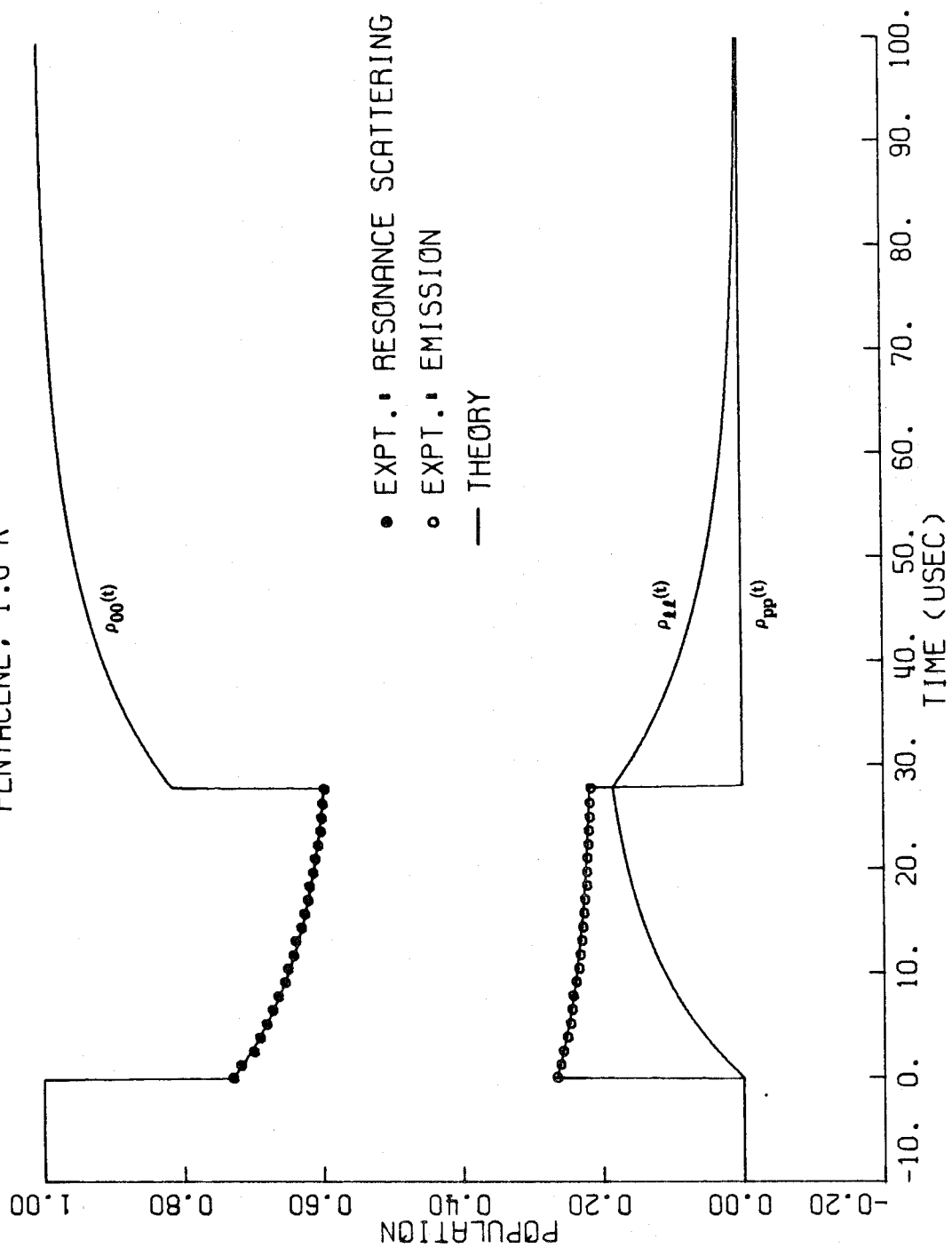
The laser scattering results (Fig. 20) are compared with theory in Fig. 22 together with the LADS emission decay at identical pulse width and laser power. As one can see, the emission signal decays by a slow transient. However, the on-resonance scattered laser signal shows a slow build-up in intensity (Fig. 20) instead of the decay predicted by the time dependence of the ground state population shown in Fig. 22. This build-up rate is identical with the ground state population

Figure 22

Shown here are plots of the population $|0\rangle$, $|p\rangle$ and $|l\rangle$ obtained from the density matrix equations in the steady-state coherence regime [Eqs. (43) and (48)], and experimental data points from the resonance scattering and LADS emission transients (see Fig. 20) at 1.8°K. The observed decay rate for $\rho_{pp}(t)$ is identical to the build-up rate of resonance scattering intensity. The best fit value for both is $13.7 \pm 0.4 \mu\text{sec}$. Resonance scattering data have been plotted on $\rho_{00}(t)$ to show that it corresponds to a depletion of population from the ground state.

LEVEL POPULATION DYNAMICS • STEADY-STATE COHERENCE REGIME

PENTACENE, 1.8 K



decay rate as shown by the excellent fit of experimental scattering data to theoretical ground state population as a function of time (Fig. 22).

From the experiments of Williams *et al.*⁶¹ on I_2 one knows that following a laser pulse excitation on-resonance, the lifetime of the molecular scattering process is governed by the natural (spontaneous) lifetime of the excited state, while off-resonance the scattering lifetime is determined by the excitation pulse characteristics. During the excitation pulse, however, the time dependence of the scattering intensity should reflect the approach of $|0\rangle$ and $|p\rangle$ towards equilibrium. If the background scattering of the laser beam (due to crystal imperfections, etc.), i.e., the off-resonance scattering of Fig. 20, is much larger than molecular resonance scattering then the observed scattering signal (on-resonance) will show a slow build-up transient due to self-absorption effects rather than the slow decay due to molecular scattering. In our experiments, background scattering is strong and thus the observed build-up characterizes the time dependence of self-absorption in the sample. One knows that the absorption coefficient is proportional to the population difference between the levels involved in the absorption process. Using Eqs. (43) and (48) of the density matrix, the population difference between $|0\rangle$ and $|p\rangle$ can be determined. One obtains an expression that decays exponentially (following the initial jump; Fig. 22) at a rate given by τ_0^{-1} towards an equilibrium value of $(\Gamma_{p\ell} + \Gamma_{p0})\Gamma_{\ell 0}/\lambda_+\lambda_-$. Since the amount of background scattered laser light reaching the detector increases as the absorption decreases, the observed build-up in the laser scattering signal is consistent with

a decrease in the absorption of the sample as population is lost to the slow decay channel. This interpretation is supported by (1) the fact that the absolute scattering intensity increases off-resonance with no build-up or decay⁶⁴ and (2) this same effect is seen at much lower concentration (1×10^{-8} m/m) where although absorption is lower, total molecular density is lower also. Thus the effect we see here at the 0, 0 frequency is not an artifact related to the sample concentration. Furthermore, background scattered laser light need not be of concern in emission experiments since laser light is blocked with appropriate sharp-cut filters at the detector and the relatively intense emission to upper vibronic levels of the ground state is observed exclusively.

These laser scattering experiments agree with the results obtained from emission experiments concerning the origin of the slow transient decay and are consistent with the level structure shown in Fig. 4 for pentacene.

F. Effect of temperature on dephasing in pentacene

1. Theoretical preliminaries

As shown in Fig. 21, the pure dephasing rate of pentacene, which forms an impurity in the p-terphenyl host, depends on the lattice temperature in a different manner from that of T_1 processes. The interesting questions are therefore (a) why is this true in solids and (b) can we describe this distinct behavior and fit the experimental results without yielding to a phenomenological approach?

Several models are now known to give rise to a temperature dependent linewidth and frequency shift. The models have been used to

describe vibrational dephasing in liquids and also some molecules in rigid media.

Diestler⁶⁵ has recently reviewed vibrational phase and population relaxation theory as applied to a harmonic oscillator in a heat bath. The work of Fischer and Laubereau,⁶⁶ Oxtoby and Rice,⁶⁷ and Madden and Lynden-Bell⁶⁸ have emphasized the role of T_2 and T_1 in determining the observed vibrational dephasing time. Oxtoby⁶⁹ has shown that an accurate T_2 calculation for N_2 can be obtained by means of a molecular dynamics simulation. More recently, Harris and coworkers⁷⁰ have advanced an exchange model based on the Kubo-Anderson⁷¹ theory to describe the effect of temperature on T_2 and on the line shift δ . The exchange model requires the presence of low frequency molecular or localized phonons (on the impurity molecule) that undergo changes in frequency on going to the excited state. Thus, it is expected that the temperature dependence of the dephasing will be determined by the thermalization process (like $e^{-\Delta/kT}$, where Δ is the phonon energy) into the nearby level.

This "activation" energy expression also appears to explain the temperature dependence of T_2 obtained from photon echo experiments done on optical transitions. Thus we are now faced with an interesting point; if exchange is the dominant process for the destruction of phase coherence, then there must be "selective" modes by which dephasing occurs. Furthermore, in the exchange model the role of acoustic phonons is incorporated only indirectly, even though the experiments of interest are usually carried out at temperatures below the Debye cutoff.

In what follows we highlight a theory developed by Jones and Zewail⁷² for optical dephasing in condensed phases as applied to pentacene. The expressions obtained for dephasing in terms of molecular scattering processes were originally derived by Jones *et al.*⁷³ utilizing the optical theorem of scattering theory and the Redfield's superoperator technique exploited by Snider⁷⁴ and recently by Liu and Marcus⁷⁵ for describing phase relaxation in a two-level system. We have obtained⁷² these same expressions more recently by using the projection operator technique of Zwanzig,⁷⁶ which has been applied to lineshape problems (especially in gases) in the classical work of Fano⁷⁷ and Ben-Reuven.⁷⁸ In this way, it was possible to cast the parameters of dephasing in solids as a function of temperature, and it was also possible to include the exchange terms in a nonphenomenological way. The theory (to lowest order) has been applied primarily by Diestler⁷⁹ to liquids. With reasonable models, the theory gives approximate T_2 's and provides their temperature dependence. For more details on the treatment the reader is referred to reference 72.

Theoretically, the molecule is treated as consisting of a single resonance with initial (i) and final (f) states interacting with a bath without discrimination between optical and acoustic modes. The Hamiltonian describing this system is

$$\mathcal{H} = \mathcal{H}_m + \mathcal{H}_{ph} + V \quad (50)$$

where \mathcal{H}_m is the molecular impurity (pentacene) Hamiltonian, \mathcal{H}_{ph} the phonon Hamiltonian and V the interaction term. Thus, we have

$$\mathcal{H}_m = \frac{1}{2} \begin{pmatrix} \hbar\omega_0 & 0 \\ 0 & -\hbar\omega_0 \end{pmatrix} = \begin{pmatrix} E_p & 0 \\ 0 & E_0 \end{pmatrix} \quad (51a)$$

$$\mathcal{H}_{ph} = \sum_{qj} \hbar\omega_{qj} (a_{qj}^+ a_{qj} + \frac{1}{2}) \quad (51b)$$

$$V = V_1 S + V_2 S^2 + \dots \quad (51c)$$

$$S = i \sum_{qj} \left(\frac{\hbar}{2M\omega_{qj}} \right)^{\frac{1}{2}} (qj) (a_{qj} - a_{qj}^+) \quad (51d)$$

Here, V_1 and V_2 are the coupling parameters between the molecule and the phonons, and S is a strain operator which creates (a^+) or destructs (a) a phonon (wavevector q and mode index j) as a result of the tensorial distortion of the lattice around the excited molecule. a^+a is the occupation number in the reservoir, and M is the mass.

The total dephasing rate for a system described by the above Hamiltonian is:⁷²

$$\begin{aligned} \frac{1}{T_2} &= \frac{1}{2} \left(\frac{1}{T_{10}} + \frac{1}{T_{1p}} \right) \\ &+ \frac{\pi}{\hbar} \sum_{q, q'} W_p \left| \langle 0q' | T | 0q \rangle - \langle pq' | T | pq \rangle \right|^2 \delta(E_q - E_{q'}) \\ &= \frac{1}{2} \left(\frac{1}{T_{10}} + \frac{1}{T_{1p}} \right) + \frac{1}{T_2'} \end{aligned} \quad (52)$$

where the initial and final states are 0 and p , respectively, and T_2' is the pure dephasing time. The temperature dependence of T_2' is now contained in the $\sum W_p$ which depends on the density of bath states and

the phonon thermal distribution. On the other hand, the transition (T)-matrix element difference between the initial and final states which now has the phonon states as well (qj , the phonons, are replaced by q for the sake of simplicity) determines the source of the elastic scattering "anisotropy" between the two states of the transition. In other words, if this anisotropy is large then the cross section for the T_2' process will be relatively large when compared with the cross section for the T_1 process. As we shall see from our data on pentacene, the anisotropy term temperature dependence dominates that of the T_1 term simply because the cross section of the former is very large for optical transitions.⁷⁹

We shall assume that for pentacene in p-terphenyl the lowest order contributions to T are the important ones. These processes include two-phonon scattering and can be handled if we expand T in terms of V using Dyson's equation:

$$T = V + VG_0T = V + VG_0V + \dots \quad (53)$$

where G_0 is the free propagator (Green operator). It is apparent that the two-phonon processes originate from the first order term of the strain expansion of V carried to second order in the Dyson series or the second-order term of the strain expansion carried to first order in the Dyson series. However, we note that the former contribution will be approximately on the order of the population decay rate and will be neglected in the case of interest.

Combining EQs. (51), (52), and (53), we have

$$\frac{1}{T_2} = \frac{4\pi}{\hbar} \sum_{\mathbf{q}, \mathbf{q}'} \left(\frac{\hbar \mathbf{q}^2}{2M\omega_{\mathbf{q}}} \right)^2 \langle n_{\mathbf{q}} \rangle \langle n_{\mathbf{q}'} + 1 \rangle |\langle \Delta V_2 \rangle_{p0}|^2 \delta(E_{\mathbf{q}} - E_{\mathbf{q}'}) \quad (54)$$

where the brackets, describing phonon absorption and emission, denote thermal averages and $\Delta V_2 = \langle \mathbf{p} | V_2 | \mathbf{p} \rangle - \langle 0 | V_2 | 0 \rangle$. For acoustic phonons obeying the Debye model, the density of states is quadratic in frequency, and is only nonzero up to the cut-off frequency ω_D . Using the expression for the Debye density of states function and Eq. (54) yields,

$$\frac{1}{T_2} = \text{constant} |\langle \Delta V_2 \rangle_{p0}|^2 \left(\frac{kT}{\hbar} \right)^7 \int_0^{X_D} \frac{X^6 e^X dx}{(e^X - 1)^2} \quad (55)$$

where $X_D = T_D/T$. Thus for temperatures much less than the Debye temperature, the rate of pure optical dephasing is

$$\frac{1}{T_2} = \text{constant} |\langle \Delta V_2 \rangle_{p0}|^2 T^7 \quad (56)$$

and we now recover the T^7 term. We note that this is different from the T^7 that describes linewidths determined by T_1 processes, discussed in reference 72 and in the literature by many other authors.⁸⁰ In fact, one can see that the coefficient (anisotropy term) in front of T^7 is what makes the pure dephasing term a dominant one in a way similar to elastic dephasing in gases under the binary collision approximation. Two interesting points can now be made. First, Eq. (56) is similar to the one used by Diestler⁷⁹ for describing dephasing of N_2 in Ar using the Born approximation method. Second, the other temperature terms of acoustic phonons can be obtained from Eq. (52) without (yet)

considering the mechanism of dephasing by exchange into other states. For example, if the phonon branch has an effective mode (e.g., quasi-localized or resonance⁸¹) of frequency Δ/\hbar then we obtain the Orbach-type term using the same prescription given above, but with a different cross section. To illustrate this point more clearly let us consider the case of a resonance mode that causes dephasing. This case is particularly useful for the pentacene/p-terphenyl system.

Dephasing by optical phonons is different from that which occurs by acoustic phonons. The difference arises since the optic phonon branch is described by essentially one energy, $\hbar\omega_{\text{op}} = \Delta$, at temperatures much less than Δ/k . If one assumes that the density of phonon states for this mode (optical or "resonance") is sharply peaked about Δ , then the temperature dependence is easy to ascertain [Eq. (54)]:

$$\frac{1}{T_2} = \text{constant} \frac{e^{\Delta/kT}}{(e^{\Delta/kT} - 1)^2} |\langle \Delta V_2 \rangle_{p0}|^2 \quad (57a)$$

$$= \Gamma_p e^{-\Delta/kT}; \quad \Delta \gg kT \quad (57b)$$

where Γ_p denotes a pre-exponential constant. This result provides several interesting points: (a) it applies to pentacene nicely; (b) it is derived from formal theory, and thus the comparison with experiments is not phenomenological; (c) it describes the Orbach mechanism (which is similar in form to the temperature dependence results of the exchange model) without invoking any specific modes. As discussed in reference 72, exchange comes from inter-resonance coupling, i.e., off-the-energy shell terms in the language of scattering theory.

Finally, the frequency shift δ of the transition can also be deduced as a function of temperature in the same manner. The shift is given⁷² by the sum of two terms: δ_1 which includes energy shifts of 0 and p (of the form $|\langle T \rangle|^2 / \Delta_{qq'}$) similar in meaning⁸⁰ to the T_1 term of Eq. (52), and δ' which contains an anisotropy term similar to that of T_2' and is given by

$$\delta' = \frac{\pi}{\hbar} \text{Re} \left\{ i \sum_{q, q'} W_q \langle \Delta T^- \rangle_{0p} \langle \Delta T^+ \rangle_{0p}^* \delta(E_q - E_{q'}) \right\} \quad (58a)$$

where

$$\langle \Delta T^\pm \rangle_{op} = \langle 0q | T | 0q' \rangle \pm \langle pq | T | pq' \rangle \quad (58b)$$

It is interesting to note that because the temperature dependence is determined by the density of states of the phonons, the δ' calculation for both kinds of phonons gives a temperature dependence function like that obtained for the linewidth.^{81b} Physically, this makes sense as the same processes are responsible for the shift and the linewidth--an anisotropy in the scattering amplitudes for the two states of the transition. Thus we conclude that the ratio of the linewidth to the shift is generally expected to be temperature independent, and that the use of this criterion to invoke the exchange model is not unequivocal.^{81b} Furthermore, the expression for δ' clearly indicates that the shift could be either positive or negative as observed experimentally, but the physics that determines this behavior is now more clear--the anisotropy of the scattering matrix element between the ground and the excited states. Thus for electronic transitions the shift is expected to be one-way, while for the IR transitions it might go either way. Also of significance,

Eq. (52) indicates that an electronic transition will exhibit faster dephasing than IR or spin transitions.^{79, 82}

2. Nutation, IRD, and echo results

As mentioned before, the data presented in Fig. 21 show the distinct behavior for T_2' and T_1 -type processes as a function of temperature. This distinction comes about because of Eq. (52). For the spontaneous lifetime of the $|p\rangle$ state in pentacene, we found no difference between the 1.8°K and the 4.2°K results (24.9 ± 2 nsec). Similarly, there is no dependence on temperature for τ_0 in the range 1.8-4.2°K;⁸³ i.e., 15.7 ± 1.5 μ sec. These two observations indicate that the population loss rate of the $|p\rangle$ state is not sensitive to temperatures (1.8-4.2°K) and that the pure dephasing rate, which reflects differences in the scattering amplitude of excited and ground states [Eq. (52)], is changing with temperature by acoustic and/or optical phonons of the mixed crystal, i.e., including resonance and quasilocalized modes.

If the impurity (pentacene) is dephased by phonons within the entire frequency distribution of the acoustic branch, then a T^7 temperature dependence. Eq. (56), for T_2' is expected. Thus, one would expect $1/T_2$ to be constant in the low temperature regime and increase when the T^7 process becomes active. On the other hand, a resonant phonon mode built on the electronic ground and/or excited states can make the impurity dephase according to Eq. (57), and the optical resonance will shift following Eq. (58).

From the nutation and the IRD results of Fig. 21, we obtained the following parameters from the computer fit and using Eq. (57):

Nutation: $\Delta = 16.9 \pm 1.1 \text{ cm}^{-1}$; $(T_2)_0 = 44 \pm 2 \text{ nsec}$
and $\Gamma_p = 10.14 \pm 0.3 \text{ GHz}$

IRD: $\Delta = 15.1 \pm 0.9 \text{ cm}^{-1}$; $(T_2)_0 = 44 \pm 2 \text{ nsec}$
and $\Gamma_p = 12 \pm 0.3 \text{ GHz}$

The above values for $(T_2)_0$, i. e., T_2 at very low temperatures (0 means zero degree which in our case implies 1.8°K) is in very good agreement with the OFID and echo results ($44 \pm 3 \text{ nsec}$ ⁴⁹). What is not in good agreement is Δ which is slightly smaller (~ 17 as compared to 21 cm^{-1}), and Γ_p . The difference is not that serious, however, since both of the values are obtained by fitting the data with two parameters, but we also know that the lack of data between 4.2°K and 8°K introduces some error. The important point is that all of the available results on pentacene are consistent in that they show agreement on the measured T_2 and T_1 and on the transition temperature (3.7°K) at which T_2' processes change with temperature.⁸⁴ It is interesting to note that the Δ measured for two of the higher energy sites is 18.7 cm^{-1} from the echo results.⁴⁹

With these data, we conclude that there is an effective intermediate state that dephases the impurity, although at the moment we cannot exclude all other channels discussed in Section 1. The intermediate is separated by $\sim 17 \text{ cm}^{-1}$ from the guest states. In terms of the two states involved in the optical transition of pentacene ($^1A_{1g}$ and $^1B_{2u}$), the 17 cm^{-1} state could be either a ground or excited phonon state. Neither the absorption spectra of our crystals nor the crystals of Aartsma et al.⁴⁹ have shown phonon side bands at this frequency.

Based on the fact that pentacene in p-terphenyl does not exhibit these resonance modes on the side band while tetracene does (at $\sim 7 \text{ cm}^{-1}$), Aartsma *et al.*⁴⁹ concluded that the guest and not the host is "helping" the formation of these resonance modes. To us the origin of these modes cannot be established with the few experiments available. Moreover, as pointed out by Small in several articles⁸¹ the origin of sidebands and dephasing is not necessarily coupled. If the mode is a resonant one, its absence in the side band of the terphenyl host doped with pentacene implies that it has the same frequency in the ground and excited state to within the inhomogeneous linewidth.

The values of T_2 obtained above at 1.8°K when compared with T_{1p} (24.9 nsec) indicate that $T_2 = 2T_{1p}$, to within 12%. The experimental errors are typically 4% and thus the difference may be due to self absorption (note that $\mu \sim 1$ Debye) and/or some intrinsic intersite effects. In very dilute crystals, T_{1p} reaches 23.5 nsec suggesting the decrease in radiation trapping that is expected when the crystal absorbs the light strongly. Note that reabsorption will influence T_1 while echo absorption will lead into a secondary echo⁸⁵ or T_1 spontaneous decay. It is perhaps worth mentioning that, as shown in Fig. 13, even when we excite 0_1 solely with the laser, 0_4 emission appears with a relative intensity of $\sim 3\%$. If 0_4 is acting as an intermediate dephasing level, it will contribute to the overall T_2 measurement.

The significance of Γ_p is now evident from Eqs. (56) and (57). It is a pre-exponential describing the difference in the scattering amplitudes of $|0\rangle$ and $|p\rangle$ due to the interactions with q and q' . It is

not clear to us why this should be called a lifetime of the phonon.⁴⁹ It is a lifetime if one is dealing with pure T_1 processes (kinetic approach) but for T_2 ' "scattering" events are the processes involved. More on this point will be published by Jones and Zewail elsewhere.

Finally, the value of T_2 obtained using the results in Fig. 21 at 4.2°K is consistent with the fact that at this temperature we still see IRD, and therefore the homogeneous width must be $\lesssim 60$ MHz, the maximum switched frequency of the laser. Thus, one can use these data to predict T_2 at higher temperatures. Of course, if the temperature is high enough to give say T_2 of 10 psec, then the width becomes 1.1 cm^{-1} and one might therefore measure it directly without elaborate picosecond methods.

G. Effect of inhomogeneous broadening

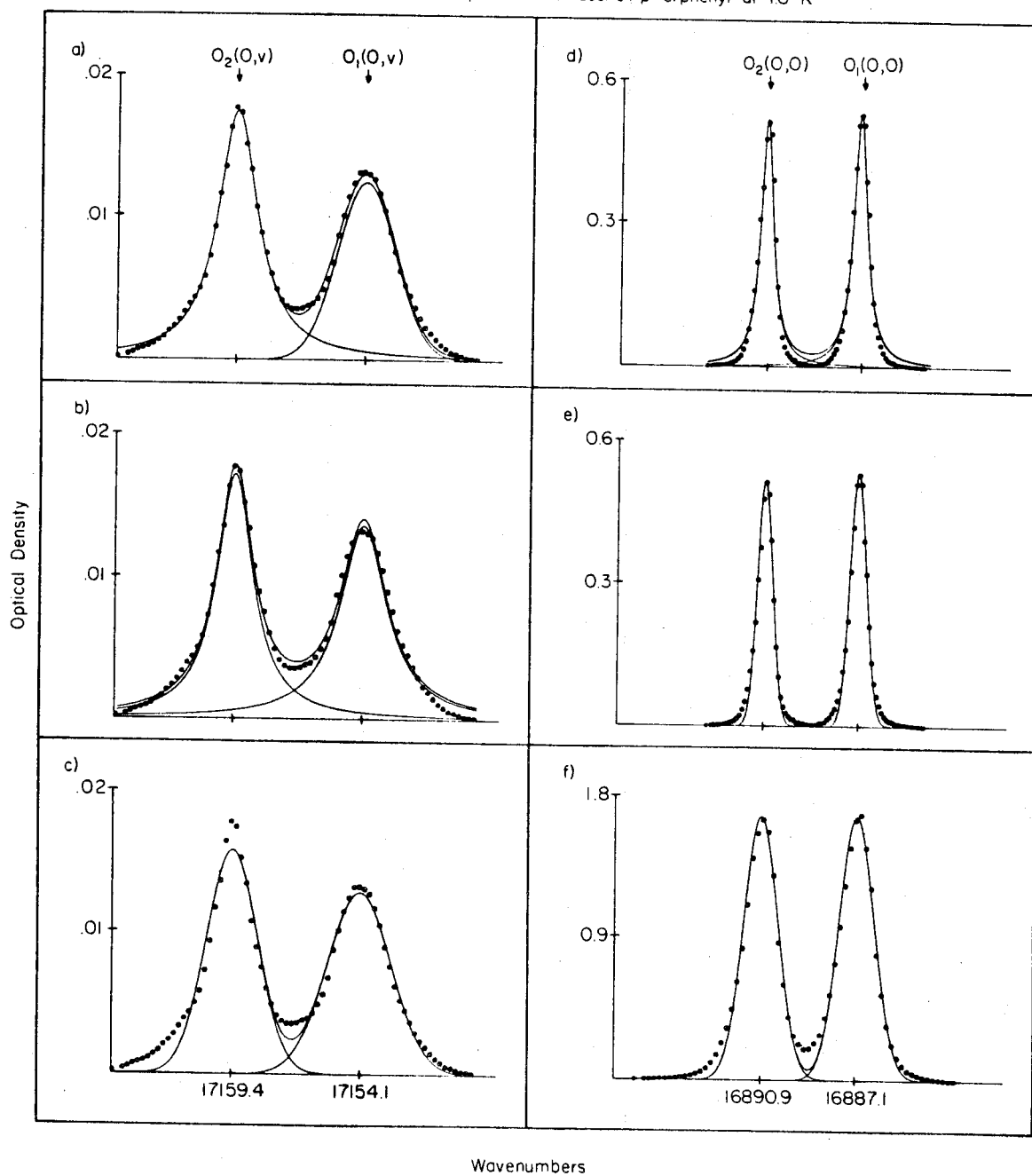
In describing the population flow in pentacene at long times, we have used the solution of ρ on resonance, and showed that the results agree with experiments quite well. In this section we discuss the effect of inhomogeneous broadening and justify the neglect of its averaging effects in the high-power limit.

Equation (41) is the on-resonance solution for $\rho_{pp}(t)$ obtained by solving the density matrix Eq. (39b) appropriate for the level structure of pentacene. To consider the effect of inhomogeneous line-shape averaging on the population dynamics, one must retain the off-resonance term of the pumping rate (i. e., $R_p = \frac{1}{2} \chi^2 \frac{\Gamma}{\Gamma^2 + \Delta^2}$), and average Eq. (41) over $g(\Delta)$. Since the only time dependence of R_p is from the known laser pulse characteristics (see pulse A of Fig. 1 in Appendix I

Figure 23

Absorption lineshapes for pentacene in p-terphenyl at 1.8°K. Experimental data (solid circles) and lineshape functions (solid lines) are shown for the vibronic lines (left) and origins (right) of sites 0_1 and 0_2 . Attempts are made to fit each line to either a Lorentzian (L) or Gaussian (G) by a least squares curve fitting computer program. The program plots the best fit for each line and also the sum. The results are (FWHM line-widths in cm^{-1} appear in parentheses): (a) $0_1 = \text{G}$ (2.82), $0_2 = \text{L}$ (1.99); (b) $0_1 = \text{L}$ (2.36), $0_2 = \text{L}$ (1.81); (c) $0_1 = \text{G}$ (3.12), $0_2 = \text{G}$ (2.48); (d) $0_1 = \text{L}$ (0.66), $0_2 = \text{L}$ (0.61); (e) $0_1 = \text{G}$ (0.79), $0_2 = \text{G}$ (0.74); (f) $0_1 = \text{G}$ (1.69), $0_2 = \text{G}$ (1.65). Spectra (a)-(e) were obtained with a low concentration ($\approx 1 \times 10^{-6}$ m/m) crystal and spectrum (f) was taken with a high concentration ($\approx 5 \times 10^{-6}$ m/m) crystal.

Absorption Lineshapes for Pentacene /p-terphenyl at 1.8°K



and Eq. (45)), Eq. (41) can be solved for $\rho_{pp}(t)$ as shown in Eq. (43) and then averaged over the lineshape. This averaging is, in general, important because it shows that the hole burned in the inhomogeneous line will saturate as R_p increases. Hence in a time resolved experiment where R_p changes indirectly the number of pumped molecules will change.

Equation (43) contains R_p and thus Δ in both the coefficients and arguments of the exponentials. Therefore, averaging of Eq. (43) in this form would have to be done numerically. However, in the high power case where R_p is greater than the relaxation rates, Eq. (43) may be simplified by a binominal expansion of the square root expression (for large R_p) in Eq. (44). This is valid in our experiments where (1) an overshoot in the emission intensity (a in Fig. 8) occurs at all laser powers used, indicating that $\rho_{pp}(t)$ is initially driven beyond its final equilibrium value, and (2) the observed decay time, τ_0 , is independent of laser power which only occurs in the high power case. The expansion shows that:

$$\lambda_+ \simeq -\left(\frac{2\Gamma_{l0} + \Gamma_{pl}}{2}\right) = -\tau_0^{-1} \quad (59a)$$

and

$$\lambda_- \simeq -2R_p \quad (59b)$$

The final form of Eq. (43) then becomes:

$$\rho_{pp}(t) \approx \frac{1}{2} \left[\left\{ \frac{\Gamma_{p\ell}}{2\Gamma_{\ell 0} + \Gamma_{p\ell}} \right\} e^{-t/\tau_0} - e^{-2R_p t} \right] + \frac{\Gamma_{\ell 0}}{2\Gamma_{\ell 0} + \Gamma_{p\ell}} \quad (60)$$

Thus, in the high power case only the build-up rate for $\rho_{pp}(t)$ needs to be averaged, a great simplification over the numerical integration which does not provide physical insight into the problem. The observed decay time τ_0 is completely determined by the magnitude of the rate constants $\Gamma_{\ell 0}$ and $\Gamma_{p\ell}$, and will not be affected by averaging over the inhomogeneous lineshape. At this point we should evaluate the fraction of the total inhomogeneous line pumped in the high power case and determine if Eq. (60) is valid. This can be done by calculating the magnitude of the off-resonance parameter Δ required to reduce R_p from the pumping rate obtained in nutation experiments (at the same power) to an effective value where the binomial expansion of the square root expression [Eq. (44)] is invalid (i.e., $R_p \approx \Gamma_{p0}$). This calculation reveals that Eq. (60) is valid for the entire power broadened linewidth ($\delta\omega_{PB}$) since $R_p > \Gamma_{p0}$ for $\Delta \leq \pm 120$ MHz. Therefore, we can average $e^{-2R_p t}$ in Eq. (60) over $\delta\omega_{PB}$ or $\delta\omega_I$ (the molecules pumped by the laser only span $\delta\omega_{PB}$) to obtain an effective pumping rate:

$$\begin{aligned} \left\langle e^{-2R_p t} \right\rangle &= \left\langle e^{\frac{-\chi^2 \Gamma t}{\Gamma^2 + \Delta^2} - \frac{\Delta^2}{\delta\omega_{PB}^2}} \right\rangle \approx \left\langle e^{\frac{-\chi^2 \Gamma t}{\Delta^2} - \frac{\Delta^2}{\delta\omega_{PB}^2}} \right\rangle \\ &= e^{-2R_{p\text{eff}} t} \end{aligned} \quad (61)$$

where

$$R_{p\text{eff}} = \frac{\chi}{\delta\omega_{PB}} \sqrt{\frac{\Gamma}{t}} .$$

This approximate solution (see Appendix II) shows that averaging the expression for the build-up rate essentially dilutes R_p by the power-broadened linewidth. Using the results of Eq. (61) and Eq. (45) which describes the exponential turn-on of the laser pulse, we obtain an expression that agrees quite well with the observed emission intensity build-up rate.

Two important conclusions can be drawn from the above discussion. First, in the high power case, inhomogeneous lineshape averaging of $\rho_{pp}(t)$ has essentially no effect on the observed transient decay time and, second, averaging of the build-up expression dilutes the pumping rate by the power-broadened linewidth, effectively. The effect of laser power on the observed transient patterns is now perhaps physically understood.

It is also clear now that by using Eqs. (60) and (61) from the high power limit and by knowing γ and τ_0 experimentally, one is able to determine unambiguously $\Gamma_{p\ell}$ and $\Gamma_{\ell 0}$, within the framework of the above approximations and especially if they are very different. This leads to the following useful formula relating γ to τ_0 :

$$\tau_0^{-1} = \frac{1}{2} \Gamma_{p\ell} (1 + \gamma^{-1}) \quad (62)$$

Thus in the high power limit, one obtains $\Gamma_{p\ell}$. We shall use these results in the coming section to help us identify the nature of $|\ell\rangle$.

H. On the structure of $\{|\ell\rangle\}$

The structure of the $\{|\ell\rangle\}$ manifold will be ascertained from more than ten independent experiments. Several of these were reported

in I and have been repeated again in this work. The following summarizes all that we have observed:

- (a) The observation of a 15 μ sec decay when the emission was monitored at right-angles to the exciting laser beam and the EO method was used with long time pulses (50-100 μ sec).
- (b) A Zeeman effect was observed on both the d.c. and the decay (see Table III).
- (c) As the temperature increases the peak of the IRD decreases.
- (d) T_2 (44 nsec) is much smaller than the 15 μ sec decay time.
- (e) The decay signal (15 μ sec) is absent when the molecule is excited above its electronic origin.
- (f) The decay time does not change with changes in the laser power (\sim 1 mwatt - 50 mwatts), but the build-up rate does.
- (g) The decay is exponential and changes as we scan the narrow-band laser within the inhomogeneous 0_1 origin.
- (h) The signal gets stronger as we increase the switching frequency, i. e., getting further away from the homogeneous width.
- (i) Exciting with a long time single pulse (LADS and not the EO) the 15 μ sec decay is only observed during the light-on cycle.
- (j) Although the inhomogeneous broadening of all sites are comparable in width (0.7 - 3 cm^{-1} depending on the concentration) T_1 and T_2 of the sites are different.
- (k) Exciting with a single mode laser, a multi-mode laser or an incoherent source gives the same T_{1p} decay time for the 0_1 origin. The lifetimes of 0_1 and 0_2 are the same at 1.8 and 4.2°K.

- (l) Exciting into the 267 cm^{-1} mode of 0_1 , neither LADS transients nor EO transients have been observed. However, the falling edge of a LADS signal still gives the same value for T_{1p} .
- (m) Exciting with the single mode into the $0, 0$ of 0_1 and monitoring the light into the $0, 0$ (scattering and emission) or into higher vibrational ground states (emission) gives identical decay times but different transient patterns (Figs. 20 and 22).

Observations (a) to (h) lead us to conclude that the narrow band excitation prepares molecular eigenstates that have much longer lifetimes, consistent with the prediction of Eq. (1). However, if this were true then (i) should show the $15\text{ }\mu\text{sec}$ decay on the falling edge of the LADS pulse. Following the observation (i) we concluded that it is possible that we have prepared a primary singlet state that decays into states that do not contain much of the singlet oscillator strength or that we just simply prepared $|p\rangle$.⁵¹ From all the observations, (i) \rightarrow (m) and also (a) \rightarrow (h), we conclude the following. The state $|p\rangle$ is excited very rapidly since χ (the pumping rate) is very large. Then during a short time light pulse coherence effects between $|0\rangle$ and $|p\rangle$ are manifested. During a long time pulse, however, the excitation (7 MHz width) is statistically going into $|\ell\rangle$, which as shown later is consistent with being a triplet manifold. The key parameter here is the decay time on the falling edge of a LADS pulse which gives a T_1 decay time that is identical to T_1 obtained from the broad band and incoherent excitations.

The interesting question now is what is the relationship between the structure of $|\ell\rangle$ and the long decay transient observed during the long-time pulse? Several possibilities exist, but we shall rule out all (that we can think of) but one.

The first possibility is that there is a slow intersystem crossing (ISC) from $|p\rangle$ to resonant or near-resonant ℓ states (built on the origin of the T_1 state) followed by fast vibrational relaxation (as in the singlet manifold) and then decay from the triplet origin to $|0\rangle$. The second possibility is a fast decay from $|p\rangle$ into resonant ℓ states (either hot vibrational levels of T_1 or a new state like T_2) followed by slow vibrational relaxation or electronic relaxation, to the bottom of T_1 , and then decay from T_1 to $|0\rangle$ by radiative and nonradiative channels. A third possibility is a fast decay from $|p\rangle$ into ℓ , a fast decay from resonant ℓ to T_1 and a slow decay from T_1 to the ground state.

Several points support the slow depletion out of $|p\rangle$. First, although it will not be surprising to us if vibrational relaxation is slow at 1.8 K for certain modes⁸⁶ in large molecules, it will be difficult to accept that vibrational relaxation is fast in the singlet and slow in triplet manifolds. Furthermore, as shown by Lim and his co-workers,⁸⁷ and by others, the internal conversion rate between triplets ($T^* \rightarrow T$) in anthracenes is typically $2 \times 10^{10} \text{ sec}^{-1}$ while the radiative rate for $T_2 \rightarrow T_1$ is typically $2 \times 10^5 \text{ sec}^{-1}$. The energy gap between T_2 and T_1 in anthracene is $\sim 11,200 \text{ cm}^{-1}$. In general, as the gap gets smaller, there seem to be a trend in large molecules in that the rate of internal conversion increases (energy gap low) except at very low energy gaps ($< 2000 \text{ cm}^{-1}$) where it decreases again.⁸⁸ As in anthracenes, we do not know how many triplets are involved in the ISC. What can be inferred from the experiments, however, is that ISC in pentacene is slow and not $\sim 10^8 \text{ sec}^{-1}$ as in other aromatic hydrocarbons, in which

a determination has been made, with the exception of pyrene (ISC rate constant = $3 \times 10^4 \text{ sec}^{-1}$). This point can be shown using Eq. (62).

Since we know γ and τ_0 experimentally for pentacene, Eq. (62) in the high power limit dictates that Γ_{pl} be at hand. In fact, if the overshoot is very large, $\gamma^{-1} \rightarrow 0$, then $\Gamma_{pl} = 2/\tau_0$. For measured values of $\tau_0 = 19.6 \text{ } \mu\text{sec}$ and $\gamma = 0.9$ in an EO experiment, the best fit from the steady-state coherence equations gives $\Gamma_{pl}^{-1} = 20.4 \text{ } \mu\text{sec}$ and Γ_{l0}^{-1} (ISC from $T_1 \rightarrow S_0$) = $37.6 \text{ } \mu\text{sec}$. Using Eq. (62), we obtain for the same values of γ and τ_0 , $\Gamma_{pl}^{-1} = 20.7 \text{ } \mu\text{sec}$. Similarly, from a LADS experiment: for $\tau_0 = 14.7 \text{ } \mu\text{sec}$ and $\gamma = 0.82$, $\Gamma_{pl}^{-1} = 16.3 \text{ } \mu\text{sec}$ and $\Gamma_{l0}^{-1} = 26.6 \text{ } \mu\text{sec}$ from the steady-state coherence equations, and $\Gamma_{pl}^{-1} = 16.4 \text{ } \mu\text{sec}$ from Eq. (62), thus ensuring the self-consistency of the high power approximation. [Note that as mentioned in the text, if LADS and the EO experiments were done under identical conditions, then τ_0 is exactly the same.⁸⁹] The important conclusion is therefore that experimentally we can determine the rate of ISC especially if Γ_{pl} and Γ_{l0} are much different. This is certainly true for the higher energy sites of pentacene in p-terphenyl at 1.8 K. Site 0₃ gives a very large overshoot $\gamma = 1.5$, and $\tau_0 \simeq 6 \text{ } \mu\text{sec}$.⁹⁰ If in pentacene the ISC rate was 10^8 sec^{-1} , as in many other aromatics, the overshoot would be enormous and the decay during the pulse would be relatively very fast.

The interesting question is: What is the driving force for ISC? For direct S_1 to T_1 coupling (i.e., no other triplets involved), the ISC of S_1 and T_1 will be comparable to that of $T_1 \rightarrow S_0$ if we assume that the electronic matrix element for the coupling and the density of states

weighted Franck-Condon factors are similar, considering a Golden Rule type expression for the rates. The lifetime of the T_1 state is 33 μsec in the vapor and 70 μsec in solution and 38 μsec from our mixed crystal work (using the theoretical fit). The energy of T_1 is approximately half-way between $S_0(|0\rangle)$ and $S_1(|p\rangle)$, see Table II. Since the energy gap between T_1 and S_1 exceeds the 4000 cm^{-1} range, C-H stretching modes are presumably the dominant accepting vibrations and the Franck-Condon weighted density of states should not be very dependent on which states are participating. Using the results of the energy gap law for ISC, one predicts an ISC rate on the order of 10^4 sec^{-1} for an energy gap of $\sim 8000\text{ cm}^{-1}$ between the excited singlet and T_1 of pentacene. Thus, on these grounds, we may conclude that Γ_{pl} and Γ_{l0} are comparable. From our results on the 0_1 site this is true, suggesting that the driving force is a direct ISC.

On the other hand, if T_2 is slightly below $|p\rangle$ in energy, then the driving force will be different. Internal conversion between T_2 and T_1 will be fast ($10^{10} - 10^4\text{ sec}^{-1}$) and this helps the irreversibility of the crossing. According to Gillispie and Lim,⁸⁷ the ISC rate is related to $\Gamma_{T_2T_1}$ ($T_2 \rightarrow T_1$ rate of internal conversion) by the square of the ratio of the spin-orbit coupling matrix element to the energy difference between $|p\rangle$ and T_2 . Thus for a rate of 10^5 sec^{-1} and $\Gamma_{T_2T_1} \simeq 10^{11}\text{ sec}^{-1}$, the T_2 state should be below $|p\rangle$ by $\simeq 1000\text{ cm}^{-1}$, knowing that the spin-orbital coupling matrix element is typically 1 cm^{-1} in these aromatics. This is the same reason which makes Lim⁸⁷ believe that in pyrene there is no reason to assume that T_2 and T_3 must be above S_1 in order to explain the low rate of ISC. Whatever the driving force is, it is clear from our

data that the rate of depleting $|p\rangle$ into T must be determined by the observed slow⁹¹ light-on transient.

The above conclusions about the nature of $\{|l\rangle\}$ are supported by the different experiments performed. The Zeeman effect results in (average) shifting of the levels, and thus influences Γ_{pl} . The fact that τ_0 is temperature independent in the range 1.8-4.2°K is also consistent, since a nearby triplet state (essentially in resonance) must be around in order to see temperature-enhanced ISC by $\sim 3 \text{ cm}^{-1}$ phonon energies. The peak of the IRD decreases because the homogeneous width is increasing. The decrease in τ_0 on going to site 0_3 suggests that the T_2 state is becoming more involved. Since the energy gap between $|p\rangle$ and T_1 is very large, sensitivity of ISC to a site energy shift of 120 cm^{-1} is not expected. On the other hand, if T_2 is very close (1000 cm^{-1} or so) then such energy changes will influence the ISC rate. For the same value of $\Gamma_{T_2T_1}$, if τ_0 becomes shorter by a factor of 3 (0_1 vs. 0_3 sites), then T_2 shifts to only 580 cm^{-1} below $|p\rangle$. It is interesting to note that these sites, 0_3 and 0_4 , have lifetimes very close to the gas phase value (see Table II) and are much different from the lifetime of 0_1 and 0_2 sites. This would be consistent with the "near" resonance role played by higher triplet states. Finally, all other observations are consistent including the fast vibrational relaxation in the solid which explains the absence of transients when the single mode of the laser was on resonance with the 267 cm^{-1} vibronic origin. The homogeneous width of this transition is larger than the 0,0 linewidth (i.e., the effective pumping rate is much less) and vibrational relaxation is fast enough to deplete population into $|p\rangle$.

VI. SUMMARY AND CONCLUSIONS

In this paper we have attempted to address the question of what happens to large molecules, specifically pentacene, excited by narrow- and wide-band lasers focusing on the radiationless decay (optical T_1) and the phase relaxations (optical T_2') processes that the molecule undergoes. The following summary highlights some of the important points and observations.

1. Optical T_2 has been measured using nutation and free induction decay techniques. For pentacene in a p-terphenyl host at 1.8 K, T_2 (44 nsec) $\approx 2T_1$ (23.5 nsec), suggesting that spontaneous emission to the ground state is causing the dephasing of the "two-level" system. Optical T_2 , which has contributions from T_1 and T_2' processes, changes as a function of temperature while T_1 does not. This was explained by the possible presence of quasi-localized or resonance modes, which have large amplitude at the guest impurity and are $\sim 17 \text{ cm}^{-1}$ away from the origin. We also did not rule out other possibilities (like T_2') ignored before.
2. Optical T_1 is caused by radiative and nonradiative decay to the ground state while T_2' is caused by the difference in the scattering amplitudes between the ground and excited states [see Eq. (52)]. This matrix element difference, together with the phonon occupation number and density of states provide the temperature dependence and details the origin of pure dephasing processes. In obtaining expressions for these dephasing rates we have shown that the origin of dephasing can be explained without requiring specific modes in

the crystal and that exchange between transitions will provide similar temperature dependences. We also present explicit expressions for cross sections of T_2' and T_1 processes.

3. Experimentally, we have learned several things in doing these transients to obtain T_1 and T_2 . First, when the crystal absorbs too much light (e.g., singlet states) one has to be careful about radiation trapping that makes T_1 appear longer. Coherent emission, on the other hand, when reabsorbed does not seem to influence the T_2 measurement if one is confined to the limit of optically thin samples that obey Beer-Lambert's law. Second, it is very important to identify the effect of crystal inhomogeneous broadening and laser spatial transverse profile on the observed transients especially in the nutation experiments. Third, crystals with good optical quality are essential for observing the coherent transients in the forward direction of the laser. Finally, the laser pulse repetition rate could influence the observed decay characteristics for all the transients if it was high enough such that population in the $\{|l\rangle\}$ manifold had not returned completely to the ground state. To insure that each laser pulse found the system at equilibrium, the repetition rate was kept at ≤ 10 KHz in our experiments where no effects on the transient decay was observed.
4. The pentacene level structure was handled theoretically by dividing the problem into two time regimes: the coherent transient regime, where the time of observation is comparable to T_2 and the Rabi time, and the steady state coherence regime where the time of observation is much longer than T_2 . In the latter regime we used the Wilcox-

Lamb theory which enables one to use density matrix equations rather than a purely kinetic approach (averaging over inhomogeneous broadenings, etc., is added phenomenologically). In this manner $\{|\ell\rangle\}$ was included in the equation of motion directly. For the transient coherence regime, where the off-diagonal elements of the density matrix have not decayed, the transients were handled using the two-level system approach available in the literature and modified to suit the pentacene level structure.

5. Because of $|\ell\rangle$, coherent transients of large molecules show unique and additional features (that do not exist in the two-level small molecule limit) which depend on whether the transient is observed following long time preparation or using short pulses. Since optical free induction decay transients occur when the laser is switched off-resonance, one is monitoring the decay of the off-diagonal density matrix elements from some initial value (usually steady-state, i.e., $\rho_{0p}^{(\infty)}$). This can be done using Eq. (39) setting the time derivatives equal to zero. The result simply involves replacing T_{1p0} in Eqs. (34)-(36) by $(2\Gamma_{\ell 0} + \Gamma_{p\ell})/\{\Gamma_{\ell 0}(\Gamma_{p0} + \Gamma_{p\ell})\}$. Thus, inclusion of the $\{|\ell\rangle\}$ manifold in the OFID expression does not affect the transient decay at low powers. It does, however, increase the influence of the power broadening term upon the observed decay at high power, and alters the calculation of μ .
6. Optical T_2 , in general, does not necessarily equal $2T_1$, and thus measurement of T_1 from line shape analysis could be dangerous. From Fig. 23, where we fit the observed high-resolution spectra

(of low absorbance crystals) into Lorentzians or Gaussians, it is clear that one has to be careful about obtaining dephasing times from the analysis. A Gaussian fit, which is "usually" indicative of inhomogeneous broadening, could not be obtained for the 0, 0 transitions of 0_1 and 0_2 . This is perhaps due to self-absorption and/or the incomplete randomness of impurity distribution in the host. We note that these lines must be inhomogeneously broadened since we know T_2 exactly. For the vibronic bands, the best fits we obtained ($OD \sim 0.015$) are a Lorentzian for 0_2 and a Gaussian for 0_1 . Taking a Lorentzian lineshape as a criterion for homogeneous broadening we calculate a dephasing time of 5.4 psec. If vibrational relaxation is the dominant dephasing channel at these low temperatures (i.e., $T_{2V} = 2T_{1V}$), then the vibrational relaxation time is 2.7 psec,⁹² and the ratio of the homogeneous width of the 0, 0 to 0, v (267 cm^{-1}) is $\sim 10^{-4}$.

7. As far as the theoretical treatment goes, the detailed structure of the $\{|l\rangle\}$ manifold does not enter into the picture directly, unless we are interested in the details of intramolecular relaxations (internal conversion and intersystem crossing). We share the view of Lim et al.⁸⁷ that higher triplets could be involved in these aromatics and we present some observations that are consistent with these ideas. The experiments show that the rate of intersystem crossing in pentacene is slow even though the crossing to the bottom of T_1 may proceed by fast vibrational relaxation or fast electronic ($T' \rightarrow T_1$) internal conversion.

8. The yield for ISC based on the above results is about 2×10^{-3} , i.e., two molecules for every 1000 $|p\rangle$ molecules make it to the triplet state. Note that this number might confuse the reader because we mentioned before that γ could be as large as 1.5 (e.g., for site 3). In other words, a very large fraction of the molecules is in the triplet. This is true because the pulse has been on for a long time, and thus molecules are constantly fed into the triplet. By triplet, of course, we mean the vibronic states with the spin substates X, Y, and Z. The reason we ignored being explicit with these spin states is because they do not add any new feature into our treatment since we assume that the total population in $|p\rangle$, $|0\rangle$, and $|\ell\rangle$ is always constant. Our ρ does not in a direct way care about the fine structure of ℓ and takes the following form:

$$\rho = \begin{pmatrix} \rho_{00} & \rho_{0p} & & & \\ \rho_{p0} & \rho_{pp} & & & \\ \hline & & \rho_{\ell_1\ell_1} & & \\ & & & \rho_{\ell_2\ell_2} & \\ & & & & \rho_{\ell_x\ell_x} \end{pmatrix}$$

and

$$\text{Tr}\rho = 1$$

9. In the pentacene system (extinction coefficient $\sim 10^4$), the on- and off-resonance scattering experiments reveal a long transient decay and also the importance of self-absorption which is responsible for

the inverted transient pattern in Figs. 20 and 22. These on- and off-resonance scattering experiments are useful in that they are sensitive in part to ground state population. Excellent fit between theory and experiments in pentacene was found.

10. Finally, narrow-band excitation of molecules with narrow-band CW lasers demands knowledge of the exact pulse (EO and LADS) shape and width in order to determine the effective bandwidth and the coherence properties of the source. For the pentacene studies we can vary this effective width from essentially the residual width of CW source to values exceeding the homogeneous line width of the transition (7.1 MHz), as shown in Fig. 1 of Appendix I.

ACKNOWLEDGMENTS

This work was supported by a grant from the National Science Foundation. We would like to acknowledge the contribution of and discussion with several people during the course of this work. W. Lambert has helped us in obtaining the results on the lineshape analysis and some of the LADS experiments. K. Jones has contributed to section F and discussions with him throughout the work were productive. A. Nichols has provided us with the solution of the integral in Appendix II. Finally, we would like to thank Dr. N. J. Bridge and Drs. A. Lami and P. Grigolini for communicating unpublished results and Professor J. Jortner for stimulating discussions.

References and Footnotes

- ¹G. B. Kistiakowsky and C. S. Parmenter, J. Chem. Phys. 42, 2942 (1965); E. M. Anderson and G. B. Kistiakowsky, J. Chem. Phys. 48, 4787 (1968); C. S. Parmenter and A. H. White, J. Chem. Phys. 50, 1631 (1969).
- ²A. E. Douglas, J. Chem. Phys. 45, 1007 (1967).
- ³For reviews on the subject see: G. W. Robinson in: Excited States, edited by E. C. Lim (Academic Press, New York, 1974), Vol. I, p. 1; S. A. Rice in: Excited States, edited by E. C. Lim (Academic Press, (1975), Vol. 2, p. 111; J. Jortner and S. Mukamel in: The World of Quantum Chemistry, edited by R. Daudel and B. Pullman (Reidel, Boston, 1974); K. F. Freed, Topics Appl. Phys. 15, 23 (1976).
- ⁴G. W. Robinson and R. P. Frosch, J. Chem. Phys. 37, 1962 (1962); ibid. 38, 1187 (1963).
- ⁵M. Bixon and J. Jortner, J. Chem. Phys. 50, 3284 (1969); ibid. 50, 4061 (1969).
- ⁶U. Fano, Phys. Rev. 124, 1866 (1961).
- ⁷K. F. Freed, J. Chem. Phys. 52, 1345 (1970).
- ⁸W. Rhodes, J. Chem. Phys. 50, 2885 (1969); W. Rhodes, R. B. Henry, and M. Kasha, Proc. Natl. Acad. Sci. USA, 63, 31 (1969); W. Rhodes, Chem. Phys. Lett. 11, 179 (1971); W. Rhodes, Chem. Phys. 4, 259 (1974); ibid. 22, 95 (1977).
- ⁹C. A. Langhoff and G. W. Robinson, Mol. Phys. 26, 249 (1973); ibid. 29, 613 (1975); C. A. Langhoff, Chem. Phys. 20, 357 (1977).

- ¹⁰W. Weisskopf and E. Wigner, *Z. Physik*, 63, 54 (1930).
- ¹¹A. H. Zewail, T. E. Orlowski, and K. E. Jones, *Proc. Natl. Acad. Sci. USA* 74, 1310 (1977); see also reference 12.
- ¹²A. H. Zewail, T. E. Orlowski, and D. R. Dawson, *Bull. Am. Phys. Soc.* 21, 1283 (1976); A. H. Zewail, *Proceedings of SPIE*, 82, 26 (1976); A. H. Zewail, D. E. Godar, K. E. Jones, T. E. Orlowski, R. R. Shah, and A. Nichols in: Advances in Laser Spectroscopy I, edited by A. H. Zewail (SPIE Publishing Co., 1977) Vol. 113, p. 42.
- ¹³M. Kasha, *Chem. Rev.* 41, 401 (1947); H. B. Klevens and J. R. Platt, *J. Chem. Phys.* 17, 470 (1949); R. Pariser, *J. Chem. Phys.* 24, 250 (1956); D. R. Kearns, *J. Chem. Phys.* 36, 1608 (1962); T. E. Peacock and P. T. Wilkinson, *Proc. Phys. Soc.* 83, 525 (1964); G. G. Hall, *Proc. Roy. Soc. A*, 213, 113 (1952).
- ¹⁴N. A. Kurnit, I. D. Abella, and S. R. Hartmann, *Phys. Rev. Lett.* 13, 567 (1964); G. B. Hocker and C. L. Tang, *Phys. Rev. Lett.* 21, 591 (1968); N. Takeuchi and A. Szabo, *Phys. Lett.* 50A, 361 (1974); R. G. Brewer and R. L. Shoemaker, *Phys. Rev. A* 6, 2001 (1972); R. G. Brewer and A. Genack, *Phys. Rev. Lett.* 36, 959 (1976).
- ¹⁵A. H. Zewail, T. E. Orlowski, and D. R. Dawson, *Chem. Phys. Lett.* 44, 379 (1976); A. H. Zewail, T. E. Orlowski, K. E. Jones, and D. E. Godar, *Chem. Phys. Lett.* 48, 256 (1977); A. H. Zewail, D. E. Godar, K. E. Jones, T. E. Orlowski, R. R. Shah, and A. Nichols in: Advances in Laser Spectroscopy I, edited by A. H. Zewail (SPIE Publishing Co., 1977) Vol. 113, p. 42.

- ¹⁶G. B. Hocker and C. L. Tang, Phys. Rev. 184, 356 (1969); R. G. Brewer and R. L. Shoemaker, Phys. Rev. Lett. 27, 631 (1971); C. L. Tang and B. D. Silverman, Physics of Quantum Electronics, edited by Kelley, Lax, and Tannenwald (McGraw-Hill, New York, 1966).
- ¹⁷R. G. Brewer and R. L. Shoemaker, Phys. Rev. A 6, 2001 (1972); F. A. Hopf, R. F. Shea, and M. O. Scully, Phys. Rev. A 7, 2105 (1973).
- ¹⁸T. E. Orlowski, K. E. Jones, and A. H. Zewail, Chem. Phys. Lett. 54, 197 (1978).
- ¹⁹W. R. Harshbarger and M. B. Robin, Acc. of Chem. Res. 6(2) 329 (1973).
- ²⁰A. Yariv, Proc. IEEE, 52, 719 (1964).
- ²¹J. E. Kiefer, T. A. Nussmeier, and F. E. Goodwin, IEEE J. Quantum Electron. QE-8, 173 (1972).
- ²²J. L. Hall, Atomic Physics 3, edited by S. J. Smith, G. K. Walters, and L. H. Volsky (Plenum, New York, 1973), p. 615.
- ²³R. L. Shoemaker and E. W. Van Stryland, J. Chem. Phys. 64, 1733 (1976). (See also p. 1739 of this reference, and reference 93).
- ²⁴R. G. Brewer and A. Genack, Phys. Rev. Lett. 36, 959 (1976).
- ²⁵A. H. Zewail and T. E. Orlowski, Chem. Phys. Lett. 45, 399 (1977); A. H. Zewail, D. E. Godar, K. E. Jones, T. E. Orlowski, R. R. Shah, and A. Nichols in: Advances in Laser Spectroscopy I, edited by A. H. Zewail (SPIE Publishing Co., 1977) Vol. 113, p. 42.
- ²⁶A. Genack, R. M. Mcfarlane, and R. G. Brewer, Phys. Rev. Lett. 37, 1078 (1976).

- ²⁷A. H. Zewail, T. E. Orlowski, R. R. Shah, and K. E. Jones, Chem. Phys. Lett. 49, 520 (1977).
- ²⁸R. Adler, IEEE Spectrum 4, 42 (1967).
- ²⁹G. Beck, Rev. Sci. Instrum. 47, 537 (1976).
- ³⁰S. W. Provencher, J. Chem. Phys. 64, 2772 (1976).
- ³¹D. W. Marquardt, J. Soc. Industrial Appl. Math. 11, 431 (1963).
- ³²P. C. Haarhof, Mol. Phys. 7, 101 (1962).
- ³³K. F. Freed, Topics Current Chem. 31, 105 (1972); W. M. Gelbart, D. F. Heller, and M. L. Elert, Chem. Phys. 7, 116 (1975); J. M. Delory and C. Tric, Chem. Phys. 3, 54 (1974).
- ³⁴This kind of coherence in the excited state should not be confused with the coherence created between the excited state relative to the ground state by the laser field.
- ³⁵See, e.g., M. Sargent, M. O. Scully, and W. E. Lamb, Jr., Laser Physics (Addison-Wesley Publishing Co., 1974); L. Allen and J. H. Eberly, Optical Resonance and Two-Level Atoms (Wiley-Interscience, 1975).
- ³⁶P. Grigolini and A. Lami, Chem. Phys. Lett. 55, 152 (1978); ibid. Chem. Phys. 30, 61 (1978).
- ³⁷R. P. Feynman, F. Vernon, and R. W. Hellworth, J. Appl. Phys. 28, 49 (1957).
- ³⁸It is important to note that in the NMR language one speaks of T_1 only when both levels are decaying by the same rate. In general, if the two levels have different rates, then the system appears statistically open and one must consider the time evolution of the total population

as well as the other usual terms ($\rho_{pp}-\rho_{00}$, ρ_{0p} and ρ_{p0}). Under these circumstances one may group the decay rate terms that belong to the ($\rho_{pp}-\rho_{00}$) expression and, perhaps, define these terms as the T_1^{-1} rate constant (see Eq. (11)), keeping in mind that the definition of T_1 in the usual Bloch equations demands that the excited and ground state T_1 's are approximately the same. Finally, one can see that the level structure we are considering for pentacene (described by Eq. (10)) represents a system where the ground state is not decaying and the population dynamics in the two levels is determined only through T_{1p0} . Note that from (10), $\dot{\rho}_{00} + \dot{\rho}_{pp} = 0$ at all times, when $\chi = 0$.

- ³⁹A. Schenzle and R. G. Brewer, Phys. Rev. A 14, 1756 (1976).
- ⁴⁰T. E. Orlowski, K. E. Jones, and A. H. Zewail, Chem. Phys. Lett. 50, 45 (1977).
- ⁴¹K. E. Jones, A. H. Nichols, and A. H. Zewail, J. Chem. Phys. accepted for publication.
- ⁴²L. R. Wilcox and W. E. Lamb, Jr., Phys. Rev. 119, 1915 (1960);
W. E. Lamb, Jr. and T. M. Sanders, Jr., Phys. Rev. 119, 1901 (1960).
- ⁴³J. R. Ackerhalt and B. W. Shore, Phys. Rev. A, 16, 277 (1977);
J. R. Ackerhalt and J. H. Eberly, Phys. Rev. A. 14, 1705 (1976);
B. L. Beers and L. Armstrong, Jr., Phys. Rev. A. 12, 2447 (1975).
- ⁴⁴A. P. Marchetti, W. C. McColgin, and J. H. Eberly, Phys. Rev. Lett. 35, 387 (1975).
- ⁴⁵N. J. Bridge, private communication.

- ⁴⁶J. H. Meyling and D. A. Wiersma, Chem. Phys. Lett. 20, 383 (1973).
- ⁴⁷G. J. Small, J. Chem. Phys. 52, 656 (1970).
- ⁴⁸R. M. Hochstrasser and P. N. Prasad, J. Chem. Phys. 56, 2814 (1972).
- ⁴⁹T. J. Aartsma, J. Morsink, and D. A. Wiersma, Chem. Phys. Lett. 47, 425 (1977); ibid. 42, 520 (1976).
- ⁵⁰N. J. Kruse and G. J. Small, J. Chem. Phys. 56, 2985 (1972).
- ⁵¹See reference 25 (Advances in Laser Spectroscopy I), and reference 18.
- ⁵²D. A. Wiersma, in The Proceeding of the Eighth Molecular Crystal Symposium, Santa Barbara, California (1977).
- ⁵³R. M. Hochstrasser and T. Lin, J. Chem. Phys. 49, 4929 (1968).
- ⁵⁴P. W. Atkins and P. R. Stannard, Chem. Phys. Lett. 47, 113 (1977).
- ⁵⁵M. A. El-Sayed, MTP International Reviews of Science Spectroscopy, edited by A. D. Buckingham and D. A. Ramsey (Butterworths, London, 1972), p. 119.
- ⁵⁶K. F. Freed, J. Chem. Phys. 64, 1604 (1976).
- ⁵⁷R. H. Clarke and H. A. Frank, J. Chem. Phys. 65, 39 (1976); R. H. Clarke and J. M. Hayes, Chem. Phys. Lett. 27, 556 (1974).
- ⁵⁸T. Azumi, C. M. O'Donnell, and S. P. McGlynn, J. Chem. Phys. 45, 2735 (1966).
- ⁵⁹R. H. Clarke, R. E. Connors, and J. Keegan, J. Chem. Phys. 66, 358 (1977).
- ⁶⁰M. A. El-Sayed and R. Leyerle, J. Chem. Phys. 62, 1579 (1975).
- ⁶¹P. F. Williams, D. L. Rousseau, and S. H. Dworketsky, Phys. Rev. Lett. 32, 196 (1974).

- ⁶²J. M. Friedman and R. M. Hochstrasser, Chem. Phys. 6, 155 (1974); J. O. Berg, C. A. Langhoff, and G. W. Robinson, Chem. Phys. Lett. 29, 305 (1974); S. Mukamel and J. Jortner, J. Chem. Phys. 62, 3609 (1975); S. Mukamel, A. Ben-Reuven, and J. Jortner, Phys. Rev. A12, 947 (1975); R. M. Hochstrasser and F. Novak, Chem. Phys. Lett. 48, 1 (1977); J. Carlsten and M. G. Raymer in: Laser Spectroscopy, edited by J. Hall and J. Carlsten (Springer Series in Optic Sciences, Springer-Verlag, N.Y., 1977), Vol 7.; F. Novak, J. Friedman, and R. M. Hochstrasser in: Laser and Coherence Spectroscopy, edited by J. Steinfeld (Plenum, N.Y., 1978).
- ⁶³A. H. Zewail in: Laser Spectroscopy, edited by J. Hall and J. Carlsten (Springer-Verlag, N.Y., 1977) Vol. 7, p. 268.
- ⁶⁴The background scattered light off-resonance is almost a factor of two larger (at the end of the laser pulse) than the corresponding level on resonance. This is not shown in Fig. 20 where data have been normalized by keeping the photomultiplier current the same.
- ⁶⁵D. J. Diestler, Mol. Phys. 32, 1091 (1976).
- ⁶⁶S. F. Fischer and A. Laubereau, Chem. Phys. Lett. 35, 6 (1975).
- ⁶⁷D. Oxtoby and S. A. Rice, Chem. Phys. Lett. 42, 1 (1976).
- ⁶⁸P. A. Madden and R. M. Lynden-Bell, Chem. Phys. Lett. 38, 163 (1976).
- ⁶⁹D. Oxtoby in: Advances in Chemical Physics, edited by I. Prigogine and S. A. Rice (to be published).

- ⁷⁰C. B. Harris, J. Chem. Phys. 67, 5607 (1978); also in Advances in Laser Chemistry, edited by A. H. Zewail (Springer Series in Chemical Physics, Springer-Verlag, N.Y., 1978). The last article summarizes some new findings.
- ⁷¹P. W. Anderson, J. Phys. Soc. Japan, 9, 316 (1954); R. Kubo and K. Tomita, J. Phys. Soc. Japan 9, 888 (1954).
- ⁷²K. E. Jones and A. H. Zewail in: Advances in Laser Chemistry, edited by A. H. Zewail (Springer Series in Chemical Physics, Springer-Verlag, N.Y., 1978).
- ⁷³A. H. Zewail, K. E. Jones, and T. E. Orlowski, Spec. Lett. 10, 115 (1977); the proof of the master equation in this paper can be found in reference 72.
- ⁷⁴R. F. Snider, J. Chem. Phys. 32, 1052 (1960).
- ⁷⁵W. Liu and R. A. Marcus, J. Chem. Phys. 63, 272 (1975).
- ⁷⁶R. Zwanzig in: Lectures in Theoretical Physics, edited by W. E. Brittin (Interscience, N.Y., 1961), Vol. III, p. 106.
- ⁷⁷U. Fano, Phys. Rev. 131, 259 (1973).
- ⁷⁸A. Ben-Reuven in: Advances in Chemical Physics, edited by I. Prigogine and S. A. Rice (Wiley, N.Y., 1975), Vol. 23, p. 235.
- ⁷⁹K. E. Jones, A. H. Zewail, and D. Diestler in: Advances in Laser Chemistry, edited by A. H. Zewail (Springer Series in Chemical Physics, Springer-Verlag, N.Y., 1978), and references therein.
- ⁸⁰D. E. McCumber, J. Math. Phys. 5, 221 (1964); D. E. McCumber and M. D. Sturge, J. Appl. Phys. 34, 1682 (1963); B. DiBartolo, Optical Interactions in Solids (Wiley, N.Y., 1968).

- ⁸¹(a) G. J. Small, J. Chem. Phys. 54, 3300 (1971); ibid. 58, 2015 (1973); (b) Note that using these modes for the T_1 term of Eq. (52) one can obtain the familiar T^4 terms for the shift as well as the other forms of the high temperatures regime.
- ⁸²K. E. Jones and A. H. Zewail, to be published.
- ⁸³We should mention that when we quote temperatures in this paper we mean the temperature measured by the sensor very near the crystal. We do not know the actual temperature "inside" the crystal.
- ⁸⁴In these fits we plot the intensity which is an exponential function of $1/T_2$ which in turn changes with temperature according to the T^7 of the $e^{-\Delta/kT}$ dependence. We have found that these two fits are indistinguishable. The difference is largest between 4.2°K and 6°K where we have no data. Note that for the $e^{-\Delta/kT}$ function the signal intensity is an exponential of an exponential.
- ⁸⁵I. Abella, N. Kurnit, and S. Hartmann, Phys. Rev. 141, 391 (1966).
- ⁸⁶At low temperatures slow vibrational relaxation in the excited state of benzene in hydrogen was found by P. Frosch (G. W. Robinson, private communication). The slow relaxation implies that the benzene mode is not able to dump that high energy into the "inert" matrix.
- ⁸⁷G. Gillispie and E. C. Lim, J. Chem. Phys. 65, 2022 (1976); E. C. Lim (private communication of unpublished work).
- ⁸⁸J. B. Birks, Photophysics of Aromatic Molecules (Wiley-Interscience, N.Y., 1970); E. Schlag, S. Schneider, and S. F. Fischer, Ann. Rev. Phys. Chem. 22, 465 (1971).
- ⁸⁹Note that in an IRD experiment, we eliminate the d.c. background and amplify the a.c. transient signal which may be 10-30% of the d.c.

level. For LADS transients we observe both the d.c. and the a.c. components. Thus at very low powers, IRD can give much more accurate τ_0 's than LADS.

⁹⁰W. Lambert and A. Zewail, unpublished work.

⁹¹It is for the same reason that we exclude the possibility that the observed slow decay is due to ground state vibrational relaxation. Because if so, the molecules will leave $|p\rangle$ at $(24)^{-1}$ nsec⁻¹ rate (spontaneous emission to ground states) and the overshoot will be very large and the light-on transient will decay rapidly.

⁹²The early measurement of Marchetti et al. (reference 44) indicated that vibrational relaxation is much slower ($\sim 2 \times 10^{-10}$ sec). Recent work (Marchetti, private communication) has established that the early measurement was due to an artifact, and that the 267 cm^{-1} is much broader, consistent with our findings.

⁹³R. Shoemaker in: Laser and Coherence Spectroscopy, edited by J. Steinfield (Plenum, N.Y., 1978), p. 197.

APPENDIX I

FOURIER TRANSFORMS OF THE LASER PULSES USED IN THIS WORK

The effective bandwidth of the CW single-mode laser varies between 60 KHz and 6 MHz depending upon the time scale of the experiment. When we utilize the EO and LADS techniques to produce pulses from this laser, frequency broadening will occur as the pulse width decreases. To quantify this effect we calculated Fourier transforms for various pulse shapes and widths (see Fig. 1) in order to determine a lower limit to the frequency bandwidth of the single-mode dye laser in our experiments.

If $f(t)$ represents the functional form of the laser pulse in time, then its Fourier transform will be defined as:

$$F(\omega) = C_N \int_{-\infty}^{\infty} f(t) e^{-i\omega t} dt \quad (I1)$$

where C_N is a normalization factor such that the value of the transform at the center frequency (here $\omega = 0$) is 1. For the pulses shown in Fig. 1, which have identical widths T , and rise and fall times Γ_p^{-1} , the transforms are:

$$F_A(\omega) = C_N \left\{ \frac{2 \sin \omega T/2}{\omega} + \left(\frac{\Gamma_p - i\omega}{\Gamma_p^2 + \omega^2} \right) \left[e^{-i\omega T/2} - e^{i\omega T/2} \right] \right\} \quad (I2)$$

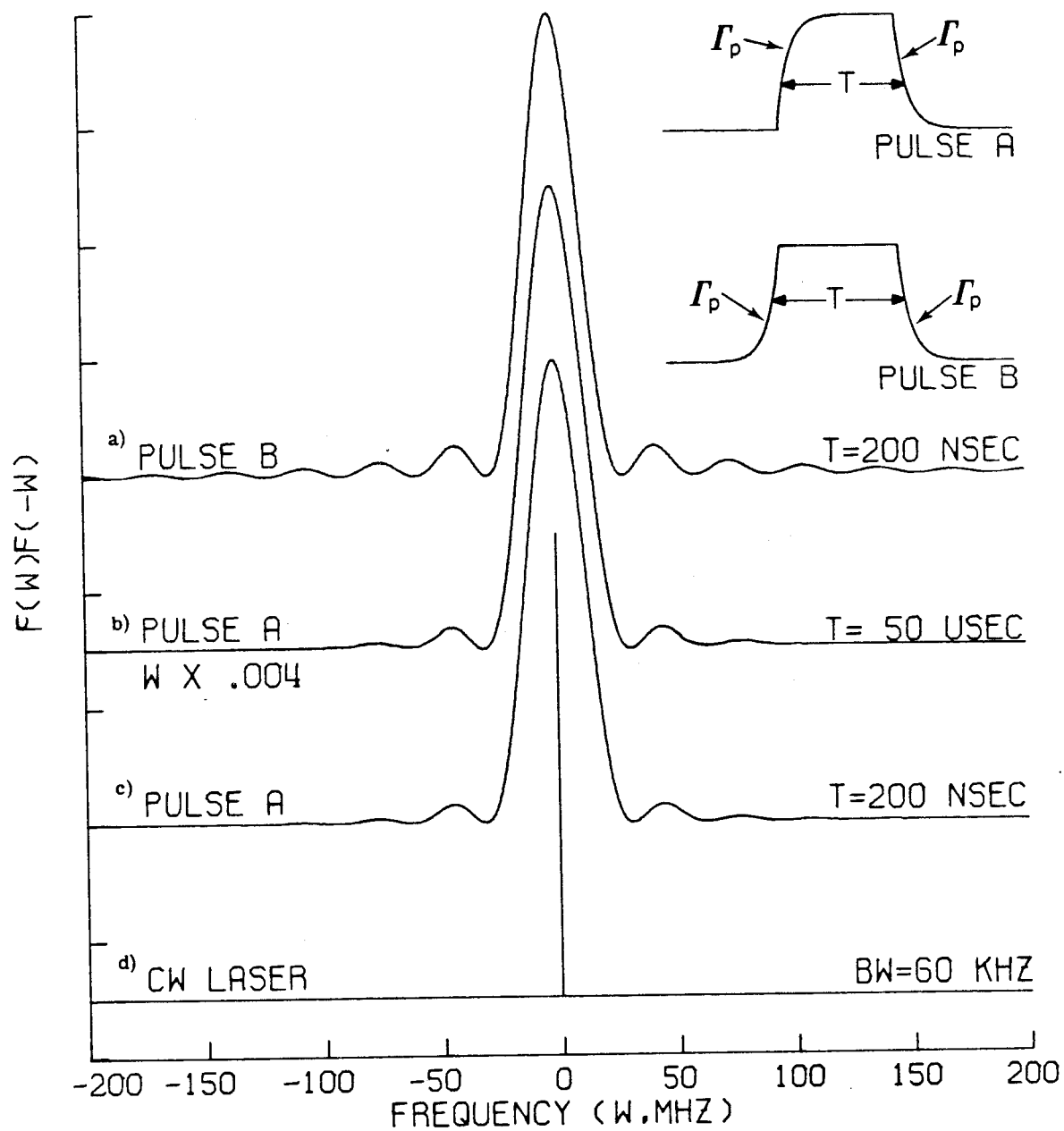
and

$$F_B(\omega) = C'_N \left\{ \frac{\sin \omega T/2}{\omega} + \frac{1}{\Gamma_p^2 + \omega^2} \left[\Gamma_p \cos \frac{\omega T}{2} + \omega \sin \frac{\omega T}{2} \right] \right\} \quad (I3)$$

Figure 1

Depicted here are Fourier transforms of laser pulses. Pulse A and B have identical widths T , and rise and fall times, Γ_p^{-1} of 10 nsec. Spectra (a) and (c) correspond to 200 nsec wide laser pulses and their bandwidths (FWHM) are 26.1 and 27.5 MHz, respectively, Spectrum (b) corresponds to a 50 μ sec wide A pulse and its bandwidth is 111.3 KHz. Shown at the bottom (spectrum d) is the effective bandwidth (60 KHz, see ref. 1) of the single-mode CW dye laser on the time scale of the slow transients observed in pentacene.

FOURIER TRANSFORMS OF LASER PULSES



To obtain $F_A(\omega)$ as shown in Eq. (I2), a term containing $e^{-\Gamma_p T/2}$ was ignored. This is valid for our experiments where $T \gg \Gamma_p^{-1}$ such that $e^{-\Gamma_p T/2} \approx 0$. Since $F_A(\omega)$ is complex, we will calculate the energy spectra of the pulses which are always real functions. The energy spectrum is related to the Fourier transform in the following way:

$$S(\omega) = F(\omega)F(-\omega) \quad (\text{I4})$$

For pulse A,

$$S_A(\omega) = 4C_N^2 \frac{\sin^2 \omega T/2}{\omega^2} \frac{\Gamma_p^2}{\Gamma_p^2 + \omega^2} \quad (\text{I5})$$

and for pulse B,

$$S_B(\omega) = F_B^2(\omega) \quad (\text{I6})$$

since $F_B(\omega)$ is real. Eqs. (I5) and (I6) are plotted versus ω in Fig. 1 for a pulse width of 200 nsec which is the width used in the OFID and nutation experiments. Neglecting the small sidebands, the frequency bandwidths (FWHM) are 27.5 and 26.1 MHz for A and B pulses, respectively. The energy spectrum of pulse A is slightly broader than that of pulse B. This occurs because the area under pulse A is less than that of B. Continuing along these lines, the energy spectrum of a step-function pulse (infinitely fast rise and fall time) of the same width as A and B is even broader (FWHM = 27.8 MHz).

In our experiments, pulse A accurately describes the pulses we observe using both the EO and LADS techniques. Therefore, we used this pulse to determine the bandwidth of the long laser pulses used

in IRD experiments. Shown in Fig. 1 is the energy spectrum (Eq. (15) versus ω) for a 50 μ sec A pulse. Here, the frequency scale has been reduced ($\omega \times 0.004$) indicating that the bandwidth for this pulse is much narrower (FWHM = 111.3 KHz).

Now, since the experiments are performed with a train of pulses rather than just one the effects of repetition rate on the form of the transforms must be considered. If the laser pulse is repeated ad infinitum at regular intervals T_i , where T_i is the pulse separation, then all of the transform is removed except for delta function samples at $\omega = \pm n \frac{2\pi}{T_i}$ where n is an integer. However, the envelope of the transform does not change. Most of the experiments on pentacene were performed at pulse repetition rates of 10 KHz. Therefore, the energy spectra for pulse trains are identical to those shown in Fig. 1 (i.e., they have the same overall width) except that they have delta function samples separated by approximately 63 KHz.

Finally, to illustrate the broadening effects introduced by pulsing a CW laser, shown at the bottom of Fig. 1 is the effective bandwidth of the single-mode dye laser on the time scale of the slow transients observed in pentacene. Wu and Ezekiel have shown¹ that the linewidth is 60 KHz (μ sec time scale) and determined primarily by residual FM jitter.

The important points of this section are: (1) for short (200 nsec) pulses, the bandwidth of the single-mode laser is temporally limited and almost 500 times larger than the effective CW bandwidth and (2) for long (50 μ sec) pulses the laser bandwidth is determined almost entirely by residual FM jitter.

References

- ¹F. Y. Wu and S. Ezekiel, Laser Focus, March 1977, p. 78.

APPENDIX II

APPROXIMATE SOLUTIONS FOR INTEGRALS IMPORTANT FOR
INHOMOGENEOUS LINEWIDTH AVERAGING

The solution of the integral written here in general form as:

$$I = \frac{1}{\sqrt{\pi} \beta} \int_{-\infty}^{\infty} e^{\frac{-\alpha}{\gamma^2 + \Delta^2} - \frac{\Delta^2}{\beta^2}} d\Delta \quad (\text{II1})$$

is required to determine both $r_2(t)$ [Eq. (15) of Ch. IV] and $\rho_{pp}(t)$ (in the high power limit of the steady-state coherence regime) averaged over the inhomogeneous linewidth. Since, to our knowledge, there is no analytic solution for this integral, it is usually approximated as:

$$I = \frac{1}{\sqrt{\pi} \beta} \int_{-\infty}^{\infty} e^{\frac{-\alpha}{\Delta^2} - \frac{\Delta^2}{\beta^2}} d\Delta \quad (\text{II2})$$

which is analytic. To show that this approximation is valid in general for $\gamma^2 \ll \beta^2$ the integral may be evaluated by an asymptotic expansion of the exponential in a Taylor series about the maxima of the argument.

With the argument of the exponential given by:

$$f(\Delta) = \frac{-\alpha}{\gamma^2 + \Delta^2} - \frac{\Delta^2}{\beta^2} \quad (\text{II3})$$

taking successive derivatives reveals that maxima in $f(\Delta)$ occur at $\Delta = \pm (\sqrt{\alpha} \beta - \gamma^2)^{\frac{1}{2}}$ if $\alpha \beta^2 > \gamma^4$, and at $\Delta = 0$ if $\alpha \beta^2 < \gamma^4$. Expanding $f(\Delta)$ in a Taylor series about $\Delta = (\pm \sqrt{\alpha} \beta - \gamma^2)^{\frac{1}{2}}$ and keeping only the first term in Δ one obtains:

$$f(\Delta) = -\left(\frac{2\sqrt{\alpha}}{\beta} - \frac{\gamma^2}{\beta^2}\right) - 4\left(\frac{1}{\beta^2} - \frac{\gamma^2}{\alpha^{1/2}\beta^3}\right)\left(\Delta - \left(\pm \sqrt{\alpha}\beta - \gamma^2\right)^{\frac{1}{2}}\right)^2 \quad (\text{II4})$$

Therefore, the integral I may be expressed as:

$$I \approx \frac{1}{\sqrt{\pi}\beta} \sum_{\substack{\text{over} \\ \pm \text{ roots}}} \exp\{f(\Delta)\} d\Delta \quad (\text{II5})$$

$$\begin{aligned} &= \frac{2}{\sqrt{\pi}\beta} e^{-\left(\frac{2\sqrt{\alpha}}{\beta} - \frac{\gamma^2}{\beta^2}\right)} \frac{\sqrt{\pi}}{2\sqrt{\frac{1}{\beta^2} - \frac{\gamma^2}{\alpha^{1/2}\beta^3}}} \\ &= \frac{e^{-\left(\frac{2\sqrt{\alpha}}{\beta} - \frac{\gamma^2}{\beta^2}\right)}}{\sqrt{1 - \frac{\gamma^2}{\alpha^{1/2}\beta}}} \quad (\text{II6}) \end{aligned}$$

Using the same techniques, the result for the integral with f expanded about $\Delta = 0$ is:

$$I \approx \frac{e^{-\frac{\alpha}{\gamma^2}}}{\sqrt{1 - \frac{\alpha\beta^2}{\gamma^4}}} \quad (\text{II7})$$

For our purposes, the useful result will be Eq. (II6). This can be shown by substituting for α , γ , and β the appropriate variables from Eq. (15) of Ch. IV for $r_2(t)$ and Eq. (60) of Ch. IV for $\rho_{pp}(t)$.

First, from Eq. (15), $\alpha = \chi^2 t / 2T$, $\gamma = \chi$ and $\beta = \delta\omega_I$. From experiment, $\chi = 0.23$ GHz (see pg.250), $T = (T_{1p0}^{-1} - T_2^{-1})^{-1} = 56.3$ nsec

and $\delta\omega_I = 24$ GHz (see Fig. 15 of Ch. IV). Thus, $\alpha\beta^2 \gg \gamma^4$ when $t \gg 0.2$ nsec. Therefore, Eq. (II6) is valid for describing all but the very short time behavior of $\langle r_2(t) \rangle$. Furthermore, considering the above values of the parameters, Eq. (II6) reduces to the form shown in Eq. (18) of Ch. IV for $\langle r_2(t) \rangle$ which was obtained using the approximation shown in (II2). Now, from the appropriate integral for $\rho_{pp}(t)$ in Eq. (60), $\alpha = \chi^2 \Gamma t$, $\gamma = \Gamma$, and $\beta = \delta\omega_{PB}$. With these parameters $R_{peff} = \chi / \delta\omega_{PB} \sqrt{\Gamma/t}$ which is identical to the previous result.

APPENDIX III

AN APPROACH TO SHOW THAT r_1 IS AN ODD FUNCTION OF
THE OFF-RESONANCE PARAMETER, Δ

In terms of r_1 and r_2 , ρ_{ba} may be expressed as:

$$\rho_{ba} = \frac{1}{2} (r_1 + ir_2) \quad (\text{III1})$$

such that

$$\dot{\rho}_{ba} = \frac{1}{2} (\dot{r}_1 + i\dot{r}_2) \quad (\text{III2})$$

Eq. (30c) of Chapter I for the equation of motion can then be written as:

$$\dot{r}_1 + i\dot{r}_2 = \left(-\frac{1}{T_2} + i\Delta\right)(r_1 + ir_2) + i\chi r_3 \quad (\text{III3})$$

Here r_3 has been substituted for $\rho_{aa} - \rho_{bb}$. The real and imaginary parts of Eq.(III3) may be separated to obtain the optical Bloch equations for r_1 and r_2 :

$$\dot{r}_1 = -\frac{1}{T_2} r_1 - \Delta r_2 \quad (\text{III4})$$

$$\dot{r}_2 = \chi r_3 + \Delta r_1 - \frac{1}{T_2} r_2 . \quad (\text{III5})$$

Eq.(III5) has been solved in Chapter IV and reference 7 of Chapter I and found to be an even function in Δ . Eq.(III4) may be rewritten to show explicitly its dependence on Δ :

$$e^{-t/T_2} \left\{ \frac{d}{dt} \left(r_1 e^{t/T_2} \right) \right\} = -\Delta r_2 . \quad (\text{III6})$$

Thus,

$$\frac{d}{dt} \left(r_1 e^{t/T_2} \right) = -e^{t/T_2} \Delta r_2 \quad (\text{III7})$$

and integrating over time one obtains:

$$r_1 = -e^{-t/T_2} \int_0^t e^{t'/T_2} \Delta r_2 dt' . \quad (\text{III8})$$

Since, r_2 is even in Δ , r_1 must be odd and so averaging Eq. (III8) over the inhomogeneous lineshape will provide the result:

$$\langle r_1 \rangle = 0 .$$

PROPOSITIONS

PROPOSITION I

Measurements of vibrational lifetimes and spin-orbit
relaxation rates in matrix isolated NO

Vibrational relaxation (VR) in molecules isolated in condensed phases has been studied extensively in the recent past. Emphasis has been placed on diatomic molecules¹⁻⁸ isolated in rare gas matrices because theoretical models have been developed for this simple case.⁹⁻¹⁷ Most of these models view the relaxation as a multiphonon process in which a single quantum of vibrational energy of the guest diatomic is converted into several host lattice phonons. Because of the analogy between these multiphonon processes and electronic relaxation processes important for large isolated polyatomic molecules, this field has attracted considerable attention.

There is some controversy involving the energy gap law and the strong temperature dependence for the vibrational relaxation rate that multiphonon theory predicts. Several exceptions and the complications involved are worth noting. Certain systems (e.g., CN/Ar)⁷ have been studied in excited electronic states where it is found that VR occurs rapidly by intersystem crossing and internal conversion rather than by a direct mechanism. Because of these competing processes it is difficult to ascertain the details of the direct coupling of the guest vibrational modes to the lattice. In other systems (NH/Ar, ND/Ar)³, where vibrational lifetimes are short ($< 1 \mu\text{sec}$ in the $A^3\Pi$ state) with no temperature dependence in the range 8-25°K, it has been suggested that rotation^{14,15} or other orientational motion¹⁷ of the guest diatomic is an important local accepting mode. These processes are completely ignored in the original multiphonon theory. Energy transfer between isotopic species has been found to be an important competing channel in CO/Ar⁵. In this system,

rotation is considered unimportant and the observed vibrational lifetime is essentially radiative. To further complicate matters, several of the diatomics studied (NH, OH, C_2^- , CN) are isolated in the host matrix after photolysis of a precursor molecule (NH_3 , H_2O , C_2H_2 , HCN). Therefore, atomic impurities and unphotolyzed starting material may be nearby the "isolated" diatomic providing additional energy transfer channels that are difficult to quantify.

To avoid the complications introduced by competing decay channels in electronically excited states and the possibility of energy transfer to impurities as a result of photolysis, it is proposed that vibrational relaxation be studied in the ground electronic state of the stable diatomic NO in an argon matrix at low temperature. It is also proposed that spin-orbit relaxation be investigated in this system to verify whether this process can indeed be slow as suggested by McCarty and Robinson¹⁸ and whether it introduces a VR channel.

Nitric oxide is somewhat of a unique molecule. It is the only stable diatomic molecule with a non-zero electronic angular momentum. Its ground electronic state has two spin-orbit components, $X^2\Pi_{1/2}$ and $X^2\Pi_{3/2}$ separated by 123.2 cm^{-1} .¹⁹ Table I summarizes the energies (cm^{-1}) for the first three vibrational levels of the $^2\Pi$ ground state obtained from high resolution gas phase measurements.^{20,21} These gas phase energies will be shifted slightly in a matrix. Red shifts of $4\text{--}5\text{ cm}^{-1}$ have been observed for CO^5 and N_2^{22} in argon matrices.

At 4.2°K , essentially all of the NO molecules will reside in the $^2\Pi_{1/2}$ state ($V=0$) since the thermal population of $^2\Pi_{3/2}$ can be neglected. Therefore, the first step would involve measuring the lifetime of $^2\Pi_{1/2}$

Table I

v	$2\Pi_{1/2}$	$2\Pi_{3/2}$
0	0	123.2
1	1876.1	1999.0
2	3724.1	3846.9
3	5544.1	5666.6

($V=1$) following excitation from $2\Pi_{1/2}$ ($V=0$). To accomplish this, one needs an excitation source at $\approx 5.3\mu$. The source must be tunable, since the position of the line is not known exactly in the matrix. A new frequency mixing technique capable of generating continuously tunable IR output from 3.5μ to 13μ has recently been introduced.²³ It involves mixing of the Stokes wave generated by stimulated Raman scattering²⁴ in a high pressure H_2 cell with the tunable output of a $LiNbO_3$ parametric oscillator.²⁵ The pump source is a 1.06μ amplified Nd:YAG laser whose output is split (50/50) to pump both the parametric oscillator and the H_2 cell. Up to 6 kW peak power in a 5 nsec pulse has been obtained with a linewidth of 0.1 cm^{-1} . Following excitation of the sample at the $2\Pi_{1/2}$ ($V=0$) \rightarrow $2\Pi_{1/2}$ ($V=1$) transition, the lifetime of $V=1$ could be determined by monitoring the emission using an InSb detector. Although dynamic response has been a problem with IR detectors in the past, detectors are now available with response times of 100 nsec or less.²⁶

From gas phase integrated absorption measurements the radiative lifetime of NO is found to be 80 msec.²⁷ If VR is indeed slow, and one can neglect the effects of rotation, then one would measure the radiative

lifetime in the matrix. This is indeed the case for CO/Ar⁵. However, the observed lifetime does decrease in CO/Ar when the temperature is raised above 24°K. It would be interesting to see if the onset of the temperature effect occurred at a lower temperature for NO, since it has a noticeably smaller vibrational energy spacing. This temperature effect could be due to nonradiative channels involving specific localized phonon modes and should be investigated carefully. Although it is not clearly understood why rotation plays no role in CO VR in a matrix, rotational constants for CO and NO are similar, and it is possible that rotation is unimportant in NO as well.

Upon measuring the lifetime of $V=1$ the next higher vibrational mode should be studied. Theory⁹⁻¹³ suggests that VR is faster in upper vibrational levels, since the host-guest coupling is taken to be linear in the guest vibrational coordinate. This has been observed in some of the systems studied. For example, in CN/Ar⁷, the relaxation rate in the $A^2\Pi$ state does increase with the extent of vibrational excitation. Lifetimes of 10, 90 and 670 nsec have been measured for $V = 4, 3$, and 2 respectively. Although the VR mechanism in this system is thought to involve intersystem crossing to vibrational levels high in the ground state manifold which cross back rather than relax directly, the experimental results do obey the energy gap law, which implies that the relaxation process has a multiphonon character. On the other hand, no dependence of the vibrational lifetime on V was found for CO/Ar⁵. In this system, relaxation is essentially radiative and energy transfer processes involving isotopic species complicate the interpretation of the relaxation mechanism. These isotopic species constitute 1.3% of the total number of

CO molecules. In NO, isotopic species ($N^{15}O^{16}$, $N^{14}O^{18}$, $N^{15}O^{18}$) amount to only 0.4% of the total number of NO molecules. Therefore, at low concentration these energy transfer processes will not interfere as much, and the observed relaxation behavior may differ considerably.

To excite the ${}^2\Pi_{1/2}$ ($V=2$) state, one needs a tunable excitation source near 2.69μ . Recently, F-center lasers have been developed that provide tunable IR excitation from 0.9μ to 3.3μ .^{28,29} An F-center consists of a single electron trapped at a halide ion vacancy in an alkali halide crystal. They are created in the crystal by X-ray bombardment. Laser action has been demonstrated in crystals where one of the six metal ions immediately surrounding the vacancy is foreign. Following absorption of a visible photon, the F-center relaxes to a new configuration and subsequently emits a near IR photon before relaxing back to its original configuration. This discussion is not meant to explain the physics of color centers. Let it be stated at this point that a type $F_A(II)$ color center in lithium doped KCl will provide tunable excitation in the required region. This laser medium can provide a very narrow linewidth (100 kHz) and operates either CW or pulsed. It can be pumped with the frequency-doubled (0.53μ) output of the Nd:YAG laser mentioned previously. Thus, time resolution would be approximately 5 nsec.

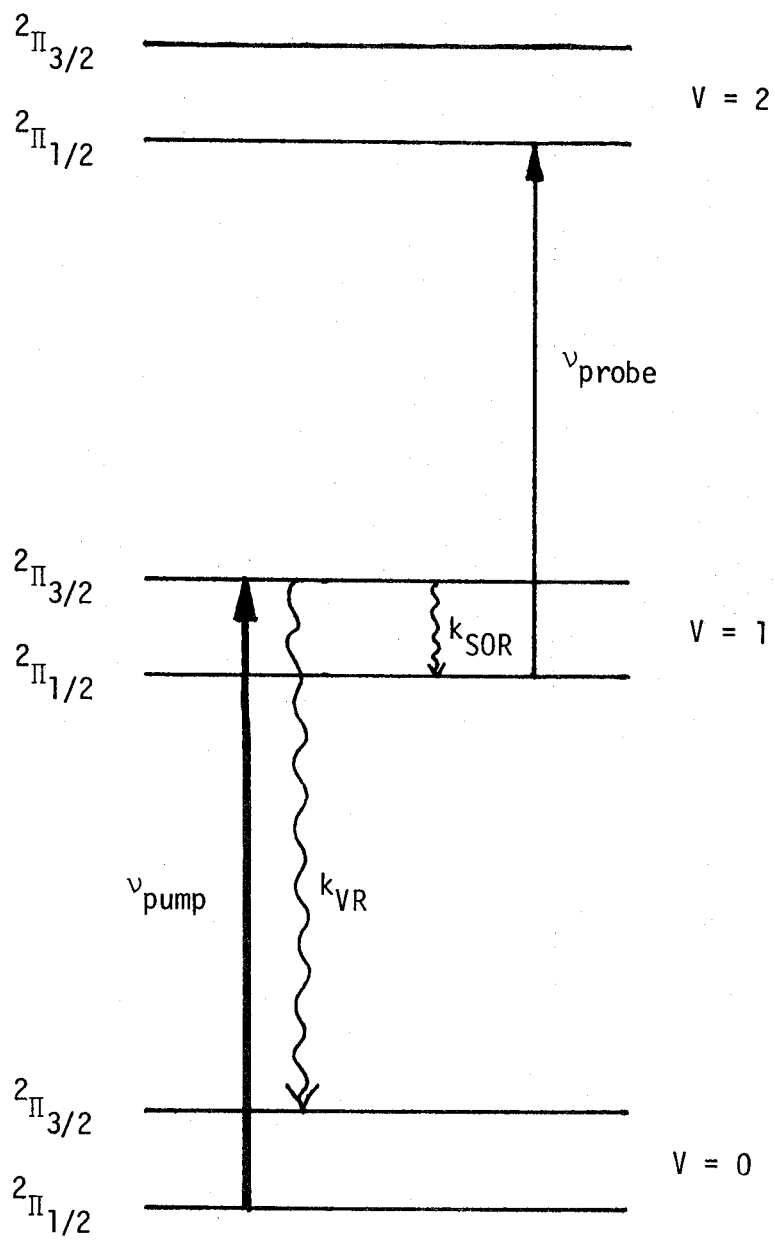
Following excitation with the F-center laser, the lifetime of the ${}^2\Pi_{1/2}$ ($V=2$) state can be measured by monitoring the emission as before, using an InSb detector. The temperature dependence of this lifetime should be investigated as well to establish whether or not $V=1$ and $V=2$ relax similarly.

Upon determining the lifetime for both vibrational levels and whether the energy gap law predicted by the multiphonon theory applies in this system, the spin-orbit relaxation (SOR) between the components of each vibrational level should be considered. This process can be examined with a double resonance technique as shown in Fig. 1 and described below.

In this double resonance experiment, one laser pumps the ${}^2\Pi_{1/2} (V=0) \rightarrow {}^2\Pi_{3/2} (V=1)$ transition. Although this transition is forbidden (Hund's Case (a)) it has been observed²⁰ before in the gas phase spectrum of NO using conventional IR excitation. With the moderately high powers available in the pulsed IR laser as described earlier, it should be possible to pump this transition as shown in Fig. 1. If spin-orbit relaxation is fast (e.g., due to some mechanism involving the participation of lattice phonons), then the build-up in absorption of the ${}^2\Pi_{1/2} (V=1) \rightarrow {}^2\Pi_{1/2} (V=2)$ transition monitored by ν probe should follow the laser excitation pulse (i.e., 5 nsec) or the detector response if one monitors the absorption. Now, if SOR is slow compared to the radiative and VR times of the ${}^2\Pi_{3/2}$ state, then no absorption would be seen. In the interesting intermediate case, the build-up in absorption would provide the relaxation rate between the spin-orbit components. At this point it should be noted that the lasers mentioned previously have adequate resolution to probe the $(1 \rightarrow 2)$ transition without exciting the $(0 \rightarrow 1)$ transition simultaneously.

Since the energy separation between the spin-orbit components is small, one might expect the relaxation process to be fast using energy gap arguments. It is not known, however, what influence this process would have

Figure 1: Energy level diagram for NO illustrating the double resonance method of measuring the spin-orbit relaxation rate.



on vibrational relaxation. In one system (NH/Ar), there is considerable controversy over the rate of spin-orbit relaxation in the $A^3\Pi$ state. McCarty and Robinson¹⁸ (MR) show spectra for NH in Ar which indicate that NH freely rotates in both its ground $X^3\Sigma^-$ and $A^3\Pi$ states in this environment. Upon assignment of the emission lines observed to various spin-orbit components of each state, they suggested that SOR is on the order of the lifetime of the electronic transition, $\approx 1 \times 10^{-6}$ sec. Bondybey and Brus³ (BB) however, claim that rotation is hindered in the $A^3\Pi$ state with a barrier of 320 cm^{-1} , and that SOR is fast ($< 10 \text{ nsec}$). In the MR experiment, NH was prepared from NH_3 in a microwave discharge, while in the BB experiment, NH was prepared by photolysis of NH_3 .

The experiment on NO could help resolve this anomaly. It can be isolated cleanly in the matrix and its large spin-orbit interaction could make it a better candidate to examine SOR and its participation, if any, in VR.

In summary, NO appears to be a molecule worth studying in an attempt to further the understanding of VR in simple isolated systems. Not only could it add new information about the energy gap law, it also introduces the possibility of determining whether spin-orbit relaxation should be considered in the mechanism of vibrational relaxation in these simple systems.

References

1. D. S. Tinti and G. W. Robinson, J. Chem. Phys., 49, 3229 (1968).
2. L. E. Brus and V. E. Bondybey, J. Chem. Phys., 63, 786 (1975).
3. V. E. Bondybey and L. E. Brus, J. Chem. Phys., 63, 794 (1975).
4. V. E. Bondybey, J. Chem. Phys., 65, 5138 (1976).
5. H. Dubost and R. Charneau, Chem. Phys., 12, 407 (1976).
6. L. J. Allamandola, H. M. Rojhanalab, J. W. Nibler, and T. Chappell, J. Chem. Phys., 67, 99 (1977).
7. V. E. Bondybey, J. Chem. Phys., 66, 995 (1977).
8. V. E. Bondybey and C. Albiston, J. Chem. Phys., 68, 3172 (1978).
9. H. Y. Sun and S. A. Rice, J. Chem. Phys., 42, 3826 (1965).
10. A. Nitzan and J. Jortner, Mol. Phys., 25, 713 (1973).
11. D. J. Diestler, J. Chem. Phys., 60, 2692 (1974).
12. A. Nitzan, S. Mukamel, and J. Jortner, J. Chem. Phys., 60, 3929 (1974); ibid., 63, 200 (1975).
13. S. H. Lin, H. D. Lin, and D. Knittel, J. Chem. Phys., 64, 44 (1976).
14. K. F. Freed, D. L. Yeager, and H. Metiu, Chem. Phys. Lett., 49, 19 (1977).
15. R. B. Gerber and M. Berkowitz, Phys. Rev. Lett., 39, 1000 (1977).
16. D. J. Diestler, in Topics in Applied Physics, ed. by F. K. Fong (Springer, Berlin, 1976), Vol. 15.
17. D. J. Diestler, E. W. Knapp, and H. D. Ladouceur, J. Chem. Phys., 68, 4056 (1978).
18. M. McCarty, Jr. and G. W. Robinson, J. Am. Chem. Soc., 81, 4472 (1959).
19. T. C. James and R. J. Thibault, J. Chem. Phys., 41, 2806 (1964).

20. T. C. James, J. Chem. Phys., 40, 762 (1964).
21. M. D. Olman, M. D. McNelis, and C. D. Hause, J. Mol. Spectrosc., 14, 62 (1964).
22. T. E. Orlowski, M. S. Thesis, California Institute of Technology, 1976.
23. S. J. Brosnan, R. N. Fleming, R. L. Herbst, and R. L. Byer, Appl. Phys. Lett., 30, 330 (1977).
24. N. Bloembergen, Amer. J. Phys., 35, 989 (1967).
25. R. L. Byer in Quantum Electronics, ed. by H. Rabin and C. L. Tang (Academic Press, New York, 1975), Vol. I.
26. For example, Mullard A264 InSb detector.
27. R. M. Green and C. L. Tien, J. Quant. Spectrosc. Radiat. Transfer, 10, 805 (1970).
28. L. F. Mollenauer and D. H. Olson, J. Appl. Phys., 46, 3109 (1975).
29. G. Litfin, R. Beigang, and H. Welling, Appl. Phys. Lett., 31, 381 (1977).

PROPOSITION II

Measurement of the intersystem crossing (ISC) rates in excited electronic states of 3,4-benzopyrene using a triplet-triplet absorption technique.

3,4-benzopyrene is a large aromatic molecule with a very small energy gap (2000 cm^{-1}) between its first and second excited singlet states.¹ The coupling between these two electronic states as a result of this small energy gap is a classic example of the "dense intermediate case".²⁻⁴ The radiative decay of the second excited singlet state (S_2) in this regime exhibits the characteristics of the small molecule limit^{2,5} for a finite set of strongly coupled levels. Consequently, emission is observed from S_2 with a lifetime much longer than that expected on the basis of the integrated oscillator strength and approximately equal to the lifetime of S_1 . Although the radiative properties of S_1 and S_2 for 3,4-benzopyrene have been studied extensively in the past,^{1,6-8} not much emphasis has been placed upon nonradiative processes. Since the lifetime of S_2 is much longer than that found for upper excited states in more "typical" aromatic molecules, it represents somewhat of a unique system to study the effects of electronic and excess vibrational energy upon the rate of intersystem crossing for strongly coupled states. It is proposed therefore, to measure the intersystem crossing rates for S_1 and S_2 of 3,4-benzopyrene in the gas phase as a function of temperature, pressure (inert gas) and laser frequency using a narrow band dye laser for state selectivity and a triplet-triplet absorption technique.

Because of the interesting radiative properties for molecules as a result of interstate coupling in the dense intermediate case, the essential details of the coupling in this regime will be presented.

For a large molecule with two excited electronic states separated by a small energy gap, a small number of zero-order vibronic levels $\{\phi_\ell\}$ in the S_1 manifold will be strongly coupled (large Franck-Condon vibrational overlap factors) with a vibronic level ϕ_s of S_2 . These ϕ_ℓ levels have been called "promoting modes"^{9,10} and strong coupling is assumed to occur only for modes that are nontotally symmetric (S_1 and S_2 are taken as nondegenerate states of different symmetry). The zero-order Born-Oppenheimer (BO) levels ϕ_s and $\{\phi_\ell\}$ are characterized by the energies $E_s, \{E_1, \dots, E_n\}$ and by the widths $\gamma_s, \{\gamma_1, \dots, \gamma_n\}$. The widths are defined as:

$$\gamma_i = \Gamma_i + \Delta_i$$

where Γ_i is the radiative width of level i , and Δ_i is the corresponding nonradiative width. Δ_i arises from intersystem crossing to the triplet manifold (s) and internal conversion to the ground electronic state. Its measurement is of concern here.

The physical model for the strongly coupled levels involves the assumption:

$$|V_{s\ell}| \gg |E_\ell - E_\ell| \quad (2)$$

where ϕ_ℓ and ϕ_ℓ are adjacent levels in the ℓ manifold, and $V_{s\ell}$ is the non-adiabatic coupling term. In a situation of strong coupling, the states that diagonalize the decay matrix cannot be assigned in terms of the zero-order states ϕ_s and $\{\phi_\ell\}$ such that a molecular eigenstate¹¹ basis set given by:

$$\psi_m = a_{sm}\phi_s + \sum_\ell b_{\ell m}\phi_\ell \quad (3)$$

is more useful. From the time evolution of the compound state in the Weisskopf-Wigner approximation, one can determine the widths of the molecular eigenstates in terms of the widths of the original zero-order levels. It is assumed that 1) no correlation exists among the decaying levels (i.e., a diagonal decay matrix), 2) $\langle \gamma_\ell \rangle$ is the mean decay width of a state in the ℓ manifold, and 3) the coupling is uniform such that $V_{s\ell}$ can be replaced by $\langle V \rangle$ and $E_\ell - E_\ell$, by $\langle \epsilon \rangle$. Within the framework of these assumptions, the diagonal elements of the decay matrix will be roughly comparable, and the decay rates for the states defined by Equation (3) take the form:⁴

$$\gamma_m = \frac{\gamma_s}{n} + \langle \gamma_\ell \rangle \quad (4)$$

In Equation (4), n is the number of strongly coupled levels given by:⁴

$$n = \frac{\pi \langle V \rangle^2}{\langle \epsilon \rangle^2} \quad (5)$$

Several interesting points can be made about the results shown in Equation (4). First, eigenstates whose energies are close to either the zero-order B0 ϕ_ℓ or ϕ_s state will have single exponential decays with approximately the same lifetime. Second, the total decay rate corresponding to the zero-order ϕ_s state is "diluted" by an amount corresponding to the number of strongly coupled levels. This is the origin of the statement made earlier that the radiative decay of ϕ_s obeys the small molecule limit where lifetimes longer than that expected from oscillator strength measurements have been observed.⁵ Finally, since the rates, γ_i , have radiative and nonradiative contributions, the nonradiative channels are "diluted" as well.

The nonradiative channels should be investigated carefully and directly for the following reasons. First, although the radiative lifetimes in the s and ℓ spectral regions have been found equal for several dense intermediate case molecules^{1,12} including 3,4-benzopyrene,⁶ in most cases only a few measurements have been made in the intermediate region between the origins of the ϕ_ℓ and ϕ_s manifolds. In this region, with a narrowband laser, it may be possible to probe the eigenstates more selectively to determine the detailed structure of the coupling, $V_{s\ell}$. This coupling should affect nonradiative channels also (Eqs. 1,4,5). Second, a narrowband laser will effectively test the assumption that there are no correlations among the decay channels, since closely spaced, strongly coupled levels can provide radiative interference effects¹³ (i.e., quantum beats) if their widths exceed their spacing, while eigenstates well separated relative to their widths do not. These interference effects may possibly manifest themselves in the nonradiative channels.

To theoretically handle the nonradiative decay involving inter-system crossing to triplet manifolds, it is usually assumed that the triplet manifolds correspond to the statistical limit^{3,14,15} where the density of triplet levels ϕ_T in the vicinity of ϕ_ℓ and ϕ_s is large. It is further assumed that ϕ_ℓ and ϕ_s decay into their own quasicontinua (i.e., diagonal nonradiative decay matrix) such that the nonradiative widths may be characterized (neglecting internal conversion processes) by the expressions:

$$\Delta_\ell = 2\pi |V_{\ell,T\ell}|^2 \rho_{T\ell} \quad (6)$$

$$\Delta_s = 2\pi |V_{s,Ts}|^2 \rho_{Ts} \quad (7)$$

where $\rho_{T\ell}$ and ρ_{Ts} are the density of states in the $\phi_{T\ell}$ and ϕ_{Ts} triplet manifolds.

The object of the experiments described below will be to measure intersystem crossing rates in 3,4-benzopyrene following selective excitation throughout the energy region given by E_{ℓ} and E_s to determine the nonradiative widths given by Equations (6) and (7). This new information may help possibly in the understanding of the intramolecular coupling between the s and T and the ℓ and T manifolds, and indirectly provide information about the coupling between s and ℓ .

Much is known about the radiative processes important for 3,4-benzopyrene. In the gas phase^{1,6} (115°C, <.1 torr) emission is seen from both S_1 (at 24,800 cm^{-1}) and S_2 (at 26,800 cm^{-1}) following excitation into a vibronic line of S_2 at 28,800 cm^{-1} . The emission which follows a single exponential has a lifetime⁶ of ≈ 70 nsec at both origins with some evidence of interference effects⁶ (quantum beats) superimposed on the decay! These interference effects, if real, indicate that certain levels must be closely spaced relative to their widths. The fluorescence yield¹ for S_2 is almost 10% relative to S_1 , and this yield increases with both temperature and excitation frequency. The addition of an inert gas (n-hexane) quenches¹ the emission from S_2 relative to S_1 . The triplet yield has been measured in solution (toluene) and found to be 0.6.¹⁶ Because the triplet yield is large, measurement of the intersystem crossing rates by triplet-triplet absorption should be possible and may aid in the understanding of the temperature and pressure effects upon the observed radiative properties.

The proposed experiments require a narrow band tunable excitation source between 24,000 and 29,000 cm^{-1} . Single-mode CW tunable dye lasers have very narrow linewidths (≈ 10 MHz) and recent advances have improved single-mode power to the point that intracavity frequency doubling is practical. The most significant advance¹⁷ involves the use of a ring-shaped cavity such that the laser can operate in a traveling wave configuration rather than the conventional standing wave arrangement. Single mode output powers of up to 1 watt (CW) have been achieved with rhodamine 6G, and 55 mW in the UV has been obtained with intracavity frequency doubling. With the dyes oxazine 1 and oxazine 750 and a KDP intracavity frequency doubling crystal, a ring dye laser could provide tunable narrow band excitation in the required region. Time resolution could be obtained using Bragg diffraction from an acousto-optic modulator to deflect the laser beam into the sample¹⁸ for a short pulse. Transient triplet-triplet absorption spectra could be observed with a tungsten lamp at right angles to the laser beam. This lamp would be on continuously, and after passing through the sample it would be focussed upon the slit of a spectrometer whose output would be monitored by a photomultiplier.

The first step in the experiment would involve obtaining frequency resolved triplet-triplet absorption spectra following laser pulses. This could be accomplished using a scanning-gate boxcar integrator to look at the signal coming from the detector for a very narrow time interval following each laser pulse. One would get a frequency-resolved transient absorption spectrum with this technique by scanning the spectrometer with the boxcar gate fixed in time relative to the laser pulse position. Time-resolved spectra, on the other hand, would be obtained by scanning

the boxcar gate position with the spectrometer fixed. Thus, by using both of the above methods in a systematic way, one can get both frequency and time information for the transient absorption process.

Since the tungsten lamp output varies with frequency, it would be advantageous (in terms of sensitivity) to remove this effect which manifests itself as a sloping background superimposed on the spectra. This can be done in a way that also corrects for the frequency dependent detector and spectrometer efficiencies as well. If one splits the signal from the detector, sending half to the original boxcar and half to another boxcar whose gate width is set to the laser pulse separation, then the ratio of the output of each boxcar gives the corrected time-resolved spectrum. This technique is much simpler than conventional ways of correcting spectra which typically require two matched detectors.

With the above techniques one should be able to obtain both the frequency and time-resolved transient triplet-triplet absorption spectra. From the build-up and decay of the intensity of the observed lines (at low laser power) one should be able to extract both the rate of intersystem crossing and the triplet lifetime. If certain lines appear at short times (relative to the laser pulse) and disappear later as other lines build up, then one has the chance of measuring and possibly identifying absorption from upper triplet states. There are many other effects to study. Of obvious concern and importance are the temperature and pressure dependence of the transient spectra because of the known effect¹ these variables have upon the radiative properties of 3,4-benzopyrene.

A temperature dependent intersystem crossing rate has been observed for anthracene¹⁹ before, and it has been attributed to participation of a second triplet manifold in the vicinity of the lowest excited singlet. Since the emission from S_2 in 3,4-benzopyrene increases with temperature, a different kind of temperature-dependent process such as collision-induced emission may be in effect.

The pressure dependence of the intersystem crossing rate should be interesting in this system because of the selective quenching of emission from S_2 observed upon addition of an inert gas (n-hexane) to the sample cell. This may show up as an enhanced ISC rate and thus stronger T-T absorption.

Possibly most interesting will be the effect of laser frequency upon the ISC process. Several examples in the literature can be found where plots of nonradiative decay rates versus excitation energy exhibit breaks at energies corresponding to the origins of various excited singlet states.²⁰⁻²² These experiments suggest that the initial state involved in the radiationless transition may be a "compound state"²⁰ or molecular eigenstate as given by Equation (3). Thus, measurements of these radiationless decay rates in 3,4-benzopyrene as a function of excitation energy may possibly add more insight into the details of the coupling in molecules corresponding to the dense intermediate case.

References

1. P. A. Geldof, R.P.H. Rettschnick, and G. J. Hoytink, *Chem. Phys. Lett.*, 4, 59 (1969).
2. M. Bixon and J. Jortner, *J. Chem. Phys.*, 50, 3284 (1969).
3. K. Freed and J. Jortner, *J. Chem. Phys.*, 50, 2916 (1969).
4. A. Nitzan, J. Jortner, and P. M. Rentzepis, *Proc. R. Soc. Lond.*, A327, 367 (1972).
5. A. E. Douglas, *J. Chem. Phys.*, 45, 1007 (1967).
6. P. Wannier, P. M. Rentzepis, and J. Jortner, *Chem. Phys. Lett.*, 10, 102 (1971).
7. C. E. Easterly, L. G. Christophorou, R. P. Blaunstein, and J. G. Carter, *Chem. Phys. Lett.*, 6, 579 (1970).
8. P.A.M. Van den Bogaardt, R.P.H. Rettschnick, and J.D.W. Van Voorst, *Chem. Phys. Lett.*, 18, 351 (1973).
9. S. H. Lin, *J. Chem. Phys.*, 44, 3759 (1966).
10. S. H. Lin and R. Bersohn, *J. Chem. Phys.* 48, 2732 (1968).
11. M. Bixon and J. Jortner, *J. Chem. Phys.*, 48, 715 (1968).
12. P. Wannier, P. M. Rentzepis, and J. Jortner, *Chem. Phys. Lett.*, 10, 193 (1971).
13. U. Fano and J. H. Macek, *Rev. Mod. Phys.*, 45, 553 (1973).
14. M. Bixon and J. Jortner, *J. Chem. Phys.*, 50, 4061 (1969).
15. W. Rhodes, *J. Chem. Phys.*, 50, 2889 (1969).
16. C. A. Parker, Photoluminescence of Solutions (Elsevier, Amsterdam, 1968), p. 315.
17. H. W. Schröder, L. Stein, D. Frölich, B. Fugger, and H. Welling, *Appl. Phys.*, 14, 377 (1977).

18. T. E. Orłowski, K. E. Jones, and A. H. Zewail, Chem. Phys. Lett., 54, 197 (1977).
19. T. F. Hunter and R. F. Wyatt, Chem. Phys. Lett., 6, 221 (1970).
20. E. C. Lim and C. Huang, J. Chem. Phys., 58, 1247 (1973).
21. S. Hadley, Conference on Radiationless Transitions in Gaseous Molecules, Boulder, Colorado, 1972.
22. E. C. Lim and J. O. Uy, J. Chem. Phys., 56, 3374 (1972).

Proposition III

Study photosensitized redox reactions at semiconductor surfaces

The efficient interconversion of optical and chemical energy is a difficult problem that has received a lot of attention in recent years. Success in the development of chemical lasers and photo-electrochemical cells using semiconductor electrodes are indications of the achievements thus far. Recently, the electrolysis of water¹⁻³ has been accomplished upon irradiation of a TiO_2 semiconductor electrode in an electrochemical cell with ultraviolet ($< 4150\text{\AA}$) light. It is proposed that this chemical reaction might be accomplished upon irradiation of a dye adsorbed to the surface of a semiconductor crystal with visible light.

1. Electrolysis of H_2O in photoelectrochemical cells

The mechanism of the electrolysis of water at an illuminated TiO_2 electrode is thought to involve excitation of an electron from the valence band to the conduction band creating a hole (h^+).⁴ The band gap in TiO_2 is approximately 3 eV⁵ and thus UV photons are required for this process. Oxidation of water occurs at the TiO_2 surface while evolution of H_2 proceeds at the platinum electrode in the electrochemical cell. The reaction occurs in acidic or basic electrolytes with quantum efficiencies⁶ (ϕ) for the conversion of optical to chemical energy of between 10^{-2} and 10^{-1} .

The electrolysis of water has subsequently been observed at the surface of several other semiconductors upon irradiation with UV light. These semiconductors include SnO_2 ⁷ (band gap = 3.5 eV,⁸ $\phi = .01$); SrTiO_3 ⁶ (band gap = 3.4 eV,⁹ $\phi = .20$); KTaO_3 ¹⁰ (band gap = 3.5 eV,¹¹ $\phi = .06$); and WO_3 ¹² (band gap = 2.8 eV,¹² $\phi = .005$). For SrTiO_3 , efficient electrolysis occurred without biasing the semiconductor. All of the other systems (including TiO_2) required a bias but always much less

than that required (1.23V) to electrolyze H_2O at standard conditions. The need for this bias is thought to involve overcoming cell impedances and to achieve an effective depletion region at the surface of the electrode.⁴ For example, a positive bias on an n-type semiconductor favors hole migration to the electrode surface, while electrons move toward the bulk. This process improves the photocurrent yield by inhibiting $h^+ - e^-$ recombination.

A few other photoelectrochemical reactions have been observed using semiconductor electrodes. In basic solution (pH 14), the oxidation of S^{-2} and Te^{-2} at the surface of GaP¹³ and CdTe¹⁴ has been observed upon visible irradiation into the conduction band of each semiconductor. Efficiencies have approached 10%. Photoelectrochemical cells using these electrodes appear to be very useful because the substance oxidized at the semiconductor is reduced at the counter electrode (platinum) such that no net chemical change occurs in the electrolyte. With this arrangement sustained photocurrents are possible.

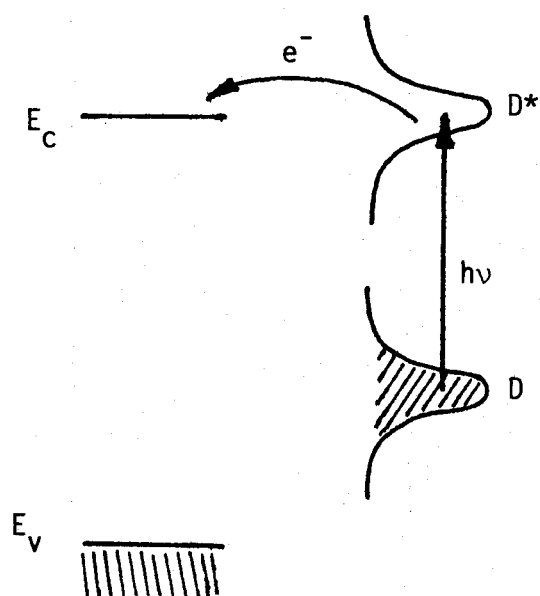
Photosensitized electron transfer reactions have been observed at semiconductor electrode surfaces and are discussed in the following sections.

2. Photosensitized electron injection

It is possible to inject an electron into the conduction band of a semiconductor by irradiating a dye adsorbed on the surface which has an excited state that overlaps the conduction band of the semiconductor (see Figure 1). This phenomenon has been observed for ZnO (band gap 3.2 eV) in the presence of Rhodamine B.^{15,16} It is not known whether

Figure 1

Photosensitized electron-injection



the dye transfers an electron from an excited singlet or triplet state. The triplet is longer lived, yet the dye is adsorbed to the surface of the semiconductor and the interaction could be strong enough to allow electron transfer from the short-lived singlet. The dye is oxidized in the process. In the ZnO-Rhodamine B (10^{-4} M, pH 2, 1 M KCl) system, the anodic photocurrent reaches a maximum at the absorption peak of the dye (5500 Å) and is greater than three orders of magnitude above the unsensitized photocurrent level.

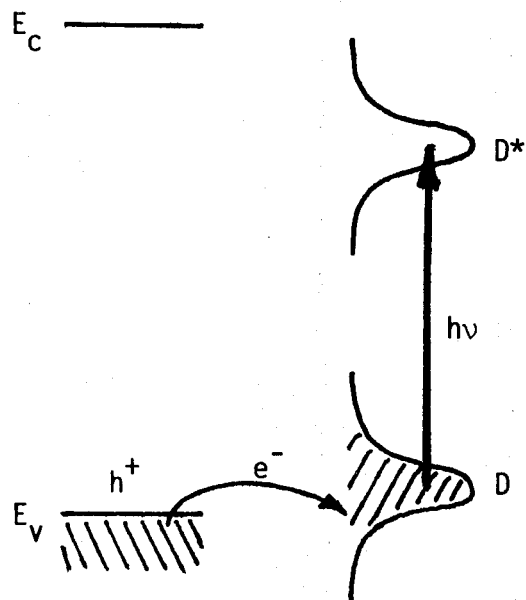
3. Photosensitized hole-injection

Cathodic photocurrents have also been sensitized by dyes absorbed on the surface of certain semiconductors.^{17,18} In this case, hole-injection can occur if the ground state energy level of the dye overlaps with the valence band of the semiconductor. Irradiation of the dye excites an electron into an upper level. An electron from the valence band of the semiconductor reduces the dye by filling the ground state dye level creating a hole in the valence band as shown in Figure 2. It is necessary for the excited state of the dye to fall below the conduction band of the semiconductor to observe cathodic photocurrents. Hole-injection has been observed in Cu₂O-Rhodamine B¹⁷ and GaP-Rhodamine B¹⁸ systems. In both cases, photocurrents were not observed with dye absent.

4. Importance of flat-band potentials

Before making use of electron and hole injection to accomplish redox reactions, one must know the energy of the band edges of semi-

Figure 2
Photosensitized hole-injection



conductors in relation to the series of standard redox potentials, the electrochemical scale for the free energy of electrons in electrolytes. The flat-band potential¹⁹ of the semiconductor allows one to estimate the position of the band edges versus a normal hydrogen electrode (NHE) or other standard electrode. The flat-band potential (V_{fb}) represents the difference in Fermi level between the semiconductor and reference electrode and is the intercept of a plot of $1/C^2$ versus V (Mott-Schottky plot)²⁰ where C is the capacitance of the semiconductor and V is the applied voltage. The conduction band edge can then be found from the expression:⁴

$$E_C = E_F - kT \ln(N_D/N_C) \quad (1)$$

Here, E_C is the conduction band energy (eV), E_F is the Fermi level energy ($E_F = -qV_{fb}$), N_D is the donor density calculated from the slope of the Mott-Schottky plot, and N_C is the effective density of states at the lower edge of the conduction band. The band gap then determines the position of the valence band. These calculations were done by Gomes and Cardon²¹ for a series of semiconductors, and their results appear in Figure 3 and Table I.

5. Photosensitized oxidation of water by hole-injection

Hole-injection into the valence band of GaP was observed by Memming and Tributsch¹⁸ for GaP-Rhodamine B systems in 1M KCl upon irradiation at 5700Å. This places the ground state energy level of Rhodamine B at less than -0.80 eV on the energy level diagram of

Figure 3

Semiconductor band edge energies (eV) versus NHE

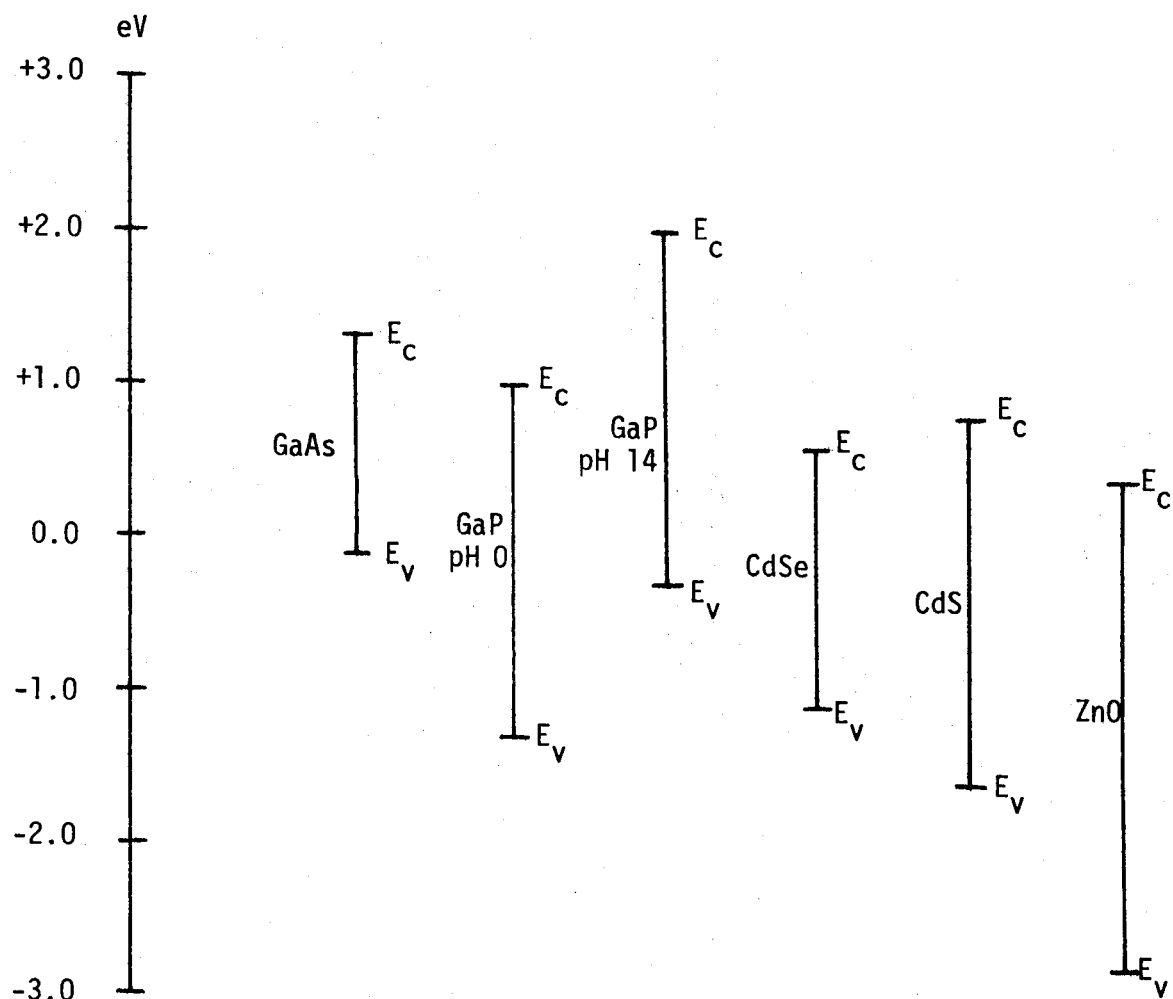
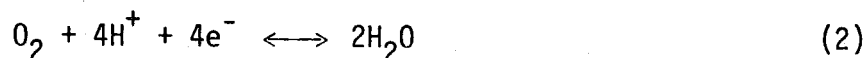


Table I Semiconductor band edge energies versus NHE

Semiconductor	Medium	E_C (eV) vs NHE	E_V (eV) vs NHE
GaAs	1M KOH	+ 1.3	- 0.1
GaP*	1M H ₂ SO ₄	+ 1.0	- 1.3
	1M NaOH	+ 2.0	- 0.3
CdSe	2M KCl	+ 0.6	- 1.1
CdS	2M KCl	+ 0.8	- 1.6
ZnO*	pH 9.2	+ 0.4	- 2.8

*It has been found that the positions of the bands of several semiconductors shift toward higher energies as the pH increases.^{21,22}

Figure 3, since overlap with the valence band of GaP is necessary for this process. O₂ evolution was not reported in this system. A possible explanation lies in the reduction potential of the reaction:



at pH 7. Using the Nerst equation and an E^0 value of + 1.23V,²³ the potential is + 0.82V versus NHE at pH 7. This places the electron energy at which Equation 2 occurs below the valence band of GaP in Figure 3. Thus, oxidation of water is not expected.

It is conceivable, however, that O₂ evolution might be observed at a GaP semiconductor surface in the proper environment. At pH 0 (1M H₂SO₄) the valence band of GaP lies at - 1.3 eV (from Table I). This is below the electron energy at which O₂ evolution occurs (-1.22 eV at pH 0) and so if one was able to inject holes into the surface of GaP,

the oxidation of H_2O should proceed.

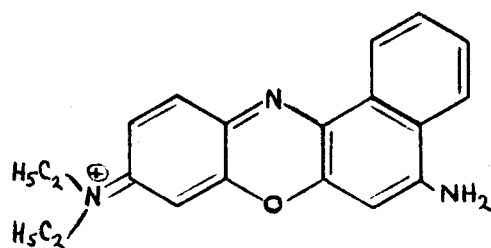
Although there is no published data that I know of on redox potentials for xanthene dyes such as Rhodamine B, the observation of hole-injection in GaP-Rhodamine B systems at pH 7 indicates that the ground state of this dye has an electron energy near -1 eV. However, since the conduction band of GaP is much lower at pH 0, Rhodamine B would not be a suitable dye for hole-injection into the semiconductor because its excited state undoubtedly overlaps the conduction band of GaP. A suitable dye would be one with an absorption band at longer wavelength. Therefore, a reasonable first set of experiments to try would involve irradiating a GaP semiconductor in acid solution with Nile Blue, oxazine 9, or dye 140 (an amidopyrylium dye) absorbed to its surface.

Nile Blue and oxazine 9 have absorption maxima (EtOH) at 6350\AA and 6010\AA , respectively, and have been found to be much more stable photochemically than xanthene dyes like the Rhodamines.²⁴ Dye 140 has an absorption maximum at 6600\AA (see Figure 4 for structures). The dye should be excited with monochromatic light near the absorption maximum. However, the optimum position might be at lower energy where there is less chance of transfer from the excited state of the dye to the conduction band of GaP.

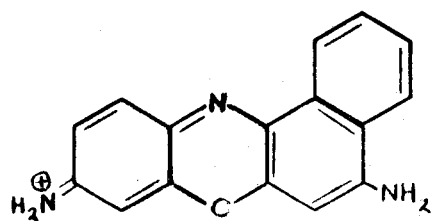
If overlap between dye in its ground state and the valence band of GaP was sufficient for hole-injection, the oxidation of water with subsequent evolution of O_2 from the surface of the crystal should occur. The evolution of O_2 might not be noticed, however, if it

Figure 4

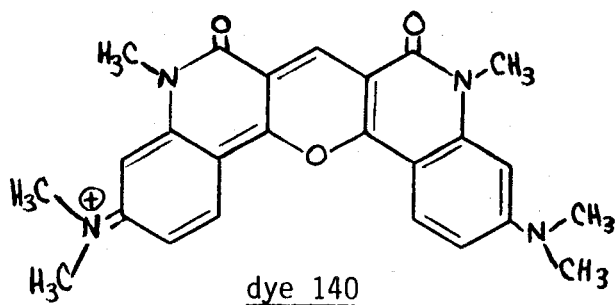
Dyes for photosensitized hole-injection
into GaP



Nile Blue



Oxazine 9

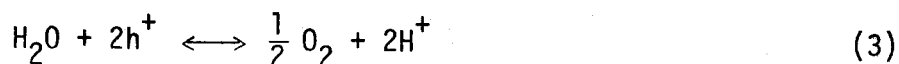


dye 140

immediately oxidizes the dye. Therefore, it might be necessary to add an oxidant or to have an electrode present to oxidize the dye after electron transfer from GaP to allow evolution of O_2 from the solution. The energy level diagram for the process is shown in Figure 5.

It would be advantageous to have the dye transfer its extra electron in a way that does useful chemistry. If another semiconductor was close by, and it had a conduction band that overlapped the excited state of the dye, it might be possible to oxidize the dye with an electron-injection process.

CdS is a possible candidate for the job. Although CdS decomposes^{25,26} upon hole-injection due to dissolution, it is stable toward electron-injection processes. Its conduction band lies at + 0.8 eV and its valence band lies at - 1.6 eV (Table I). Thus, it should be possible to transfer an electron from the excited dye to the conduction band of CdS. The electron energy of the conduction band should be high enough to see evolution of hydrogen at the surface. This has been observed in GaP¹⁸ upon irradiation with light ($\approx 5500\text{\AA}$) into its conduction band at pH 7. The complete energy level diagram for the redox reaction is shown in Figure 6. At the surface of GaP, oxygen should be evolved:



while at the surface of CdS, hydrogen should be evolved:



There are several modifications one could make in the system if the desired chemistry did not occur. Perhaps of most importance is the

Figure 5

Chemical reaction at p-GaP surface: $\text{H}_2\text{O} + 2\text{h}^+ \rightarrow \frac{1}{2} \text{O}_2 + 2\text{H}^+$

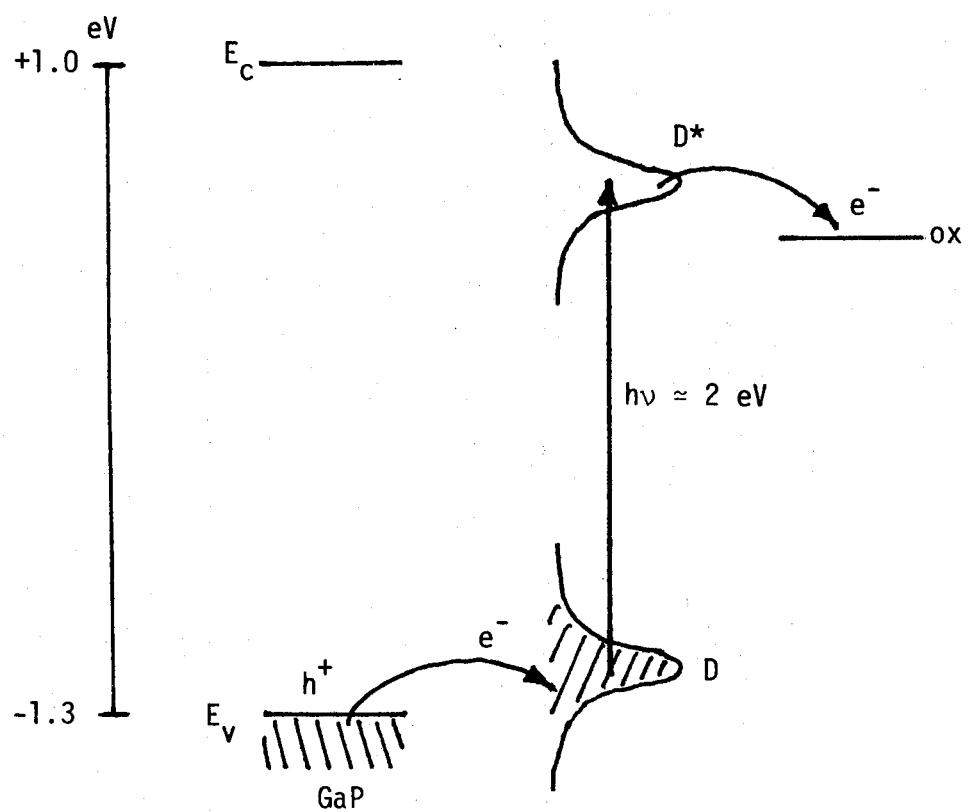
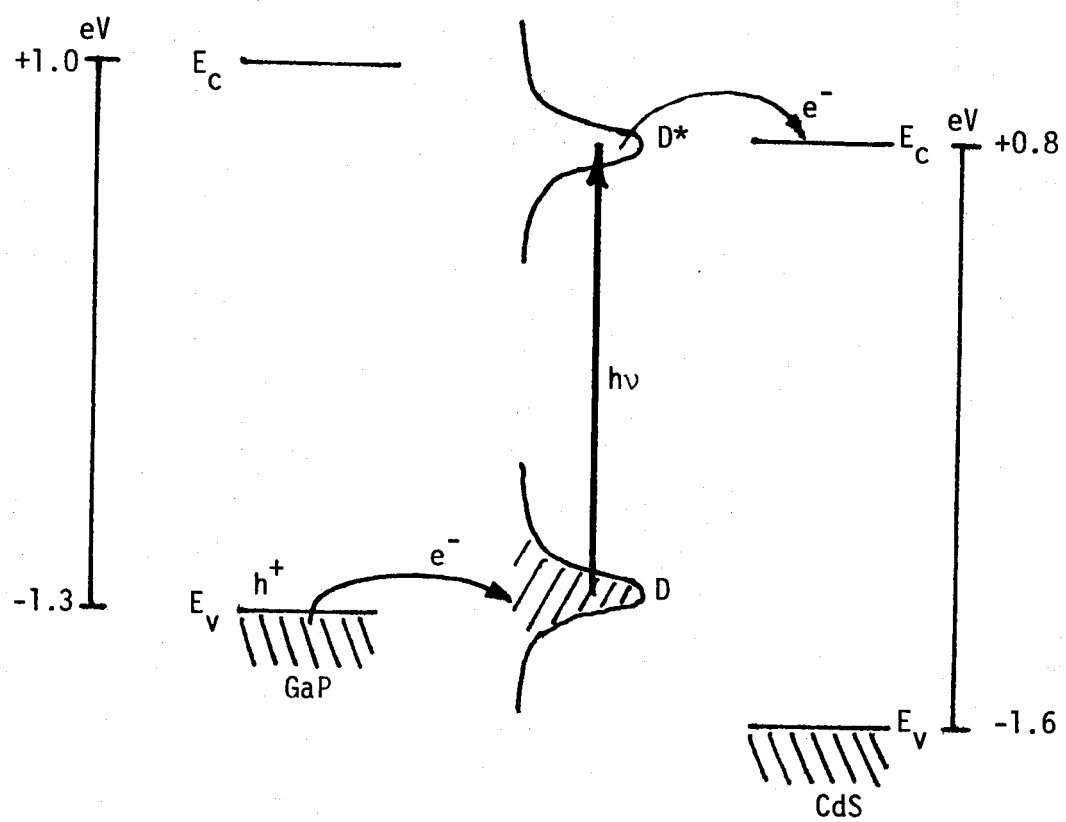


Figure 6

Energy level diagram for the redox reaction



fact that the energy band edges of the semiconductors are sensitive to both pH^{21,22} and temperature⁸ of the electrolyte to which they are exposed. Thus, shifting of the band edges can be done if necessary for better overlap of the valence band of the semiconductor with the ground state of the dye (hole injection) or better overlap of the conduction band of the semiconductor with the excited state of the dye (electron injection). For example, if one could shift the band edges of SrTiO_3 or KTaO_3 which have very high quantum efficiencies such that good overlap occurred with the ground state of the adsorbed dye, then the efficiency of the electrolysis might improve dramatically. Other dye-semiconductor combinations could be tried and even if the electrolysis of water could not be achieved, other chemical redox reactions could be studied in order to improve the efficiency and further the understanding of the details of the electron-transfer process.

References

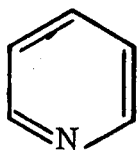
1. A. Fujishima and K. Honda, *Nature*, 238, 37 (1972).
2. M. S. Wrighton, D. S. Ginley, P. T. Wolcyanski, A. B. Ellis, D. L. Morse, and A. Linz, *Proc. Nat. Acad. Sci. USA*, 72, 1518 (1975).
3. A. Nozik, *Nature (London)*, 257, 383 (1975).
4. H. Gerischer in *Physical Chemistry*, ed. by H. Eyring, D. Henderson, and W. Jost (Academic Press, N.Y., 1970), Vol. IXA.
5. D. C. Cronmeyer, *Phys. Rev.*, 87, 876 (1952).
6. M. S. Wrighton, A. B. Ellis, P. T. Wolczanski, D. L. Morse, H. B. Abrahamson, and D. S. Ginley, *J. Am. Chem. Soc.*, 98, 2774 (1976).
7. M. S. Wrighton, D. L. Morse, A. B. Ellise, D. S. Ginley, and H. B. Abrahamson, *J. Am. Chem. Soc.*, 98, 44 (1976).
8. M. Nagasawa and S. Shionoya, *J. Phys. Soc. Japan*, 30, 1118 (1971).
9. M. I. Cohen and R. F. Blunt, *Phys. Rev.*, 168, 929 (1968).
10. A. B. Ellis, S. W. Kaiser, and M. S. Wrighton, *J. Phys. Chem.*, 80, 1325 (1976).
11. D. Khang and S. H. Wemple, *J. Appl. Phys.*, 36, 2925 (1965).
12. G. Hodes, P. Cohen, and J. Manassen, *Nature (London)*, 260, 312 (1976).
13. A. B. Ellis, J. M. Bolts, S. W. Kaiser, and M. S. Wrighton, *J. Am. Chem. Soc.*, 99, 2848 (1977).
14. A. B. Ellis, S. W. Kaiser, J. M. Bolts, and M. S. Wrighton, *J. Am. Chem. Soc.*, 99, 2839 (1977).
15. H. Gerischer and H. Tributsch, *Ber. Bunsenges. Phys. Chem.*, 72, 437 (1968).

16. H. Tributsch and H. Gerischer, Ber. Bunsenges. Phys. Chem., 73, 251 (1969); ibid. 850 (1969).
17. H. Gerischer, Photochem. and Photobio., 16, 243 (1972); Ber. Bunsenges. Phys. Chem., 77, 771 (1973).
18. R. Memming and H. Tributsch, J. Phys. Chem., 75, 562 (1971).
19. J. F. Dewald, Bell Syst. Techn. J., 39, 615 (1960).
20. N. F. Mott, Proc. Roy. Soc. (London), A171, 27 (1939); W. Schottky, Z. Phys., 113, 367 (1939); ibid., 118, 539 (1942).
21. W. P. Gomes and F. Cardon, Zeitschrift für Physikalische Chemie Neue Folge, 86, 330 (1973).
22. K. L. Hardee and A. J. Bard, J. Electrochem. Soc., 122, 739 (1975).
23. R. E. Dickerson, H. B. Gray, and G. P. Haight, Chemical Principles (Benjamin, California, 1973).
24. K. H. Drexhage, in Topics in Applied Physics, ed. by F. P. Schafer (Springer-Verlag, Berlin, 1973), Vol. I.
25. K. Bohnenkamp and H. J. Engell, Z. Elektrochem., 61, 1184 (1957).
26. U. Harten, Z. Naturforsch., 16, 1401 (1961).

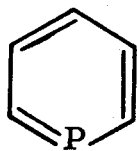
PROPOSITION IV

Synthesize new substituted styrenes by alkylating group V heterobenzenes using vinyl triflates

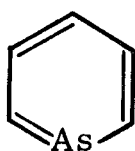
The group V heteroaromatic compounds, pyridine a, phosphabenzene b, arsabenzene c, stibabenzene d, and bismabenzene e form an interesting chemical series in that elements of an entire column of the periodic table are incorporated into aromatic rings.



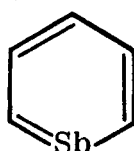
a



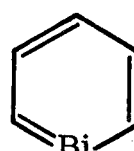
b



c



d



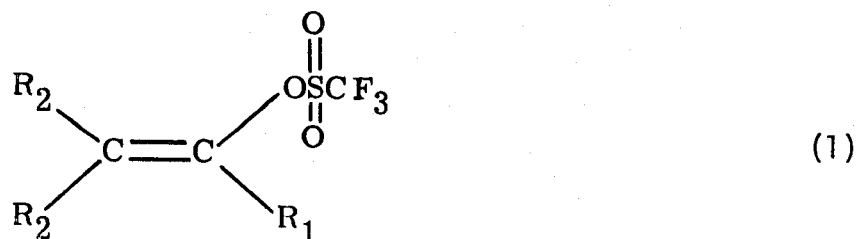
e

Studying the relative chemical reactivity of the members of this series in various types of reactions should provide information about the nature of π bonding between carbon and group V elements as well as lend insight into the details of the reaction mechanisms themselves. It is proposed that several of the group V heterobenzenes (b,c,d) can be alkylated in a Friedel-Crafts electrophilic aromatic substitution reaction with vinyl triflates to form new substituted styrenes. A comparison of the relative reactivities of b,c,d towards alkylation could 1) provide information about the influence of the heteroatom upon the electron density in the aromatic ring and 2) possibly add support to the belief that the mechanism of vinyl triflate alkylation involves a vinyl cation intermediate and not a carbonium ion as invoked for other Friedel-Crafts alkylations.²

Except for the highly labile bismabenzene, e, the group V heterobenzenes are stable, isolatable compounds. Microwave spectral studies³⁻⁶

indicate that all of the heterobenzenes are planar. Carbon-carbon bond lengths are extremely close (0.01\AA) to the C-C bond in benzene (1.395\AA). Although the C-X bonds (where X = heteroatom) are much longer than the C-C bonds, the CXC bond angles are smaller than the CCC bond angle in benzene (120°) such that the structural strain introduced in the ring by the addition of the large heteroatom is minimized. With the exception of pyridine, whose chemistry is very different from the other members due to the basicity of nitrogen, the heterobenzenes undergo Diels-Alder type cycloaddition reactions,⁷ certain electrophilic aromatic substitution reactions,⁸ and can form transition metal complexes.^{8,9} Recently, it has been found⁸ that the heteroatoms of phosphabenzene and arsabenzene show no basic properties toward proton acids or alkylating agents. For this reason, it may be possible to alkylate these heterobenzenes (and perhaps stibabenzene as well) using vinyl triflates to form new substituted styrenes. To justify this hypothesis, a discussion of the alkylation of aromatic substrates using vinyl triflates is necessary.

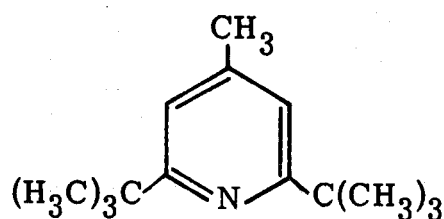
Vinyl triflates are highly reactive species containing a trifluoromethanesulfonate (TFMS) group as shown below:



where TFMS = CF_3SO_3 and R_1, R_2 are alkyl and/or aryl substituents. Since it has been established that triflic acid, $\text{CF}_3\text{SO}_3\text{H}$, is the strongest

Brønsted acid (proton donor) known, the CF_3SO_3^- anion should be one of the best leaving groups available. This is the origin of the reactivity of vinyl triflates.

It has been discovered^{1,11} that both activated and deactivated aromatic substrates (i.e., substrates with substituents that either donate or withdraw electron density from the ring) can be alkylated with certain vinyl triflates. The reaction occurs under mild conditions, without the usual Friedel-Crafts catalysts (e.g., AlCl_3). It requires the presence of a sterically hindered nonnucleophilic base, 2-6-di-tert-butyl-4-methylpyridine (2).

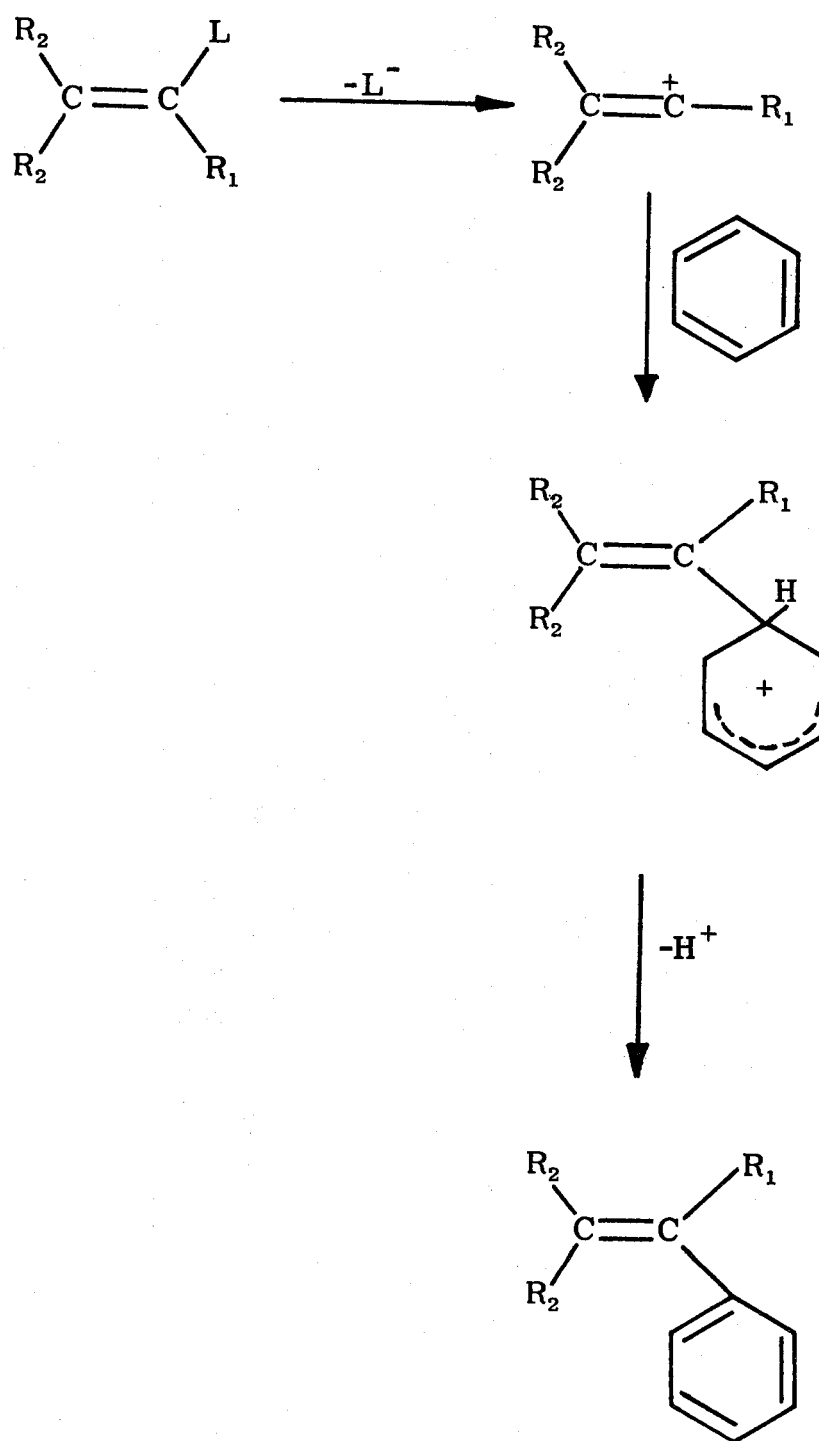


(2)

This base neutralizes the triflic acid liberated in the reaction, but does not interact with potential electrophilic intermediates (i.e., vinyl cations) due to steric hindrance.¹² Any interaction of this type would prevent alkylation. The mechanism of aromatic alkylation using vinyl triflates is thought to occur via a vinyl cation as shown in Fig. 1. In the diagram, $\text{L} = \text{CF}_3\text{SO}_3^-$ and for simplicity the aromatic substrate is taken to be benzene. The third step in this mechanism involves an intermediate with a positive charge delocalized on the aromatic ring. Because of this, alkylation of deactivated aromatic substrates (which already have reduced electron density in the ring due to an electron with-

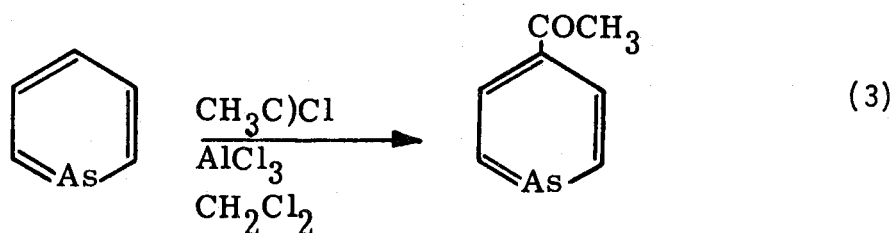
Figure 1. Mechanism of aromatic alkylation with vinyl triflates

Fig. 1

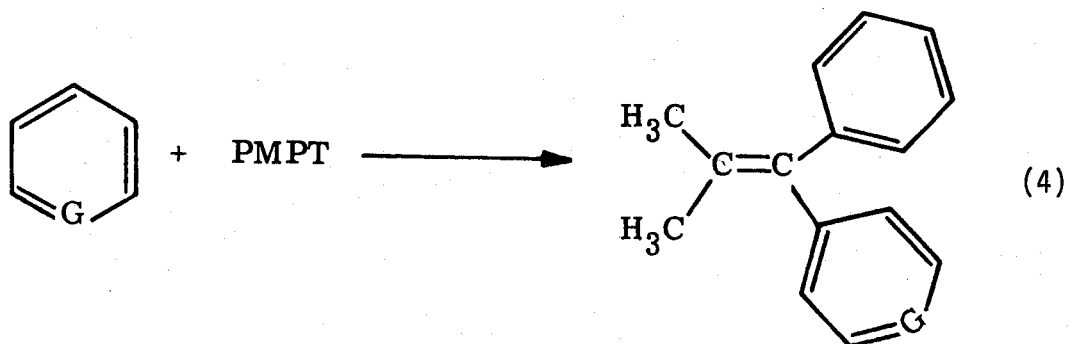


drawing substituent) is difficult, yet it has been accomplished for chlorobenzene¹ with good yield using 1-phenyl-2-methyl-1-propen-1 yl triflate ($R_1 = C_6H_5$, $R_2 = CH_3$ in (1)). This vinyl triflate (to be referred to as PMPT later) was used because 1) the vinyl cation thought to be produced is stabilized by the aryl group (R_1) and 2) it has no β hydrogens. Vinyl triflates with β hydrogens have been found¹ to undergo elimination reactions more favorably than alkylation.

Now that the mechanism and requirements for vinyl triflate alkylation of aromatic substrates have been presented, the reasons why group V heterobenzenes (b,c,d) should react to form styrenes will be given. First, as mentioned previously, the heteroatoms of phosphabenzene, arsabenzene, and possibly stibabenzene show no basic properties toward proton acids or alkylating agents. Therefore they should not interact with electrophilic intermediates (vinyl cations in this case) and electrophilic aromatic substitution should proceed if the substrate is reactive enough. Second, vinyl triflates are highly reactive species that can alkylate aromatic substrates under mild conditions without catalysts. This should make it more favorable to alkylate stibabenzene which is known to polymerize above room temperature.¹³ Finally, arsabenzene⁸ undergoes a Friedel-Crafts acylation reaction as shown below:



This reaction usually occurs for aromatic substrates that are at least as reactive as the halobenzenes. Therefore, arsabenzene must be as reactive as, say, chlorobenzene toward electrophilic aromatic substitution. As mentioned before, chlorobenzene undergoes vinyl triflate alkylation (primarily para-substitution) so if the other group V heterobenzenes (b,d) are as reactive or nearly as reactive as arsabenzene, then they should all undergo vinyl triflate alkylation to give the following styrene products:



where G = P, As, Sb.

Comparing the relative reaction rates and product yields for the resulting substituted styrenes should give some indication of the relative ability of the group V heteroatoms to stabilize the reaction intermediate. Also, comparison studies of the spectroscopy of the products with the benzene derivative (i.e., G = C) could provide new information about the influence of the heteroatom upon the electronic structure of these products.

References

1. P. J. Stang and A. G. Anderson, J. Am. Chem. Soc., 100, 1520 (1978).
2. G. A. Olah, Friedel-Crafts Chemistry (Wiley-Interscience, N.Y., 1973).
3. R. L. Kuczkowski and A. J. Ashe III, J. Mol. Spectrosc., 42, 457 (1972).
4. R. P. Lattimer, R. L. Kuczkowski, A. J. Ashe III, and A. L. Meinzer, J. Mol. Spectrosc., 57, 428 (1975).
5. R. L. Kuczkowski, G. Fong, and A. J. Ashe, III, J. Mol. Spectrosc., in press.
6. G. O. Sorensen, L. Mahler, and N. Rastrup-Anderson, J. Mol. Struct., 20, 119 (1974).
7. A. J. Ashe III and M. D. Gordon, J. Am. Chem. Soc., 94, 7596 (1972).
8. A. J. Ashe III, Acc. Chem. Res. 11, 153 (1978).
9. J. Deberity and H. Noeth, J. Organometal. Chem., 49, 453 (1973);
H. Vahrenkamp and H. Noeth, Ber., 106, 2227 (1973).
10. C. McCallum and A. D. Pethybridge, Electrochim. Acta, 20, 815 (1975).
11. P. J. Stang, Acc. Chem. Res., 11, 107 (1978).
12. H. C. Brown and B. Kanner, J. Am. Chem. Soc., 75, 3865 (1953).
13. A. J. Ashe III, J. Am. Chem. Soc., 93, 6690 (1971).

PROPOSITION V

Study dephasing processes in molecules capable of forming intramolecular exciplexes using picosecond laser excitation and the three-pulse photon echo method

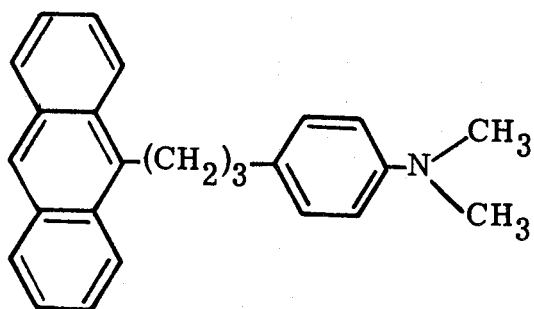
An exciplex is a complex of an electronically excited molecule with another chemically distinct molecule in its ground state. It only exists in the excited state and dissociates into its ground state component molecules upon radiative or radiationless relaxation. The binding energy of the complex is provided by charge transfer. However, if the difference between donor ionization energy (D_E) and acceptor electron affinity (A_E) is small, ground state charge transfer (CT) complexes are formed. Therefore, a necessary criterion for exciplex formation is that ($D_E - A_E$) be large enough to prevent the formation of ground state CT complexes. Intramolecular exciplexes can be formed if a molecule has two distinct aromatic parts separated from each other by some aliphatic chain or other group.

Much experimental¹⁻⁵ and theoretical⁷ effort has been devoted to the problem of understanding the orientational requirements for the formation of an intramolecular exciplex and its electronic structure following the local excitation of one of the aromatic groups of the molecule. From exciplex formation rates in certain systems, it is thought that internal rotation of the aliphatic chain is necessary to get the two aromatic groups in a favorable geometric position for the charge transfer interaction.³ Several questions come to mind regarding this orientational requirement. One may ask what happens in the molecule during the time period following photon absorption in one aromatic group and before the exciplex is fully formed. Is there any energy redistribution in the excited chromophore before it interacts with the other aromatic group? Does excess vibrational energy influence the rate of exciplex formation? How would the approach of the other aromatic group influence the dephas-

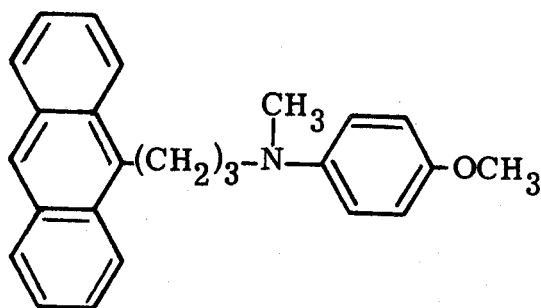
ing rate of the locally excited group? For that matter, although one assumes that there is no interaction between the two chromaphores in the ground state, can one treat the groups independently when one speaks about dephasing processes of the system? Information that may help to find the answers to some of these questions can be obtained by studying the molecular dynamics of these systems. In particular, it should be useful to obtain 1) the coherence of the system (i.e., the dephasing time of the locally excited chromaphore + ground state chromaphore); 2) the lifetime of the excited chromaphore; 3) the formation rate and lifetime of the exciplex; and 4) the dephasing time of the locally excited chromaphore when isolated (i.e., just the free chromaphore). This information should provide insight into the relationship between the dephasing rate and the exciplex formation rate in the system and also provide an indication of just how "isolated" the chromaphores actually are in the ground state. Previous studies on intramolecular exciplexes have been done in solution¹⁻⁵ as a function of solvent polarity and viscosity. Exciplex formation rates, lifetimes and emission spectra have been obtained for several systems. To answer some of the questions posed earlier and specifically to determine the coherence properties of these systems, it is proposed that several molecules capable of forming intramolecular exciplexes be studied at low pressure in the gas phase where the influence of the solvent upon both the rate of exciplex formation and the resulting exciplex structure is removed.

The systems chosen for these studies have already been examined in solution. They are diaromatic molecules of the form $X-(CH_2)_3-Y$ where X is anthracene and Y is an aromatic amine. Shown below are their

structures:

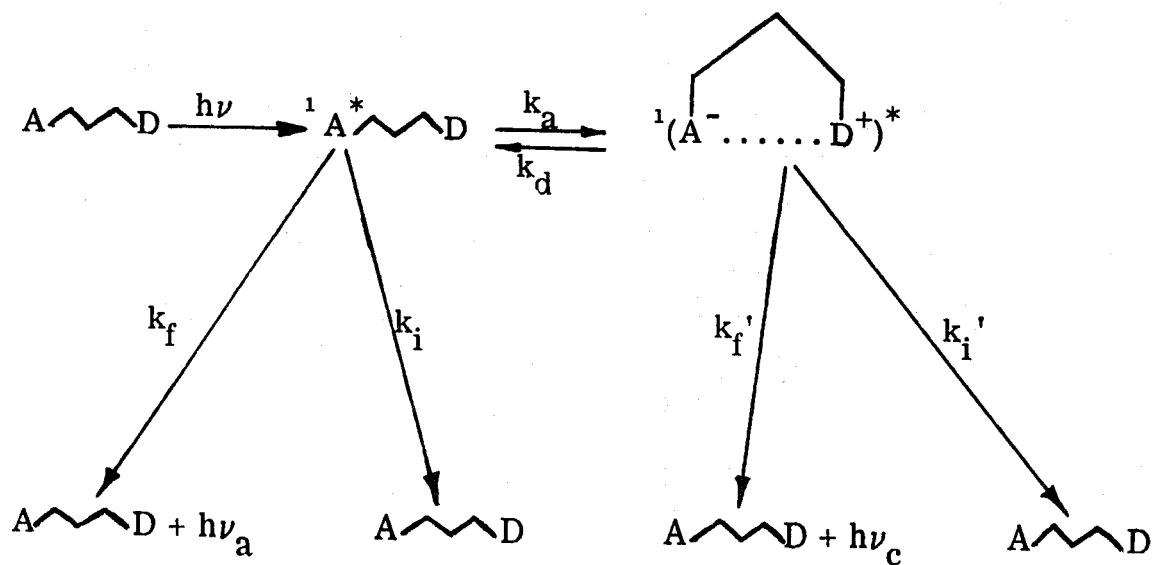


I



II

In these molecules it has been found that anthracene acts as an electron acceptor (A) and the aromatic amine an electron donor (D) in the charge transfer interaction in the excited state. The mechanism for intramolecular exciplex formation and decay can be described as follows:



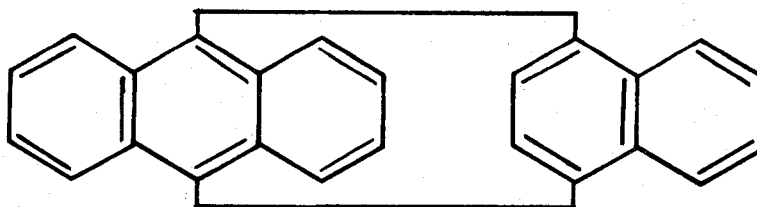
Following absorption into the lowest allowed singlet of the anthracene part of the molecule, a locally excited anthracene moiety is formed. This intermediate either emits at a rate given by k_f , decays nonradiatively at k_i (here k_i represents the total nonradiative decay, i.e., intersystem crossing and internal conversion) or if the proper orientation of D is obtained (during the excited state lifetime), goes on to form the exciplex. The exciplex also has radiative and nonradiative relaxation channels as shown in the diagram. In solution, much has been learned about the details of this mechanism. Because the information is useful for an understanding of the photophysics of exciplex formation, a summary of some of the results will be presented below.

First, the absorption spectra of I² and II⁴ are identical with the sum of the spectra of 9-methylanthracene and the respective aromatic amine. Therefore, it is thought that no appreciable ground state interaction between the aromatic groups occurs. One should be careful at this point not to draw any conclusions about the dephasing (T_2) channels between the aromatic groups simply from the spectra. Second, the emission spectrum of the anthracene part of both I and II resembles that of anthracene itself.^{2,4} In I, the lifetime is about equal to that of anthracene in solution (3-6 nsec).⁸ In II, the lifetime is strongly temperature dependent, equalling that of anthracene only at low temperature ($\approx 120^\circ\text{K}$). At room temperature the lifetime of the anthracene-like emission in II is 0.7 nsec. From these results (in nonpolar solvents) and quantum yield measurements it has been concluded that the rate of exciplex formation is much higher in II than in I.

Third, exciplex emission spectra^{2,4} for I and II are broad and red-shifted from the anthracene emission. The lifetime of the exciplex emission (both I and II) is about 100 nsec. In I, the emission shifts to lower energy with increasing solvent polarity. This has been attributed to the polar nature of the exciplex state. Further evidence for this comes from the $S_1 \rightarrow S_n$ absorption spectra of the anthracene part of I. In polar solvents, peaks can be identified² with those of the anthracene anion. This implies a high degree of charge separation in the exciplex. Finally, the time constant (k_a^{-1}) for exciplex formation has been measured for I using picosecond absorption spectroscopy. In a nonpolar solvent (n-hexane) k_a^{-1} was found to be 900 psec³ at room temperature. For II k_a^{-1} was estimated as < 1 nsec.

With this information in hand, the proposed experiments are as follows. First, it would be interesting to measure the dephasing time (T_2) of both I and II following coherent excitation into the lowest allowed singlet transition in the anthracene moiety ($^1A_{1g} \rightarrow ^1B_{2u}$ origin at $\approx 27,500 \text{ cm}^{-1}$ for the free molecule⁹) in the gas phase at low pressure. Exciplex formation represents a unique kind of intramolecular energy transfer in these systems in that a predominantly localized excitation is spread out over another part of the molecule upon proper orientation of the two aromatic groups. Several questions relating to dephasing can be posed. One may ask how close the second aromatic group has to be and what orientation it needs to affect the phase coherence created in the "two-level" system in anthracene selected by the laser. Can the aliphatic chain connecting the two portions of the molecule provide a communication channel between the two groups such that phase coherence is lost well

before an exciplex is formed or is phase coherence lost (assuming no collisions during the lifetime of the excited state) only by formation of the exciplex and radiative and nonradiative (T_1) processes of the locally excited anthracene moiety? Hopefully, the experiments mentioned above might answer these questions. Second, the dephasing time of anthracene itself under similar conditions should be measured to determine the relative importance of exciplex formation compared with other dephasing channels in the molecule. Finally, it would be interesting to measure the dephasing rate in another type of diaromatic molecule containing anthracene to see if it might provide additional insight into intramolecular dephasing processes. For example, [2.2](1,4)-naphthaeno(9,10)anthracenophane contains both anthracene and naphthalene connected with aliphatic chains as shown below:



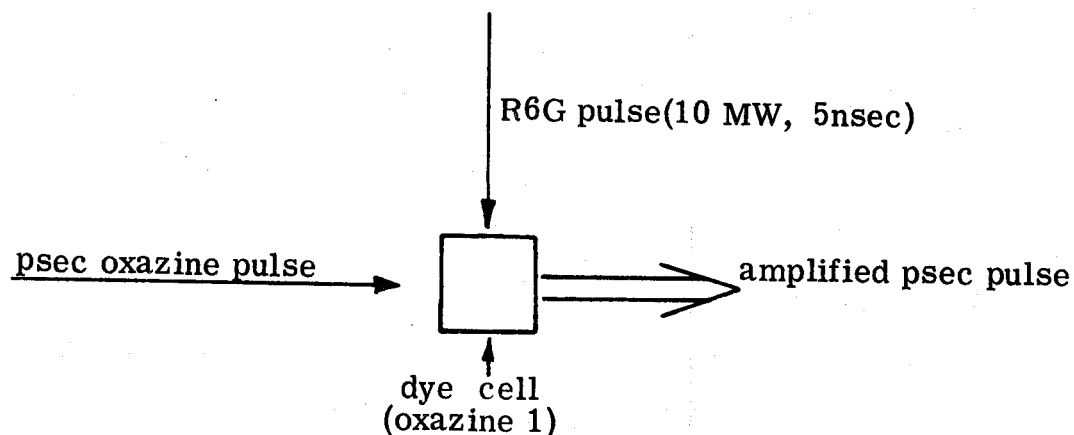
III

Since anthracene is bonded to naphthalene at two positions, the interaction between groups may be stronger resulting in even faster dephasing. Of course, it is not known at this point if the groups can achieve a favorable orientation for exciplex formation or weaker interaction for that matter. Measuring the dephasing rate may provide clues concerning the nature of the intramolecular interaction. These suggested dephasing experiments will require a picosecond dye laser and can be done most

easily using the three-pulse photon echo method.¹¹ Since the time constant for exciplex formation in I is 900 psec (in solution), one must have the time resolution of a picosecond laser to coherently excite anthracene and have sufficient time to measure the decay of the photon echo which provides the dephasing time. It has already been established that the three-pulse photon echo method for measuring the dephasing rate in a system is sensitive enough to work at low pressure in the gas phase.¹¹ This is due to the fact that one probes the spontaneous emission from the system with this method at 90° to the exciting beam, which can be done with extremely sensitive detectors. Therefore, the only technical difficulties in doing these experiments are 1) to get picosecond pulses with sufficient power in the region of the origin of the lowest allowed singlet in anthracene ($\approx 3600\text{\AA}$), and 2) to obtain the necessary laser pulse sequence ($\pi/2, \pi, \pi/2$) to perform the experiment.

The first problem can be solved in the following way. Synchronously-pumped mode-locked cavity dumped (SPMLCD) picosecond dye lasers are now available. They have pulse widths of 5-20 psec and peak powers of over 1.5 kW. For these experiments, a SPMLCD picosecond dye laser consisting of a krypton laser pumping a dye laser containing oxazine 1 should provide picosecond pulses from 6800-8200 \AA . These pulses can be frequency doubled using a KDP crystal to provide pulses at the required wavelength ($\approx 3600\text{\AA}$). However, the peak power of the doubled pulses with this laser arrangement will probably be too low to do the experiment. To overcome this problem, a dye amplifier would have to be used. Briefly, this would entail transverse excitation of a cell containing oxazine 1 with a pulse

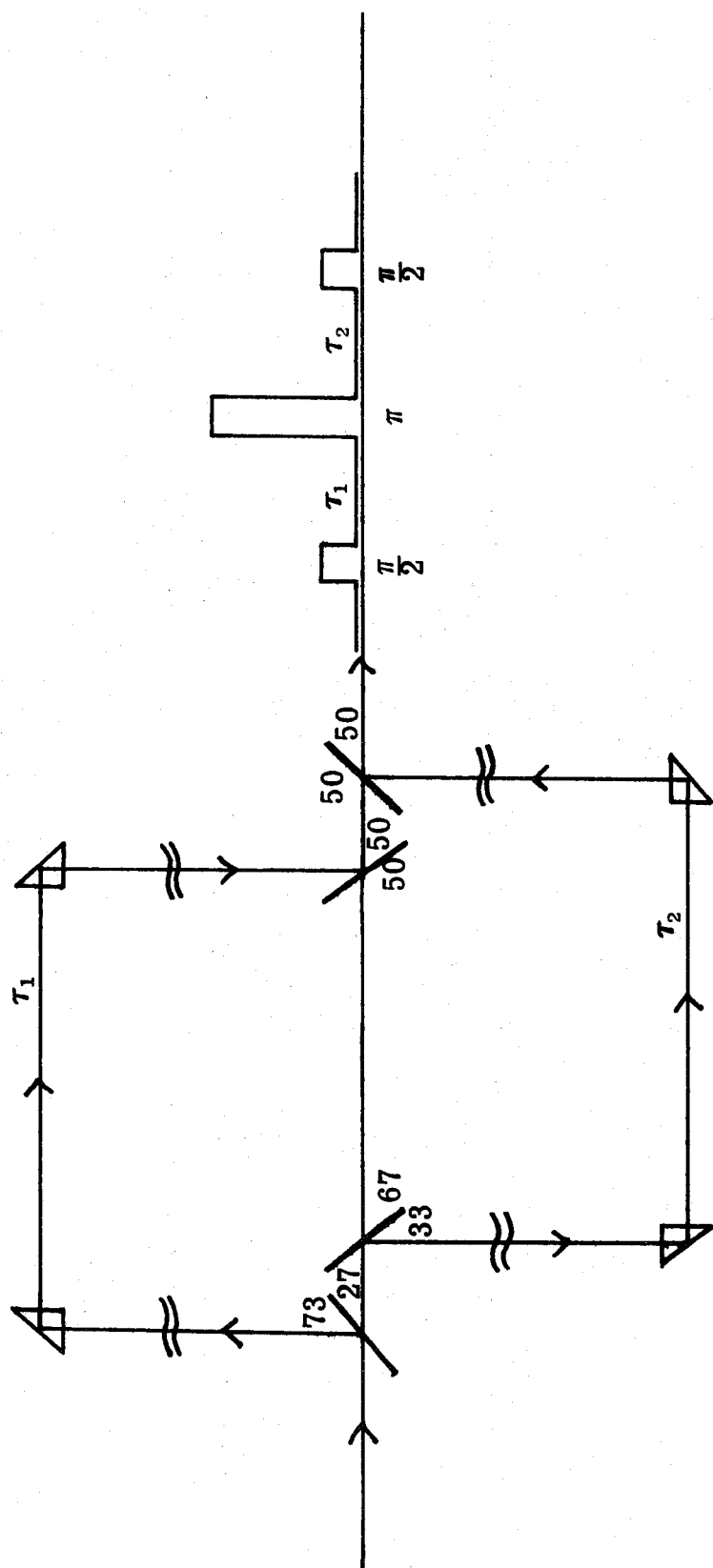
from a doubled and amplified Nd:YAG pumped rhodamine 6G dye laser¹³ synchronized with the arrival of a picosecond pulse from the oxazine dye laser as shown below:



Using a sequence of three cells and appropriate spatial and spectral filtering between stages, this amplification system has provided gains of 10^3 - 10^5 in other applications.^{14,15} Following the amplifier, the pulse would be doubled using KDP as before to obtain the required frequency. With this laser arrangement, there would be sufficient tunability to do the experiment at the origin of the transition in anthracene as well as at the first few vibronic lines to determine the effects of excess vibrational energy upon the various dephasing processes.

The second problem can be solved using a combination of beam splitters and optical delay lines as shown in Fig. 1. Since all of the pulses are of the same width, the proper excitation sequence requires that the intensity of the first and third pulses be one-fourth that of the second. This is because a $\pi/2$ pulse is obtained from the relation:

Figure 1. Schematic of an optical arrangement for splitting a single pulse into three pulses with the intensity ratio (1:4:1). Optical delay lines provide variable pulse separations.



$$\left(\frac{\mu \cdot \epsilon}{h}\right)t = \pi/2 \quad (1)$$

where μ is the transition dipole moment and ϵ is the laser field amplitude. An estimate of the field amplitude necessary to produce a $\pi/2$ pulse for a pulse width (t) of 10 psec can be obtained from the oscillator strength of the anthracene transition ($f = 0.4$).¹⁶ This corresponds to a dipole moment of $\mu = 0.6$ debye and therefore, for a 10 psec pulse, an ϵ of $\approx 9 \times 10^6$ V/m is required to satisfy equation (1). If the laser beam is focussed to a 100μ spot, a pulse of less than 1 kW peak power will provide this field. Peak power levels of this magnitude should be obtainable using the dye amplifier even considering the losses introduced by the optical arrangement for creating the pulse sequence.

The decay of the photon echo, which provides T_2 as stated earlier, is obtained by varying the delay times (τ_1, τ_2) between pulses and monitoring the intensity of the spontaneous emission at $\tau_1 = \tau_2$. This dephasing time (T_2) when combined with a lifetime measurement (T_1) obtained using one excitation pulse, can provide information about pure dephasing events (T_2') in the system since:

$$\frac{1}{T_2} = \frac{1}{2} \left(\frac{1}{T_{1e}} + \frac{1}{T_{1g}} \right) + \frac{1}{T_2'} \quad (2)$$

where T_{1g} and T_{1e} are the lifetimes of the ground and excited states, respectively. For electronic transitions $T_{1e} \ll T_{1g}$ so one usually ignores the $1/T_{1g}$ term in (2) and obtains T_2' knowing T_2 from the photon echo and T_{1e} from the spontaneous emission lifetime. Recent theoretical

work¹⁷ has related T_2' to the anisotropy between the scattering amplitudes of the ground and excited states of the "two-level" system selected by the laser. If one assumes that phase destroying events as a result of elastic collisions are unimportant in these systems at low pressure where the excited state lifetime is less than that required for collisions, then one can establish whether or not intramolecular dephasing channels exist in these systems. If $T_2 = 2T_{1e}$, then by Eq. (2), $T_2' = 0$. On the other hand, if $T_2 < 2T_{1e}$, then $T_2' \neq 0$. If it is found that intramolecular dephasing does occur in these systems, one may ask what the anisotropy in scattering amplitudes between the excited and ground states refers to. One approach to this problem would be to attribute this anisotropy to differences in the coupling of each level to the continua of vibrational levels from other manifolds. Not enough is known at this point however to understand these processes. Much more experimental and theoretical work in the area of intramolecular relaxation is needed. Perhaps these experiments may provide some new information concerning these important processes in large molecules.

References

1. E. A. Chandross and H. T. Thomas, Chem. Phys. Lett., 6, 393 (1971).
2. T. Okada, T. Fujita, M. Kubota, S. Masaki, N. Mataga, R. Ide, Y. Sakata, and S. Misumi, Chem. Phys. Lett., 14, 563 (1972).
3. T. J. Chuang, R. J. Cox, and K. B. Eisenthal, J. Am. Chem. Soc., 96, 6828 (1974).
4. F. Pragst, H. J. Hamann, K. Teuchner, M. Naether, W. Becher, and S. Daehne, Chem. Phys. Lett., 48, 36 (1977).
5. M. Migita, M. Kawai, N. Mataga, Y. Sakata, and S. Misumi, Chem. Phys. Lett., 53, 67 (1978).
6. M. Itoh, T. Mimura, H. Usui, and T. Okamoto, J. Am. Chem. Soc., 95, 4388 (1975).
7. For a review see J. B. Birks, Progr. Reaction Kinetics, 5, 4109 (1969).
8. D. S. Kliger and A. C. Albrecht, J. Chem. Phys., 50, 4109 (1969).
9. G. Kortum and B. Vinck, Z. Physik Chem., B52, 263 (1942).
10. A. Iwama, T. Toyoda, T. Otsubo, and S. Misumi, Chem. Lett., 587 (1973).
11. See section B of Chapter II, and section C of Chapter III of this thesis.
12. e.g., Spectra-Physics Corporation.
13. e.g., Quanta-Ray PDL-1 plus Quanta-Ray DCR-1A Nd:YAG.
14. M. M. Sabour, Opt. Comm., 22, 202 (1977).
15. E. Ippen and C. V. Shank, to be published.
16. R. Pariser, J. Chem. Phys., 24, 250 (1956).
17. K. E. Jones and A. H. Zewail, in Advances in Laser Chemistry, ed. by A. H. Zewail (Springer, Berlin, 1978).